

**Identifying Key Variables Associated with the Temporal and Spatial  
Distribution of Prolific Marine Petroleum Source Rock (MPSR) Units  
and its Application to the Taconic Foreland Basin, eastern New York**

Abstract of  
a thesis presented to the Faculty  
of the State University of New York  
at Albany  
in partial fulfillment of the requirements  
for the degree of  
Master of Science  
College of Arts and Sciences  
Department of Geological Sciences

C. Mark Achong  
1993

## ABSTRACT

Correctly identifying key variables associated with the temporal and spatial distribution of prolific marine petroleum source rock (MPSR) units is of critical importance towards the future development of models accurately predicting their existence and effective exploitation. The geographic positioning and prevailing paleoclimatic conditions on paleocontinental reconstructions, in combination with the processes controlling the drowning of continental margins and parameters associated with the establishment of high biologic productivity and long term anoxic conditions within the water column, have been pursued as first-order constraints controlling the development of some prolific marine petroleum source rock (MPSR) deposits. From this, a model has been developed that accounts for the enhanced preservation of regional type-II MPSR deposits on low paleolatitudinally-positioned continental margins and shelves that have undergone depression with respect to sea level. Two 'shelf-drowning' mechanisms, continental passive margin subsidence combined with eustacy, and tectonically-induced subsidence by the loading of continental margins, are presented as effective processes that contribute towards the more efficient accumulation and preservation of some extensive marine petroleum source rock (MPSR) units.

The potential utility of this model is examined by a comprehensive analysis of an extensive active continental margin MPSR unit deposited within the late medial Ordovician Taconic Foreland Basin of eastern New York and a prolific late medial Cretaceous continental passive margin MPSR unit deposited within the Maracaibo Basin of northwestern Venezuela. The integrated use of organic geochemistry, programmed pyrolysis, and geochemical analyses of the Taconic Foreland Basin demonstrates that the Utica Formation was an organic-rich and a prolific, although now spent, MPSR unit. The existence of the Utica Formation is believed to have been the result of 'channeled-flow upwelling', within a bathymetrically-constricted collisional foreland basin, which was spatially positioned at a subsiding continental margin entering a subduction zone. The penecontemporaneous impingement of the oxygen minimum zone of the water column at the drowned continental shelf caused the establishment of long-term anoxic conditions on the outer

slope of the developing foreland basin. This consequently increased the potential for the preservation, subsequent burial and compaction, and eventual conversion of organic-rich muds into a regionally important source rock unit.

Geochemical analysis of the late medial Cretaceous derived petroleum oils of the Maracaibo Basin also requires the existence of one regional MPSR unit, the La Luna Formation. This is consistent with the combination of eustatic sea level rise, and thermal subsidence, of the northern South American passive continental margin and shelf during medial Cretaceous times being coincident with the development of high biologic productivity conditions within the overlying photic zone of the water column. This was a direct result of the low paleolatitudinal positioning of the northern coastline of South America during medial Cretaceous times. The subsequent movement of the Caribbean Plate through the Proto-Caribbean Seaway in turn controlled the timing and maturation of the MPSR unit, becoming younger as collision and foredeep sedimentation progressed eastwards.

**Identifying Key Variables Associated with the Temporal and Spatial  
Distribution of Prolific Marine Petroleum Source Rock (MPSR) Units  
and its Application to the Taconic Foreland Basin, eastern New York**

A thesis presented to the Faculty  
of the State University of New York  
at Albany  
in partial fulfillment of the requirements  
for the degree of  
Master of Science  
College of Arts and Sciences  
Department of Geological Sciences

C. Mark Achong  
1993



## ACKNOWLEDGMENTS

There is a 'supporting cast of thousands', each of whom deserve recognition for their respective contributions towards the production of this thesis. I hope that I have acknowledged below all those who have assisted me through my graduate study at the State University of New York at Albany.

First and foremost, for their patience, academic guidance, and associated 'colourful' moments throughout my M.S. study, special thanks goes to my thesis committee, Dr. James L. Pindell (Dartmouth College), Dr. John W. Delano (State University of New York at Albany), especially Dr. William S.F. Kidd (State University of New York at Albany), and the entire Geological Sciences faculty and associated staff (especially Diane Patton) of the State University of New York at Albany. They deserve credit for providing me with the necessary encouragement and scientific direction (even though sometimes it was a serpentine, tortuous, experience that I shall not soon forget) throughout my graduate studies. I must also take this time to re-emphasize my gratitude towards Dr. William S.F. Kidd for initially getting me involved with this project, as well as his insightful and thought-provoking commentary regarding global politics, contemporary culture, and Archean plate tectonics during the late November deer-hunting season while 'hunting' for calcareous shale outcrops for my field study, and seeing me through this process to the very end.

For their scientific assistance, I would like to thank Dr. Rhodes for the use of machinery at the Ronald B. Gilmore X-Ray Analytical Facility at the University of Massachusetts at Amherst, and his associates' hospitality during my stay, and Dr. S.T. Ahmedali of McGill University for the excellent geochemical analyses of my samples, and his courteous nature during the harrowing six month wait that it took to get the analyses of my samples.

For their comradeship, the 'Hogan's Heroes' of the Department of Geological Sciences at the State University of New York at Albany, the graduate students, are acknowledged. While every graduate student that I encountered while at Albany made my stay that much more enjoyable, special thanks goes to (soon to be) Drs. Y.D. Park and B.Z. Hanson for instilling within

me the necessary diligence, tenacity, and vigilance towards the pursuit of scientific knowledge, and the most fond memories of my graduate career at the State University of New York at Albany. Special mention goes to Michael "Long live Britannia" Edwards for his colourful discussions regarding American and British society, R&B music, and structural geology, Susi "the Xenolist" Vogel for her eloquent thoughts on phase equilibria, geochemical thermodynamics, and German food, Micheal 'Double Agent' Hascke for his realistic, as well as timely, appraisements of life as a struggling 'graduate student-in-training' geologist, and Andreas "Mr. Perfect 100" Plesch for keeping me on my toes scientifically as well as academically.

For their financial support, I would like to thank Dr. Audri Bissada of Texaco Inc. for acquiring financial support for the analysis of my samples, summer living expenses during the summer of 1992, and additional scientific advice regarding the petroleum generative capacity of the calcareous black shales of the Taconic Foreland Basin. Also, thanks goes out to Betty Shadrick, and Jonathan Bartow of the Office of Graduate Studies of State University of New York at Albany, for the coordination and continued acquisition of graduate fellowship funding throughout my graduate study.

Finally, I would like to thank my family, namely my parents and my sisters, for their patience, support, periodic financial backing, and understanding during my tenure at Albany, as well as Dwight Pierre, Todd G. Day, Pedro McKnight Jr., Ken Glover, Andrew Kurtz for their additional support and pertinent advice, when all of us were in the 'graduate-school trenches'. Last, but definitely not least, a very special degree of thanks goes to Karlene A. A. Anderson (Cornell, B.S. '94) for helping me to finally realize that when one tries to make their goals and aspirations become reality (Note: the upcoming assertion will not hold true for scientific endeavors, especially when it comes to material dealt within this thesis), "if the dreams are *indeed* really big enough, then the facts really don't matter". I will always be in your debt for the support that you were so willing to give when I needed you to be there for me.

## TABLE OF CONTENTS

<u>Chapter</u>	<u>Page</u>
ABSTRACT	ii
ACKNOWLEDGMENTS	v
TABLE OF CONTENTS	viii
LIST OF TABLES	xi
LIST OF FIGURES	xii
I. CHAPTER 1: INTRODUCTION	1
II. CHAPTER 2: METHOD OF STUDY AND STUDY AREA	15
III. CHAPTER 3: GEOLOGICAL EVOLUTION OF THE CARIBBEAN INTER-PLATE REALM: IMPLICATIONS FOR THE DEPOSITION, MATURATION AND MIGRATION OF HYDROCARBONS DERIVED FROM A PRÓLIFIC MARINE PETROLEUM SOURCE ROCK (MPSR) UNIT DEPOSITED WITHIN THE MARACAIBO BASIN, NORTHWESTERN VENEZUELA	
3.1 Introduction	30
3.2 Regional Plate-Tectonic Overview	35
3.2.1 Formation of the proto-Caribbean Seaway: Creation of a Submerged Margin along northern South America during Tithonian (140 Myr) through Campanian (84 Myr) Times	35
3.2.2 Late medial Cretaceous Paleoclimatic Reconstruction	40
3.2.3 Evidence Establishing the La Luna Formation as a Passive Continental Margin MPSR Unit deposited during late medial Cretaceous Times	43
3.2.4 Commencement of Collisional Foredeeps and Marginal Basins During late Cretaceous through Paleocene Times	46
3.2.5 Formation of the Cuban and Maracaibo Collisional Foredeeps and Cayman Trough during latest Paleocene through Eocene Times	49

3.2.6	Tectonic Disruption of Paleocene-Eocene Petroleum Reservoirs During Oligocene Times	50
3.2.7	Collision of the Panamanian-Costa Rican Arc and its Related Consequences for Hydrocarbon Evolution During Miocene Times	51
3.3	Geochemistry of Maracaibo Basin, Northwestern Venezuela	53
3.3.1	Introduction: General Regional Overview	53
3.3.2	Organic Matter and Source Rocks of the Maracaibo Basin	58
3.3.3	Hydrocarbon Generation in the Maracaibo Basin	62
3.3.4	Mechanism for Expulsion of Hydrocarbons in the Maracaibo Basin	64
3.3.5	Migration History of Hydrocarbons within the Maracaibo Basin	67
3.4	Conclusions	69
3.4.1	Validation of La Luna Formation as a Prolific Passive Continental Margin MPSR Unit as a Consequence of Wind-Driven Upwelling during the late medial Cretaceous	69
IV.	CHAPTER 4: REGIONAL OVERVIEW AND GEOCHEMICAL ANALYSIS OF THE TACONIC FORELAND BASIN, LATE MEDIAL ORDOVICIAN: THE UTICA FORMATION AS A PROLIFIC, SPENT, MARINE PETROLEUM SOURCE ROCK (MPSR) UNIT	
4.1	Introduction	71
4.2	Regional Overview of the Taconic Foreland Basin, eastern New York	73
4.2.1	Geologic Setting of the Taconic Foreland Basin	73
4.2.2	Tectonic Evolution of the Collisional Foredeep	81
4.2.3	Depositional Environment of the Taconic Foreland Basin	83
4.2.4	Paleoecological Assessment of the Collisional Foredeep	86
4.2.5	Late medial Ordovician Paleoclimatic Distribution	88
4.3	Geochemical Analysis of the Taconic Foreland Basin	92
4.3.1	Pyrolysis Analysis of Representative Transect of the Taconic Foreland Basin	92
4.3.2	Verification of Anoxic Conditions During Deposition of the Utica Formation	101
4.3.3	Establishment of Primary Productivity Conditions within the Taconic Foreland Basin	109
4.3.4	Provenance Determination within the Taconic Foreland Basin	119
4.3.5	Preliminary Geochemical Analyses and Implications for Previously Unmapped Faults within the Taconic Foreland Basin	123
4.4	Conclusions	123
4.4.1	Re-Evaluation of the Utica Formation as an Extensive, Spent, Marine Petroleum Source Rock (MPSR) Unit during late medial Ordovician times	127
V.	CHAPTER 5: CONCLUSIONS	
5.1	Conclusions	131
5.1.1	Overall Conclusions	131
5.1.2	Future Work and Study	135

## APPENDICES

I.	DETERMINATION OF STRATIGRAPHIC POSITION OF SAMPLES	137
II.	PROGRAMMED PYROLYSIS OF SAMPLES	139
III.	X-RAY FLUORESCENCE OF SAMPLES	142
IV.	LOI DETERMINATION OF SAMPLES	149
V.	ORIGINAL FIELD NOTES DESCRIPTIONS OF SELECTED SAMPLE LOCALITIES	146
VI.	PALEOGEOGRAPHIC AND PALEOCLIMATIC RECONSTRUCTION TECHNIQUES	163
	Vi.i Introduction	
	Vi.ii Atmospheric Circulation	
	Vi.ii.i Derivation of ideal, present-day, zonal circulation patterns	164
	Vi.ii.ii Modification of ideal present-day zonal circulation into present-day cellular circulation patterns	169
	Vi.iii Wind-Driven Upwelling	
	Vi.iii.i Conditions for wind-driven upwelling	172
	Vi.iii.ii Coastal wind-driven upwelling	176
	Vi.iii.iii Open-oceanic divergences and upwelling	177
	Vi.iii.iv The connection between primary productivity and wind-driven upwelling: Is there actually one ?	180
	Vi.iv Paleoclimatic Reconstruction Modeling	
	Vi.iv.i Paleogeographic Reconstructions	183
	Vi.iv.ii Bathymetric considerations of wind-driven upwelling	186
	Vi.iv.iii Non-numerical, qualitative, paleoclimatic modeling	187
	Vi.iv.iv Numerical paleoclimatic modeling	189
	Vi.iv.v Comparison between both paleoclimatic models: Which one is better ?	191

## REFERENCES

192

LIST OF TABLESPage

Table I -	Locality Samples, Taconic Foreland Basin, eastern New York	18
Table II -	Locality Samples, Taconic Foreland Basin, eastern New York	19
Table III -	Locality Samples, Taconic Foreland Basin, eastern New York	20
Table IV -	Eastern Transect Samples, Taconic Foreland Basin, eastern New York	23
Table V -	Middle Transect Samples, Taconic Foreland Basin, eastern New York	24
Table VI -	Western Transect Samples, Taconic Foreland Basin, eastern New York	25
Table VII -	Programmed Pyrolysis Samples, Taconic Foreland Basin, eastern New York	28
Table VIII -	X-Ray Fluorescence Samples, Taconic Foreland Basin, eastern New York	29
Table IX -	LOI Weight Loss Calculations, Taconic Foreland Basin, eastern New York	145
Table X -	Source rock characteristics of the stratigraphic sequences within the Maracaibo Basin	59
Table XI -	Quantity, Quality, Thermal Maturity of Taconic Foreland Basin Samples	93
Table XII -	Modeling of Total Original Organic Carbon, Taconic Foreland Basin, eastern New York	99
Table XIII -	Major element analyses of samples from Taconic Foreland Basin, eastern New York	110
Table XIV -	Trace element analyses of samples from Taconic Foreland Basin, eastern New York	120

**LIST OF FIGURES****Page**

Figure 1.1 -	Distribution of effective source rocks through geologic time	2
Figure 1.2 -	Crude oil composition emphasizing principal fields of occurrence of crude oils from different depositional environments	3
Figure 1.3a -	Components of hydrocarbon source rocks	5
Figure 1.3b -	Relationships between kerogen-types, elemental composition, and organic maturation pathways	6
Figure 1.4 -	Principal periods of deposition of extensive oil source rocks and major coal deposits compared with global transgressive and regressive events	7
Figure 1.5 -	Relative areal extent compared against effectiveness of source rocks by paleolatitudinal zones <sup>1</sup>	9
Figure 1.6 -	Effectiveness of source rocks deposited in various structural forms	10
Figure 1.7 -	Explanation of the enhanced accumulation and preservation of MPSR units at continental margins undergoing topographic depression	13
Figure 2.1 -	Map showing location of the Mohawk Valley, eastern New York	17
Figure 2.2 -	Stratigraphic correlation chart of the Late Ordovician Taconic Foreland Basin strata	21
Figure 2.3 -	Generalized geologic map of the Taconic foredeep, eastern New York State	22
Figure 2.4 -	Map showing locations of transects and associated sample locations	26
Figure 3.1 -	Diagram of the West Indies structure	31
Figure 3.2 -	Geographical location map of the Caribbean region	32
Figure 3.3 -	Diagram of present-day plate separation between North and South America	36
Figure 3.4 -	General stratigraphy of the Maracaibo Basin	37
Figure 3.5 -	Late medial Cretaceous paleogeographic reconstruction and paleo-upwelling distribution	41
Figure 3.6 -	Sediment Accumulation Rate Curves of the Maracaibo Basin	45

Figure 3.7 -	Cross sections of episutural foredeep basins within the Caribbean region	47
Figure 3.8 -	General stratigraphy of the Maracaibo Basin	49
Figure 3.9 -	Neogene structural development of NW South America	52
Figure 3.10 -	Location of the Maracaibo Basin with names of various oil fields	54
Figure 3.11 -	Oil types and their distribution within the Maracaibo Basin	56
Figure 3.12 -	Sketch of hydrocarbon migration in the Maracaibo Basin during late Eocene-Oligocene times	57
Figure 3.13 -	Shale density-depth plot for an unspecified well in the western Maracaibo Basin	66
Figure 3.14 -	Sketch of hydrocarbon migration within the Maracaibo Basin during end middle Miocene-Recent times	68
Figure 4.1 -	Eustatic sea-level curves for the Phanerozoic	74
Figure 4.2 -	Generalized stratigraphic section of the Taconic Foreland Basin	75
Figure 4.3 -	Stratigraphy of the Trenton Group	77
Figure 4.4 -	Facies pattern of the Trenton Group	78
Figure 4.5a-c -	Plate-tectonic model for the Taconic Orogeny involving arc-passive collision and schematic block diagram of the Taconic collisional foredeep	82
Figure 4.6 -	Paleogeographic Distribution of Ordovician paleo-upwelling zones	89
Figure 4.7 -	Plot of Hydrogen Indices (HI) versus Oxygen Indices (OI) of Taconic Foreland Basin samples	94
Figure 4.8a -	Graphical Comparison of present-day TOC values of the Taconic Foreland Basin	96
Figure 4.8b -	Graphical Comparison of Organic Modeling of the Taconic Foreland Basin	98
Figure 4.9 -	Diagrammatic representation of the overall process of sedimentary pyrite formation	102
Figure 4.10 -	Plot of Total S <sub>pyrite</sub> (%) = Total Sulfur (%) versus Total Organic Carbon (%) for samples of the Taconic Foreland Basin	104



Figure 4.11 - Ternary plot of $\text{Al}_2\text{O}_3$ -U-TiO <sub>2</sub> concentrations of Taconic Foreland Basin samples	106
Figure 4.12 - Plot of U versus $\text{P}_2\text{O}_5$ concentrations of Taconic Foreland Basin samples	107
Figure 4.13 - Ternary plot of $\text{Al}_2\text{O}_3$ - $\text{P}_2\text{O}_5$ -TiO <sub>2</sub> concentrations of Taconic Foreland Basin samples	112
Figure 4.14 - Plot of $\text{P}_2\text{O}_5/\text{TiO}_2$ versus stratigraphic height of Taconic Foreland Basin samples	113
Figure 4.15 - Plot of $\text{P}_2\text{O}_5/\text{Al}_2\text{O}_3$ versus stratigraphic height of Taconic Foreland Basin samples	114
Figure 4.16 - Ternary plot of $\text{Al}_2\text{O}_3$ -BaO-TiO <sub>2</sub> concentrations of Taconic Foreland Basin samples	115
Figure 4.17 - Plot of BaO/TiO <sub>2</sub> versus stratigraphic height of Taconic Foreland Basin samples	117
Figure 4.18 - Plot of $\text{P}_2\text{O}_5/\text{Al}_2\text{O}_3$ versus stratigraphic height of Taconic Foreland Basin samples	118
Figure 4.19 - Ternary plot of $\text{Al}_2\text{O}_3$ -Nb-TiO <sub>2</sub> concentrations of Taconic Foreland Basin samples	121
Figure 4.20 - Ternary plot of $\text{Al}_2\text{O}_3$ -Zr-TiO <sub>2</sub> concentrations of Taconic Foreland Basin samples	122
Figure 4.21 - Plot of CaO versus stratigraphic height of Taconic Foreland Basin samples	124
Figure 4.22 - Plot of $\text{Al}_2\text{O}_3$ versus stratigraphic height of Taconic Foreland Basin samples	125
Figure 4.23 - Proposed mechanism of enhanced organic production within the Taconic Foreland Basin	129
Figure V.i - Unmodified positions of selected samples, Taconic Foreland Basin	152
Figure V.ii - Unmodified positions of selected samples, Taconic Foreland Basin	157
Figure V.iii - Unmodified positions of selected samples, Taconic Foreland Basin	158
Figure VI.i - Idealized surface atmospheric circulation, showing easterly and westerly wind belt systems	166

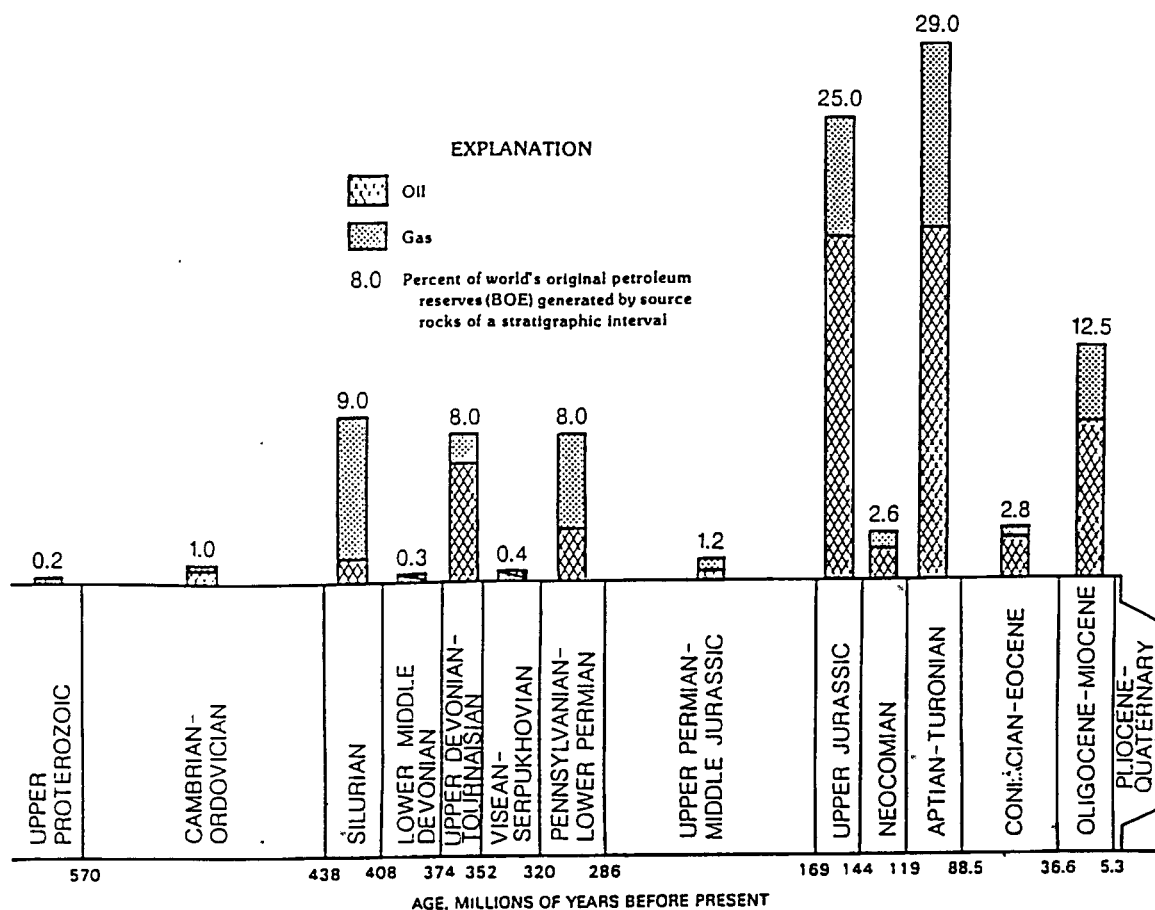
Figure VI.ii - Idealized surface atmospheric circulation, showing pressure belt systems and associated wind belt system development	168
Figure VI.iii - Idealized surface atmospheric circulation modification for summer and winter hemispheres-given a hypothetical continental landform	170
Figure VI.iv - Primary organic production in the present-day ocean	173
Figure VI.v - Ekman spiral and relationship between net water transport and wind direction	175
Figure VI.vi - Schematic diagram highlighting various wind-driven upwelling mechanisms	178

## CHAPTER 1: INTRODUCTION

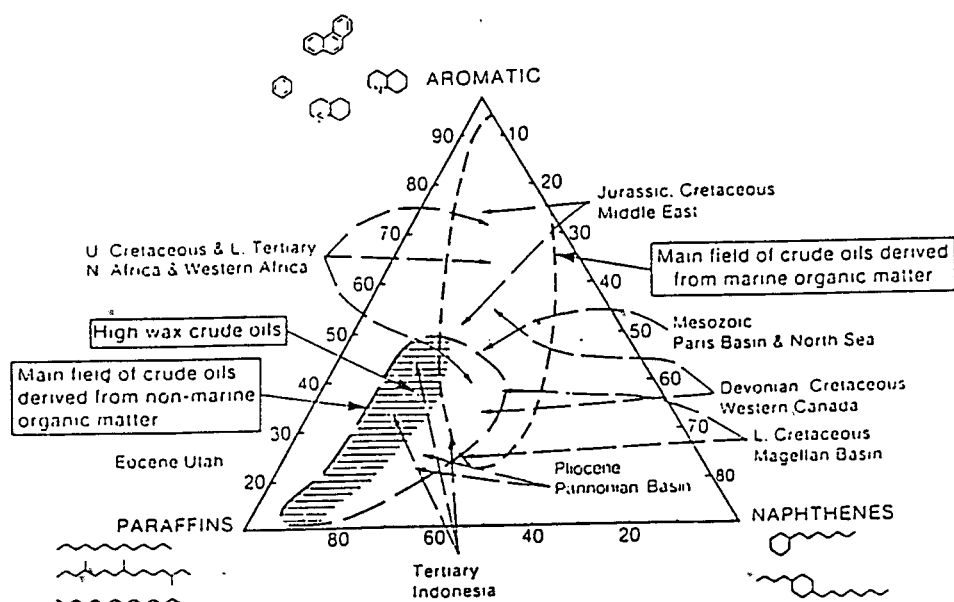
Petroleum geologists have tried recently to capitalize on the phenomenon of an observed uneven distribution of hydrocarbon deposits throughout the Phanerozoic. Six key stratigraphic time intervals - the late medial Ordovician, the Silurian, upper Devonian, Pennsylvanian-Lower Permian, Upper Jurassic, medial Cretaceous and Oligocene-Miocene - have produced more than 90 percent of the total projected global hydrocarbon budget ( $2200 \times 10^9$  barrels of oil), yet represent only 31 percent of Phanerozoic time (Fig. 1.1) (Ulmishek and Klemme, 1990). Several attempts, discussed below, have been made at identifying a specific key variable that would accurately predict the pattern of hydrocarbon deposits.

A source rock is a volume of rock that has generated or is generating and expelling hydrocarbons in appreciable enough quantities to form commercial oil and gas accumulations (Brooks et al., 1987). Hydrocarbon products are formed by the thermal maturation of organic matter within the source rock. Source rocks are derived either from marine or non-marine sources. Marine petroleum source rocks (MPSRs) accumulate as oil-prone sediments under marine conditions, but can also contain terrigenously-derived organic matter. While some marine clastics can be dominated by terrigenous organic matter, non-marine petroleum source rocks mostly accumulate within lakes and river basins, containing a mixture of freshwater algae and land plant material. Because hydrocarbon products are dependent upon the composition, depositional environment, thermal history and possible alteration of source rocks, hydrocarbon products formed from marine sources are generally more aromatic and less paraffinic than hydrocarbon products derived from non-marine source rocks (Fig. 1.2) (Brooks et al., 1987).

Sedimentary organic matter in the source rocks is divisible into two fractions. One is the portion of organic matter soluble in organic solvents or mineral acids known as bitumen, while



**Figure 1.1 - Distribution of effective source rocks through geologic time in percent of the world's original deposits generated by these rocks. Percent numbers are derived from summation of original petroleum deposits, in barrels of oil equivalent (BOE), of basins shown on the lithofacies and structural forms of the principal stratigraphic intervals. Reserve data for other intervals are approximated from a review of the main basins containing source rocks in these intervals. Separation of deposits into gas and oil is approximate (After Ulmishek and Klemme, 1991).**

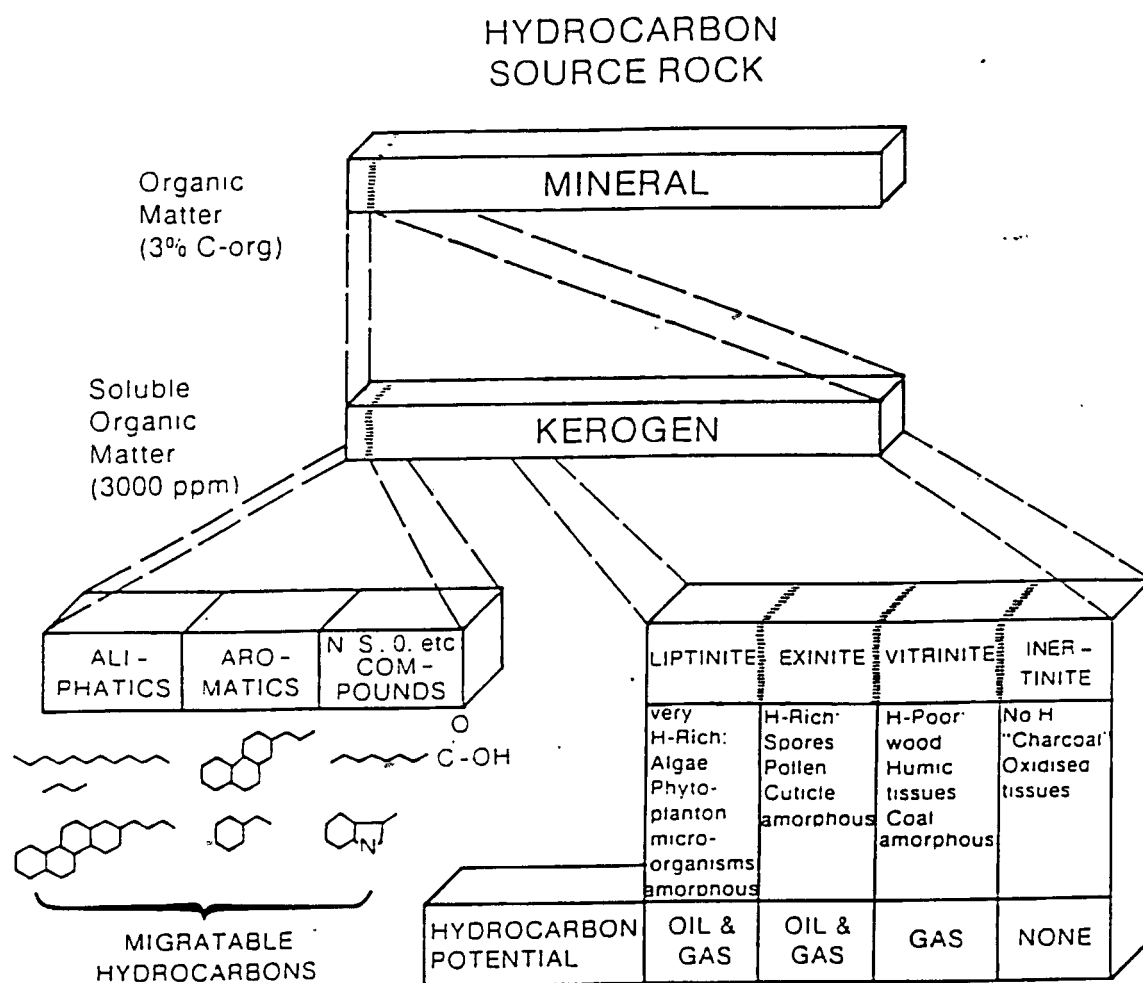


**Figure 1.2** - Crude oil composition highlighting the principal fields of occurrence of crude oils from marine and non-marine origin (After Tissot and Welte 1978, 1984) (Taken from Brooks et al, 1990).

the other is the insoluble organic matter, called kerogen, that yields hydrocarbon products upon cracking (heating) (Fig. 1.3a). Using C, H, O elemental abundances, it has been possible to classify three distinct types of kerogen according on their ability to generate hydrocarbons (oil and gas) (Fig. 1.3b) (Brooks et al., 1987).

Liptinite, type-I kerogen, possesses high H/C ratios with low O/C ratios and is primarily derived from algal material deposited in fine grained sediments within an anoxic, shallow water environment (Demaison and Moore, 1980). The Eocene Green River Oil Shale is the 'classic' example of type-I kerogen that primarily yields oil upon cracking. Exinite, type-II kerogen, also has high H/C ratios, but lower than type-I kerogen, and intermediate O/C ratios. It is derived from autochthonously-derived marine sediments that are the result of high primary productivity of phytoplankton, bacterial organisms and zooplankton, above an anoxic environment (Brooks et al., 1987). It can also be derived, to a lesser extent, from allochthonously-derived plant material such as spores, pollen, and cuticles. It produces oil and gas upon cracking. Vitrinite, type-III kerogen, possesses low H/C ratios and higher O/C ratios than both types-I and -II and is derived from woody fragments of terrestrially-derived plant material. Because of its allochthonous nature, with respect to the water column, it is usually refractory when deposited, being highly resistant to further degradation effects after deposition; it primarily yields gas upon heating. Inertinite, type-IV kerogen, possesses low H/C and O/C ratios and is the end product of the thermal maturation and degradation of the previous kerogen types, having no potential for future oil and/or gas generation. Because hydrocarbon deposits generated by type-I kerogen source rock units have been calculated to represent only 2.7% of the global total (Ulmishek and Klemme, 1990) and type-III kerogen produces primarily gas products upon cracking, type-II kerogen, found only in marine petroleum source rock (MPSR) units, is believed to be the key kerogen fraction that can yield prolific hydrocarbon deposits under favorable conditions.

Tissot (1979) tried to correlate between inferred global marine transgressions and the observed intervals of enhanced production and preservation of marine organic matter (Fig. 1.4)



**Figure 13a** - Components of hydrocarbon source rocks. Kerogen is subdivided into principal organic material of liptinite, exinite, vitrinite, and inertinite. Each of the organic materials have different potential for hydrocarbon generation (After Brooks et al., 1990).

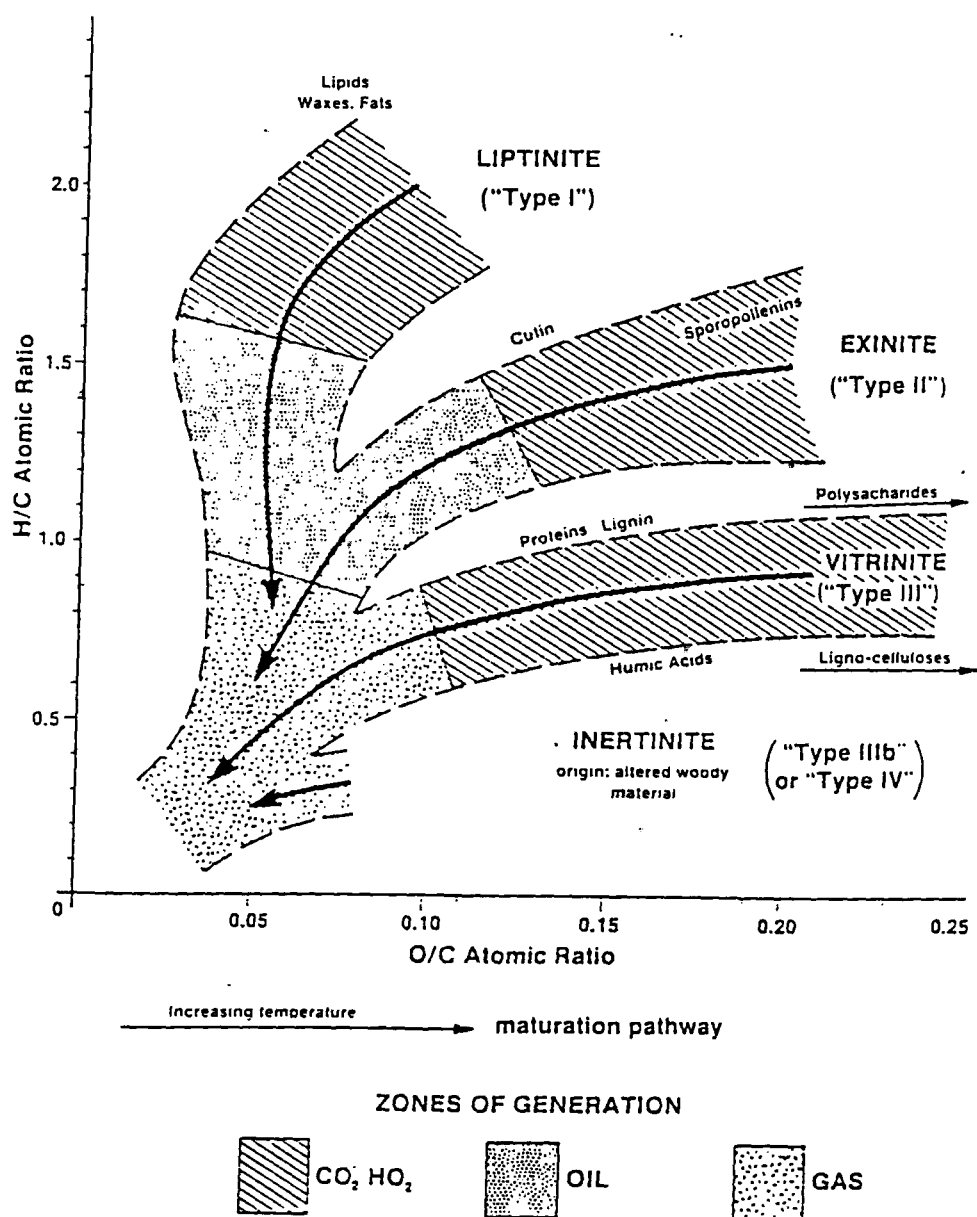


Figure 1.3b - Relationships between kerogen-types, elemental composition, and organic maturation pathways (From Brooks, 1981a) (Taken from Brooks et al., 1990).



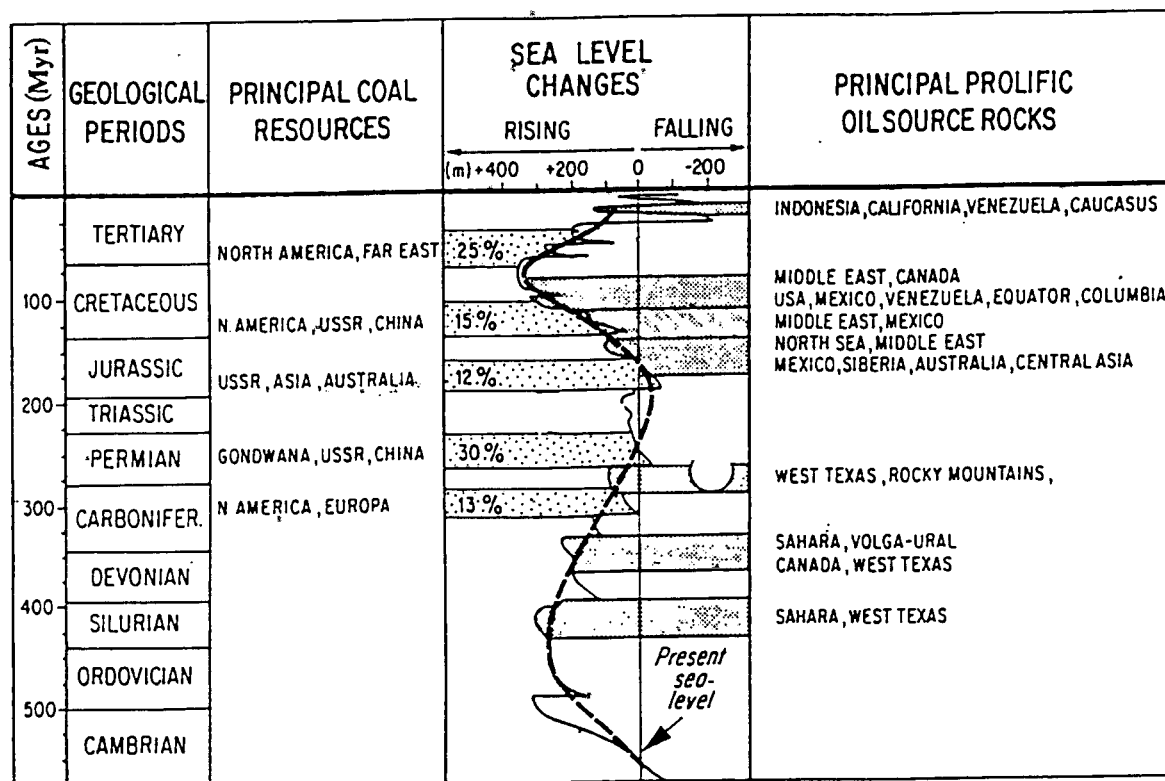
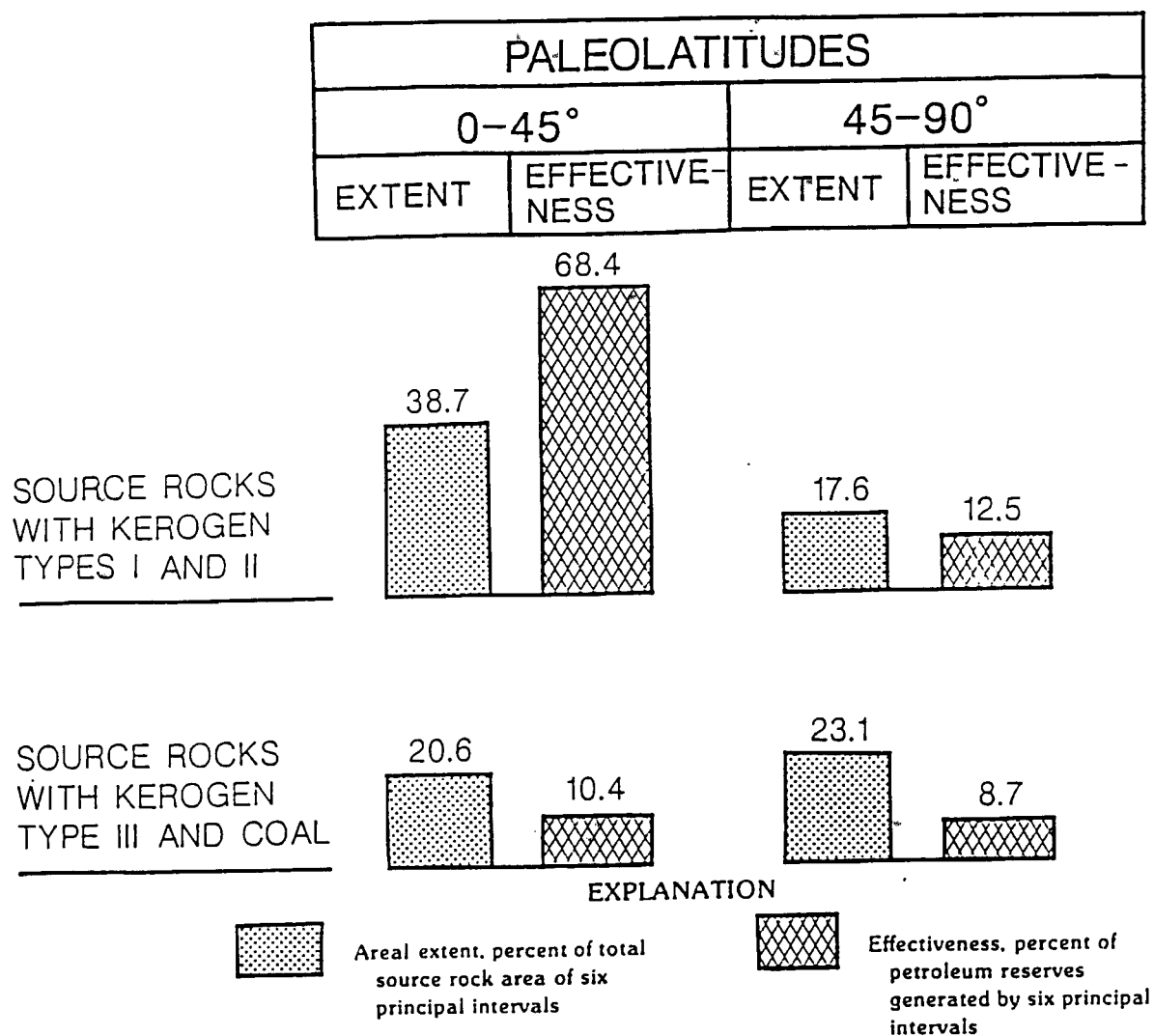


Figure 1.4- Principal periods of deposition of extensive oil source rocks and major coal deposits compared with global transgressive and regressive events. The periods considered for petroleum source rocks are responsible for more than  $900 \times 10^8 (\text{kg}) (\text{Myr})^{-1}$  of oil during the first transgressive pulse (570-200 Myr) and more than  $900 \times 10^9 (\text{kg}) (\text{Myr})^{-1}$  during the second (200-0 Myr) transgressive pulse (Taken from Tissot, 1979).

(Tissot, 1979). However, Demaison and Moore (1980) pointed out that if global sea-level changes were the only key variable for times of enhanced formation of petroleum source rock deposits, then enhanced accumulation and production of organic matter at present-day abyssal depths would be expected. However, according to (Demaison and Moore, 1980), this is observed not to be the case.

Parrish (1982) examined the significance of paleolatitudinal position of continents towards controlling enhanced hydrocarbon deposition (Parrish, 1982; Parrish and Curtis, 1982; Parrish, 1982a). Low to moderate paleolatitude positioning, with associated warm and moist climates, has been suggested to be conducive to the deposition of oil-prone source rocks (Ulmishek and Klemme, 1990). This is based on the observation that almost 60 percent of the total source-rock area of the six key stratigraphic time intervals has been deposited in paleolatitudes less than 45° north or south of the equator (Fig. 1.5); however, this would be expected from plain geometry, not allowing for the fact that the surface area between 45° latitude north and south accounts for over seventy percent of the Earth's surface. The majority of paleocontinental landforms have been positioned in low paleolatitudes throughout the Phanerozoic (Kidd, personal communication, 1993). Parrish (1982, 1982a) used paleogeographic reconstructions and paleoclimatological inferences to predict that 55 percent of all observed source-rock units were a consequence of wind-driven upwelling. However, the inaccuracy of her technique at predicting high-latitude hydrocarbon sites (Barron, 1985), and the observed widespread deposition of black shales in the Atlantic during Mesozoic times, limits its potential usefulness (Ulmishek and Klemme, 1990) in locating yet-to-be discovered extensive MPSR sites.

Recently, a perceived correlation between certain structural forms developed during regional orogenic events and the quantity and quality of source-rock deposition at these sites has been established. Three key structural forms - intracontinental platforms, circular sags, and linear sags - have been observed to have produced 75 percent of the total original deposits of the six key stratigraphic time units (Ulmishek and Klemme, 1990). It is believed that these structural forms somehow allow for the enhanced deposition and preservation of organic matter (Fig. 1.6)



**Figure 1.5** - Relative areal extent compared against effectiveness of source rocks by paleolatitudinal zones. The effectiveness is measured in amounts of original petroleum reserves generated by source rocks. Both total area of source rocks of the six principal stratigraphic intervals and total petroleum reserves generated by these source rocks are normalized to 100 percent (Taken from Ulmishek and Klemme, 1990).

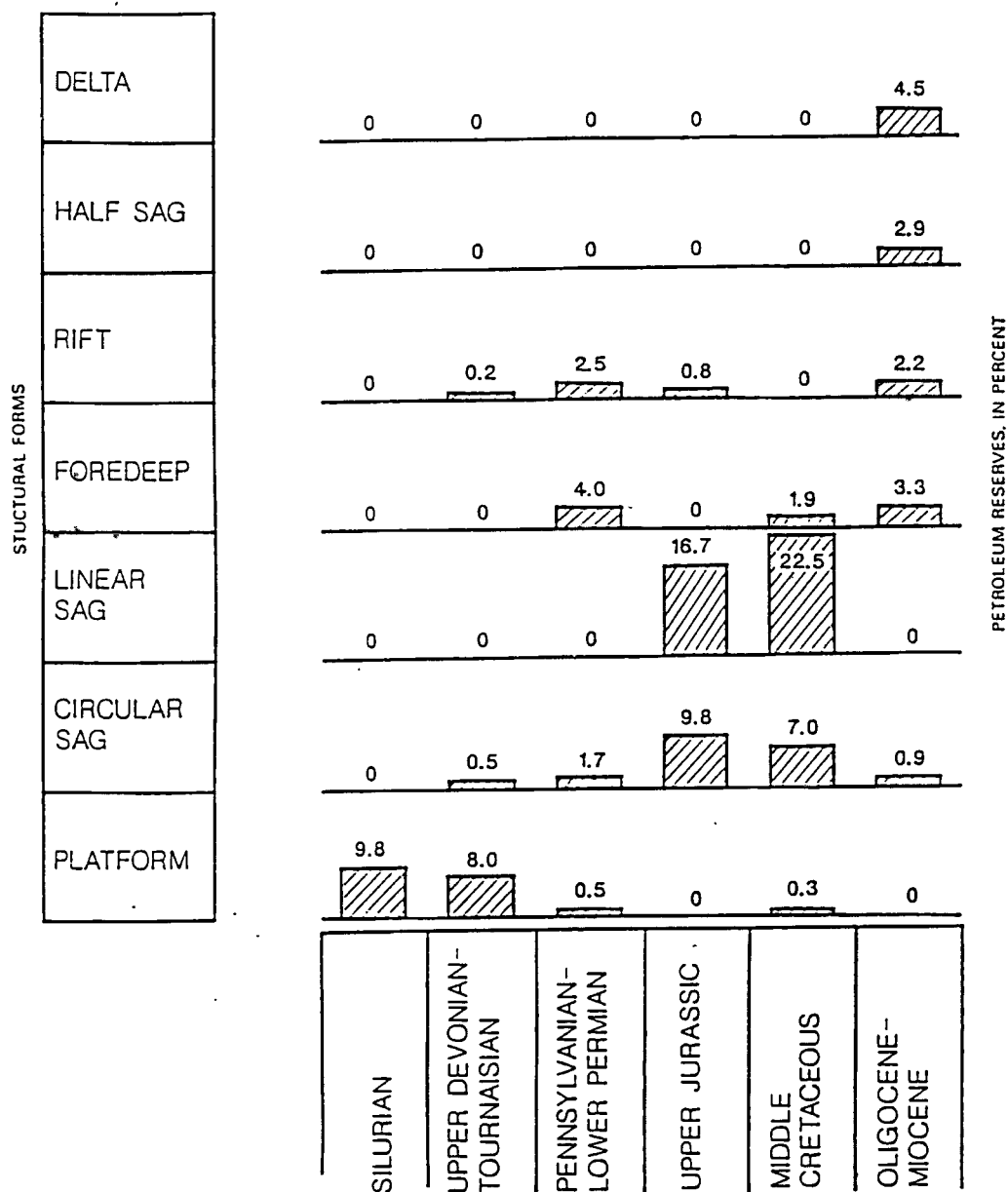


Figure 1.6 - Effectiveness of source rocks deposited in various structural forms within each of the six principal stratigraphic intervals, in percent of original petroleum generated by source rocks of the six intervals. The reserve amounts are calculated and are related to specific structural forms from data shown on the lithofacies and tructural forms maps of (Ulmishek and Klemme, 1990) (Taken from Ulmishek and Klemme, 1990).

(Ulmishek and Klemme, 1990). However, Demaison and Moore (1980) also pointed out the difficulty in using only 'morphotectonic' forms in predicting locations of enhanced source rock deposition. Allochthonous, terrigenous-derived, refractory organic matter presently accounts for as much as 50 percent of the total organic carbon flux to present-day central open-ocean environments (Stein, 1991). One could argue that the total organic carbon concentration in any basin is totally independent of the prevailing marine conditions at the actual deposition site. Instead, the total quantity of organic carbon deposited at a site could be dependent only on the mechanisms that control terrigenous organic carbon input. Demaison and Moore (1980) concluded that only when total organic carbon values are observed to be greater than 3 percent can it be quantitatively said that such structural forms actually promote the enhanced deposition of prolific marine petroleum source-rock units.

The previous discussion highlights the difficulty of identifying only one key variable for the origin of prolific marine petroleum source rock (MPSR) units. In all probability, the factors that control the accumulation of organic matter in the marine realm - the production of marine organic matter, the preservation rate of organic matter and the supply of terrestrially-derived organic matter can all be important, and are dependent upon morphotectonic development, eustatic sea level changes, paleocontinental positioning and global paleoclimatic conditions existing at the time of deposition.

This investigation analyses the ability of using the combined techniques of paleogeography and paleoclimatology, with determining probable mechanisms associated with the drowning of continental margins and factors controlling primary biologic productivity and long-term anoxic conditions within the water column, towards predicting the temporal and spatial distribution of some extensive MPSR units. Specifically, it is proposed that regional type-II rock deposition is significantly enhanced at low-paleolatitudinally positioned continental margins and shelves that become topographically depressed with respect to sea-level. Two mechanisms that cause for the drowning of continental margins are reviewed within the context of this thesis:

Continental Passive Margin Thermal Subsidence Combined with Eustasy. During times of high sea-level stand, such as the late medial Ordovician, the Silurian, upper Devonian and the late medial Cretaceous (Haq et al., 1987), the drowning of continental margins and shelves in combination with their thermal subsidence developed extensive shallow epicontinental seas. This would have permitted the encroachment of deep-water pelagic facies upon the outer parts of these drowned continental margins and shelves. The deposition of organic-rich muds would also have been augmented by the paleogeographic positioning of these drowned continental margins and shelves at paleolatitudinal positions conducive towards the development of upwelling zones. This is exemplified by the deposition of deep-water organic-rich pelagic units on the northwestern passive margin of South America during medial Cretaceous times.

Tectonically-Induced Subsidence By the Loading of Continental Margins. The lithospheric flexure of an underthrust plate undergoing consumption at a destructive plate margin (i.e. subduction zones) causes the formation of two topographic highs, specifically the flexural bulge and a volcanic arc complex, relative to sea-level. Eventually, the continued consumption of lithospheric material at subduction zones causes the drowning of the continent's active margin and shelf. This allows for the deposition of huge thicknesses of orogenic clastic sediments within developing foreland basins, formed as a consequence of this tectonically-driven process. If correctly oriented parts of these developing foreland basins were positioned within low paleolatitudes, the development of highly productive upwelling zones, and extensive MPSR deposits, would have occurred. This is exemplified by the drowning of the proto-North American eastern continental margin and shelf during medial Ordovician times.

Both of the proposed 'shelf-drowning' mechanisms would have produced extensive MPSR units because of the subsequent depression of the continental margin and shelf below the average depth of wave base within the water column (70-80 meters below sea-level (Pindell, personal communication, 1993)) (Figure 1.7). If either of these mechanisms were occurring on a continental margin that was located at the right paleoposition where an upwelling zone caused the enhanced

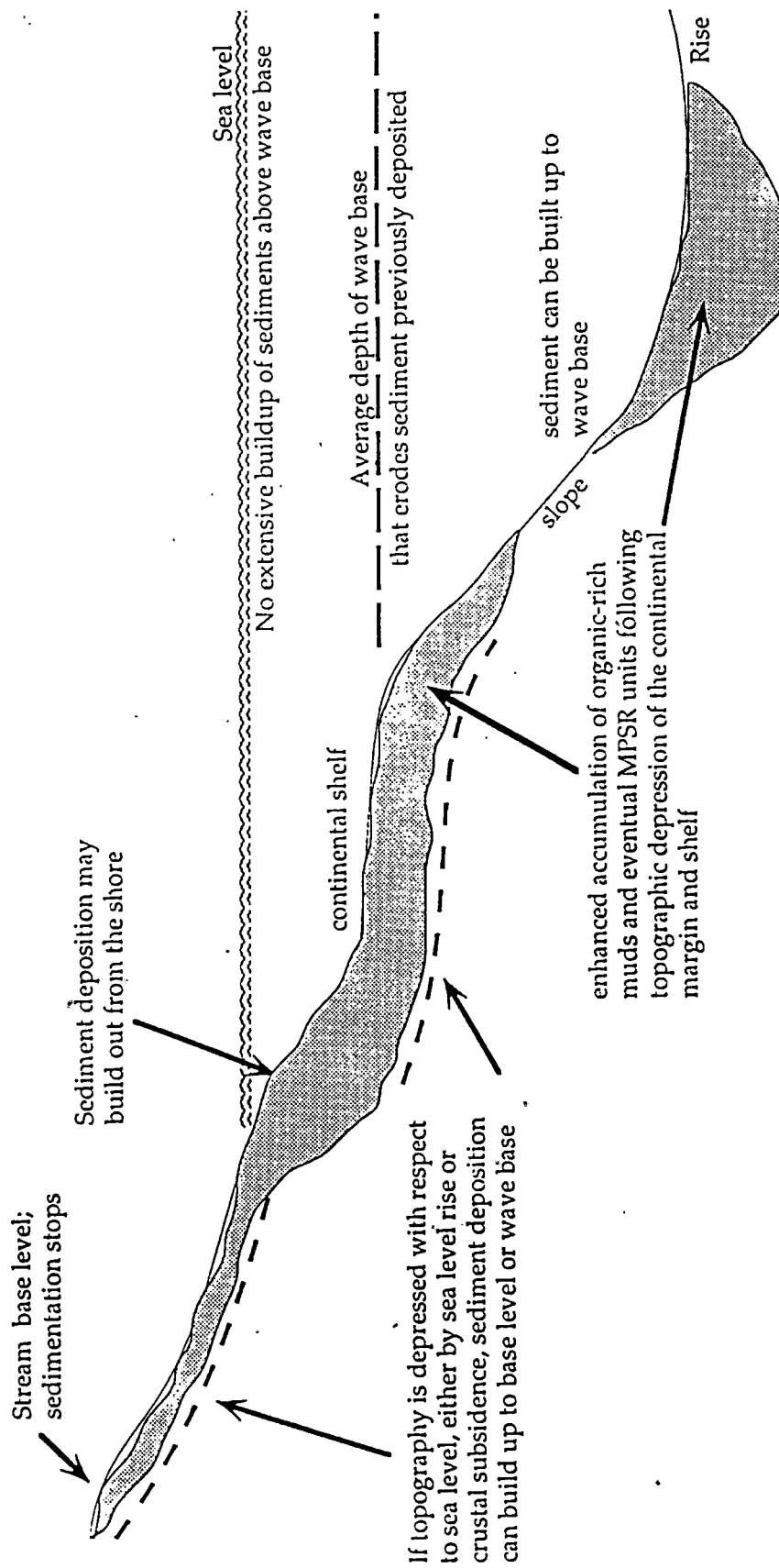


Figure 1.7 - Explanation of how surficial depression (subsidence) of continental margins and shelves, with respect to sea level, can enhance the accumulation and preservation of MPSR units (modified from Press and Seiver, 1986).

the production of algal blooms in the photic zone of the water column. Consequently, 'organic rain', formed by the decay of planktonic organisms from the photic zone of the water column, would have produced extensive deposition of organic-rich muds. The resulting effect of higher sea-levels, due to the topographic depression of the continental margin and shelf, coinciding with higher primary biologic productivity within the water column would have been the exhaustion the oxygen budget in the water column. This would have caused the establishment of long-term anoxic conditions on these drowned continental shelves and foreland basins, at a passive and active continental margins respectively. In addition, the deposition of continental shelf-sediments below the average water depth where wave action can rework, degrade, and redistribute previously-deposited sediments, would have also contributed towards its accumulation and long term preservation. Eventually, commercial-size quantities of marine source rock material could have accumulated within such areas previously described and possibly undergo burial-induced maturation.

This thesis examines two specific marine petroleum source rock (MPSR) units that represents each of the two types of 'continental margin and shelf drowning' mechanisms previously mentioned. Each one was positioned at an ideal paleolatitude which was conducive for the development of upwelling zones, which were spatially located above their associated drowned continental margins. This allowed for the enhanced deposition, accumulation, and preservation of organic-rich muds, serving as precursors to prolific MPSR units. Specifically, these are the passive continental margin deposits of the late medial Cretaceous La Luna Formations of northwestern Venezuela and the active continental margin deposits of the late medial Ordovician Utica Formation of eastern North America.



## CHAPTER 2: METHOD OF STUDY AND STUDY AREA

The potential utility of the proposed depositional model is considered in two parts. First, a detailed compilation was undertaken of stratigraphic, lithologic, and tectonic data from previously published material on two pertinent foreland basins, the late medial Ordovician Taconic Foreland Basin of eastern New York and the late medial Cretaceous Maracaibo Basin of northwestern Venezuela. This part of the study sought to find out common trends in the basins selected for study under equivalent conditions of topographic depression of continental margins and shelves with respect to sea level and low paleolatitudinal positioning, high primary biologic productivity as well as long term anoxic conditions existing within the water column. Collected information included the following for each basin:

- stratigraphic section and brief tectonic history of pertinent time interval
- identification of prime source rock horizons and their relative ages
- type of source rock material and their relative abundances
- estimation of the quantity of oil produced or remaining in proved reservoirs
- proof of correlation of the time of thrusting relative to sedimentation of source rocks.

This data, compiled by previous authors, was used to test the idea that the drowning of continental margins and shelves at low paleolatitudes can enhance the accumulation and preservation of high quality, type-II, source rock deposition.

Second, to further test the applicability of this model, a detailed field study and geochemical analysis of the late medial Ordovician Taconic Foreland Basin was undertaken, which served as the focal point of new research undertaken within the context of this thesis. This part of the study sought to prove whether or not the organic-rich calcareous shales of the Utica Formation of the Taconic Foreland Basin was a result of the drowning of the low paleolatitudinally-positioned eastern margin of North America during medial Ordovician times. From this, a specific explanation of the occurrence of a prolific, although now spent, MPSR unit

developing off the eastern margin of North America was constructed in terms of the key variables identified as controlling the temporal and spatial distribution of some extensive MPSR units.

The area of study from distal shelf to the basin floor is about 120 kilometers (Hay and Cisne, 1988) extending throughout the Mohawk Valley from Albany to Utica (Fig. 2.1). Shales, from fourteen localities, all of late medial Ordovician age, were sampled for detailed geochemical analysis (Tables I, II, III). All samples range in age between the graptolite zones of *Diplograptus multident* and *Climacograptus pymageus* (Fig. 2.2) (Fisher, 1977). Under ideal conditions, the samples would have been taken along one or more single time horizons down a dip section across the foreland basin. However, the failed subduction of the Appalachian passive margin caused the formation of a complex normal block-faulted zone flanking the Taconic thrust front (Fig. 2.3). This has resulted in inadequate stratigraphic control to define such a horizon, particularly given the generally poor exposure of the Utica Formation throughout the selected field area. Therefore in the absence of adequately precise stratigraphic control, samples were taken in three vertical stratigraphic transects positioned along an overall dip section (the direction that active plate margin convergence was occurring) as a substitute (Table IV, V, VI, Fig. 2.4). The diachronous nature of the Utica Formation, becoming younger to the west within the Taconic Foreland Basin, is not seen as a problem within the context of this thesis. The ability to test the usefulness of the proposed 'shelf-drowning' mechanisms for predicting the temporal and spatial distribution of some prolific MPSR units will not be obscured. Instead, performing detailed geochemical analyses on a migrating, organic-rich, facies unit, such as the Utica Formation, allows the possibility of predicting optimum times for the deposition of organic-rich sediments within a 'drowning' continental margin for the production high quality, type-II, source rock material. For methods concerning the determination of the inferred stratigraphic position of the samples see Appendix I.

Coupled with the new inorganic geochemical analyses, and interpretations of the acquired data, of the calcareous shales of the Utica Formation, organic geochemical analyses were performed by Texaco Inc. on some samples taken from the basin under review. This included

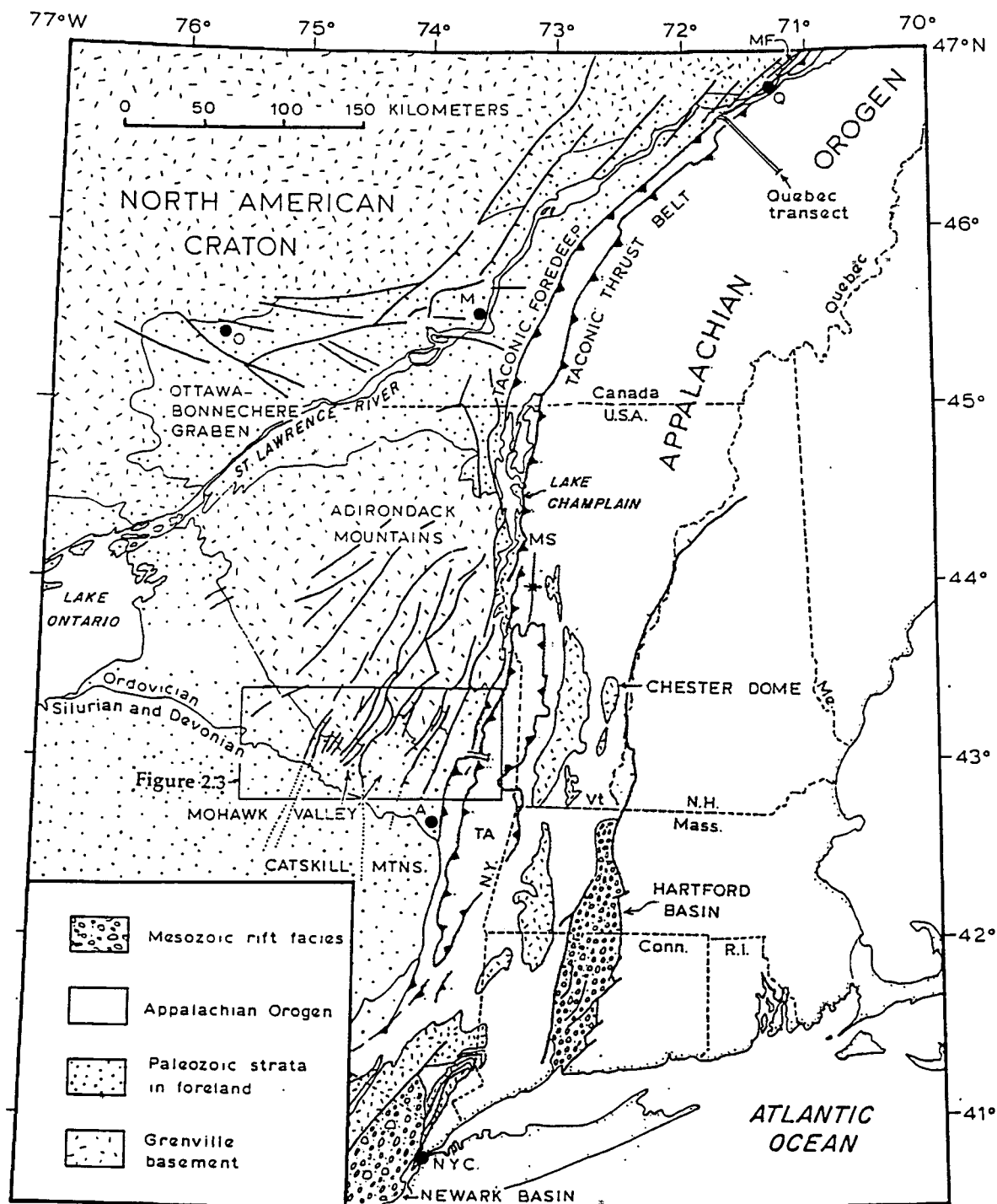


Figure 2.1 - Map showing the Taconic Foreland fold-thrust belt and adjacent foreland in New York, Vermont and Quebec, and the partial location of the Quebec transect from Bradley and Kidd (1991). Ordovician flexure-induced normal faults (heavy lines, barbed on the downthrown side, dashed in subsurface of Catskill region) strike subparallel with contractional structures in the orogen. Abbreviations: A, Albany; M, Montreal; MF, Montmorency Fault, MS, Middlebury Synclinorium; MV, Mohawk Valley; NYC, New York City; O, Ottawa; Q, Quebec City; TA, Taconic Allochthon. Rectangle shows area of Figure 2.3 (Modified from Bradley and Kidd, 1991).

**Table 1: Sample Locality List, Taconic Foreland Basin**

Locality Identification Code	Strat Position, ft	Strat Position, m	Longitude (deg.min.ss) N	Latitude (deg.min.ss) E	County
<i>Central Bridge (30A FF)</i>					
30A FF 01	2077.32	633.33	74.15.58	42.42.41	Schoharie, New York
<i>Wolf Hollow (WH FF)</i>					
WH FF 01	1083.97	330.48	74.04.26	42.55.35	Schenectady, New York
<i>Bean Hill Creek (BHC US)</i>					
BHC US 07 (*)	931.90	284.12	74.13.18	42.51.41	Montgomery, New York
BHC US 06	902.50	275.15	74.13.17	42.51.42	Montgomery, New York
BHC US 05	865.30	263.81	74.16.16	42.51.42	Montgomery, New York
BHC US 04 (*)	826.10	251.86	74.13.14	42.51.43	Montgomery, New York
BHC US 03	793.80	242.01	74.13.10	42.51.44	Montgomery, New York
BHC US 02	767.60	234.02	74.13.08	42.51.45	Montgomery, New York
BHC US 01 (*)	728.90	222.23	74.13.05	42.51.46	Montgomery, New York
<i>Youngs Lake (YKS US)</i>					
YKS US 01 (*, +)	630.00	192.07	74.15.24	42.51.52	Montgomery, New York
<i>Schoharie Creek (SC US)</i>					
SC US 02	586.60	178.84	74.17.17	42.53.20	Montgomery, New York
SC US 01	486.60	148.35	74.17.20	42.53.29	Montgomery, New York
<i>Tennille Creek (TC US)</i>					
TC US 02	449.20	136.95	74.10.06	42.52.50	Montgomery, New York
TC US 01 (*, +)	401.60	122.44	74.10.04	42.52.58	Montgomery, New York
<i>Chuctanunda Creek (AS US)</i>					
AS US 14 (+)	237.00	72.26	74.12.53	42.55.49	Montgomery, New York
AS US 13	204.00	62.20	74.12.53	42.55.49	Montgomery, New York
AS US 12 (+)	172.40	52.56	74.12.54	42.55.53	Montgomery, New York
AS US 11 (+)	134.40	40.98	74.12.54	42.55.53	Montgomery, New York
AS US 10 (+)	127.30	38.81	74.12.54	42.55.53	Montgomery, New York
AS US 09 (*)	97.30	29.66	74.12.55	42.55.58	Montgomery, New York
AS US 08 (+)	90.40	27.56	74.12.57	42.55.57	Montgomery, New York
AS US 07	80.90	24.66	74.12.57	42.55.57	Montgomery, New York
AS US 06	72.70	22.16	74.12.57	42.55.57	Montgomery, New York
AS US 05	64.50	19.66	74.12.57	42.55.57	Montgomery, New York
AS US 04 (*, +)	54.70	16.68	74.12.51	42.56.04	Montgomery, New York
AS US 03 (+)	46.30	14.12	74.12.51	42.56.04	Montgomery, New York
AS US 02	42.50	12.96	74.12.51	42.56.04	Montgomery, New York
AS US 01	39.60	12.07	74.12.51	42.56.04	Montgomery, New York

(\*) Programmed Pyrolysis

(+) XRF Geochemical Analysis

**Table II: Sample Locality List, Taconic Foreland Basin**

Locality Identification Code	Strat Position, ft	Strat Position, m	Longitude (deg.min.ss) N	Latitude (deg.min.ss) E	County
<i>Otsuquago Creek (OTC FF)</i>					
OTC FF 01 (*, +)	1139.60	347.44	74.47.51	42.54.39	Herkimer, New York
<i>Yatesville Creek (YC US, YC FF)</i>					
YC FF 02 (+)	1069.71	326.13	74.27.00	42.51.57	Montgomery, New York
YC FF 01 (+)	1044.01	318.30	74.27.00	42.51.57	Montgomery, New York
YC US 02 (*)	997.56	304.13	74.27.00	42.51.59	Montgomery, New York
YC US 01	939.80	286.52	74.27.00	42.51.59	Montgomery, New York
<i>Nowadaga Creek (NC US, NC DF)</i>					
NC US 08 (*, +)	560	170.73	74.50.00	42.58.41	Herkimer, New York
NC US 07	535	163.11	74.49.36	42.58.33	Herkimer, New York
NC US 06 (+)	470	143.29	74.49.11	42.58.40	Herkimer, New York
NC US 05 (*, +)	390	118.90	74.48.11	42.58.56	Herkimer, New York
NC US 04 (+)	330	100.61	74.48.04	42.59.15	Herkimer, New York
NC US 03	195	59.45	74.47.32	42.59.49	Herkimer, New York
NC US 02	100	30.49	74.47.07	43.00.06	Herkimer, New York
NC DF 01 (*)	0	0.00	74.46.40	43.00.25	Herkimer, New York
<i>Cunajoharie Creek (CC US, CC TL)</i>					
CC US 21 (*)	262.4	80.00	74.34.22	42.52.42	Montgomery, New York
CC US 20	248.9	75.88	74.34.22	42.52.42	Montgomery, New York
CC US 19 (*, +)	229.9	70.09	74.34.04	42.52.45	Montgomery, New York
CC US 18	201.2	61.34	74.33.57	42.52.46	Montgomery, New York
CC US 17	164.2	50.06	74.33.57	42.52.46	Montgomery, New York
CC US 16 (*, +)	142.3	43.38	74.33.55	42.52.48	Montgomery, New York
CC US 15 (*)	97.5	29.73	74.34.06	42.52.59	Montgomery, New York
CC US 14	82.8	25.24	74.34.06	42.53.00	Montgomery, New York
CC US 13 (+)	81.9	24.97	74.34.06	42.53.00	Montgomery, New York
CC US 12	63.8	19.45	74.34.06	42.53.06	Montgomery, New York
CC US 11 (*)	54.5	16.62	74.34.06	42.53.06	Montgomery, New York
CC US 10 (+)	31.5	9.60	74.34.06	42.53.54	Montgomery, New York
CC US 09 (*, +)	27.9	8.51	74.34.06	42.53.54	Montgomery, New York
CC US 08 (+)	24.6	7.50	74.34.06	42.53.54	Montgomery, New York
CC US 07 (*)	20.6	6.28	74.34.19	42.53.57	Montgomery, New York
CC US 06 (*, +)	17.2	5.24	74.34.19	42.53.57	Montgomery, New York
CC US 05	13.3	4.05	74.34.19	42.54.03	Montgomery, New York
CC US 04 (*, +)	10.6	3.23	74.34.19	42.54.03	Montgomery, New York
CC US 03 (*, +)	7.2	2.20	74.34.33	42.54.02	Montgomery, New York
CC US 02 (*, +)	2.9	0.88	74.34.33	42.54.02	Montgomery, New York
CC TL 01	-4.92	-1.50	74.34.33	42.54.01	Montgomery, New York

(\*) Programmed Pyrolysis  
(+) XRF Geochemical Analysis

**Table III: Sample Locality List, Taconic Foreland Basin**

Locality Identification Code	Strat Position, ft	Strat Position, m	Longitude (deg.min.ss) N	Latitude (deg.min.ss) E	County
<i>Route 171, Illion (171 FF)</i>					
171 FF 02	839.0	255.78	75.06.10	43.01.30	Herkimer, New York
171 FF 01 (+)	814.0	248.16	75.06.10	41.01.30	Herkimer, New York
<i>Warter Hill Creek (HHC US, TL, DF)</i>					
HHC US 21	698.6	212.99	75.00.27	43.07.42	Herkimer, New York
HHC US 20	644.5	196.49	75.00.22	43.07.31	Herkimer, New York
HHC US 19	603.5	183.99	75.00.22	43.07.31	Herkimer, New York
HHC US 18	593.7	181.01	75.00.22	43.07.31	Herkimer, New York
HHC US 17	570.7	173.99	75.00.20	43.07.29	Herkimer, New York
HHC US 16	492	150.00	75.00.19	43.07.27	Herkimer, New York
HHC US 15	439.5	133.99	75.00.17	43.07.26	Herkimer, New York
HHC US 14	367.4	112.01	75.00.14	43.07.24	Herkimer, New York
HHC US 13	341.1	103.99	75.00.14	43.07.24	Herkimer, New York
HHC US 12	316.8	96.59	75.00.14	43.07.24	Herkimer, New York
HHC US 11	283.7	86.49	75.00.13	43.07.22	Herkimer, New York
HHC US 10 (+)	259.8	79.21	75.00.10	43.07.21	Herkimer, New York
HHC US 09	218.5	66.62	75.00.06	43.07.19	Herkimer, New York
HHC US 08 (+)	182.1	55.52	75.00.04	43.07.18	Herkimer, New York
HHC US 07	150.9	46.01	75.00.03	43.07.16	Herkimer, New York
HHC US 06	114.8	35.00	75.00.01	43.07.13	Herkimer, New York
HHC US 05	85.3	26.01	75.00.01	43.07.13	Herkimer, New York
HHC US 04	52.5	16.01	75.00.00	43.07.10	Herkimer, New York
HHC DF 03	19.7	6.01	75.00.00	43.07.10	Herkimer, New York
HHC TL 02	-21	-6.40	74.59.59	43.07.05	Herkimer, New York
HHC TL 01	-137	-41.77	74.59.57	43.07.01	Herkimer, New York
<i>Ohlisa Creek (OC FF)</i>					
OC FF 01	1239.61	377.93	74.04.26	42.57.20	Herkimer, New York

(\*) Programmed Pyrolysis  
(+) XRF Geochemical Analysis

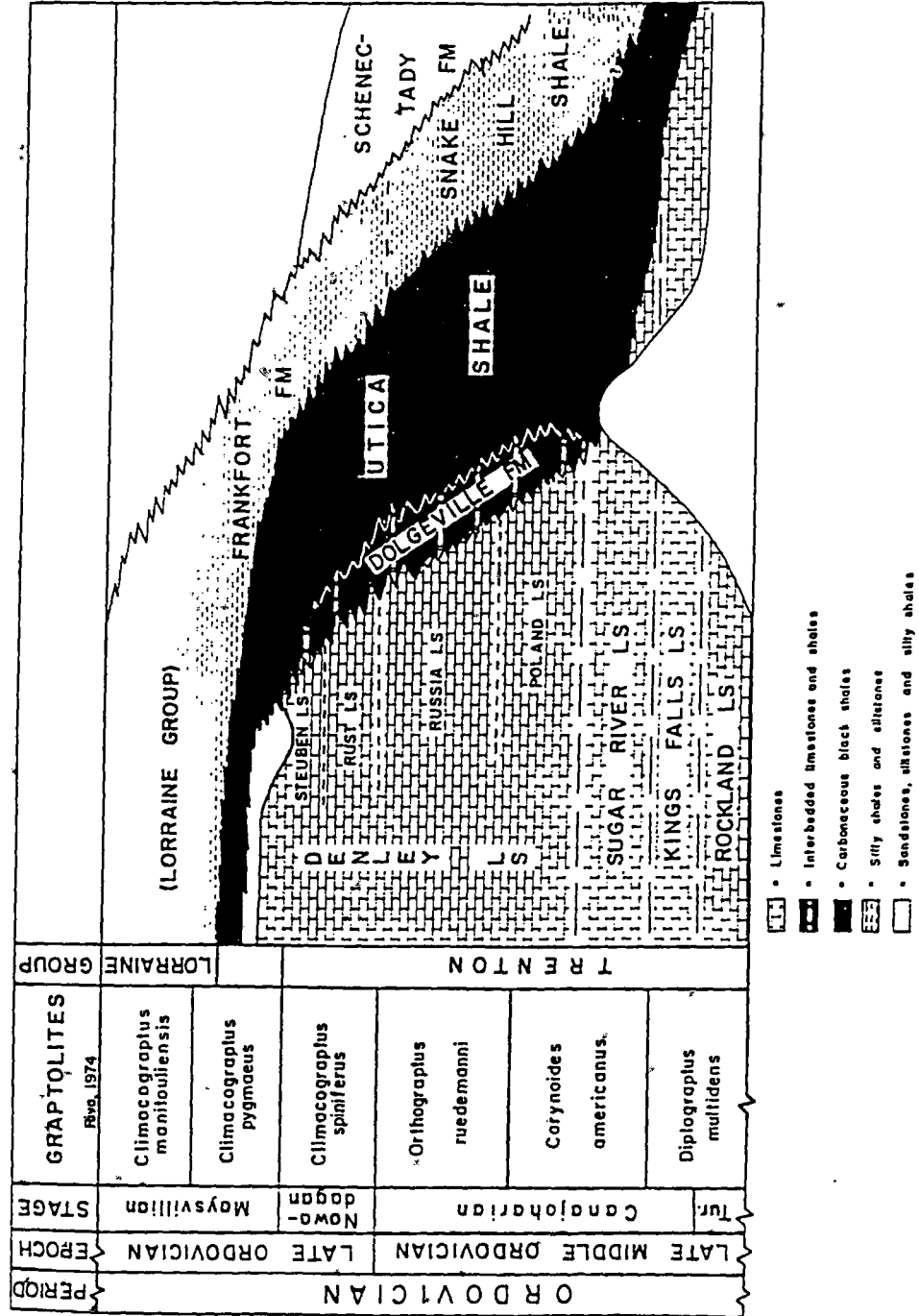


Figure 2.2 - Stratigraphic correlation chart of the Late Ordovician Taconic Foreland Basin strata of the Trenton Group (modified after Fisher, 1977) (After Hay and Cisne, 1988).

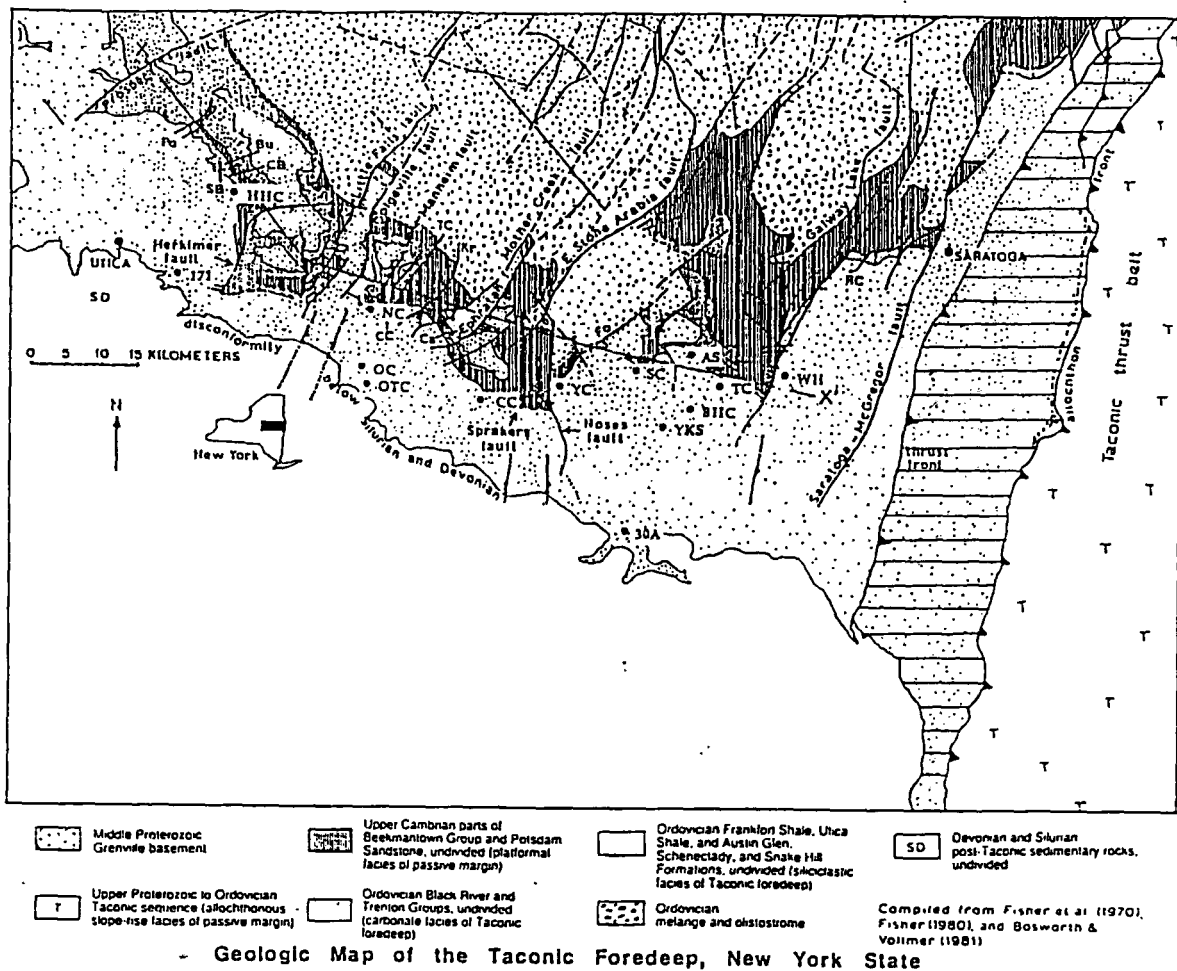


Figure 2.3 - Generalized geologic map, with locations of samples used in this study, of the Taconic foredeep, eastern New York State. Ordovician normal faults are located west of, and strike parallel with, Ordovician thrusts, which crop out in the eastern part of the map area. Simplified from Fisher and others (1970), with modifications from Fisher (1980) in the area between and including the Manheim and Hoffman faults, from Bosworth and Vollmer (1981) for the position of the frontal thrusts. The Mohawk Valley approximately follows the line of section X-X'. Abbreviations for minor faults: Po, Poland; SB, Shedd Brook; Bu, Buttermilk Creek; Ca, Caroga Creek; CB, City Brook; CC, Crum Creek; Kr, Kringsbrush; Fu, Fultonville; Fo, Fonda; RC, Rock City Falls. Hatch lines within Ordovician strata represent medium-deformed units adjacent to the Taconic thrust front (i.e. Austin Glen Formation). Abbreviations: CC, Canajoharie Creek; BHC, Bean Hill Creek; YC, Yatesville Creek; AS, Chuctunuda Creek; NC, Nowadaga Creek; SC, Schoharie Creek; OC, Ohisa Creek; OTC, Otsquago Creek; TC, Terwilliger Creek; HHC, Harter Hill Creek; WH, Wolf Hollow; 171, Illion; 30A, Central Bridge; YKS, Youngs Lake (After Bradley and Kidd, 1991).



**Table IV: Eastern Transect Samples, Taconic Foreland Basin**

Sample Control Number	Strat Position, ft	Strat Position, m	Longitude (deg.min.ss) N	Latitude (deg.min.ss) E	County
30A FF 01	2077.32	633.33	74.15.58	42.42.41	Schoharie, New York
WH FF 01	1083.97	330.48	74.04.26	42.55.35	Schenectady, New York
Utica Fm - Frankfort Fm Contact					
BHC US 07 (*)	987.80	301.16	74.13.18	42.51.41	Montgomery, New York
BHC US 06	931.90	284.12	74.13.17	42.51.42	Montgomery, New York
BHC US 05	902.50	275.15	74.16.16	42.51.42	Montgomery, New York
BHC US 04 (*)	865.30	263.81	74.13.14	42.51.43	Montgomery, New York
BHC US 03	826.10	251.86	74.13.10	42.51.44	Montgomery, New York
BHC US 02	793.80	242.01	74.13.08	42.51.45	Montgomery, New York
BHC US 01 (*)	767.60	234.02	74.13.05	42.51.46	Montgomery, New York
YKS US 01 (*, +)	728.90	222.23	74.15.24	42.51.52	Montgomery, New York
SC US 02 (+)	630.00	192.07	74.17.17	42.53.20	Montgomery, New York
SC US 01 (+)	586.60	178.84	74.17.20	42.53.29	Montgomery, New York
TC US 02 (+)	486.60	148.35	74.10.06	42.52.50	Montgomery, New York
TC US 01 (*, +)	449.20	136.95	74.10.04	42.52.58	Montgomery, New York
AS US 14 (+)	401.60	122.44	74.12.53	42.55.49	Montgomery, New York
AS US 13	237.00	72.26	74.12.53	42.55.49	Montgomery, New York
AS US 12 (+)	204.00	62.20	74.12.54	42.55.53	Montgomery, New York
AS US 11 (+)	172.40	52.56	74.12.54	42.55.53	Montgomery, New York
AS US 10 (+)	134.40	40.98	74.12.55	42.55.58	Montgomery, New York
AS US 09 (*)	127.30	38.81	74.12.57	42.55.57	Montgomery, New York
AS US 08 (+)	97.30	29.66	74.12.57	42.55.57	Montgomery, New York
AS US 07	90.40	27.56	74.12.57	42.55.57	Montgomery, New York
AS US 06	80.90	24.66	74.12.57	42.55.57	Montgomery, New York
AS US 05	72.70	22.16	74.12.57	42.55.57	Montgomery, New York
AS US 04 (*, +)	64.50	19.66	74.12.51	42.56.04	Montgomery, New York
AS US 03 (*)	54.70	16.68	74.12.51	42.56.04	Montgomery, New York
AS US 02	46.30	14.12	74.12.51	42.56.04	Montgomery, New York
AS US 01	42.50	12.96	74.12.51	42.56.04	Montgomery, New York
	39.60	12.07	74.12.51	42.56.04	Montgomery, New York

(\*) Programmed Pyrolysis  
(+) XRF Geochemical Analysis

Table V: Middle Transect Samples, Taconic Foreland Basin

Sample Control Number	Strat Position, ft	Strat Position, m	Longitude (deg.min.ss) N	Latitude (deg.min.ss) E	County
OC FF 01	1239.61	377.93	74.04.26	42.57.20	Herkimer, New York
OTC FF 01 (*,+)	1139.60	347.44	74.47.51	42.54.39	Herkimer, New York
YC FF 02 (+)	1069.71	326.13	74.27.00	42.51.57	Montgomery, New York
YC FF 01 (+)	1044.01	318.30	74.27.00	42.51.57	Montgomery, New York
Utica Fm - Frankfort Fm Contact					
YC US 02 (*)	999.61	304.76			
YC US 01	997.56	304.13	74.27.00	42.51.59	Montgomery, New York
NC US 08 (*,+)	939.80	286.52	74.27.00	42.51.59	Montgomery, New York
NC US 07	560	170.73	74.50.00	42.58.41	Herkimer, New York
NC US 06 (+)	535	163.11	74.49.36	42.58.33	Herkimer, New York
NC US 05 (*,+)	470	143.29	74.49.11	42.58.40	Herkimer, New York
NC US 04 (+)	390	118.90	74.48.11	42.58.56	Herkimer, New York
NC US 03	330	100.61	74.48.04	42.59.15	Herkimer, New York
NC US 02	195	59.45	74.47.32	42.59.49	Herkimer, New York
NC DF 01 (*)	100	30.49	74.47.07	43.00.06	Herkimer, New York
CC US 21 (*)	0	0.00	74.46.40	43.00.25	Herkimer, New York
CC US 20	262.4	80.00	74.34.22	42.52.42	Montgomery, New York
CC US 19 (*,+)	248.9	75.88	74.34.22	42.52.42	Montgomery, New York
CC US 18	229.9	70.09	74.34.04	42.52.45	Montgomery, New York
CC US 17	201.2	61.34	74.33.57	42.52.46	Montgomery, New York
CC US 16 (*,+)	164.2	50.06	74.33.57	42.52.46	Montgomery, New York
CC US 15 (*)	142.3	43.38	74.33.55	42.52.48	Montgomery, New York
CC US 14	97.5	29.73	74.34.06	42.52.59	Montgomery, New York
CC US 13 (+)	82.8	25.24	74.34.06	42.53.00	Montgomery, New York
CC US 12	81.9	24.97	74.34.06	42.53.00	Montgomery, New York
CC US 11 (*)	63.8	19.45	74.34.06	42.53.06	Montgomery, New York
CC US 10 (+)	54.5	16.62	74.34.06	42.53.06	Montgomery, New York
CC US 09 (*,+)	31.5	9.60	74.34.06	42.53.54	Montgomery, New York
CC US 08 (+)	27.9	8.51	74.34.06	42.53.54	Montgomery, New York
CC US 07 (*)	24.6	7.50	74.34.06	42.53.54	Montgomery, New York
CC US 06 (*,+)	20.6	6.28	74.34.19	42.53.57	Montgomery, New York
CC US 05	17.2	5.24	74.34.19	42.53.57	Montgomery, New York
CC US 04 (*,+)	13.3	4.05	74.34.19	42.54.03	Montgomery, New York
CC US 03 (*,+)	10.6	3.23	74.34.19	42.54.03	Montgomery, New York
CC US 02 (*,+)	7.2	2.20	74.34.33	42.54.02	Montgomery, New York
CC TL 01	2.9	0.88	74.34.33	42.54.02	Montgomery, New York
	-4.92	-1.50	74.34.33	42.54.01	Montgomery, New York

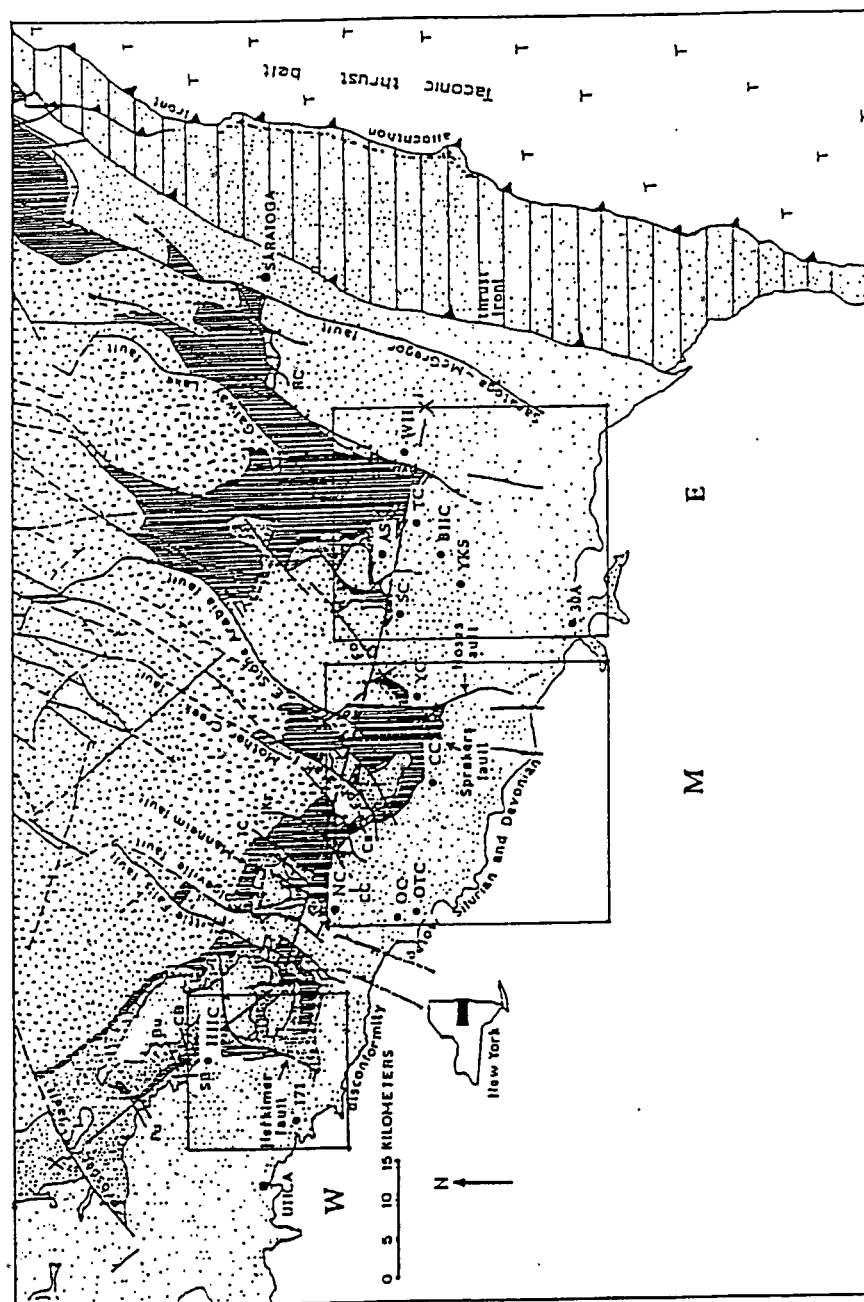
(\*) Programmed Pyrolysis  
(+) XRF Geochemical Analysis

**Table VI: Western Transect Samples, Taconic Foreland Basin**

Sample Control Number	Strat Position, ft	Strat Position, m	Longitude (deg.min.ss) N	Latitude (deg.min.ss) E	County
171 FF 02	838.9584	255.78	75.06.10	43.01.30	Herkimer, New York
171 FF 01 (+)	813.9648	248.16	75.06.10	41.01.30	Herkimer, New York
Ulrica Fm -Frankfort Fm Contact	738.98	225.3			
IIIC US 21	698.6	212.99	75.00.27	43.07.42	Herkimer, New York
IIIC US 20	644.5	196.49	75.00.22	43.07.31	Herkimer, New York
IIIC US 19	603.5	183.99	75.00.22	43.07.31	Herkimer, New York
IIIC US 18	593.7	181.01	75.00.22	43.07.31	Herkimer, New York
IIIC US 17	570.7	173.99	75.00.20	43.07.29	Herkimer, New York
IIIC US 16	492	150.00	75.00.19	43.07.27	Herkimer, New York
IIIC US 15	439.5	133.99	75.00.17	43.07.26	Herkimer, New York
IIIC US 14	367.4	112.01	75.00.14	43.07.24	Herkimer, New York
IIIC US 13	341.1	103.99	75.00.14	43.07.24	Herkimer, New York
IIIC US 12	316.8	96.59	75.00.14	43.07.24	Herkimer, New York
IIIC US 11	283.7	86.49	75.00.13	43.07.22	Herkimer, New York
IIIC US 10 (*)	259.8	79.21	75.00.10	43.07.21	Herkimer, New York
IIIC US 09	218.5	66.62	75.00.06	43.07.19	Herkimer, New York
IIIC US 08 (*)	182.1	55.52	75.00.04	43.07.18	Herkimer, New York
IIIC US 07	150.9	46.01	75.00.03	43.07.16	Herkimer, New York
IIIC US 06	114.8	35.00	75.00.01	43.07.13	Herkimer, New York
IIIC US 05	85.3	26.01	75.00.01	43.07.13	Herkimer, New York
IIIC US 04	52.5	16.01	75.00.00	43.07.10	Herkimer, New York
IIIC DF 03	19.7	6.01	75.00.00	43.07.10	Herkimer, New York
IIIC DF 02	-21	-6.40	74.59.59	43.07.05	Herkimer, New York
IIIC DF 01	-137	-41.77	74.59.57	43.07.01	Herkimer, New York

(\*) Programmed Pyrolysis

(+) XRF Geochemical Analysis



**Figure 2.4 -** Locations of transects of this study. Legend is the same as Figure 2.3. Abbreviations: E, Eastern Transect; M, Middle Transect; W, Western Transect (Modified from Bradley and Kidd, 1991).

measurements of the quantity, quality, and thermal maturation of organic matter. This was accomplished by pyrolysis and vitrinite reflectance analyses of a subset of the original sample suite (Table VII), selected to give as clear a view of the overall geochemistry of the Utica Formation and Frankfort Formation as possible for a moderate number of samples. Additional technical support from Texaco Inc. enabled inference of the possible quantity and quality of hydrocarbon content during optimum times of petroleum generation (Bissada, personal communication, 1993). For reasoning behind the selection of the subset of samples chosen, and for methods of preparation and analyses, see Appendix II.

X-Ray fluorescence analyses of a second subset of samples of the original sample suite were made, for determination of the whole rock major and trace-element geochemistry (Table VIII). This enabled the qualitative determination of anoxic and primary productivity conditions existing in the basin during the deposition of the calcareous shales of the Utica Formation. For methods of preparation and analyses see Appendix III. In addition, a comprehensive review of how paleogeographic and paleoclimatic reconstructions, from previously published material, were utilized for predicting the temporal and spatial distribution of some prolific MPSR units and its application to Maracaibo Basin and the Taconic Foreland Basin. From this, regional, type-II, source rock deposition was assessed as a function of the topography of selected continental margins and shelves, paleogeographic positioning, prevailing global paleoclimatic conditions, biologic productivity and long term anoxic conditions established within the overlying water column. A similar assessment of the Maracaibo Basin of northwestern Venezuela was taken from previously published sources. This was integrated with the Utica Formation study for the construction of a new general model that could explain enhanced regional source rock deposition on low paleolatitudinally positioned continental margins and shelves in terms of biologic productivity, oxygen concentrations within the water column as a function of depth, prevailing paleoclimatic conditions, and paleogeographic reconstructions through time.

**Table VII: Programmed Pyrolysis Sample List, Taconic Foreland Basin**

Sample Control Number	Strat Position, ft	Strat Position, m	Longitude (deg.min.ss) N	Latitude (deg.min.ss) E	County
OTC FF 01	1139.60	347.44	74.47.51	42.54.39	Herkimer, New York
YC US 02	997.56	304.13	74.27.00	42.51.59	Montgomery, New York
BHC US 07	931.90	284.12	74.13.18	42.51.41	Montgomery, New York
BHC US 04	826.10	251.86	74.13.14	42.51.43	Montgomery, New York
BHC US 01	728.90	222.23	74.13.05	42.51.46	Montgomery, New York
YKS US 01	630.00	192.07	74.15.24	42.51.52	Montgomery, New York
NC US 08	560	170.73	74.50.00	42.58.41	Herkimer, New York
TC US 01	401.60	122.44	74.10.04	42.52.58	Montgomery, New York
NC US 05	390	118.90	74.48.11	42.58.56	Herkimer, New York
CC US 21	262.4	80.00	74.34.22	42.52.42	Montgomery, New York
HHC US 10	259.8	79.21	75.00.10	43.07.21	Herkimer, New York
CC US 19	229.9	70.09	74.34.04	42.52.45	Montgomery, New York
HHC US 08	182.1	55.52	75.00.04	43.07.18	Herkimer, New York
CC US 16	142.3	43.38	74.33.55	42.52.48	Montgomery, New York
CC US 15	97.5	29.73	74.34.06	42.52.59	Montgomery, New York
AS US 09	97.30	29.66	74.12.55	42.55.58	Montgomery, New York
AS US 04	54.70	16.68	74.12.51	42.56.04	Montgomery, New York
CC US 11	54.5	16.62	74.34.06	42.53.06	Montgomery, New York
CC US 09	27.9	8.51	74.34.06	42.53.54	Montgomery, New York
CC US 07	20.6	6.28	74.34.19	42.53.57	Montgomery, New York
CC US 06	17.2	5.24	74.34.19	42.53.57	Montgomery, New York
CC US 04	10.6	3.23	74.34.19	42.54.03	Montgomery, New York
CC US 03	7.2	2.20	74.34.33	42.54.02	Montgomery, New York
CC US 02	2.9	0.88	74.34.33	42.54.02	Montgomery, New York
NC DF 01	0	0.00	74.46.40	43.00.25	Herkimer, New York

**Table VIII: X-Ray Fluorescence Sample List, Taconic Foreland Basin**

Sample Control Number	Strat Position, ft	Strat Position, m	Longitude (deg.min.ss) N	Latitude (deg.min.ss) E	County
OTC FF 01	1139.60	347.44	74.47.51	42.54.39	Herkimer, New York
YC FF 02	1069.71	326.13	74.27.00	42.51.57	Montgomery, New York
YC FF 01	1044.01	318.30	74.27.00	42.51.57	Montgomery, New York
171 FF 02	738.984	255.78	75.06.10	43.01.30	Herkimer, New York
YKS US 01	630.00	192.07	74.15.24	42.51.52	Montgomery, New York
SC US 02	586.60	178.84	74.17.17	42.53.20	Montgomery, New York
NC US 08	560	170.73	74.50.00	42.58.41	Herkimer, New York
SC US 01	486.60	148.35	74.17.20	42.53.29	Montgomery, New York
NC US 06	470	143.29	74.49.11	42.58.40	Herkimer, New York
TC US 02	449.20	136.95	74.10.06	42.52.50	Montgomery, New York
TC US 01	401.60	122.44	74.10.04	42.52.58	Montgomery, New York
NC US 05	390	118.90	74.48.11	42.58.56	Herkimer, New York
NC US 04	330	100.61	74.48.04	42.59.15	Herkimer, New York
AS US 14	237.00	72.26	74.12.53	42.55.49	Montgomery, New York
CC US 19	229.9	70.09	74.34.04	42.52.45	Montgomery, New York
AS US 12	172.40	52.56	74.12.54	42.55.53	Montgomery, New York
CC US 16	142.3	43.38	74.33.55	42.52.48	Montgomery, New York
AS US 11	134.40	40.98	74.12.54	42.55.53	Montgomery, New York
AS US 10	127.30	38.81	74.12.54	42.55.53	Montgomery, New York
AS US 08	90.40	27.56	74.12.57	42.55.57	Montgomery, New York
CC US 13	81.9	24.97	74.34.06	42.53.00	Montgomery, New York
AS US 04	54.70	16.68	74.12.51	42.56.04	Montgomery, New York
AS US 03	46.30	14.12	74.12.51	42.56.04	Montgomery, New York
CC US 10	31.5	9.60	74.34.06	42.53.54	Montgomery, New York
CC US 09	27.9	8.51	74.34.06	42.53.54	Montgomery, New York
CC US 08	24.6	7.50	74.34.06	42.53.54	Montgomery, New York
CC US 06	17.2	5.24	74.34.19	42.53.57	Montgomery, New York
CC US 04	10.6	3.23	74.34.19	42.54.03	Montgomery, New York
CC US 03	7.2	2.20	74.34.33	42.54.02	Montgomery, New York
CC US 02	2.9	0.88	74.34.33	42.54.02	Montgomery, New York

CHAPTER 3: GEOLOGICAL EVOLUTION OF THE CARIBBEAN: IMPLICATIONS FOR THE  
DEPOSITION, MATURATION, AND MIGRATION OF HYDROCARBONS DERIVED FROM A  
PROLIFIC MARINE PETROLEUM SOURCE ROCK (MPSR) UNIT DEPOSITED WITHIN THE  
MARACAIBO BASIN, NORTHWESTERN VENEZUELA

3.1 Introduction

The evolution of the Caribbean region (Pindell and Barrett, 1990) continues to remain an active topic of research for structural as well as petroleum geologists. Some plate tectonic models (James, 1985; James, 1990) previously pursued the notion that the Caribbean region was a consequence of only simple sea floor spreading occurring between North and South America during Mesozoic and Cenozoic times. The existence of at least 90 Myr of Atlantic oceanic plate consumption beneath the Caribbean Plate, the development of numerous strike-slip basins in the area, and the inference of large scale east-west relative motion between the Americas and the Caribbean region (Pindell, 1990; St. Croix Conference), has raised serious doubts on the validity of such an explanation.

Only recently have accurate paleogeographic reconstructions of the components of the Caribbean region been constructed (Pindell and Barrett, 1990; Pindell et al., 1988). These will be of critical importance towards understanding the total generative capacity of this area and identifying future areas for exploration, and where not to explore. The model is based upon the notion that the evolution of the Caribbean could be explained by a process similar to that of 'ice rafting' (Wilson, 1966), where under certain conditions the edges of two sheets of thin ice could overlap and interfinger into narrow strips (Fig. 3.1). Expanding this idea to the Caribbean region, a plate tectonic-based model was developed that could adequately explain the current largest-scale features of the Caribbean region (Fig. 3.2) as well as the accumulation, maturation, and migration



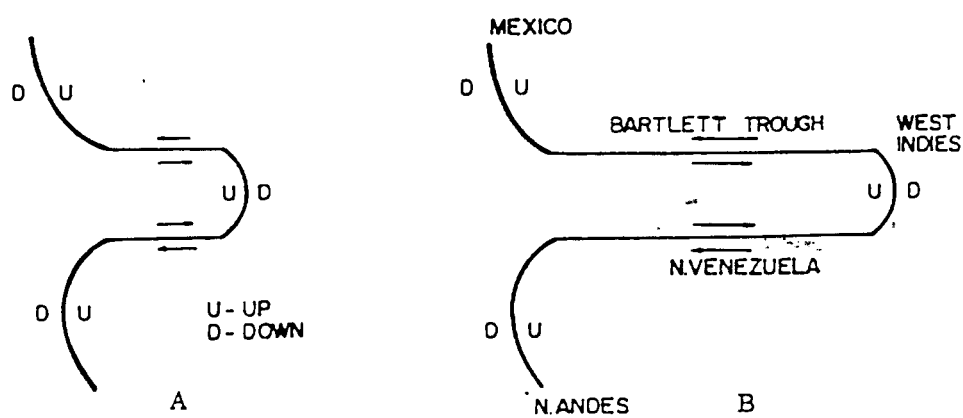


Figure 3.1 - Diagram of the West Indies structure illustrating its apparent similarity to ice-rafting (After Wilson, 1966).

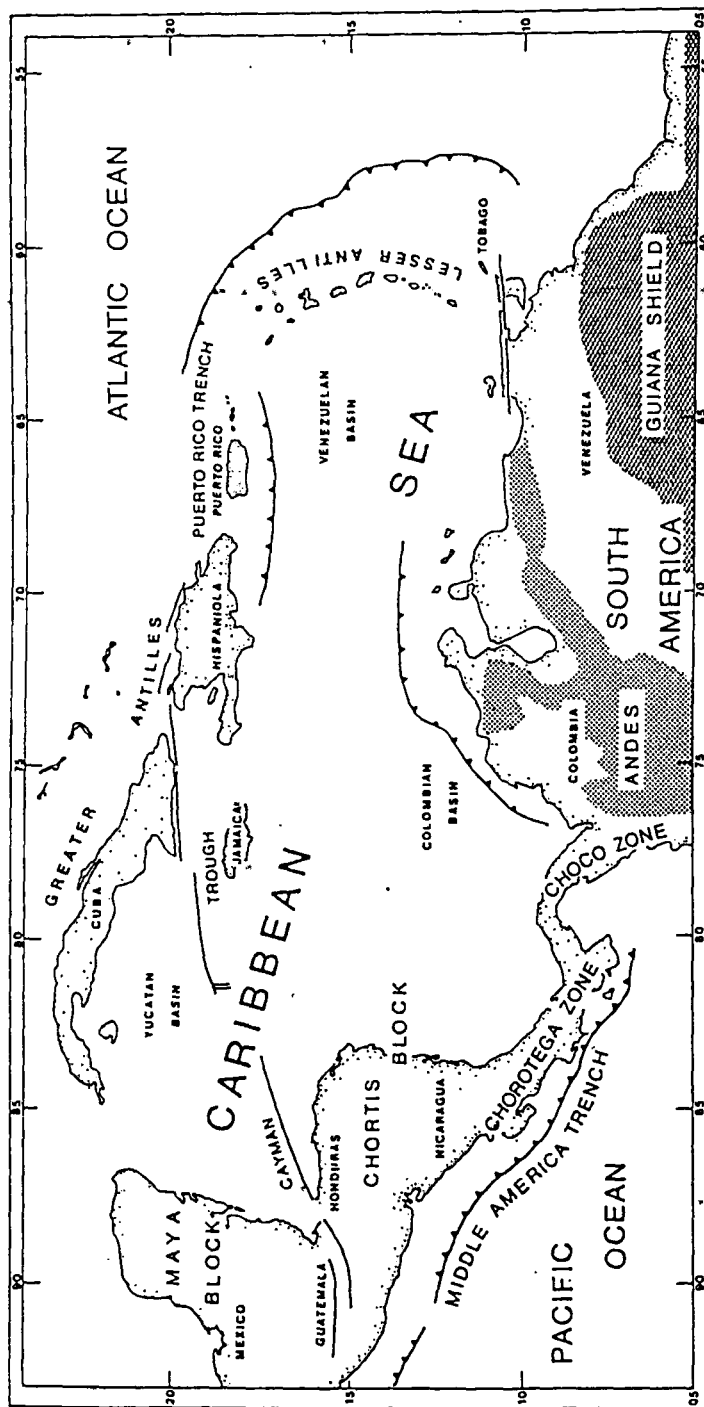


Figure 3.2 - Geographical location map of the Caribbean region, highlighting the largest-scale features of the region (From McDonald, 1990).

of petroleum and gas deposits in the area (Pindell, 1991).

The key to this model was firmly based that the Caribbean Plate is allochthonous with respect to North and South America (Pindell and Barrett, 1990). This is confirmed by various geophysical and geochemical techniques. The model breaks up the development of the Caribbean region into two phases:

- 1) rapid SW-NE extension between North and South America from late Jurassic through medial Cretaceous times, following Pangean continental disruption. This allowed for the formation of a proto-Caribbean ocean basin between the Yucatan block and the North and South American continents.
- 2) large scale E-W relative motion of the Caribbean plate from medial Cretaceous times until Recent times, causing the passive margins of the proto-Caribbean oceanic basin to become tectonically loaded. Large collisional foredeep sections (such as the Eocene of the Maracaibo Basin of northwestern Venezuela) were formed diachronously as the Caribbean Plate migrated relatively eastwards, which loaded previously deposited MPSR units with synorogenic flysch acting as potential reservoir rocks. Minor amounts of Cenozoic-age MPSR units were also deposited within this area.

The movement of the Caribbean Plate through the proto-Caribbean oceanic basin also controlled the timing and maturation of the source rocks previously deposited there; along the southern margin of the basin maturation of these units become younger eastward as the collision and foredeep sedimentation progressed eastwards during the Tertiary.

The major concern here is to present a general overview of the tectonic evolution of the Caribbean region, addressing key factors that have affected the evolution of hydrocarbon deposits within the Maracaibo Basin. Specifically these will include deducing the paleogeographic and paleoclimatic conditions existing during the late medial Cretaceous, off the northern South American coast, which enhanced biological productivity within the overlying water column, showing that eustatically-driven subsidence of the northern South American margin was conducive

for significant MPSR accumulation, and that the development of long-term anoxic conditions enabled the efficient preservation of the organic matter. Doing so will develop general explanations regarding the deposition of extensive MPSR units formed during the late medial Cretaceous off the northern coast of South America.

## 3.2 Regional Plate-Tectonic Overview

### 3.2.1 Formation of the proto-Caribbean Seaway: Creation of a Submerged Margin along northern South America During Tithonian (140 Myr) through Campanian (84 Myr) Times

Pindell et al. (1988) used magnetic and fracture zone data from the Central and South Atlantic to determine that following the initial disruption of Pangea between 180-160 Myr, the separation of North and South America continued from Tithonian (140 Myr) until just before Campanian (84 Myr) times. The calculated rate of angular motion between the Americas was  $.27^{\circ} \text{ Myr}^{-1}$  ( $30 \text{ km}^1 \text{ Ma}^{-1}$ ) (Pindell et al., 1988), eventually causing 3000 kilometers of plate separation between the Americas (Fig. 3.3) (Pindell, 1991).

This produced an extensive 'Atlantic-type' passive margin along northern South America, extending from Colombia through Brazil (Pindell and Barrett, 1990). The proto-Greater Antillean Island Arc formed simultaneously along the Pacific side of the gap between North and South America (Pindell and Barrett, 1990). This island arc complex played an important role in the evolution of the Caribbean region, forming collisional basins as it interacted with certain segments of the proto-Caribbean passive margins from Campanian (84 Myr) through Recent times.

The depositional environment in the northern Venezuelan margin of the evolving proto-Caribbean oceanic basin also progressively changed throughout the Cretaceous (Fig. 3.4). The original depositional environment was fluvial in nature during the earliest Cretaceous, evidenced by the deposition of the Rio Negro Sandstone. During Aptian-Albian times, the deposition of the Apon, Lisure, and Maracas Formations of the Collogo Group is due to the depositional environment becoming a shallow carbonate platform (Talukdar et al., 1986). These are grainstone and ooid bar deposits that contain lagoonal, organic-rich sediments which could have generated hydrocarbon deposits to a limited degree (James, 1990). However, the key MPSR unit of the area, the La Luna Formation, was deposited during Cenomanian through Santonian times.

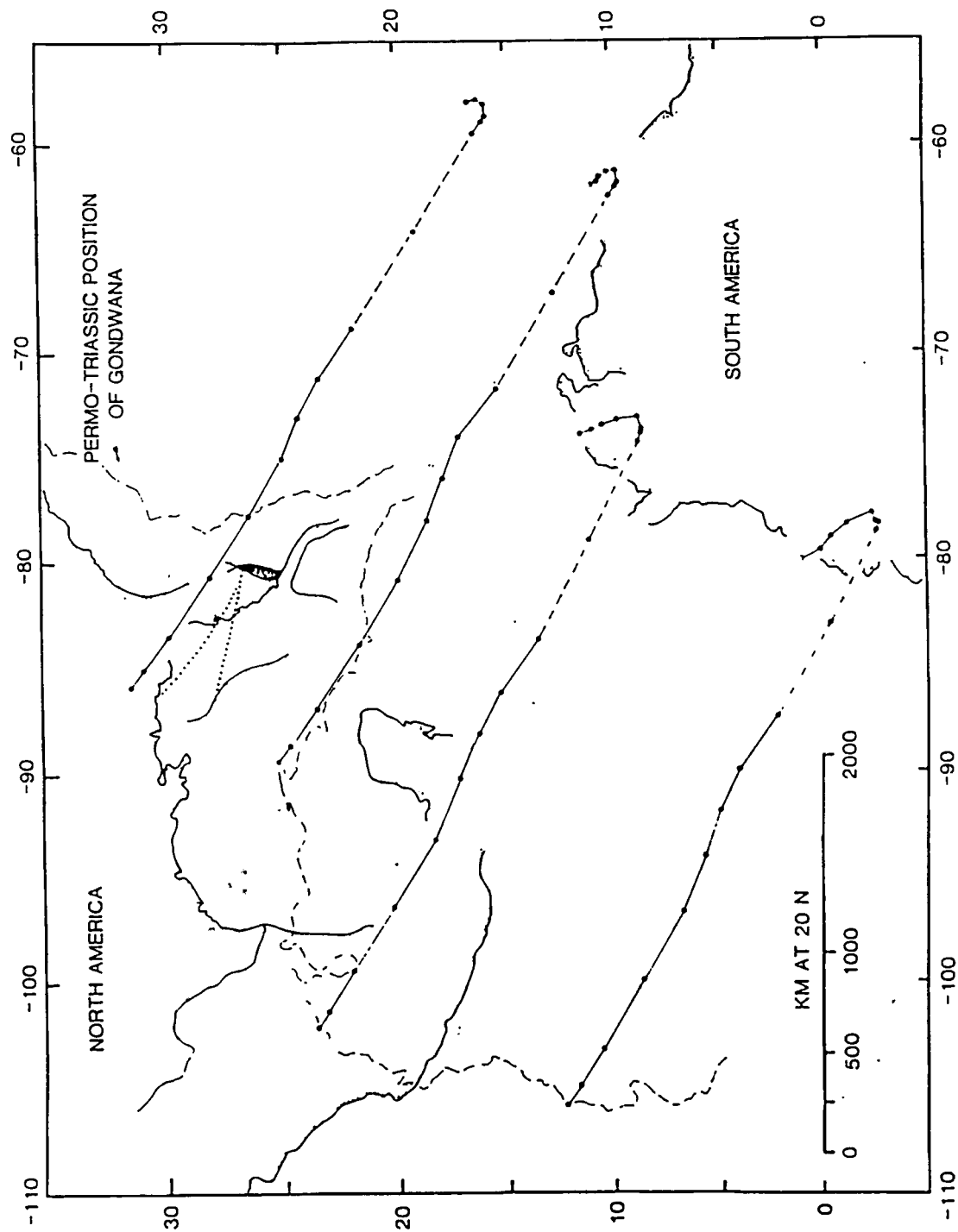


Figure 3.3 - Diagram of present-day plate separation between North and South America following Pangean disruption and NE-SW movement (After Pindell et al., 1988).


GEOLOGICAL TIME	WEST		EAST		DEPOSITIONAL ENVIRONMENT
PLEISTOCENE	ONIA		EL MILAGRO		CONTINENTAL
PLIOCENE		BETI-JOQUE	LA PUERTA	CONTINENTAL	
		ISNOTU		FLUVIAL (WEST)	
	MIOCENE	LA VILLA LOS RANCHOS	LAGUNILLAS		FLUVIO-DELTAIC (EAST)
EL FAUSTO		LA ROSA			FLUVIAL (WEST) MARINE (EAST)
		OLIGOCENE		ICOTEA	FLUVIAL
EOCENE	LA SIERRA	PAUJI		FLUVIAL (WEST) MARINE (EAST)	
	MIRADOR	MISOA		FLUVIO-DELTAIC	
			TRUJILLO		FLUVIAL (WEST) MARINE (EAST)
PALEOCENE	OROCUE	MARCELINA	GUASARE		FLUVIO-DELTAIC (WEST) MARINE (EAST)
CRETACEOUS	MITO JUAN			MARINE	MARINE OXIC
	COLON				
	CAPACHO	LA LUNA			OPEN MARINE ANOXIC (EAST)
	COGOLLO				CARBONATE PLATFORM
	RIO NEGRO				FLUVIAL
PRE-CRETACEOUS	BASEMENT				

Figure 3.4 - General stratigraphy of the Maracaibo Basin showing the position of the La Luna Formation, the Cretaceous regional seal and the reservoirs of oils related to La Luna source rocks (Talukdar et al., 1987).

This fine grained, dark gray to black, argillaceous limestone-calcareous shale is organic-rich (average TOC value 3.80%) and is finely laminated with abundant planktonic and pelagic fossils present. The total stratigraphic thickness of the unit is between 400-700 foot (121-213 meters) (Talukdar et al., 1986). The high observed content of Type-II (marine) kerogen of this unit, coupled with the absence of benthonic fossils, abundant planktonics, and finely laminated sediments point to its euxinic depositional environment. The coincidence of the highest eustatic sea levels of the Mesozoic during the late medial Cretaceous (Haq et al., 1987), its inferred paleolatitude location, and possibly above normal bottom water temperatures may have contributed to the enhanced source rock quality of this unit. Above the La Luna Formation lies the Campanian-Maastrichian Colon Formation, and its lateral equivalents. It is a 1000 foot (328 meters) bituminous, reported-'shale' that probably acted as an imperfect regional seal for the La Luna Formation. Debate still persists as to whether or not the Colon Formation represents the last phase of passive margin deposition occurring on the northern South American margin, or if it represents the onset of outer trench slope deposition within the developing foreland basin (Pindell, personal communication, 1993). The most characteristic aspect of the Colon Formation is its marked decrease in TOC values relative to the underlying La Luna Formation; TOC values for the Colon Formation average only .80%. This could be a consequence of marine oxic conditions being established during its deposition, or detrital sedimentation rates being higher than organic carbon flux rates into the basin. Until samples spanning the entire thickness of the La Luna and Colon Formations become accessible for detailed geochemical analyses, the question of what factor(s) could have resulted in the dramatic decreases in TOC value in the Colon Formation will remain unanswered. Oxygen and carbon isotope stratigraphy could infer whether or not biologic productivity was the deciding factor controlling TOC values in the Colon Formation. Conversely, strontium, and possibly sulfur, isotope stratigraphy could point to the possibility of oxygen concentrations being the primary variable controlling TOC values within the Colon Formation. Given that sea-level stand was probably much lower during Campanian-Maastrichian times than



during Cenomanian through Santonian times, the preliminary position is taken, within the context of this thesis, that TOC values within the Colon Formation was the result of clastic dilution. A greater portion of the flexural bulge would have been above sea level during Campanian-Maastrichtian times, enabling for its erosion and deposition in to the developing foreland basin.

By the end of the Santonian, sea-floor spreading between the Americas had decreased to only  $.07 \text{ Myr}^{-1}$  (Pindell et al., 1988). This change in motion must have resulted in sea floor spreading in the proto-Caribbean Seaway ceasing, or nearly so, such that the relative motion of South America to Africa was now similar to that of North America to Africa.

### 3.2.2 Late medial Cretaceous Paleoclimatic Reconstruction

Parrish and Curtis (1982) generated late Cretaceous (Cenomanian) paleoclimatic maps for predicting paleo-upwelling locations (Fig. 3.5). By using the general qualitative rule that wind-driven upwelling occurs on the west facing coasts within subtropical high pressure belts, the model predicted major coastal paleo-upwelling zones off the western coasts of North and South America. Parrish and Curtis (1982) also predicted zonal high-latitude paleo-upwelling off the Australia and the Arctic coasts.

Coastal upwelling was predicted only for the northwestern coast of South America; numerical modeling however predicted more extensive upwelling on the northern, as well as northwestern, coasts of South America (Diagram 13C; Barrón (1985)). Barron's prediction is more consistent with sedimentological evidence (Barron, 1985). Two reasons why the qualitative model was unable to correctly predict upwelling off northern South America are:

- the geologic record of Cretaceous source rocks in the northern margin of South America was not adequately sampled, so that not enough paleoclimatically-sensitive sediments were detected to imply the existence of paleo-upwelling off the northern coast of South America when using Parrish's (1982) qualitative paleoclimatic modeling techniques.
- that qualitative paleoclimatic modeling techniques implicitly assumes a necessary continental separation for surface winds to produce wind-driven divergence within the water column. Parrish and Curtis (1982) assumed in their qualitative modeling attempts that the relative 'closeness' of North America, South America and Africa during the late medial Cretaceous was not yet conducive towards the establishment surface wind-driven divergences. Therefore, they did not predict paleo-upwelling to occur, but nonetheless it may have existed, as shown by Barron's (1985) numerical paleoclimatic modeling attempts.

Paleo-upwelling may have occurred off the northern coast of South America under two possible situations. The first, under relatively high sea-level (250-300 meters above present conditions), would have allowed extensive Cretaceous epicontinental seas to develop. Consequently, a



Figure 3.5 - Continental configuration and predicted upwelling zones during late medial Cretaceous times. Stippled areas = proposed upwelling sites. Upwelling zones from Parrish (1982). Paleogeographical configurations from Scotese (1980).

symmetric equatorial oceanic divergence could have developed over the northern margin of Cretaceous South America, allowing for extensive paleoproductivity and marine petroleum source rock deposition. The other possibility is that the upwelling, and enhanced biologic productivity, is a consequence of low latitude zonal coastal upwelling. The Cretaceous-age northern coast of South America was at the right latitudinal position and correct orientation for zonal wind driven upwelling to have produced extensive organic-rich sediment deposition (see Appendix VI). It is probably reasonable to assume that both effects operated during the late Cretaceous. Under these scenarios, using techniques developed by Betzer et al. (1984) to ascertain qualitatively productivity fluxes into the ocean, primary productivity may have ranged from 100-250  $\text{gC}_{\text{Org}}\text{m}^{-2}\text{yr}^{-1}$  during Aptian times. This would have enabled between 15-30  $\text{gC}_{\text{Org}}\text{m}^{-2}\text{yr}^{-1}$  to reach the sediment-water interface that could have been buried, using the assumption that water depths ranged from 100-250 meters, deep enough for Ekman transport mechanisms to occur in the water column.

### 3.2.3 Evidence Establishing the La Luna Formation as a Passive Continental Margin MPSR Unit Deposited within late medial Cretaceous Times

Wilson's (1966) original hypothesis proposed that the Caribbean plate had been inserted into the zone between North and South America, where the proto-Caribbean oceanic basin had been formed. This is based on the following observations:

- the occurrence of east-west transform faults presently bounding the Caribbean region
- the suggestion that the Antillean Island Arc was the tip of an eastward advancing oceanic lithospheric slab advancing eastwards, relative to the Americas
- igneous and metamorphic terranes being emplaced along the northern South American coastline.

Debate has continued regarding the two possible mechanisms producing these features within the Caribbean region:

- 1) local, Cretaceous-age deformation and penecontemporaneous emplacement, due to island-arc continental collision, along the northern South American passive continental margin.
- 2) distant, Cretaceous-age deformation, and subsequent Tertiary emplacement, of igneous and metamorphic terranes onto a northern South American continental margin that was passive throughout Mesozoic times (see Erikson and Pindell, 1993 for a comprehensive analysis of this problem).

Depending on the interpretation accepted for the evolution of the Caribbean region, the explanation for the depositional environment for the key MPSR unit of the region, La Luna Formation, will be different. While new modeling (Pindell and Barrett, 1990) requires acceptance of the La Luna Formation to be a passive margin deposit, initial explanations viewed the La Luna as a collisional foreland basin deposit. Difficulty in trying to identify tectonically isolated fragments of the various shelf and continental slope sedimentary environments, and restoring them to their original relative positions (Burke, 1988), has hampered resolution of this important issue.

Recently published data (Erikson and Pindell, 1993; Erikson and Pindell, in press) of sediment accumulation rates within the Maracaibo Basin of northern South America provides conclusive evidence showing that the La Luna Formation was a passive continental margin deposit. This evidence proves that distant Mesozoic deformation and Cenozoic emplacement of igneous and metamorphic terranes occurred on the northern South American margin. The usefulness of sediment accumulation diagrams is that they are able to distinguish between different tectonic environments producing different sedimentation patterns. Sediment accumulation curves that exhibit slow sediment accumulation rates are indicative of thermal subsidence existing within the area under examination. Uplift events, caused by island-arc collision events for example, instead show dramatic increases in sediment accumulation rates within flanking basins. From this, the interpretation of Fig. 3.6 is that the northern coastline of South America was passive throughout Mesozoic times and did not become an active continental margin until well into Cenozoic times (Fig. 3.6). If the northern coastline of South America was passive throughout the Mesozoic, then the La Luna Formation is required to be passive margin deposited MPSR unit. Unless evidence pointing to the occurrence of flexural normal faulting within the La Luna Formation during its deposition, the verification of some component of clastic sedimentary detritus within the La Luna being indicative of the development of a collisional foreland basin during medial Cretaceous off the northern Venezuelan coast, or the existence of bentonites within the Cretaceous sedimentary column within the Maracaibo Basin, indicating the relative close proximity of the volcanic arc to the northern South American margin, the depositional environment of the La Luna Formation will have to be accepted as passive continental margin in nature.

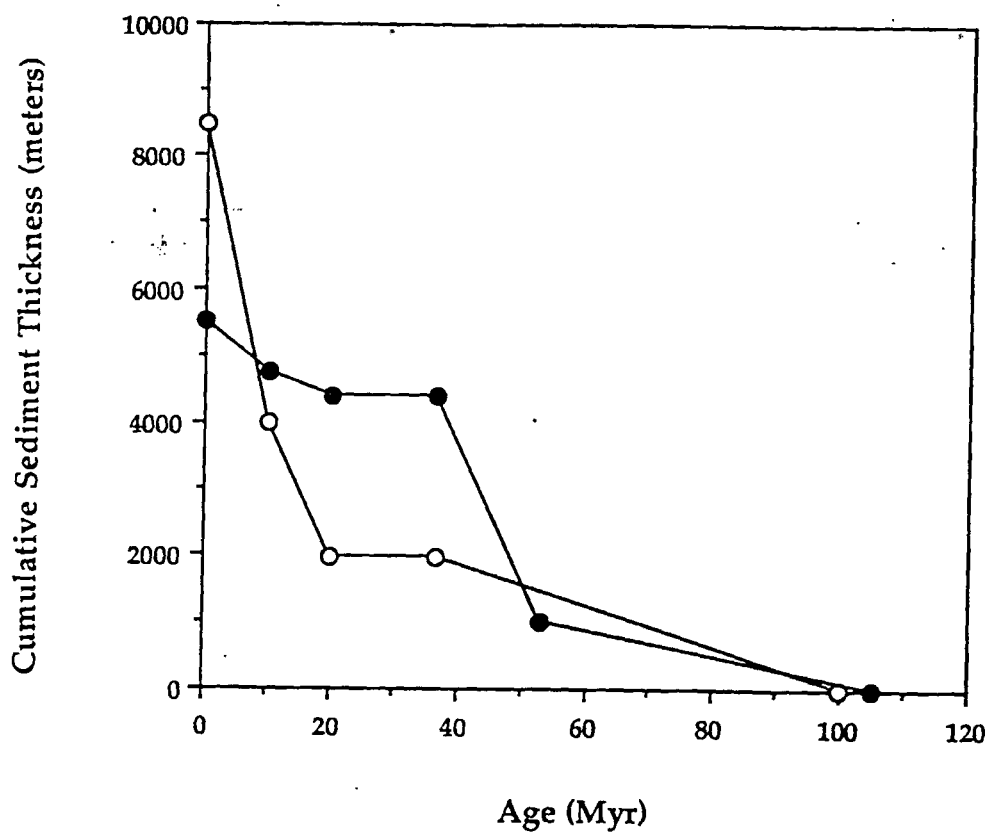


Figure 3.6 - Sediment accumulation rates within the Maracaibo Basin. Slow accumulation rates during Cretaceous are indicative of passive continental margin tectonic environment, while dramatic increases are representative of tectonic subsidence occurring within the basin. Open circles = South Maracaibo Basin; Closed circles = North Maracaibo Basin. (Modified from Erikson and Pindell, in press).

### 3.2.4 Commencement of Collisional Foredeeps and Marginal Basins During late Cretaceous through Paleocene Times

From Campanian (84 Myr) through Recent times, proto-Caribbean oceanic basin lithosphere was progressively consumed beneath the Antillean Island Arc. Consequently, large scale easterly relative motion of the Caribbean Oceanic Plateau caused some sections of the passive margins of the basin to become tectonically loaded. This caused the diachronous production of several large asymmetric collisional foredeeps (Pindell, 1991) as the Antillean Island Arc progressively collided with some sections of the proto-Caribbean passive margins (Burke, 1988).

The deposition of synorogenic flysch units in these collisional foredeeps served two important functions in the production of hydrocarbon deposits in the Maracaibo Basin. Sediment infilling of the foreland basin allowed for the thermal maturation of the earlier deposited MPSR unit, and served as potential reservoir rocks for migrating hydrocarbon deposits.

The late Cretaceous Sepur Collisional Foredeep off the Guatemalan coast was the first of these basins to form in the Caribbean region. It is interpreted as the result of the collision of the Antillean Island Arc with the Yucatan Peninsula (Fig. 3.7) (Burke, 1988). Evidence for this collisional event is recorded by the formation of the Motagua suture zone in Guatemala at the end of the Cretaceous (Burke, 1988). The progressive movement of the Antillean Island Arc complex past southern Yucatan also caused the creation of several additional basins in the area, as the Caribbean oceanic plateau moved past the Yucatan Peninsula (Burke, 1988). It is believed that the Yucatan Basin of Paleogene age, and the Grenada Basin, also of Paleogene age, are the result of this mechanism.



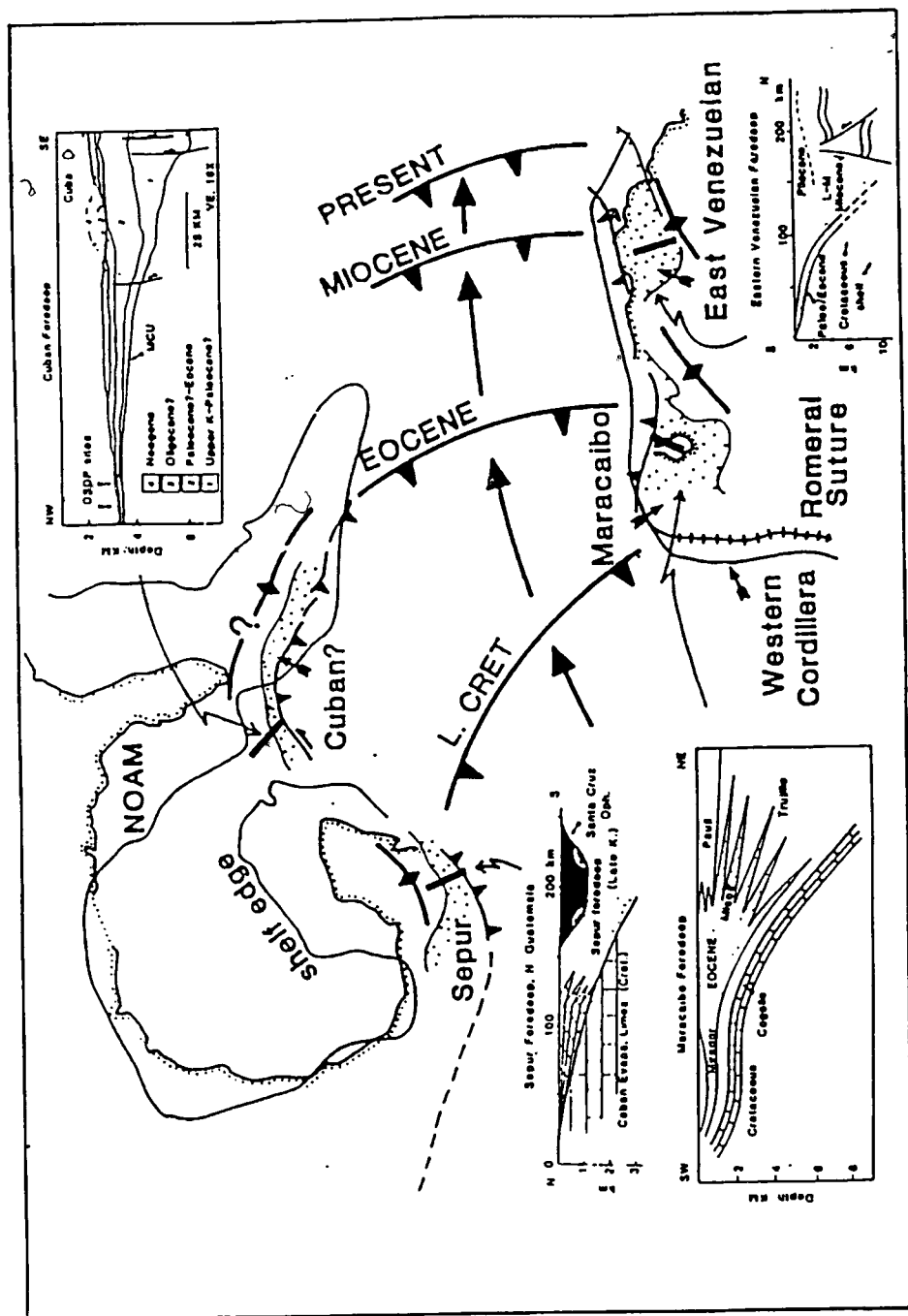


Figure 3.7 - Cross sections of episutural foredeep basins. Caribbean-American relative motion shown by heavy lines through proto-Caribbean Seaway. North and South America are plotted in Maastrichtian relative positions, and the blocks of northwestern South America are restored to their pre-Neogene positions (After Pindell, 1991).

### 3.2.5 Formation of the Cuban and Maracaibo Collisional Foredeeps during latest Paleocene through Eocene Times

During latest Paleocene-early Eocene times, the initiation of development of two additional collisional foredeeps, the Cuban and Maracaibo, occurred. The Cuban Collisional Foredeep was formed when the northern section of the Antillean Arc collided with the Bahamas and Florida Platform, forming ophiolitic nappes and back thrusting in the area. The Maracaibo foredeep of northwestern Venezuela however, was a result of the North Venezuela Nappes being emplaced onto the Venezuelan margin diachronously, in close association with the Cenozoic eastward advance of the Caribbean Plate (Pindell and Barrett, 1990). The depositional environment, critical towards the hydrocarbon evolution of the area, was also affected (Pindell and Barrett, 1990). Specifically, moderate regional uplift and local erosional shoaling occurred due to the progressive transpressional, eastward-younging, orogenesis between the Caribbean and South American plates (Bockmeulen et al., 1983; Pindell, 1991). During the Paleocene, limestones indicative of a fluvio-deltaic to marine environment were deposited with relatively low TOC values being a result of clastic dilution (Fig. 3.8), while throughout the Eocene huge thicknesses of regressive shale-deltaic sand sequences, the Misoa Formation, were deposited throughout the area (Fig. 3.8). It is the deposition of these fluvio-deltaic units that caused maturation of, and migration from, the earlier deposited MPSR unit. The maturation and migration in the northern Maracaibo Basin initially began in the Eocene and caused the southwestwards migration of the produced hydrocarbons towards Eocene-deposited sands (Bockmeulen et al., 1983; Pindell, 1991).

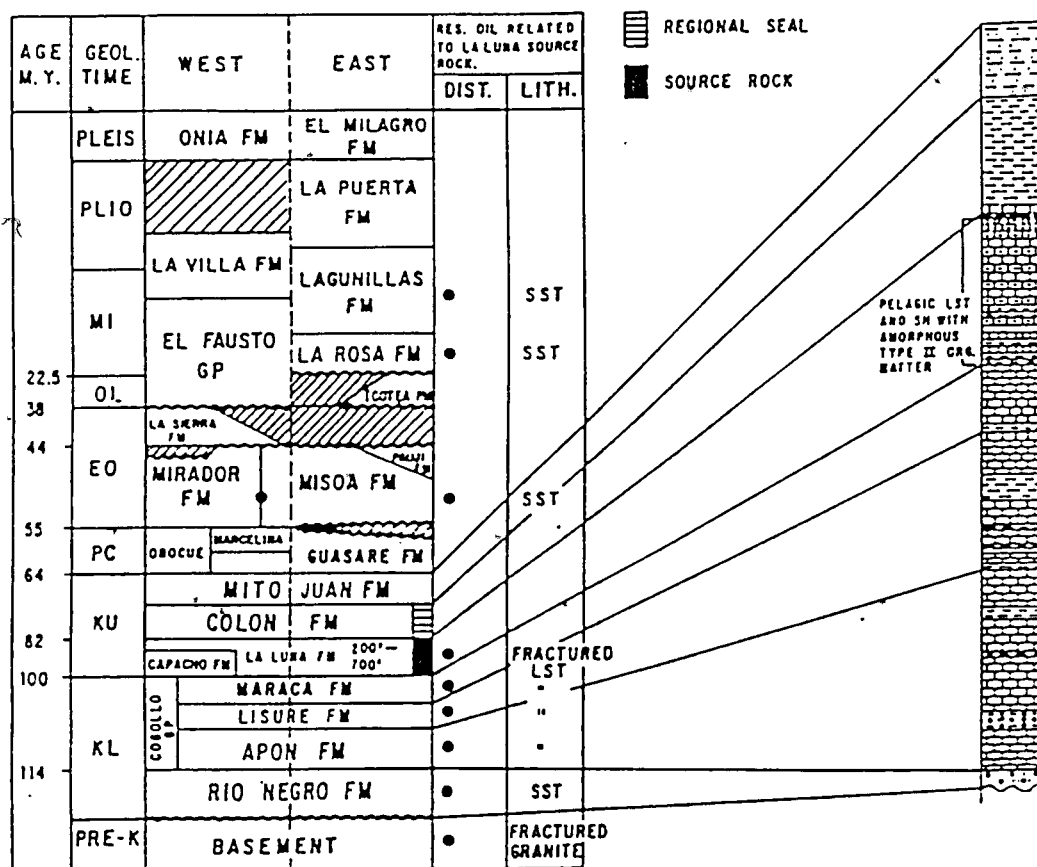


Figure 3.8 - General stratigraphy of the Maracaibo Basin (After Talukdar et al., 1987).

### 3.2.6 Tectonic Disruption of Paleocene-Eocene Petroleum Reservoirs During Oligocene Times

The tectonic disruption of Eocene-Paleocene petroleum reservoirs of the Maracaibo Basin occurred in the Oligocene. It has been postulated that this was connected to a global regressive event, the largest in the Cenozoic, occurring during this time (Bockmeulen et al., 1983). At least 2700 meters of Eocene sands were eroded, allowing for meteoric water contamination and degradation of the petroleum deposits, while concurrent faulting produced a series of north-south anticlines, serving as structural traps for the still southwestwardly migrating-petroleum deposits. However, it is highly improbable that over 2700 meters of stratigraphic section within the Maracaibo Basin could have been eroded by a global regressive event alone. Such an event would not have been localized only within northwestern sections of the northern Venezuelan coast, as postulated by Bockmeulen et al (1983). It is more likely that the Oligocene unconformity event is somehow tectonically connected to the emplacement of the North Venezuelan Nappes and the development of the Southern Caribbean Plate Boundary Zone (PBZ) (see Pindell and Barrett, 1990), resulting from the progressive Cenozoic eastward advance of the Caribbean Plate (Pindell and Barrett, 1990). As the Caribbean Plate moved eastward throughout the Cenozoic, nappe emplacement could have resulted in the 'wedging-in' of accretionary thrust sheets into the northern South American margin, with larger displacements produced in the eastern parts of the northern Venezuelan margin. The existence of such a 'triangle wedge' structure, progressively inserting itself in the Venezuelan margin, could have subsequently uplifted parts of the Venezuelan margin, especially in the northeastern sections of the basin. This mechanism could explain the development of erosion and tectonic disruption of Eocene-Paleocene reservoirs within the Maracaibo Basin proposed by Bockmeulen et al (1983) during Oligocene times, as well as the dextral sense of shearing postulated by Pindell and Barrett (1990) produced on the northern Venezuelan margin during the progressive Cenozoic eastward advance of the Caribbean Plate (Pindell and Barrett, 1990).

### 3.2.7 Collision of the Panamanian-Costa Rican Arc and its Related Consequences for Hydrocarbon Evolution During Miocene Times

With the beginning of the Miocene, the collision of the Panamanian-Costa Rican Island Arc onto South America was the next important event affecting the evolution of hydrocarbon deposits in the Maracaibo Basin (Pindell, 1991). The collision of Panama with South America subsequently produced Miocene through Recent northwards extrusion of the Maracaibo Block in northwestern Venezuela. At least 100 kilometers of strike-slip motion on the Santa Marta and Bocono Fault systems has caused the Maracaibo Block to move at least 70 kilometers northwards relative to stable South America. The ongoing collision has produced the Atrato suture zone, reminiscent of the Romeral suture zone developed earlier during the Cretaceous. This serves as the primary piece of evidence indicating an island arc-continental collision developing in the Caribbean region during this time (Pindell, 1991) (Fig. 3.9).

This has also caused the La Luna MPSR unit deposited in the southern portion of the Maracaibo Basin to thermally mature and expel hydrocarbon products. Following the Panamanian collision, uplift of the Cordillera has caused huge thicknesses of Neogene sediments (6-8 kilometers) to fill the southern part of the basin. Since Miocene times, the Caribbean Plate has continued to migrate between the Americas; however, the regional tectonic evolution of this area is being further complicated by a slight convergence between North and South America (Pindell, 1991). The formation of another collisional foredeep, the Maturin Collisional Foreland Basin has begun further eastwards on the northern Venezuelan coast.

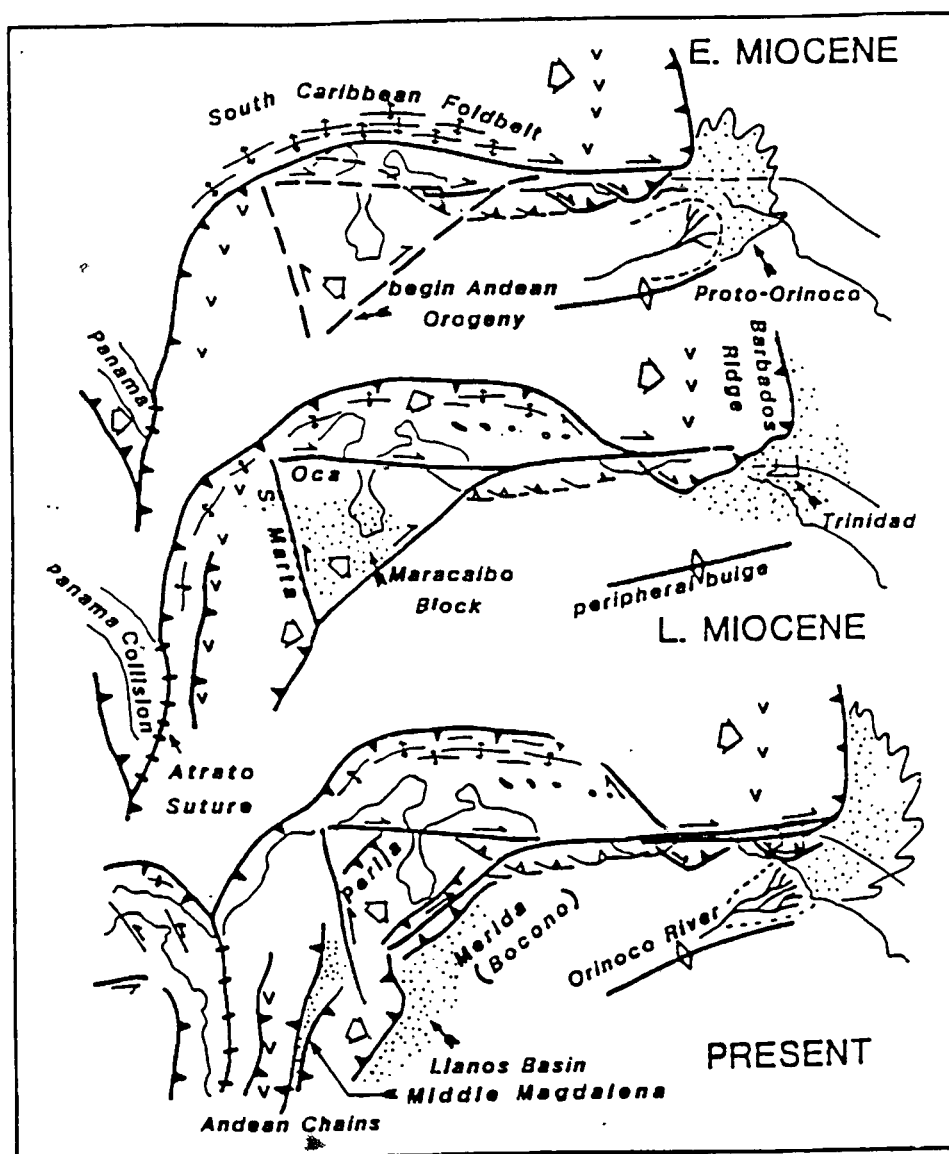


Figure 3.9 - Neogene structural development of northwestern South America, using a  $15\text{--}20\text{ mm(yr)}^{-1}$  South America-Caribbean displacement rate (Pindell, 1991)

### 3.3 Geochemistry of Maracaibo Basin, Northwestern Venezuela

#### 3.3.1 Introduction: General Regional Overview

The Maracaibo Basin of northwestern Venezuela is a large producer of petroleum, with its deposits projected at 29 billion barrels of oil (Talukdar et al., 1986). While the present structural configuration, an intermontane basin, did not exist until middle Miocene times, the Cenozoic tectonic evolution of the area was the most important control over the maturation of, and migration from, the late medial Cretaceous MPSR unit.

The drainage area where hydrocarbon deposits have subsequently migrated following expulsion covers an area approximately  $5 \times 10^4 \text{ km}^2$ . It is limited to the north by the Oca Fault, a left-lateral transform fault, while towards the northeast it is bounded by a north-northwestward trending line delineating the maximum thickness of Eocene-deposited fluvio-deltaic sediments. Mountain ranges complete the closure of the Maracaibo Basin, with the Venezuelan Andes to the south and southeast, the Santander Massif towards the southwest, and the Perija Range to the west and northwest (Fig. 3.10) (Talukdar et al., 1986).

The paucity of late Mesozoic tectonic events controlled the deposition of the key MPSR unit on the northern passive margin of South America, while active Cenozoic tectonic events induced sedimentation that drove thermal maturation, expulsion, and degradation of the La Luna MPSR unit. Geochemical analyses point to the La Luna Formation as the key MPSR unit of the Maracaibo Basin with calculations estimating that at least 90 percent of all petroleum generated in the area has been derived from it (Talukdar et al., 1990). The subsequent deposition of the shaley Colon Formation (Fig. 3.8), possessing low TOC values, during Campanian through Maastrichtian times provided a regional seal for migrating hydrocarbons. The initial thermal maturation, and expulsion of hydrocarbons from, the La Luna Formation was caused by foreland basin thrust and sediment loading, and deformation of the northern South American passive margin during early Tertiary times (Pindell, 1991).

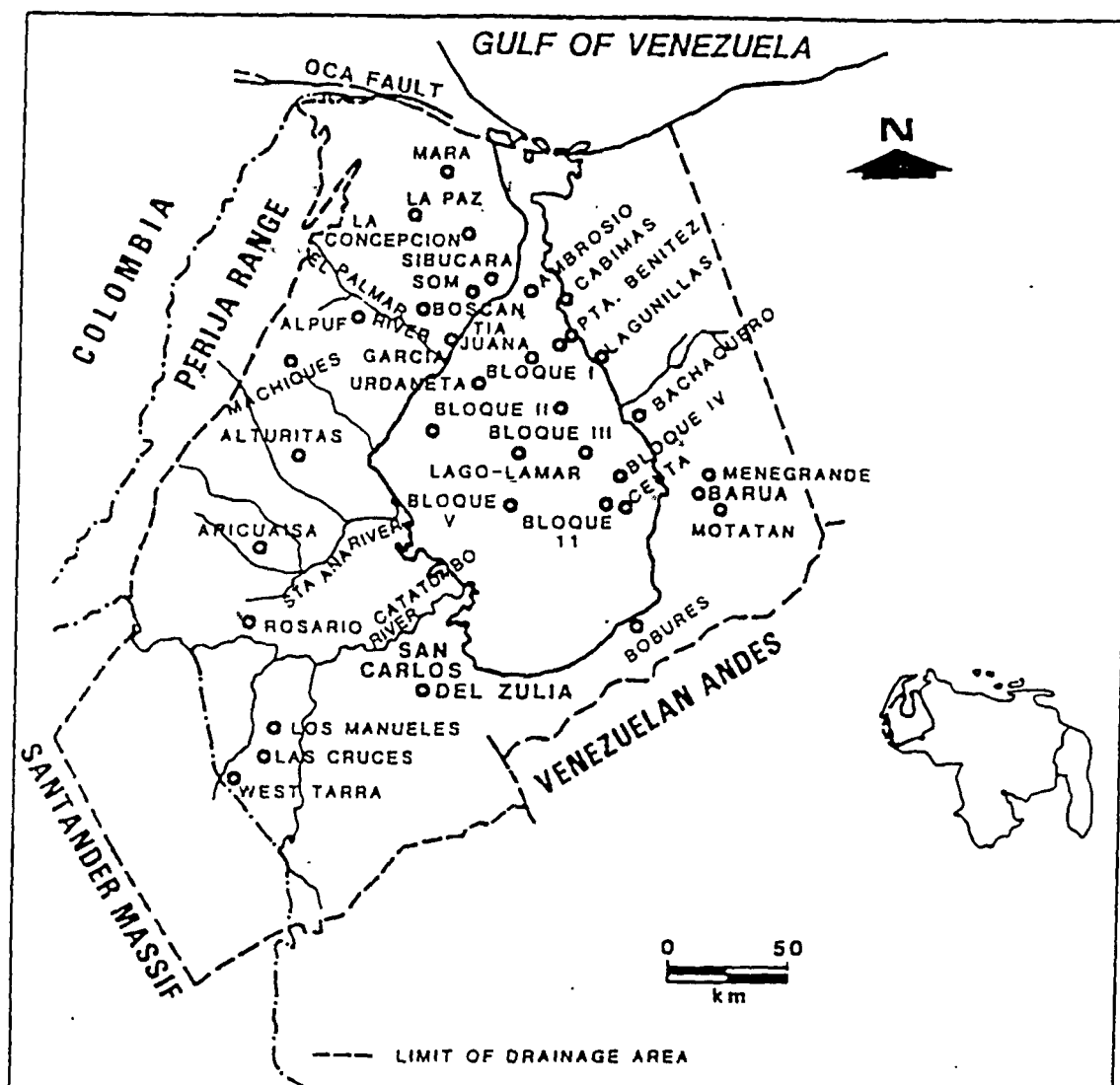


Figure 3.10 - Location of the Maracaibo Basin with names of various oil fields (After Talukdar et al., 1986).



Geochemical analyses of oils spanning the whole area of the Maracaibo Basin show that three distinct types of oil are present. Mesozoic-age marine-derived oils (i.e. the La Luna Formation), ranging from immature to highly mature, occur throughout all areas of the basin, while terrestrial-derived and mixed marine-terrestrial oils are located only in the southwestern areas of the basin (Fig. 3.11) (Talukdar et al., 1987). Thermal modeling of the basin has shown that maturation of the MPSR unit by tectonically-induced sediment loading of the passive margin occurred first in the northeastern section of the collisional foredeep during Eocene times. The area of active hydrocarbon generation subsequently broadened in an easterly direction as Eocene deltaic sediments (Eocene Misoa-Trujillo sands) (Fig. 3.12a) (Dewey and Pindell, 1986), derived from the proto-Orinoco River, migrated towards the east and subsequently thermally matured the regionally deposited MPSR unit. The southern section of the basin however, underwent hydrocarbon maturation and migration during Miocene through Recent times during and following the collision of the Panamanian-Costa Rican arc against northwestern South America.

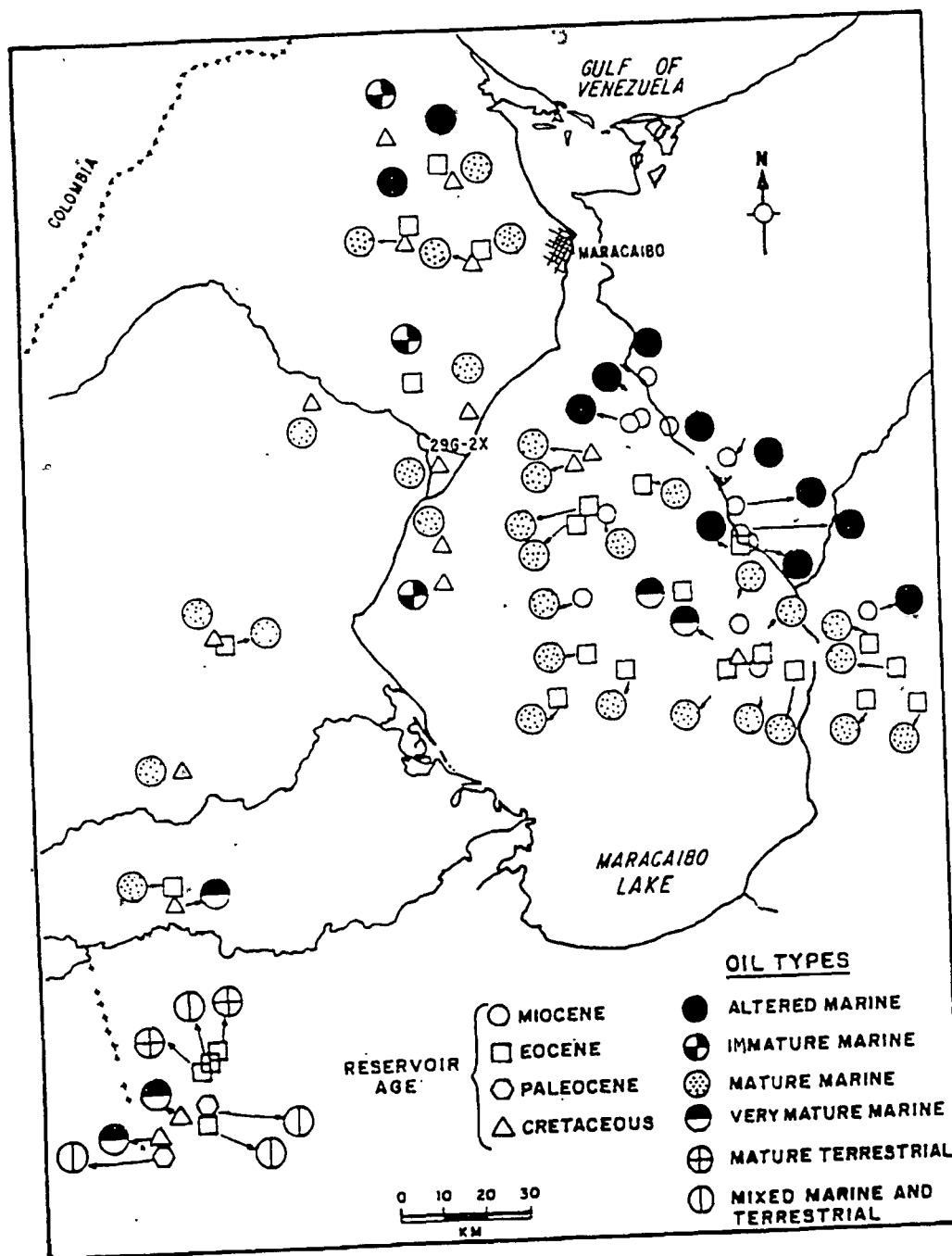


Figure 3.11 - Oil types and their distribution within the Maracaibo Basin (After Talukdar et al., 1986).

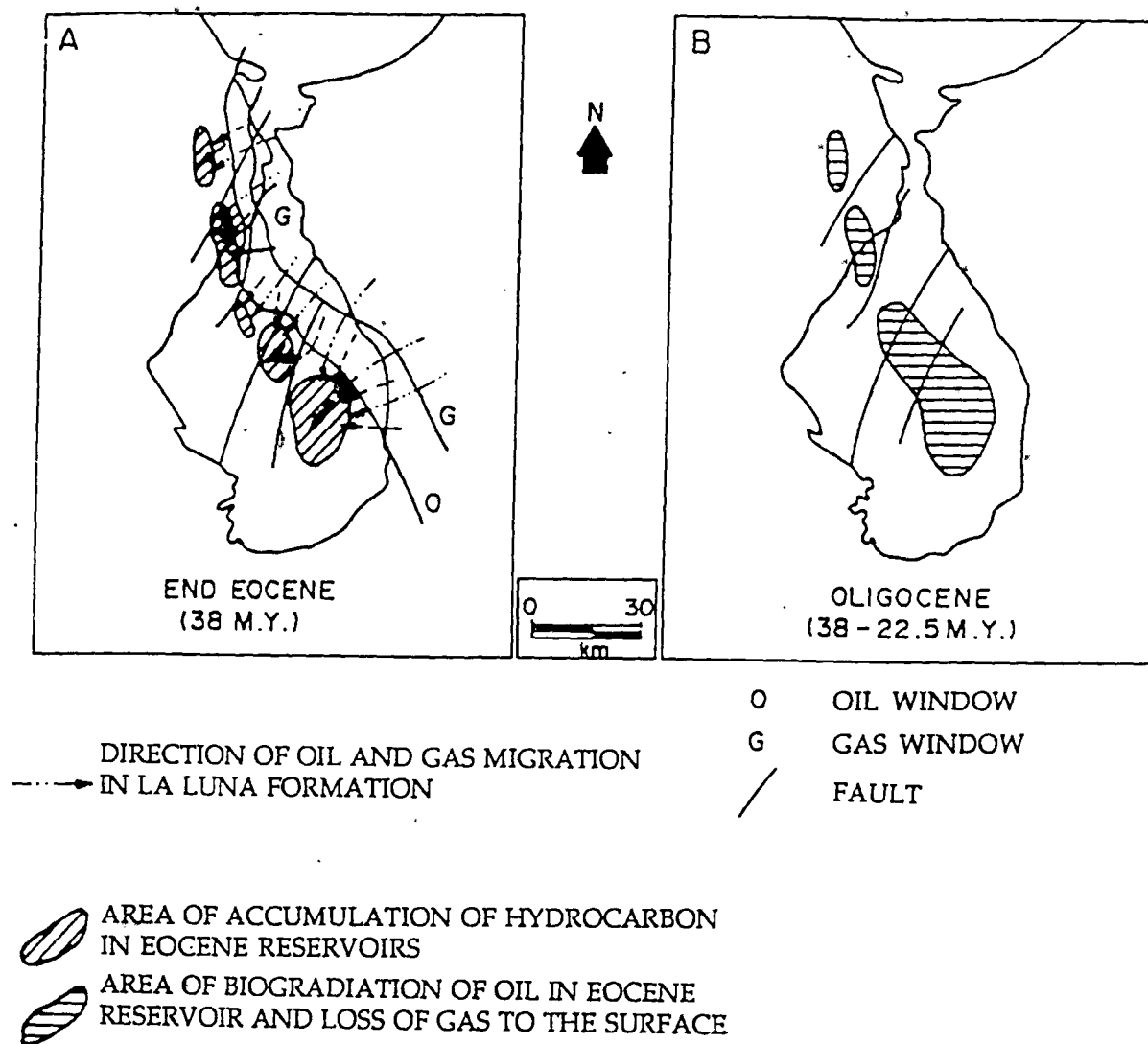


Figure 3.12 - Sketch of hydrocarbon migration in the Maracaibo Basin during late Eocene-Oligocene times  
(After Talukdar et al., 1986).

### 3.3.2 Organic Matter and Source Rocks of the Maracaibo Basin

Organic geochemical, and pyrolysis, analysis of all stratigraphic units deposited in the Maracaibo Basin, undertaken by previous authors, was compiled to determine which ones could have served as principal source rock units for hydrocarbon generation, and some of this data is published. However, much of the data still remains classified by the petroleum industry, hampering an effective, comprehensive, geochemical assessment of the Maracaibo Basin. The potential of a lithologic unit as a source rock includes the quantity and quality of organic matter deposited and preserved, as well as the thermal maturity of the unit (Talukdar et al., 1986). Talukdar et al (1986) concluded that the Cretaceous Capacho and La Luna Formations and the Apon Formation of the Collogo Group were the best candidates for source rock units in the basin (Table X).

The La Luna Formation is a fine grained argillaceous limestone and calcareous shale unit, with total thickness varying between 61-213 meters (Talukdar et al., 1987). The occurrence of rhythmic banding on the order of 20-50 centimeters between the limestones and shales, coupled with observed internal millimeter to sub-millimeter scale banding, is indicative of an open marine shelf (?) and/or abyssal environment existing during Cenomanian through Coniacian times (Talukdar et al., 1987). The lack of bioturbation in the sediments suggests deposition under anoxic conditions ( $<0.1 \text{ ml O}_2 / \text{l H}_2\text{O}$ ) a requirement to preserve finely laminated sediments (Stein, 1991).

Pyrolysis analysis of the La Luna Formation shows that it is an organic-rich unit, with its present total organic carbon (TOC) values ranging between 1.5-9.6 wt.%, and with its calculated original TOC values ranging between 2.5-10.8 wt. % (Talukdar et al., 1986). The hydrogen index of immature samples of whole rock extracts of the La Luna is about 700 mg HC/g TOC, while calculated H/C ratios are about 1.3. Based on these geochemical observations, the La Luna is interpreted as a product of marine deposition, with type-II organic matter dominating (Talukdar et al., 1987). A marine origin for the organic matter is verified by kerogen petrography with the occurrence of common amorphous marine and algal matter and rare vitrinite (Talukdar et

Table X: Source Rock Characteristics within Maracaibo Basin

Age	Formation	Source Rock lithology	TOC range (%)	TOC average (%)	Organic Matter Type	Maturity
Eocene	Trujillo	Shales	0.5-0.3	1.2	III	Overmature
Eocene	Misón	Shales	0.6-3.0	1.47	III	Mature to overmature in the east and northeast
Eocene	Mirador	Shales	0.3-2.3	0.97	III	Mature locally in the south
Paleocene	Marcelina	Shales	0.6-1.7	0.9	III	Mature locally in the west
Paleocene	Guasare	Shales	0.8-1.7	1.18	III	Mature only in the south and Ambrosio area
Cretaceous	Colon	Shales	0.5-1.1	0.8	III	Immature to overmature
Cretaceous	Capacho	Limestones, calcareous shales	0.6-8.3	3.1	III	Mature to overmature
Cretaceous	La Luna	Limestones, calcareous shales	1.5-9.6	3.8	II	Mainly mature to overmature
Cretaceous	Lisura*	Shales	0.1-2.6	0.97	II and III	Mainly mature to overmature
Cretaceous	Apon*	Limestones	0.1-2.8	1.14	II	Mainly mature to overmature

\* Formations that belong to the Collogo Group

Foreland Basin

Passive Margin

al., 1986). In addition, molecular organic geochemistry also points to a marine origin for the La Luna Formation, with the presence of steranes and terpanes being characteristic of marine origin (see Talukdar et al., 1986; Talukdar et al., 1987).

The overlying Capacho Formation of the Maracaibo Basin also possesses high TOC values (about 3.1 wt %) and high HI hydrogen index values (650 mg HC/g TOC) (Table X). However, its distribution only in the southwestern part of the basin indicates this unit played only a minor role in the evolution of petroleum deposits in the area. The underlying Apon Formation, though regionally distributed throughout the basin, varies in carbonate facies, organic matter content, and thermal maturity restricting its use as a potentially regional oil-prone source rock unit. Calculations imply that the Capacho and Apon Formations combined have accounted for only 7% of all petroleum deposits in the Maracaibo Basin while the La Luna has produced at least 90% of all petroleum deposits (Talukdar et al., 1986). Detailed organic biomarker analyses of the Apon, La Luna, and Capacho Formations verify that all three units have served as source rocks for hydrocarbon production within the Maracaibo Basin, but with the La Luna Formation serving as the primary producer for the reasons discussed above. Whole rock extracts from each of the units possess similar concentrations of normal-alkane compounds to one another, which are also observed within marine-derived oils present throughout all parts of the basin. The similarity of specific geochemical compounds within the hydrocarbons of the Maracaibo Basin, as well as the Apon, La Luna, and Capacho Formations, are used for justification of the argument that these units are the proposed source rocks for the region (Talukdar et al., 1986) (Fig. 3.11). Geochemical comparison to the overlying Lisure, Colon, and Misoa shale extracts have indicated that these units could not have served as significant source rocks for petroleum generation (Talukdar et al., 1986).

Therefore, the medial Cretaceous La Luna Formation, deposited during a relative maximum global sea level stand, is the major MPSR unit for the Maracaibo Basin. Based on the quantity, quality, and thermal maturity of the unit, it is estimated that for every  $1\text{km}^3$  of La Luna source rock

that undergoes petroleum transformation,  $290 \times 10^6$  barrels of oil can be generated, with total projected deposits of  $29 \times 10^9$  barrels of petroleum capable of being produced (Talukdar et al., 1987).

### 3.3.3 Hydrocarbon Generation in the Maracaibo Basin

Sediment accumulation from late Jurassic through Campanian in the Maracaibo Basin was responsible for the deposition of the key MPSR unit but was not sufficient to initiate petroleum generation (Bockmeulen et al., 1983) (Fig. 3.6). Loading of the northern passive continental margin of South America by the eastward advancing Caribbean Plate during Tertiary times caused foreland basin thrust loading in the area (Pindell, 1991). This initiated hydrocarbon generation of the La Luna Formation. Because the maturation of the La Luna was a function of sediment burial and/or tectonic overthrusting during the evolution of the Caribbean region, an assessment of the timing of the onset of petroleum generation is possible (Pindell, 1991) (see Fig. 3.6).

Initial petroleum generation began in the northeastern part of the Maracaibo Basin during later Eocene times with the deposition of thick fluvio-deltaic sediments, derived from the proto-Orinoco River, inducing generation of hydrocarbon products (Sweeney et al., 1990). Oils from this part of the basin are observed to be highly mature, with vanadium concentrations between 20-1100ppm, while sulfur concentrations are observed between 0.5-5.2 wt. %. Combined with the observation of a spectrum of normal alkane, and biomarker, compounds in the oils, its marine-derived nature is confirmed (Talukdar et al., 1986). The continued eastward progression, and deposition, of Misoa-Trujillo fluvio-deltaic sediments caused the southwestwardly progression of petroleum generation to occur through the rest of the Eocene (Fig. 3.12a) (Talukdar et al., 1987).

The eastward broadening zone of petroleum generation was arrested during the Oligocene, when an enormous unconformity developed with at least 9000 feet of Eocene-deposited sands being removed in the northeast (Bockmeulen et al., 1983; Pindell, 1991). Consequently, shallow oils that were located in northeastern Cretaceous and Eocene reservoirs of the basin were contaminated by meteoric water intrusion (Fig. 3.12b). This is confirmed geochemically by the paucity of normal alkane compounds in oils from the area, vanadium concentrations ranging only between 200-500ppm and high sulfur contents (Talukdar et al., 1986). Bockmeulen et al., (1983) interpreted that this erosional event is connected to the lowest observed sea level stands during the Cenozoic occurring



during this time (Bockmeulen, 1983). However, it is more likely that it was connected to evolving southern Caribbean pale boundary tectonism (Pindell and Barrett, 1990).

### 3.3.4 Mechanism for Expulsion of Hydrocarbons in the Maracaibo Basin

Petrographic analysis of La Luna whole rock extracts has enabled the determination of how petroleum was expelled, and subsequently migrated, as it underwent thermal maturation. The key observations made were the following (Talukdar et al., 1986; Talukdar et al., 1987):

- limestones show thin millimeter-scale laminations of carbonate-rich and organic-rich layers parallel to stratification, with the organic-rich layers being thin continuous bands varying in thickness between 10 $\mu$  - 200 $\mu$
- bitumen, in the organic-rich layers of the limestones, is present along microfractures on the border or within bands of organic matter parallel to stratification and within connecting microfractures, also parallel and oblique to stratification
- bitumen, within carbonate-rich layers of limestones, is found in microfractures that cross-cut stratification and within fine pores of the carbonate matrix
- kerogen being found within clay-rich argillaceous limestones as discontinuous bands parallel to stratification
- abundant microfracturing is observed in the La Luna Formation, coupled with bitumen occurring in these fractures
- low porosity (between 0-5%) permeability, and water content values being observed in La Luna Formation at depth

These observations suggest that over-pressuring of the La Luna Formation, and overlying Colon Shales, causing the formation of abundant microfractures within these units, and that the fractures provided the primary mechanism of initial petroleum migration in the Maracaibo Basin (Talukdar et al., 1987).

As liquid petroleum was generated within the unit, the volume increase would cause fluid pressure within the unit to increase. Eventually, lithostatic pressures would have developed, causing fracturing of the unit. These microfractures would have created pathways for the migrating petroleum to flow in, explaining the observation of kerogen being seen primarily parallel to

stratification while bitumen was observed to be both parallel and oblique to the stratification. As the petroleum was expelled, the system would essentially 'reset' itself, with overlying sediment being supported by the remaining dry organic matter (kerogen) and its mineral grain host until sufficient sediment accumulation allowed for the occurrence of another phase of petroleum generation and expulsion. The hypothesis of over-pressuring of the shale units is verified by a detailed comparison of shale density versus depth of key units within the Maracaibo Basin to normally-observed shale compaction gradient calculations (Fig. 3.13) (Talukdar et al., 1987).

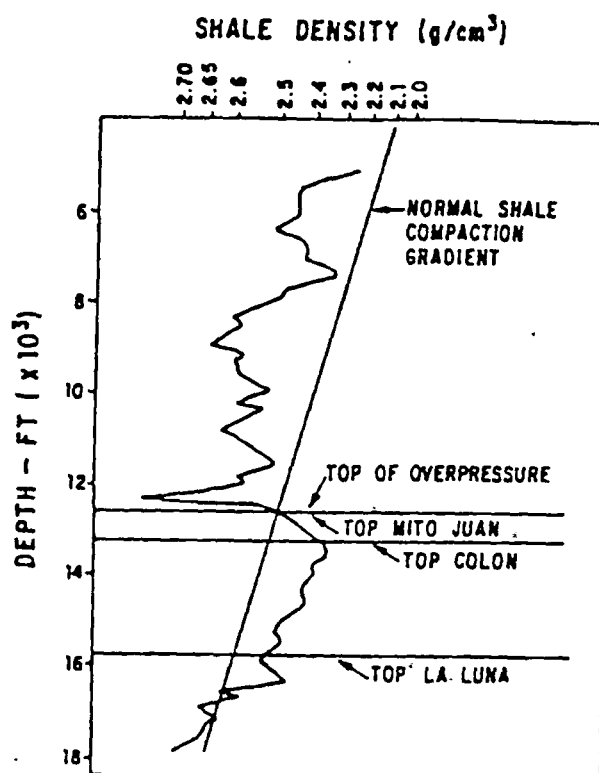


Figure 3.13 - Shale density versus depth plot for an unspecified well in the western Maracaibo Basin showing the top of overpressure zone at the Mito Juan Formation (After Talukdar et al., 1987).

### 3.3.5 Migration History of Hydrocarbons within the Maracaibo Basin

Using the simple rule of thumb that migrating hydrocarbons will always preferentially travel updip towards areas of lower pressure, a comprehensive construction of the migration of petroleum deposits in the Maracaibo is possible. Petroleum initially migrated from northeastern parts towards southwestern parts of the Maracaibo Basin (Talukdar et al., 1986), consistent with sediment loading occurring in the northeastern parts of the basin, causing down-to-northeastward tilting of the basin strata. Migrating petroleum eventually relocated itself in structural highs within Cretaceous age reservoir sequences. While the overlying Colon Shale acted as a regional cap for the migrating petroleum, eventually the regional seal was fractured, enabling petroleum to migrate vertically into shallow Eocene sandstone reservoirs (Talukdar et al., 1987).

Events associated with development of the Oligocene unconformity event tectonically disrupted the integrity of the Eocene reservoirs, being pronounced in the northeastern section of the Maracaibo Basin (Fig. 3.11b). During Miocene times however, the collision of Panama with South America enhanced sediment infilling of the southern portion of the basin, restarting migration of petroleum deposits, while also allowing migration to occur both in a northwards and southwards direction (Fig. 3.14a, b, c) (Talukdar et al., 1987). Because the Panama collision reactivated once dormant faults in the Miocene within the Maracaibo Basin, long-distance, horizontal, migration of hydrocarbons was hindered. Vertical migration pathways were subsequently developed, allowing for substantial petroleum accumulation within Eocene and Miocene-deposited reservoir rocks (Talukdar et al., 1987), while biodegradation has continued to occur in the northeastern parts of the basin, possibly a consequence of the northwards extrusion of the Maracaibo Block from western South America. This is a direct result of the continued Cenozoic eastwards motion of the Caribbean Plate (Pindell and Barrett, 1990).

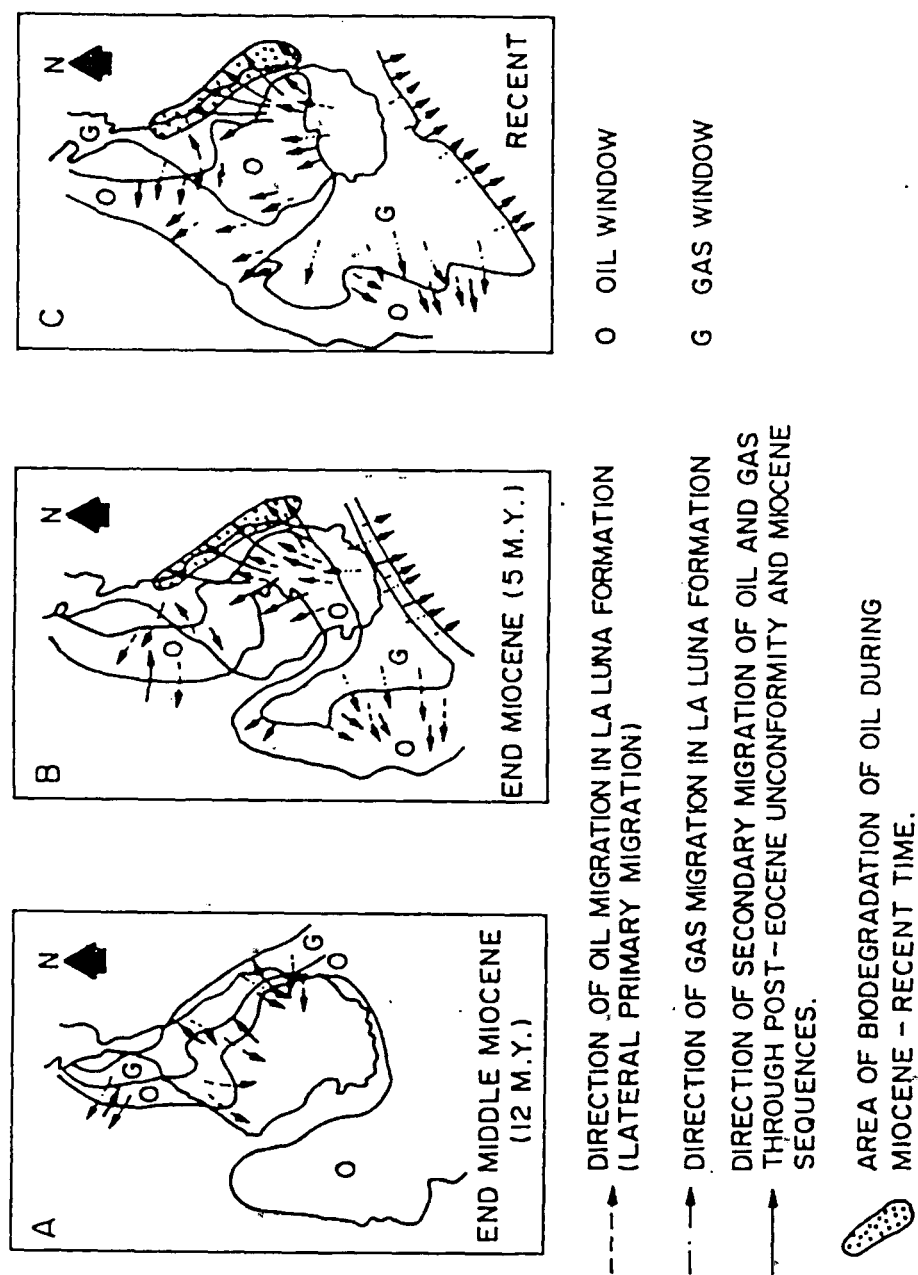


Figure 3.14 - Sketch of hydrocarbon migration within the Maracaibo Basin during end of middle Miocene-Recent times (After Talukdar et al., 1986).

### 3.4 Conclusions

#### 3.4.1 Validation of La Luna Formation as a Prolific Passive Continental Margin MPSR Unit as a Consequence of Wind-Driven Upwelling during the late medial Cretaceous

During Cenomanian through Coniacian times, a global marine transgression and highstand reached its maximum, flooding the passive margin of northern South America (Talukdar et al., 1986) with a prolific MPSR unit, the La Luna Formation, being deposited (Talukdar et al., 1987). While the Mesozoic is considered as the time of substantial MPSR deposition off the northern Venezuelan passive margin coast, throughout the Cenozoic thermal maturation and expulsion of hydrocarbons is felt, within the context of this thesis, to have been controlled by enhanced sediment production and deposition above the passive margin beds during this time. This was a direct consequence of the Caribbean Plate migrating relatively eastwards along the northern margin of the South American Plate.

In the Maracaibo Basin of northwestern Venezuela, hydrocarbon generation was initiated during the Eocene, as substantial thicknesses of deltaic sediments were deposited in the northeastern part of the basin. This caused the progressive southwesterly migration of hydrocarbons into Cretaceous and Eocene reservoirs, and the eastward progression of MPSR sediment-induced thermal maturation (Talukdar et al., 1987). During the Oligocene however, the erosion of thousands of meters of Eocene-deposited sediments arrested hydrocarbon generation and tectonically disrupted Cretaceous and Eocene reservoirs (Bockmeulen et al., 1983). During the Miocene collision of Panama with South America, high sedimentation was restarted in the southern part of the Maracaibo Basin as the ongoing island arc-continental collision produced the uplift of the Cordillera de los Andes (Talukdar et al., 1986). Hydrocarbon migration during this time was north and south-directed into Cretaceous, Eocene, and Miocene reservoirs as well as continuing in a southwesterly direction (Talukdar et al., 1986).

For the late medial Cretaceous at least one paleoclimatic model predicts extensive MPSR deposition off the northern coast of South America (Barron, 1985; Kruijs and Barron, 1990). Using the interpretation that a section of the La Luna Formation is a passive continental margin deposit, being situated near the equator, the northern South American coast was in an equatorial zonal upwelling zone. This enhanced primary productivity within the overlying water column. Enhanced preservation of deposited marine and algal organic matter is felt to be the consequence of sea-level stand being high enough (250-300 meters above present conditions), allowing for the establishment of long-term anoxic conditions on the flooded continental shelf. The positioning of the continent in a low paleolatitude also probably arrested seasonal overturning of the water column, also contributing to long-term anoxic conditions developing off the northern coast of South America.

The presence of MPSR units in the Maracaibo Basin of northwestern Venezuela shows the potential utility of using specific variables (determining the extent and causes of subsidence of continental margins and shelves in low paleolatitudes, inferring the paleogeographic and paleoclimatic conditions existing at such times, and postulating the biologic activity and oxygen concentrations within the water column) towards identifying other areas of significant MPSR deposition. The next step is the determination whether or not wind-driven upwelling can actually produce sufficient, commercial-size, quantities of organic matter for hydrocarbon deposits awaiting petroleum conversion. The late medial Ordovician Taconic Collisional Foredeep Basin provides an useful opportunity to test this hypothesis regarding the quantity of wind-driven upwelling marine organic production, since the key stratigraphic unit (the Utica Formation) was deposited at least 20 Myr before the development of significant plant forms on continents.



CHAPTER 4: REGIONAL OVERVIEW AND GEOCHEMICAL ANALYSIS OF THE TACONIC FORELAND BASIN, MEDIAL ORDOVICIAN: THE UTICA FORMATION AS A PROLIFIC SPENT, MARINE PETROLEUM SOURCE ROCK (MPSR) UNIT

4.1 Introduction

Sedimentary and tectonic effects resulting from the destruction of the eastern passive margin of Laurentia (proto-North America) through the later Ordovician can be seen from Newfoundland to Alabama. Following extensive platformal deposition on the Appalachian passive margin from Cambrian through early Ordovician times, the carbonate bank was uplifted, eroded, and subsequently drowned (Bird and Dewey, 1970; Rowley and Kidd, 1981; Bradley and Kusky, 1986). This was accommodated partially by eastward regional tilting and in part by motion on normal fault blocks in the upper part of the subsiding lithosphere (Bradley, 1989). Eventually this would form a minimum 100 kilometers-wide normal faulted zone flanking the allochthonous Taconic thrust sheet of eastern New York and western New England (Fig. 2.3) (Bradley and Kidd, 1991).

The loading, consequent lithospheric flexure, drowning of the passive margin, and attempted subduction of the proto-North American continent was due to the collision of the margin with a subduction complex at the leading edge of a magmatic arc during the medial Ordovician (Rowley and Kidd, 1981; Bradley and Kidd, 1991). Due to the oblique collision between the arc and the probably irregular-shaped Appalachian passive margin, a diachronous shelf drowning sequence developed on the rifted passive margin (Bradley, 1989). In addition to the closure of a minimum 500-900 kilometers wide 'proto-Atlantic' ocean, the Iapetus, the collision of the island arc with the margin produced a flexural foredeep, the Taconic Foreland Basin, spanning over 130 kilometers width in central New York (Fig. 2.1) (Hay and Cisne, 1988).

As the Taconic Orogeny progressed, the deposition of terrigenous-derived argillaceous and arenaceous sediments in the Taconic Foreland Basin showed a change from platformal to flysch sedimentation (Bosworth and Vollmer, 1981). A direct consequence of the Taconic Orogeny, the destruction of the Appalachian passive margin is recorded by erosion in the basin followed by an upward-deepening succession of carbonates, shales, and flysch (Bradley, 1989). Prior to this major tectonic event, the lithologic facies in the area of the Taconic Foreland Basin show evidence of a global-transgressive event occurring throughout Cambrian times, followed by an episode of shallowing in the early medial Ordovician, followed by the Taconic loading of the Appalachian passive margin during Ordovician times (Titus, 1988; Bradley and Kidd, 1991). A summary of the tectonic evolution of the Taconic Foreland Basin, compiled from previously published data, is presented. This will highlight aspects relevant to the development of the hydrocarbon potential of the Taconic Foreland Basin. Also, new, detailed organic and geochemical analyses of the foredeep sediments make it possible to infer the primary productivity, oxygen concentrations, and the quality, quantity, and thermal maturation of organic matter within the foredeep. This shows that the late medial Ordovician Utica Formation was a prolific MPSR unit during optimum times of hydrocarbon generation. This was a direct result of the drowning of the Laurentian passive margin within a low paleolatitude during late medial Ordovician times.

## 4.2 Regional Overview of the Taconic Foreland Basin, eastern New York

### 4.2.1 Geologic Setting of the Taconic Foreland Basin

A schematic diagram highlighting the series of stratigraphic units comprising the Taconic Foreland Basin (Fig. 4.2), shows that it occurred at the time of the widespread deposition of Upper Ordovician carbonates and shales. This is inferred to be indicative of the largest-inferred marine submergence of Laurentia (proto-North America) during the Paleozoic (Fig. 4.1) (Longman and Palmer, 1987). Following extensive, transgressive, platformal sedimentation from early Cambrian through early Ordovician times, the Taconic closure of the 'proto-Atlantic' caused uplifting of the shelf, with subsequent block faulting and burial with thick transgressive black, basinal, shales and turbidites (Bradley and Kusky, 1986).

The basement of the Taconic Foreland Basin sequence are Grenville-age (Fig. 4.2) metamorphic and plutonic rocks that became the continental margin of the North America craton by Cambrian times (Bradley and Kusky, 1986). Lying disconformably above it in the presently autochthonous platform is the medial Cambrian Potsdam Sandstone (Fig. 4.2), a basal siliciclastic unit. With its total thickness in the Mohawk Valley between 0-30 meters, it is indicative of the initial phase of marine transgression on this part of the passive margin (Bradley and Kusky, 1986). It is followed conformably by a package of carbonate rocks, the upper Cambrian through lower Ordovician Beekmantown Group, whose total thickness is between 0-230 meters in the Mohawk Valley. Both the Potsdam Sandstone and the Beekmantown Group are products of thermally-driven subsidence of a passive margin, as it was also experiencing a long-term episode of gradually rising sea-level (Bradley and Kusky, 1986).

Above this initial suite of carbonate rocks, there is a early middle Ordovician unconformity upon which lie a second package of carbonates, the Black River and Trenton Groups (Fig. 4.2) (Bradley and Kusky, 1986). The existence of the unconformity has been interpreted as the initiation of 'interaction' between the Laurentian passive margin and the oncoming island arc, culminating with the Taconic Orogeny in the medial Ordovician (Rowley and Kidd, 1981; Bradley and Kidd,

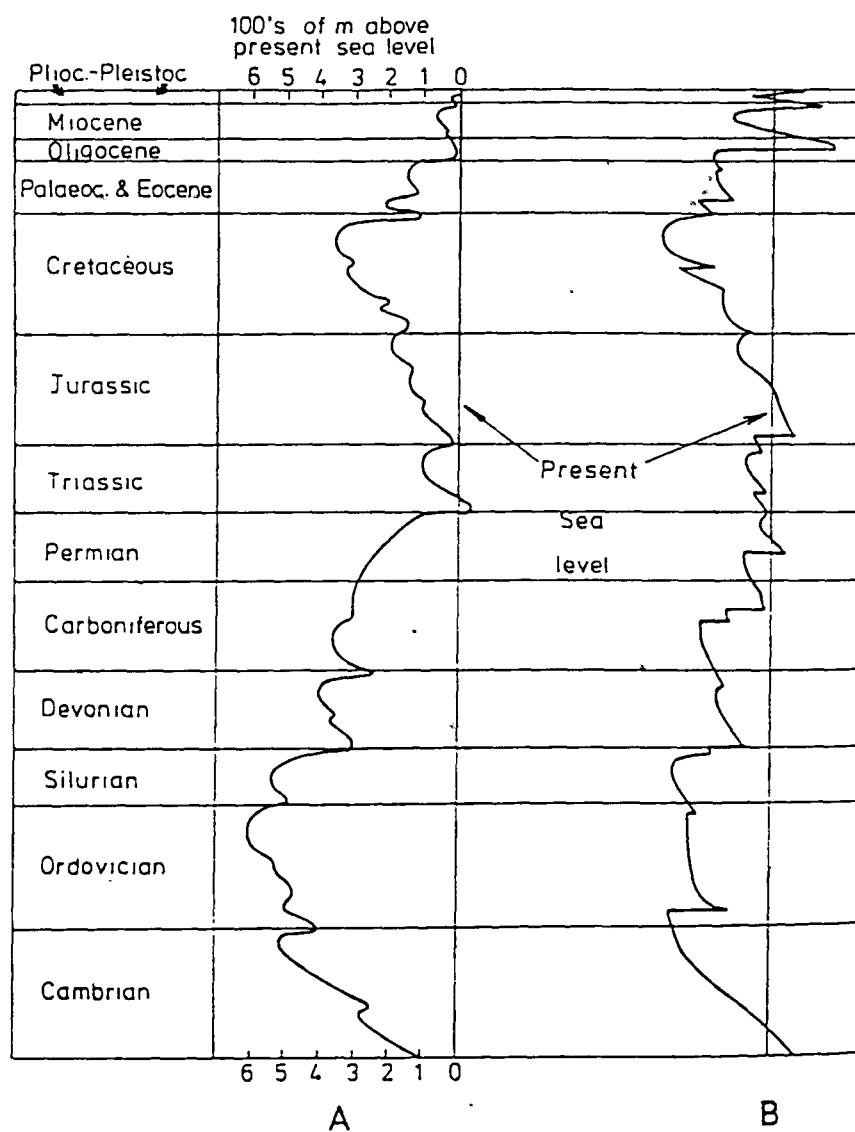


Figure 4.1 - Eustatic sea-level curves for the Phanerozoic. (A): After Hallam (1984); (B) After Vail et al., (1977). Reinterpretation by Hallam (1984) has caused the largest inferred sea-level maximum to occur during early Paleozoic times, as compared to late Cretaceous times as concluded by Vail et al., (1977). After Hallam (1984).


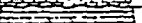


TIME	LITHOLOGY	ROCK UNIT	TECTONIC ENVIRONMENT
Medial Ordovician		Frankfort Fm. Schenectady Fm. Snake Hill Fm. Pawlet Fm.	Base of inner trench slope  Trench Floor
		Utica Fm.	Outer Trench Slope
		Trenton Group Black River Group	Eastern flank of flexural bulge
E. Ordovician		Beekmantown Gr.	Thermally subsiding passive margin
Cambrian		Potsdam Ss.	
Precambrian		Grenville Basement	

Figure 4.2 - Generalized stratigraphic section of the Taconic Foreland Basin. Exact ages are not shown because the rock units are markedly diachronous. Early Ordovician unconformity is interpreted as the passage of the peripheral bulge within the Taconic Foreland Basin (After Bradley and Kusky, 1986).

1991). As the continental shelf passed through a flexural bulge, formed in response to the bending of the lithospheric plate, the initial Cambrian through lower Ordovician carbonate sequence was variably eroded; in some small sections of the Taconic Foreland Basin, the Black River Group even lies unconformably above Grenville-age basement rock (Bradley and Kidd, 1991). The total time that the erosional event represents is estimated to be about 5 Myr (Bradley and Kusky, 1986). This second suite of carbonate rocks is a deepening-upward sequence, representative of the continental shelf being subsequently drowned after passing over a flexural bulge (Fig. 4.2).

Closer examination of the Trenton Group reveals oscillating sea-level changes superimposed upon the accelerating subsidence of the Trenton Group (Titus, 1988). The basal unit of the Trenton Group is the Napanee Limestone (Fig. 4.3). It is a thick-bedded, fossiliferous, calcisiltite indicative of a lagoonal depositional environment under oxic conditions (Fig. 4.4) (Titus, 1988). The overlying, conformable, Kings Falls and Sugar River Limestones are representative of the first transgressive/subsidence pulse of the medial Ordovician (Fig. 4.3). According to Titus (1988), the lower Kings Falls Limestone, a thick-bedded coarse calcarenite, shows primary physical structures indicative of an offshore barrier shoal environment (Fig. 4.4) (Titus, 1988). Conformable strata overlying the Kings Falls and Sugar River Limestones continue to become thinner-bedded and finer-grained supporting the interpretation of a transgressive pulse occurring during medial Ordovician times (Titus, 1988). The first pulse of transgression reached its climax with the deposition of the lower Denley Limestone (Poland Formation) (Fig. 4.3), a thick-bedded, fine-grained limestone, with the paucity of algal deposits and the abundance of graded units highlighting its deeper-water depositional environment. Further upsection into the Denley Limestone, (Russia Formation) the occurrence of blue-green algal-generated stromatolites (?) and lamination in micrites, coupled with various physical primary structures such as cross-bedding, graded beds and intraclasts however, are indicative of an intermediate period of shallowing occurring within the foreland basin (Fig. 4.4) (Titus, 1988). Evidence for the intermediate period of shallowing within the Trenton is further strengthened by the sedimentological nature of the lower

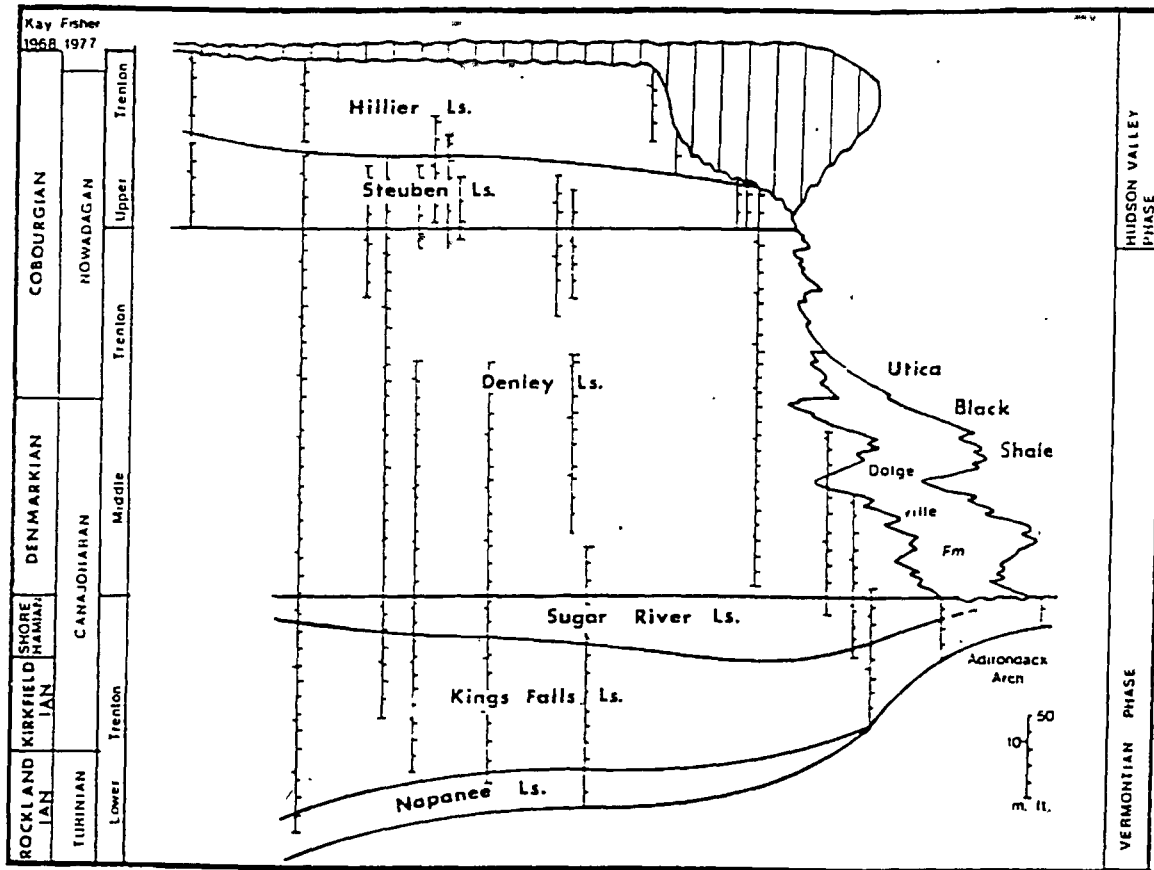


Figure 4.3 - Stratigraphy of the Trenton Group. Vertical lines are based from outcrops that Titus (1988) had studied (After Titus, 1988) Area studied approximately covers 150 kilometers.

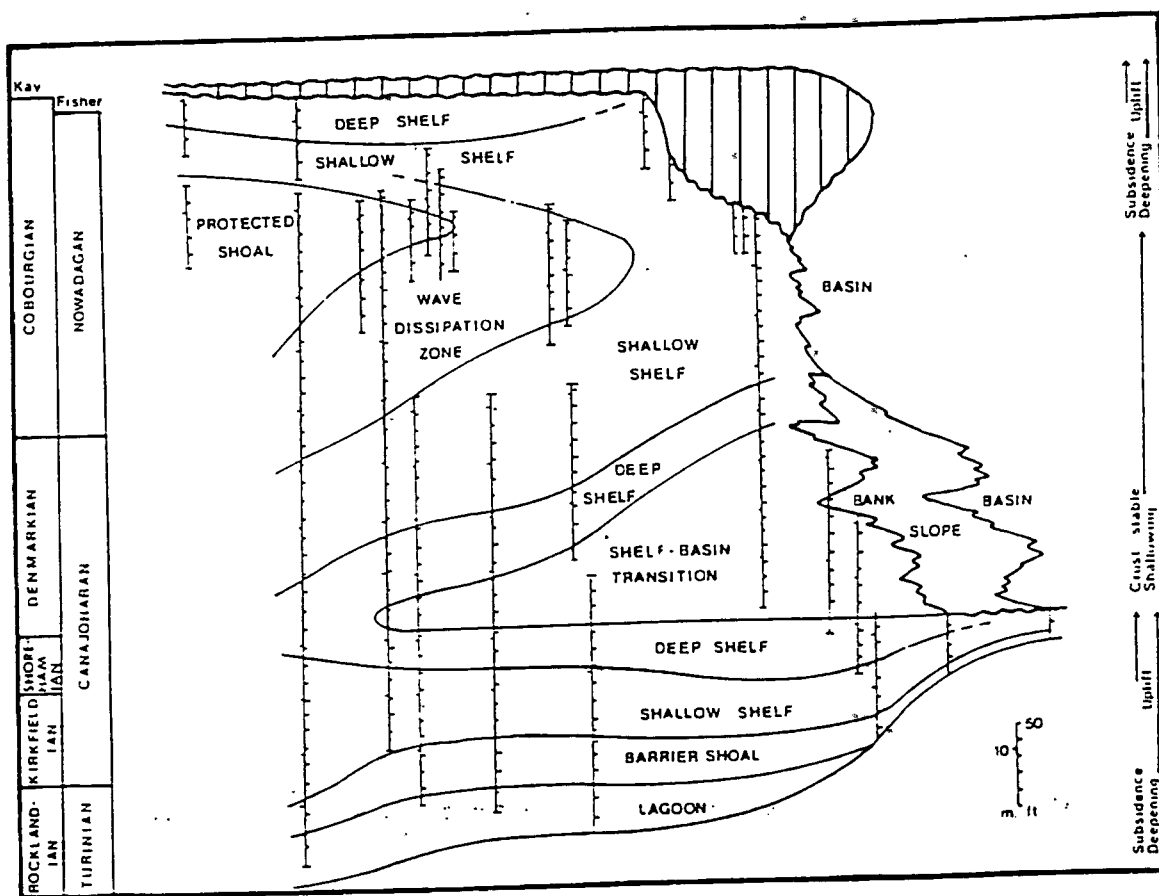


Figure 4.4 - Facies pattern of the Trenton Group. Area studied approximately covers 150 kilometers (After Titus, 1988).



Steuben Limestone, a clean, sparry, thick calcarenite (Fig. 4.3) (Titus, 1988). According to Titus (1988) however, the second phase of global transgression was soon re-initiated, evidenced by the deposition of the Hillier Limestone (Fig. 4.3), a micritic fine-grained, thin-bedded limestone, indicative of a shallow shelf transition into deeper shelf conditions (Fig. 4.4) (Titus, 1988).

Using stratigraphic thicknesses and geologic age determinations from Fisher (1977), Hay and Cisne (1988) concluded that the combined sedimentation rate for the Trenton Group was between  $20\text{-}30\text{m}(\text{Myr})^{-1}$  (Hay and Cisne, 1988). The potential error associated with this calculation is large, given the current uncertainties of geologic age determinations, and variable stratigraphic thicknesses of units within the Taconic Foreland Basin. The dating of bentonites within the Utica Formation will ultimately produce more accurate sedimentation rates of the Trenton Group, and overlying units within the Taconic Foreland Basin originally determined by Hay (1982) and Hay and Cisne (1988) (Delano, personal communication, 1992).

Continued progression upward and eastward into the section shows the Trenton Group being replaced by the Dolgeville Formation (Fig. 2.2), which represents a band of transition between the distal shelf and deeper-water deposits. In places it is composed of slump-folded, micritic ribbon limestones and hemipelagic, dark-gray to black, calcareous graptolitic shale (Hay and Cisne, 1988). It is currently thought that the Dolgeville Formation represents a gentle slope between the edge of the platform and deeper basinal shale conditions (Titus, 1988). Deposition rates of the Dolgeville Formation are estimated to have been between  $40\text{-}80\text{m}(\text{Myr})^{-1}$  (Hay and Cisne, 1988). As with the Trenton Group, the potential error associated with this calculation is large, given the current uncertainties of geologic age determinations, and variable stratigraphic thicknesses of units within the Taconic Foreland Basin. In turn, the Dolgeville grades upward and eastward into the Utica Formation, a dark-gray to black, fissile, finely laminated, hemipelagic shale with sedimentation rates estimated to have been between  $50\text{-}100\text{m}(\text{Myr})^{-1}$  (Hay and Cisne, 1988) (Fig. 4.3). Again, it must be emphasized that this sedimentation rate is associated with large potential errors, given the current uncertainties of geologic age determinations, and variable stratigraphic

thicknesses of units within the Taconic Foreland Basin. Based upon structure contour techniques, using geologic maps of Fisher (1979), in this study (see Appendix I), the stratigraphic thickness of this unit is about 300 meters in the eastern transect. A measured section within the western transect is 225 meters, and the unit thins to about 60 meters further to the northwest (Kidd, personal communication, 1993). While thicknesses of the Utica Formation can not be determined accurately east of the Hoffmans Fault, it is improbable that the Utica Formation there is much thicker than approximately 300 meters. The Utica Formation is diachronous, younger to the west. The base of the Utica Formation at Canajoharie, New York is in the *Corynoides americanus* graptolite zone of Riva (1974), while 105 kilometers further west at Frenchville, New York, it lies three zones higher within the *Climacograptus pygmaeus* graptolite zone (Fig. 2.2) (Bradley and Kusky, 1986).

Above the Utica Formation lies the Frankfort Formation, a gray shale and siltstone with thin sandy turbidites (Zerrahn, 1978), indicative of the depositional environment changing from an outer trench slope to a trench floor environment (Fig. 4.2) (Hay and Cisne, 1988). Being also time transgressive, the contact between the Utica Formation and overlying submarine fan deposits of the Frankfort Formation lies within the *C. spiniferus* graptolite zone near Amsterdam, New York, while 75 kilometers further west in Utica, New York, it is within the *C. pygmaeus* zone (Fig. 2.2) (Hay and Cisne, 1988). Sedimentation rates for the Frankfort Formation are estimated between 200-250m(My<sup>r</sup>)<sup>-1</sup>, with potential errors associated with this sedimentation rate being large for the same reasons stated above for the underlying units. Deposition of the Frankfort Formation signaled the end of the active convergence of the Taconic Orogeny. After its completion, the foredeep subsequently rebounded and was filled with east-derived, late Ordovician through Silurian, non-fossiliferous green and then red hematitic clastics of the Lorraine Group (Zerrahn, 1978).

#### 4.2.2 Tectonic Evolution of the Collisional Foredeep

From the distal shelf to the basin floor, spanning over 120 kilometers, the Taconic Foreland Basin slope is cut by a series of northeast-trending, steeply eastward-dipping normal faults (Fig. 2.3) (Bradley and Kidd, 1991). The faults are generally spaced 10-20 kilometers apart with displacements on the faults ranging from several meters in the western part of the basin to several hundred meters in the eastern part of the basin (Bradley and Kusky, 1986). Most faults strike parallel to the Taconic thrust-front, except in the extreme west of the foredeep. The normal faults throughout the collisional foredeep are a consequence of lithospheric flexure of the eastern Laurentian carbonate platform due to loading by the Taconic thrust wedge (Fig. 4.5a, b) (Bradley, 1989).

As the drowning of the Appalachian passive margin progressed, within the foreland basin the normal faulting of the outer slope migrated cratonward (Fig. 4.5c) (Bradley and Kidd, 1991). This was a result of the underthrust plate being bent beyond its elastic limit (Bradley and Kidd, 1991). In addition, regional eastward tilting, shown by the medial Ordovician facies, was associated with the syn-Taconic Orogeny cratonward fault development. Justification for the interpretation that the faults are medial Ordovician are (Cisne et al, 1982):

- the thinning, pinchout, and local absence of stratigraphic units across the top of horsts
- the presence of thicker stratigraphic units within grabens than on adjacent horsts
- all of the normal faults are observed to die out within Ordovician strata

(Bradley and Kusky, 1986)

The diachronous nature of the arc-passive margin collision is also highlighted by the observation that faults in the eastern part of the basin were active longer and accumulated greater displacements than those in the western part of the Taconic Foreland Basin (Bradley and Kidd, 1991).

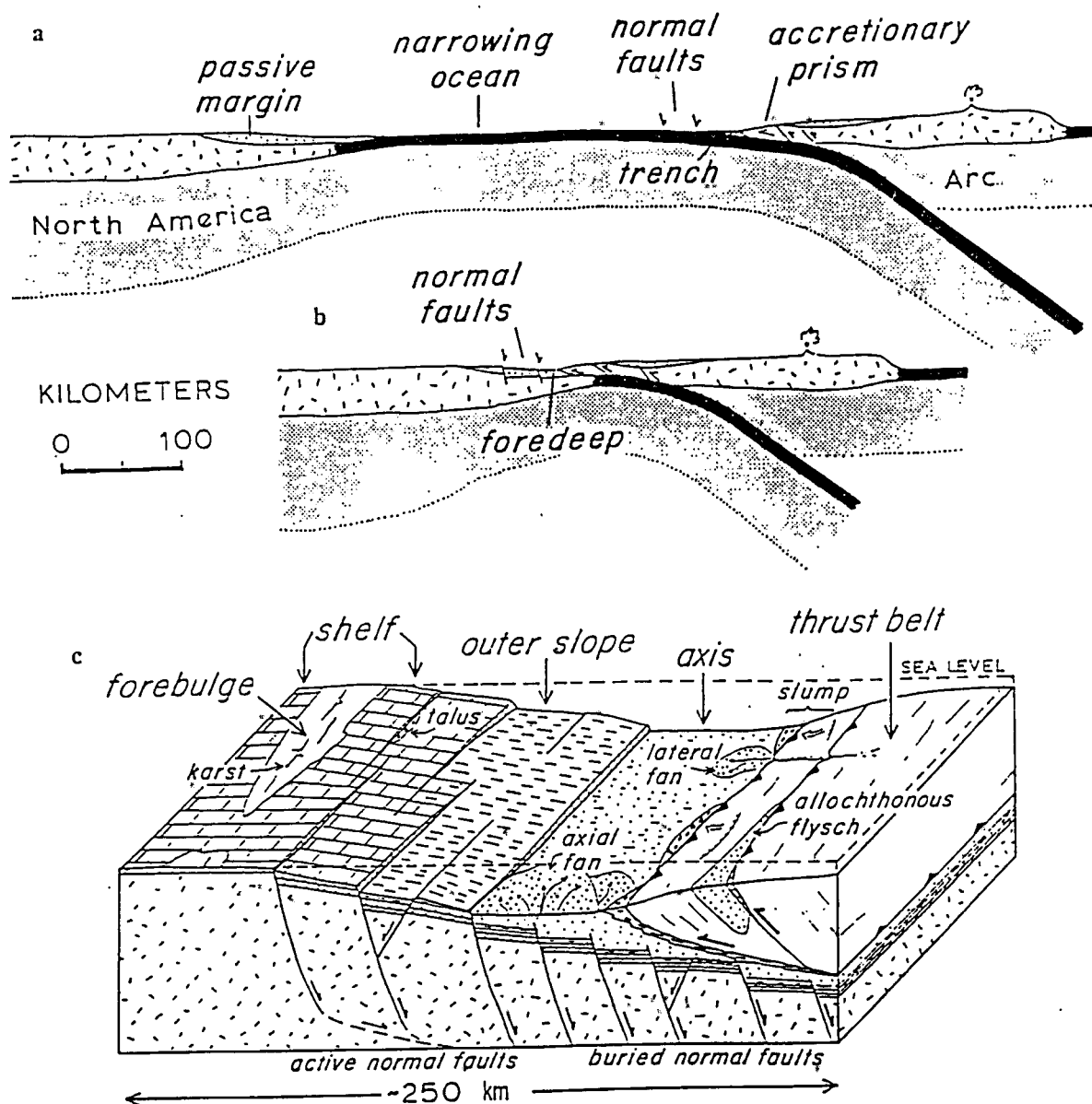


Figure 4.5 - (a and b) Plate-tectonic model for the Taconic Orogeny involving arc-passive margin collision. In Figure 4.5a, the oceanic crust of the outer trench slope was presumably cut by normal faulting; the passive margin passed through this regime of normal faulting as it approached the trench. Random dashes, continental crust; black, oceanic crust; gray, mantle lithosphere. (c) Schematic block diagram of the Taconic collisional foredeep, showing the distribution of facies belts and structural regimes shortly before plate convergence ended (After Bradley and Kidd, 1991).

#### 4.2.3 Depositional Environment of the Taconic Foreland Basin

Hay and Cisne (1988) compiled an extensive set of organic geochemical and paleobiological data in order to assess the depositional conditions of the collisional foredeep during the deposition of the various medial Ordovician stratigraphic units. Overall, it was determined that total organic carbon content changed downslope into the basin, with concentrations of 0.1-0.5 wt. % Corg found within the carbonate shelf sequence (Trenton Group), concentrations of up to 1.0 wt. % Corg on the upper slope (Dolgeville Formation) and concentrations of between 1.5-3.5 wt. % Corg on the outer slope (Utica Formation) (Hay and Cisne, 1988). Sediments deposited on the basin floor (Frankfort Formation) reversed the general trend with values averaging 0.4 wt. % Corg. However, the integration of total organic carbon (TOC) data reported by Hay (1982) and Hay and Cisne (1988) into this study, for the development of a more comprehensive assessment of the Taconic Foreland Basin, was not possible. Hay (1982), as well as Hay and Cisne (1988), published organic and carbonate carbon concentrations only from graptolite-correlated sections of the eastern-most deformed section of the Taconic Foreland Basin. TOC and carbonate carbon data from the bentonite-correlated sections of the central and western parts of the basin was not published as unmodified data. Recently published data also shows conclusively that bentonite correlations made by Hay and Cisne (1982) are incorrect (Delano et al., in press). This consequently invalidates any initial conclusions regarding organic carbon concentrations within the Taconic Foreland Basin which were based upon Hay and Cisne's (1988) previous attempts. In addition, the manipulation of reported stratigraphic sections of the Taconic Foreland Basin into 'standard-meter increments' by Hay (1982) and Hay and Cisne (1988), supposedly done for the compensation of different sedimentation rates across the basin, does not allow for the accurate determination of the original stratigraphic positions of samples plotted in graphs. The omission of the original stratigraphic position of samples, as well as the absence of detailed explanations of the techniques and reasoning used for the manipulation of the original data set, casts doubts on some of the conclusions presented by Hay (1982) and Hay and Cisne (1988). The reported long term 'anaerobic phases' recognized by Hay and

Cisne (1988), interpreted by them as due to changes within the basin and the world ocean, are based largely on stratigraphic sections from Canajoharie and Nowadaga Creeks. Original bentonite correlation attempts by Hay and Cisne (1988) suggested that these sections were contemporaneous in nature. New bentonite correlations attempts, based on major and trace element concentrations of melt encapsulated with quartz phenocryst hosts, now yields conclusive evidence that this was not the case; there was little overlap on time between stratigraphic sections from Canajoharie and Nowadaga Creeks (Delano et al., in press). In addition, while Hay and Cisne (1988) have reported a complete Canajoharie Creek section of the first 100 meters of the Utica Formation to verify their proposed 'anaerobic phases', Nowadaga Creek misses key stratigraphic sections that are reported by Hay and Cisne (1988) to represent times of these reported anaerobic phases. Tilting within the incompletely exposed Nowadaga Creek section must also have complicated the exact determination of original stratigraphic position of the samples. Geochemical inferences for the existence of previously unmapped faulting within the Taconic Foreland Basin are discussed in a section below. Therefore, conclusions that were made by Hay and Cisne (1988) and Hay (1988), must be treated cautiously. In particular, the first order increase in TOC values is primarily based on data from Nowadaga Creek only. The existence of pronounced tilting, and probable faulting, within this section therefore requires that this interpretation must be accepted, and treated, with caution.

The first-order increase of organic carbon both through time and downslope within the basin was interpreted by Hay and Cisne (1988) as the result of the combined effects of lithospheric flexure of the subducting plate and an extensive global marine transgression raising sea-levels up to 200-300 meters above present conditions. This enabled the establishment of long-term anoxic conditions on the outer slope of the foredeep. The observed TOC reversal within the Frankfort Formation was probably the result of unstable conditions existing at the basin floor allowing for episodic remixing of the bottom of the water column by turbidites, with associated regeneration of  $O_2$  concentrations in this part of the water column. It is also possible that the decrease in TOC

values observed within the Frankfort Formation was due to an increased clastic sedimentation rate (Delano, personal communication, 1993).

The interpretation that oxic conditions were present on the carbonate shelf, while suboxic conditions existed on the upper slope and basin floor, and anoxic conditions on the outer slope is strengthened by a similar variation of authigenic pyrite concentrations in the associated sediments. Authigenic pyrite, indicative of anoxic conditions (Stein, 1991), is found in the Dolgeville and Utica Formations as distinct parallel laminae at apparently random intervals, while considerably less pyrite is found within Frankfort and Trenton Group rocks (Hay and Cisne, 1988). Some trace fossils with an associated impoverished benthonic community occur within the Utica Formation, while the diversity and number of benthonic organisms within the Frankfort Formation is greater than observed within the Utica Formation (Hay and Cisne, 1988). Vertical burrowing within the Trenton Group is common, with a high degree of bioturbation relative to other sediments in the foredeep (Hay and Cisne, 1988). Hay and Cisne's (1988) field observations of well-developed fissility, uncommon benthic biogenic structures, and the occurrence of fine laminations within the Utica Formation were believed indicative of anoxic conditions ( $\leq 0.1 \text{ ml O}_2 / 1.0 \text{ l H}_2\text{O}$ ) being established on the outer slope of the foredeep (Hay and Cisne, 1988). However, observations of Utica Formation bentonites being mixed with overlying shale points to the probable existence of intermittent dysaerobic conditions during deposition of the Utica Formation (Delano et al., 1990; Delano, personal communication, 1992). Dysaerobic conditions for the Dolgeville Formation, the approximate location of the carbonate-slope transition, and for the Frankfort Formation, the area of the basin floor, are inferred by the occurrence of horizontal burrowing being more common in these, than in the Utica Formation (Hay and Cisne, 1988).

#### 4.2.4 Paleoecological Assessment of the Collisional Foredeep

Oxic conditions ( $\geq 1.0 \text{ ml O}_2 / 1.0 \text{ l H}_2\text{O}$ ) were established on the carbonate shelf during the deposition of the Trenton Group, as shown by the evidence of strong bioturbation, the presence of comparatively rich faunal assemblages, and relatively low  $C_{\text{org}}$  concentrations within the unit (Hay and Cisne, 1988). However, the faunal assemblages present within the Utica Formation, while containing abundant planktonic organisms, show evidence of an impoverished benthic (bottom-feeding) community and increased  $C_{\text{org}}$  and  $S_{\text{pyrite}}$  concentrations. This would have been a consequence of decreasing  $\text{O}_2$  concentrations downslope into the basin (Hay and Cisne, 1988). Minute parallel laminations, elevated authigenic pyrite concentrations and increasing TOC concentrations towards the thrust front, reaching a maximum on the outer slope, are the primary pieces of evidence pointing to the establishment of more pronounced reducing conditions where the Utica Formation was deposited (Hay and Cisne, 1988).

The next question to be answered is what type of organism(s) could have been produced in sufficient quantities to serve as the organic matter source. The fact that the Taconic Orogeny occurred in the late medial Ordovician, and that presently it is believed that the establishment of land plant organisms did not occur until the late early Silurian, (Spicer, 1989) precludes a terrigenous-derived organic source. Therefore, only an autochthonous marine source, a type-II kerogen, could serve as the type of organic matter produced in the Taconic Foreland Basin. While research has determined that a 'primitive' prokaryotic (no definable nucleus) organism, classified as *Gleocapsomorpha prisca*, was the key late medial Ordovician marine organism, debate still exists as to its biological nature (Longman and Palmer, 1987). One hypothesis is that this organism was similar to the cyanobacteria blue-green algal mats, as presently seen in Abu Dhabi (Longman and Palmer, 1987). However, the organic geochemistry of such organisms requires the presence of certain key biomarkers within late medial Ordovician-derived oils, such as pristane and phytane, observed in present-day blue-green algal mats, but not observed in late medial Ordovician-derived petroleum oils (Longman and Palmer, 1987). Therefore, while it has been proposed that the key



marine organism was benthonic on the outer slope of the foredeep, it has also been postulated that it was planktonic, periodically blooming above the photic zone, subsequently falling through the water column as 'organic rain' (Longman and Palmer, 1987).

#### 4.2.5 Late medial Ordovician Paleoclimatic Reconstruction

Uncertainties of paleoclimatic reconstruction are increased with increasing age (Caradocian) because of errors associated with paleo-positioning. For example, there are no paleomagnetic poles for positioning Baltica during the Cambrian and Ordovician (Scotese and McKerrow, 1990). Therefore the maps become more dependent on qualitative techniques, which could introduce larger errors.

Based upon paleomagnetic data alone, Van der Voo (1988) determined that the Laurentian craton (proto-North America) was in an equatorial position throughout Ordovician times. It was hypothesized that Laurentia subsequently rotated clockwise about 45° (Van der Voo, 1988). An equatorial positioning of proto-North America during Ordovician times is strengthened by the observed symmetric distribution of evaporites at around 15° latitude north and south of the equator (see Van der Voo, 1988). Recent examination of paleoclimatic indicators have confirmed the equatorial positioning of Laurentia, differing by only 10° latitude from the position determined by paleomagnetic data alone (Witzke, 1990). However, more recent paleogeographic reconstructions (Witzke, 1990) have placed Laurentia much closer to the paleoequator, so that this may affect the distribution of paleoclimatic indicators, upwelling zones, and prolific MPRS units determined within the context of this thesis.

Using paleogeographic maps generated by Ziegler et al. (1987), Parrish predicted mid-latitude coastal upwelling off the northwestern coasts of Laurentia, Gondwana, and Siberia (Fig. 4.6). However, these are all speculative because all possible marine petroleum source rocks (MPSR) deposited within this region during the early Paleozoic have been consumed. However, marine petroleum source rock deposition off the eastern coast of Laurentia, not proposed from qualitative modeling attempts, could have still existed during Ordovician times. Upwelling zones proposed by Parrish (1982) are only a result of coastal upwelling, which is presently the dominant upwelling mechanism producing elevated levels of productivity. However, there are additional upwelling mechanisms that could have produced substantial upwelling during times of significantly

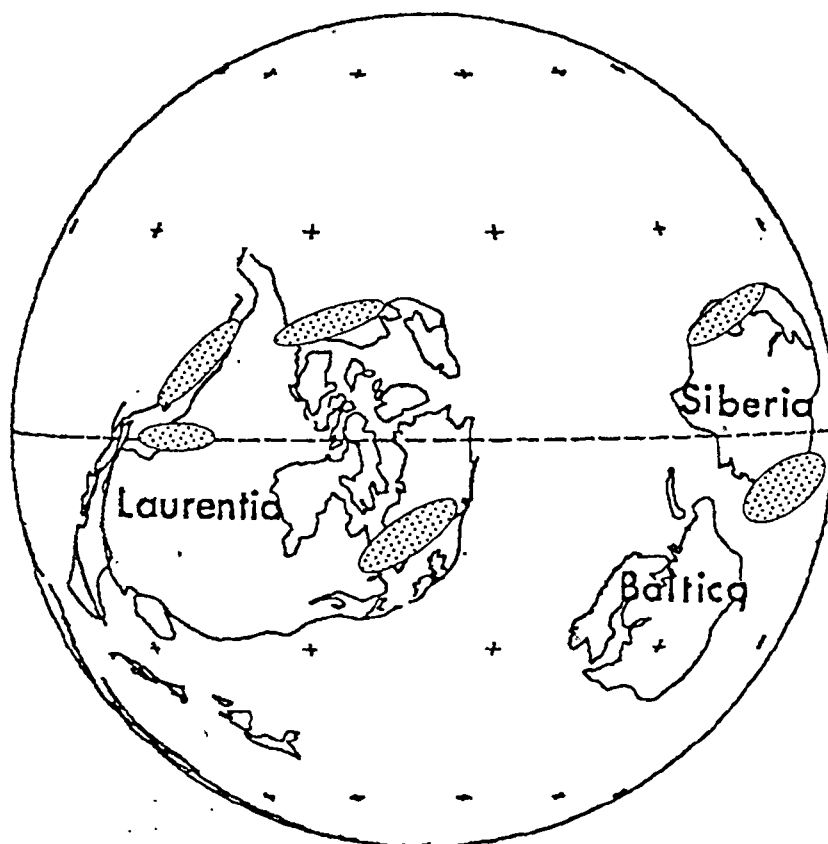


Figure 4.6 - Continental configuration and predicted upwelling zones during Landelio-Caradoc (late medial Ordovician) times. Stippled areas = proposed upwelling sites. Upwelling zones from Parrish (1982). Paleogeographic configurations from Scotese (1980).

different continental configuration and sea-level stand. One such mechanism that is proposed in the context of this thesis to have developed off the proto-North American coastline during late medial Ordovician times is that of channeled-flow upwelling. This variant of wind-driven upwelling occurs usually in an elongated seaway where surface winds are channeled allowing for high primary productivity upwind (Parrish, 1982). This is currently observed in the Gulf of California with upwelling occurring on the mainland side, when winds prevail from the north and parallel the long axis of the gulf.

During the late medial Ordovician, using paleoclimatic qualitative modeling, Parrish (1982) predicted that during *summer* intervals surface winds would have been derived from the north and would have traveled in a direction parallel to the then northeast-southwest trending coastline of Laurentia. Paleomagnetic data, as well as paleoclimatic data, is consistent with the (current southeastern) Laurentian craton margin being aligned in a northeast-southwest trending orientation (Fig. 2, of Van der Voo, 1988; Fig. 2, of Witzke, 1990) throughout Ordovician times. Also at this time, several island arcs, also in a northeast-southwest trending direction, existed off the (present eastern) margin of Laurentia, colliding with each other and Laurentia progressively. This collision had initiated in the north during the early Ordovician and culminated in late medial Ordovician with the Taconian Orogeny. The volcanic arc would have served as the border to the elongated seaway and the southwestward directed surface winds, causing southeastward directed transport of the water, would have produced channeled-flow upwelling. Inferred high sea-level stands (Haq et al., 1987) would have allowed for the preservation and deposition of organic-rich rocks cratonward onto the continent. The comparison between the Gulf of California and the Taconic Foreland Basin must be accepted cautiously however; currently the Gulf of California is more restricted than the proposed Taconic Foreland Basin Seaway. In addition, sea-level stand is not nearly as high presently as it was during the Caradocian. The key point is that based solely on non-numerical modeling, organic-rich facies present in the Taconic Foreland Basin provides strong evidence for a wind-driven paleo-upwelling zone existing at that time and location.

Another possibility for extensive MPSR deposits off the eastern coast of Laurentia is that the enhanced preservation of organic matter occurred because it was essentially an anoxic silled basin (the modern analog being the Black Sea (Demaison and Moore, 1980)). Given the fact that it was probably in a low paleolatitude, seasonal overturning would not have occurred, allowing for long-term vertical stratification of the water column. It is more probable that a combination of high primary productivity and enhanced basinwide stratification, encouraging anoxic conditions, enabled extensive MPSR deposition off the eastern coast of proto-North America. Using techniques developed by derived by Betzer et al. (1984) to ascertain organic carbon fluxes into the ocean, assuming that primary productivity at  $250\text{gC}_{\text{org}}\text{m}^{-2}\text{yr}^{-1}$  and water depth at 250m, the carbon flux reaching the ocean floor would have been about  $30\text{gC}_{\text{org}}\text{m}^{-2}\text{yr}^{-1}$ . Even if primary productivity was much lower, as seen with the Black Sea, with enhanced preservation due to structural forms that may have protected an anoxic environment from open-oceanic circulation, extensive MPSR deposition was highly probable. It is probable that both mechanisms operated during the medial Ordovician, producing an extensive MPSR deposit awaiting thermal maturation.

#### 4.3 Geochemical Analysis of the Taconic Foreland Basin

##### 4.3.1 Pyrolysis Analysis of Representative Transect of the Taconic Foreland Basin

A suite of samples from the Taconic Foreland Basin (Table VII) was chosen for the determination of the quantity, quality, and thermal maturity of organic matter within the basin by programmed pyrolysis analysis (Table XI). Analyses were performed by Texaco Inc. From this data, modeling of the original total organic carbon content of the foredeep, and the theoretical production rate of hydrocarbons following maturation, was ascertained.

Calculations based upon vitrinite reflectance, averaging 2.1% throughout all parts of the basin (Bissada, personal communication, 1993), show that all of the hydrocarbons have been expelled (Fig. 7.5, of Waples, 1980). Vitrinite reflectance is based upon the principle that the percentage of light reflected back upon shining light on vitrinite particles within a sample is directly proportional to its thermal maturity (see Waples, 1980). A plot of oxygen indices versus hydrogen indices of samples from the Taconic Foreland Basin confirms its highly mature nature, with all points plotting near the origin, while immature predominantly type-I and type-II kerogen would plot with higher hydrogen indices, indicative of their high hydrocarbon-generative potential (Fig. 4.7).

However, these values of the Taconic Foreland Basin samples must be taken as absolute minimums for several reasons. Hay (1988) reported that the mineral matrix of the Utica Formation was predominantly an illite/montmorillonite clay particle mixture, which is capable of retaining up to 85 percent of pyrolytic products (S<sub>2</sub>) by adsorption upon the mineral matrix (Peters, 1986). In addition, highly mature samples usually lack a S<sub>2</sub> peak or concentration, a lack which is observed in all the samples from the Utica, Frankfort, and Dolgeville Formations, since all potential organic matter has already been cracked (thermally decomposed). Because all samples were acquired at least 6 to 12 inches from the outcrop surface, possible depletion in S<sub>1</sub> and S<sub>2</sub>, and an increase in S<sub>3</sub>, values due to weathering were eliminated. Also, because all samples were air dried before being

Table XI: Programmed Pyrolysis Transect Sample List, Taconic Foreland Basin

Sample Control Number	Strat Position, m	Total S wt %	Organic C wt%	S1	S2	S1 + S2	S3	H index	O index	%Ro
OTC FF 01	347.44	0.87	0.56	0.02	0.09	0.11	0.29	16	51	2.1
YC US 02	304.13	1.28	0.47	0.01	0.01	0.02	0.08	2	16	2.1
BHC US 07	284.12	4.87	1.66	0.04	0.03	0.07	0.33	1	19	2.1
BHC US 04	251.86	4.74	1.91	0.03	0.01	0.04	0.1	0	5	2.1
BHC US 01	222.23	2.61	2.74	0.02	0	0.02	0.18	0	6	2.1
YKS US 01	192.07	0.5	1.23	0.02	0.01	0.03	0.37	0	30	2.1
NC US 08	170.73	3.05	2.19	0.07	0.11	0.18	0.16	5	7	2.1
TC US 01	122.44	0.85	1.85	0.02	0	0.02	0.69	0	37	2.1
NC US 05	118.90	1.52	1.45	0.05	0.04	0.09	0.19	2	13	2.1
CC US 21	80.00	1.07	2.76	0.03	0.08	0.11	0.41	2	14	2.1
HHC US 10	79.21	2.94	2.83	0.03	0.11	0.15	0.12	3	4	2.1
CC US 19	70.09	1.02	1.89	0.02	0.06	0.08	0.47	3	24	2.1
HHC US 08	55.52	2.52	2.84	0.05	0.12	0.17	0.33	4	11	2.1
CC US 16	43.38	0.94	1.98	0.02	0.07	0.09	0.46	3	23	2.1
CC US 15	29.70	1.48	1.38	0.02	0.02	0.04	0.2	1	14	2.1
AS US 09	29.66	1.5	2.42	0	0	0	0.2	0	8	2.1
AS US 04	16.68	0.37	2.39	0	0.02	0.02	0.18	0	7	2.1
CC US 11	16.60	0.91	1.71	0.01	0.08	0.09	0.47	4	27	2.1
CC US 09	8.10	1.71	2.87	0.02	0.12	0.14	0.52	4	18	2.1
CC US 07	6.30	1.75	2.23	0.02	0.04	0.06	0.39	1	17	2.1
CC US 06	5.40	1.34	1.77	0.02	0.06	0.08	0.29	3	16	2.1
CC US 04	3.20	4	1.96	0.01	0.02	0.03	0.48	1	24	2.1
CC US 03	2.20	1.2	2.64	0.01	0.1	0.11	0.23	3	8	2.1
CC US 02	0.80	3.07	1.98	0.02	0.03	0.05	0.23	1	11	2.1
NC DF 01	0.00	0.87	1.23	0.02	0.05	0.07	0.47	4	38	2.1

distillable hydrocarbons present within the rock (mg HC/g rock)

generated hydrocarbons following pyrolysis of kerogen; hydrocarbon generation

potential of the rock (mg HC/g rock)

total hydrocarbon potential of rock (mg HC/g rock)

carbon dioxide generated following kerogen pyrolysis (mg CO<sub>2</sub>/g rock)

hydrogen index (mg generated hydrocarbons/g of organic carbon)

oxygen index (mg generated CO<sub>2</sub>/g of organic carbon)

vitrinite reflectance

S1

S2

S1+S2

S3

H index

O index

%Ro

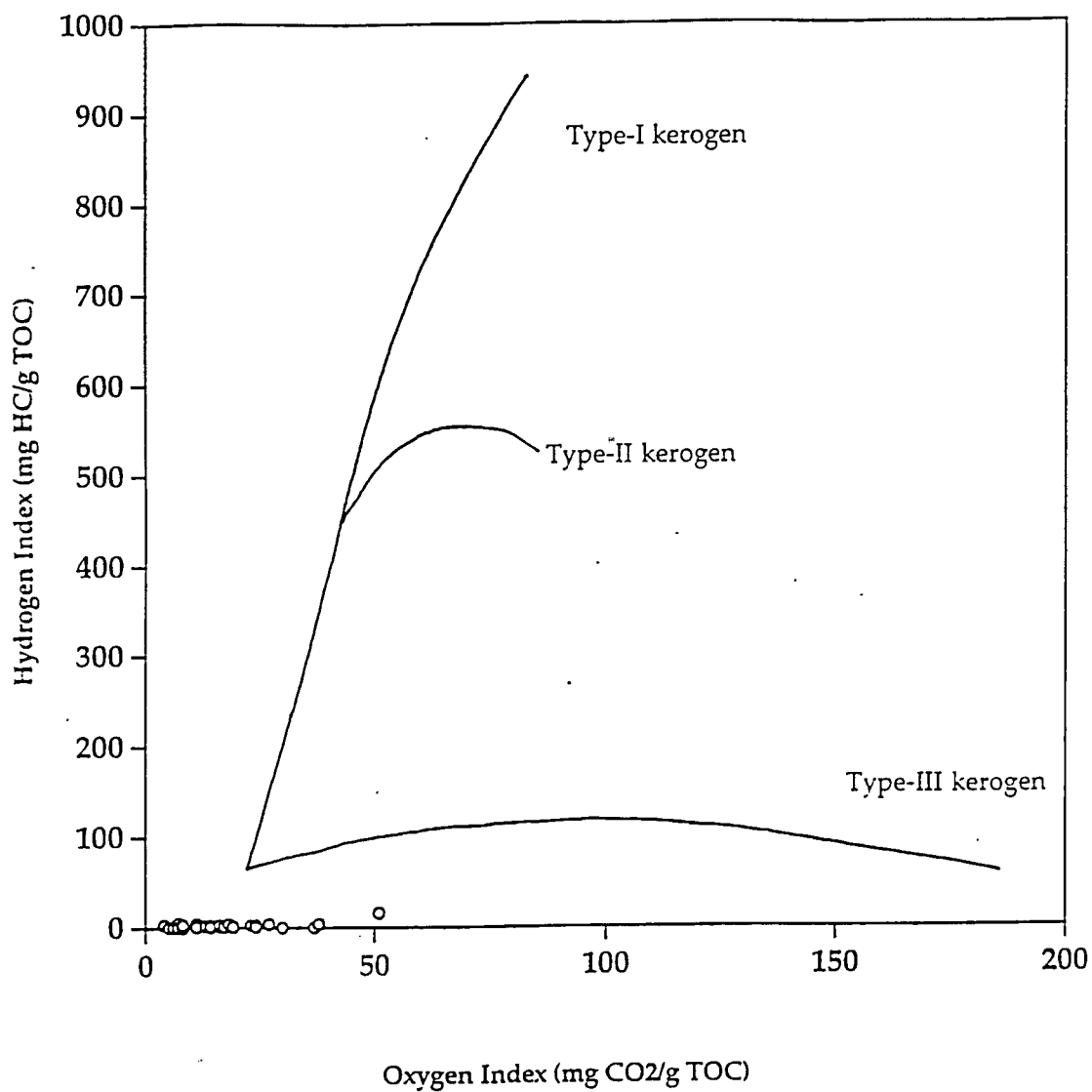


Figure 4.7 - Plot of Hydrogen Index (HI) versus Oxygen Index (OI) of samples from the Taconic Foreland Basin, with plots of average type-I, II, III kerogen trends from Waples (1980).



stored, the growth of fungi on wet samples, which could affect programmed pyrolysis by increasing S1, S2, and S3, was averted (Peters, 1986).

Since all organic matter within the foreland basin is either type-I or type-II in nature, the determination of the approximate original total organic carbon content is possible. By knowing the present-day H/C ratio of a kerogen and its thermal maturity ( $\%R_o$ ), an assessment of the H/C ratio of a kerogen when it was thermally immature can be made (Table XI) (Waples, 1980); consequently one can calculate the original TOC values of a kerogen during its deposition (Waples, 1980). The determinations of the stratigraphic positions samples from the Utica Formation were accomplished by the use of structural contouring principles. For methods concerning the determinations of the inferred stratigraphic positions of the samples see Appendix I. In collaboration with Texaco Inc., three possible scenarios of the type of organic matter deposited on the outer slope of the Taconic Foreland Basin have been pursued. Presently the average TOC value of the Utica Formation is 2.02 wt. % (range 0.47-2.87 wt. % TOC) (Table XI) (Fig. 4.8a). Several relative total organic carbon (TOC) maximums are seen from the analyzed sample data from this study. It would be tempting to identify these as the same maximums proposed by Hay (1982) and Hay and Cisne (1988). However, without the original stratigraphic position of their collected samples, or a detailed explanation of the re-normalization procedure used to standardize their samples, independent confirmation from this study of their TOC maximums within the Utica Formation is impossible. It is highly unfortunate that this is the case; independent verification of Hay and Cisne's (1988) proposed stratigraphic TOC maximums would have strengthened the argument that the Utica Formation has served as an extensive MPSR unit. However, recent work (Delano et al., in press) has indicated that initial attempts made by Hay and Cisne (1988) to reconstruct the original stratigraphy of the Taconic Foreland Basin was incorrect. In addition the TOC variations in the within sample suite from the Utica Formation in this study highlights the need for more dense sampling of the unit and the need for independently correlated, stratigraphic positioning of samples. It is probable that additional relative TOC maximums exist within the

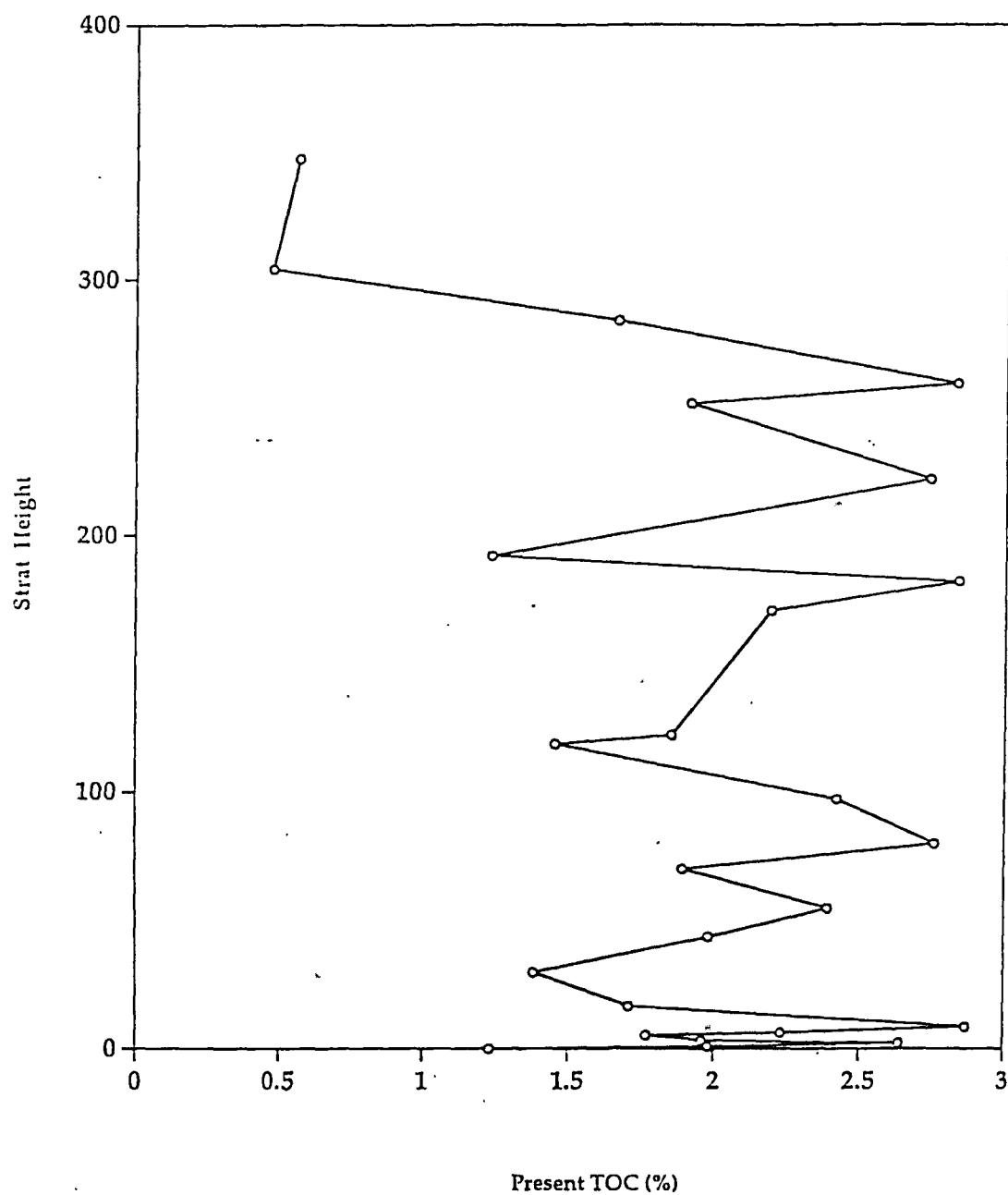


Figure 4.8a - Graph of present day TOC values (%) versus stratigraphic position (meters) of samples from the Utica, Dolgeville, and Frankfort/Schenectady Formations of the Taconic Foreland Basin. Open circles = present day TOC values.

stratigraphic units not yet identified. This is because the TOC variation seen within the densely sampled basal 20 meters of the Utica Formation is as wide as variations seen throughout the entire stratigraphic thickness of the Utica Formation (Fig. 4.8b). Additional TOC sampling of the Utica Formation could show additional maximums existing within the Utica Formation; I suggest that this strong variation in one short stratigraphic interval casts doubt on the existence of only four TOC maximums within the Taconic Foreland Basin as Hay and Cisne (1988) propose.

If the organic matter present within the Taconic Foreland Basin was all of an allochthonous-algal (plant) type-I origin, then approximately 35 percent of the total original organic carbon remains, and the average original organic carbon content within the basin was 5.76 wt. % (range 1.34-8.20 wt. % TOC) (Table XII) (Fig. 4.8b). If instead it was of autochthonous-marine type-II origin, then 50 percent of the total original organic carbon remains, with the average original TOC values at a minimum of 4.03 wt. % (range 0.94-5.74 wt. % TOC) (Table XII) (Fig. 4.8b). A mixture of type-I and II kerogen matter would have produced an average original TOC value within the basin of about 5.04 wt. %, (range 1.18-7.18 wt. % TOC) (Table XII) (Fig. 4.8b) with 40 percent of the original organic matter presently remaining (Bissada, personal communication, 1993). Based upon the reported TOC values from Texaco Inc. (Table XII), it is interpreted that the suite of samples chosen for this study is geographically, as well as stratigraphically, representative of the Taconic Foreland Basin (Bissada, personal communication, 1993). The sampling density of the stratigraphic thickness of the Utica Formation is within parameters (10-30 meters) recommended by Peters (1986) for the effective assessment and interpretation of pyrolysis data (see Peters, 1986). Also, since the variation of TOC values within localized sections of the Utica Formation, such as the Canajoharie section of the pyrolysis transect, is within the same range of values seen throughout the entire transect, the potential problem of one more densely sampled section of the transect dominating the entire transect has been avoided.

Using the type-II kerogen case as a minimum, based upon calculations from Brooks et al. (1987), for every  $1\text{km}^3$  of Utica Formation within the basin undergoing thermal maturation, (as a

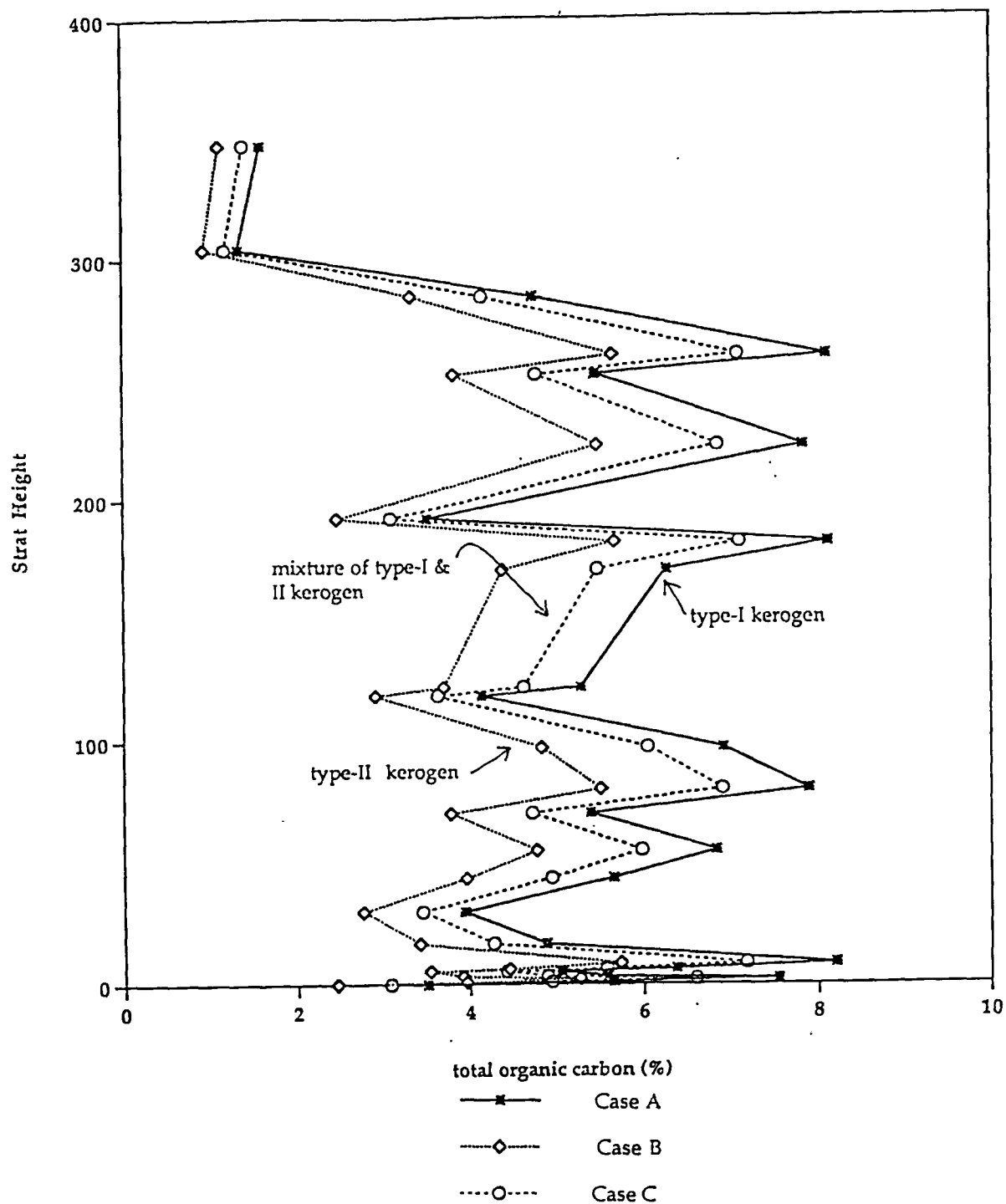


Figure 4.8b - Graph of initial total organic carbon (TOC) values (%) modeling versus stratigraphic position (meters) of samples from the Utica, Dolgeville, and Frankfort/Schenectady Formations of the Taconic Foreland Basin. Stars = Case A : 100% type-I original kerogen; Diamonds = Case B : 100% type-II original kerogen; Open circles = Case C : 66% type-I / 33% type-II initial kerogen mix.

Table XII: Total Organic Carbon (TOC) Modeling, Taconic Foreland Basin

Sample Control Number	Strat Position, m	Total S wt%	Organic C wt%	C/S ratio	Case A	Case B	Case C
OTC FF01	347.44	0.87	0.56	0.64	1.60	1.12	1.40
YC US 02	304.13	1.28	0.47	0.37	1.34	0.94	1.18
BHC US 07	284.12	4.87	1.66	0.34	4.74	3.32	4.15
BHC US 04	251.86	4.74	1.91	0.40	5.46	3.82	4.78
BHC US 01	222.23	2.61	2.74	1.05	7.83	5.48	6.85
YKS US 01	192.07	0.5	1.23	2.46	3.51	2.46	3.08
NC US 08	170.73	3.05	2.19	0.72	6.26	4.38	5.48
TC US 01	122.44	0.85	1.85	2.18	5.29	3.7	4.63
NC US 05	118.90	1.52	1.45	0.95	4.14	2.9	3.63
CC US 21	80.00	1.07	2.76	2.58	7.89	5.52	6.90
HHC US 10	79.21	2.94	2.83	0.96	8.09	5.66	7.08
CC US 19	70.09	1.02	1.89	1.85	5.40	3.78	4.73
HHC US 08	55.52	2.52	2.84	1.13	8.11	5.68	7.10
CC US 16	43.38	0.94	1.98	2.11	5.66	3.96	4.95
CC US 15	29.73	1.48	1.38	0.93	3.94	2.76	3.45
AS US 09	29.66	1.5	2.42	1.61	6.91	4.84	6.05
AS US 04	16.68	0.37	2.39	6.46	6.83	4.78	5.98
CC US 11	16.62	0.91	1.71	1.88	4.89	3.42	4.28
CC US 09	8.51	1.71	2.87	1.68	8.20	5.74	7.18
CC US 07	6.28	1.75	2.23	1.27	6.37	4.46	5.58
CC US 06	5.24	1.34	1.77	1.32	5.06	3.54	4.43
CC US 04	3.23	4	1.96	0.49	5.60	3.92	4.90
CC US 03	2.20	1.2	2.64	2.20	7.54	5.28	6.60
CC US 02	0.88	3.07	1.98	0.64	5.66	3.96	4.95
NC DF 01	0.00	0.87	1.23	1.41	3.51	2.46	3.08
Average, Utica Formation							
		1.92	2.02		5.76	4.03	5.04
Standard Deviation, Utica Formation							
		1.28	0.61		1.75	1.22	1.53

Case A: 100 % type I marine organic matter

Case B: 100% type II marine organic matter

Case C: 66% type I / 33% type II organic matter

consequence of foreland basin thrust loading or sediment burial), at least  $175 \times 10^6$  barrels of oil would have been generated during optimum conditions. Comparing this to calculated production of the late medial Cretaceous La Luna Formation, which is the source rock for the Maracaibo Basin,  $290 \times 10^6$  barrels of oil per  $1\text{km}^3$ , demonstrates that the late medial Ordovician Utica Formation must have been an extensive, prolific, marine petroleum source rock (MPSR) unit, although it is now completely spent.

A more difficult question to resolve is when did hydrocarbon production within the Utica Formation actually commence. Based upon the observation that large-scale production of hydrocarbons from type-II kerogen begins at  $80^\circ\text{C}$  (Brooks et al, 1990), and assuming a continental lithospheric thermal gradient of  $25^\circ\text{C}/\text{km}$ , at least 3.2 kilometers of sediment burial would have been needed to initiate hydrocarbon production within the Utica Formation. With the combined stratigraphic thickness of the overlying late Ordovician Lorraine Group and Queenston Formations (approximately 500 meters), petroleum conversion could not have occurred in the sampled portion of the Taconic Foreland Basin during Ordovician times. The existence of the Silurian unconformity within the Taconic Foreland Basin makes it tempting to hypothesize that hydrocarbon generation could have commenced as early as Silurian times, being arrested following the occurrence of the major erosional event. This would have been similar to the arresting of petroleum production from the La Luna Formation within the Maracaibo Basin during Oligocene times (Bockmeulen et al., 1983; Pindell, 1991). This would necessitate the existence of Silurian-age derived oils showing the effects of contamination. However, even allowing for erosion below the Devonian-Silurian unconformity, it is unlikely that sufficient quantities of Silurian sediments were deposited to initiate petroleum generation during Silurian times (Kidd, personal communication, 1993). A more plausible explanation is that the deposition of at least 2.5 kilometers of Devonian-age sediments within the eastern Acadian Foreland Basin triggered full-scale petroleum production from the Utica Formation during late Devonian times about 370 Myr ago.

#### 4.3.2 Verification of Anoxic Conditions During Deposition of the Utica Formation

Authigenic pyrite is formed by the reaction of detrital iron minerals with  $H_2S$ , while  $H_2S$ , in turn, is produced from the reduction of interstitial sulfate by bacteria using sedimentary organic matter as a reducing agent and as an energy source (Berner, 1983). The general scheme of the key reactions governing  $S_{pyrite}$  formation (Fig. 4.9), shows that three components, (a) the amount and quality of organic matter, (b) iron-detrital minerals, (c) and the availability of sulfate, are the key factors ultimately controlling  $S_{pyrite}$  formation. Each of the three reagents consequently can act as a limiting factor for  $S_{pyrite}$  formation under different sedimentary environments (Berner, 1983).

In marine oxic conditions,  $S_{pyrite}$  production is controlled by the quality and quantity of organic matter being deposited, with a positive correlation existing between  $S_{pyrite}$  and  $C_{org}$  concentrations from 0.4 to 3.0 wt.%  $C_{org}$  (Demailson and Moore, 1980). Areas with high sedimentation rates, such as upwelling zones, allow for the rapid burial of organic matter. If  $C_{org}$  fluxes are large enough, following consumption of oxygen within the water column, commencement of sulfate reduction occurs, producing free  $H_2S$  at some depth below the sediment-water interface, which by reaction with iron-minerals, allows for the eventual formation of  $S_{pyrite}$ . Using a plot of  $S_{pyrite}$  versus  $C_{org}$  matter concentrations, verification of a correlation between the two in marine oxic environments is seen, with present-day sediments containing less than 1.0 wt. %  $S_{pyrite}$  for every 2.0 wt. %  $C_{org}$  matter (Berner, 1983).

In freshwater conditions however, sulfate concentrations are usually two orders of magnitude lower than in marine oxic environments. Consequently,  $S_{pyrite}$  formation is limited by sulfate availability, which becomes quickly exhausted under such conditions. This results in a poor correlation between  $C_{org}$  and  $S_{pyrite}$  formation (Fig. 6, of Berner, 1983), thus  $S_{pyrite}$  is essentially independent of  $C_{org}$  values in freshwater environments. (Berner, 1983).

Under marine anoxic conditions,  $O_2$  has already been consumed within the water column and  $H_2S$  is present in the bottom waters of the water column, allowing the production of  $S_{pyrite}$

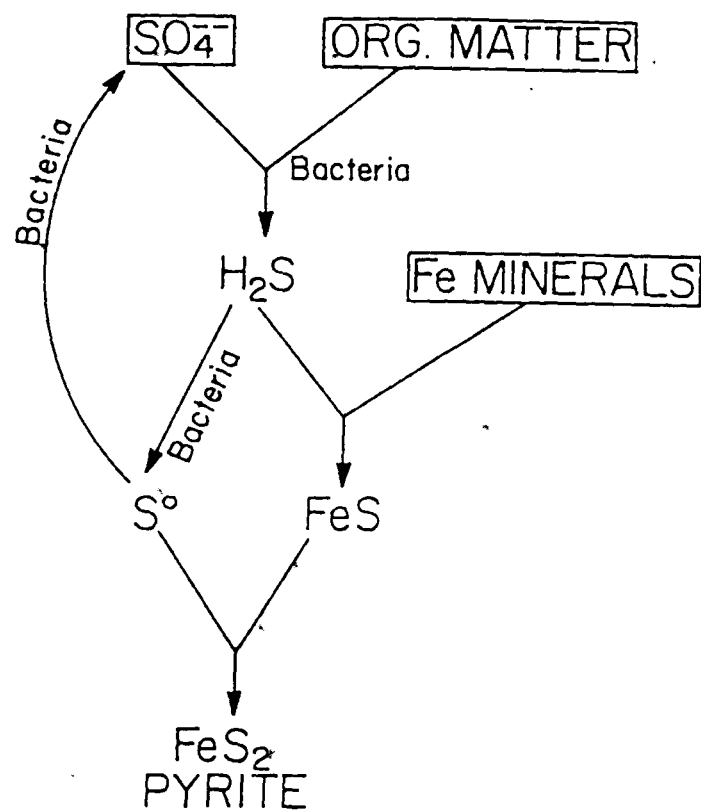


Figure 4.9 - Diagrammatic representation of the overall process of sedimentary pyrite formation (After Berner, 1972) (From Berner, 1983).



both at and below the sediment-water interface. Consequently,  $S_{pyrite}$  also exhibits a poor correlation with  $C_{org}$ , with low organic carbon concentrations possessing higher  $S_{pyrite}$  concentrations relative to present-day marine oxic environments (Berner, 1983). Therefore, a plot of  $S_{pyrite}$  versus  $C_{org}$  concentrations of samples from the Taconic Foreland Basin should confirm the existence of anoxic conditions during the deposition of the Utica Formation (Fig. 4.10; Table XII). For this study, it is assumed that the concentration of  $S_{pyrite}$  within a sample is equal to the total sulfur concentration of the sample.

Analysis of Figure 4.10 shows that qualitatively, anoxic conditions did exist on the outer slope of the foreland basin. The larger spread of values of the Taconic Foreland Basin however, both above and below the regression line, are a consequence of several factors. When sediments are composed almost entirely of calcium carbonate ( $CaCO_3$ ), there are insufficient detrital iron-minerals to produce pronounced  $S_{pyrite}$  within the sediment column. Even with an abundance of sulfate,  $H_2S$ , and  $C_{org}$  within the sediment column, if the sediment is dominated by  $CaCO_3$ ,  $S_{pyrite}$  formation will always be limited (Berner, 1983), elevating  $C_{org}/S_{pyrite}$  ratios relative to normal anoxic conditions observed in Figure 4.10.

Because terrestrially-derived plant material did not develop until the late Early Silurian (Spicer, 1989), the Utica Formation could only have contained autochthonous-marine and allochthonous-algal derived organic matter buried within the marine realm. The present-day marine anoxic  $C_{org}/S_{pyrite}$  values shown in Fig. 4.10 are a consequence of up to 50% of the organic carbon being derived from refractory, highly resistant, type-III kerogen organic matter. Without this 'inert' organic matter being present during Ordovician times, marine anoxic  $C_{org}/S_{pyrite}$  values would be lower than observed under present-day conditions, since organic matter consumption would have been more efficient, resulting in lower  $C_{org}/S_{pyrite}$  ratios. This is possibly indicated for samples from the Taconic Foreland Basin (Fig. 4.10); with samples perhaps plotting closer to the normal marine-oxic conditions regression line established for Quaternary marine sediments.

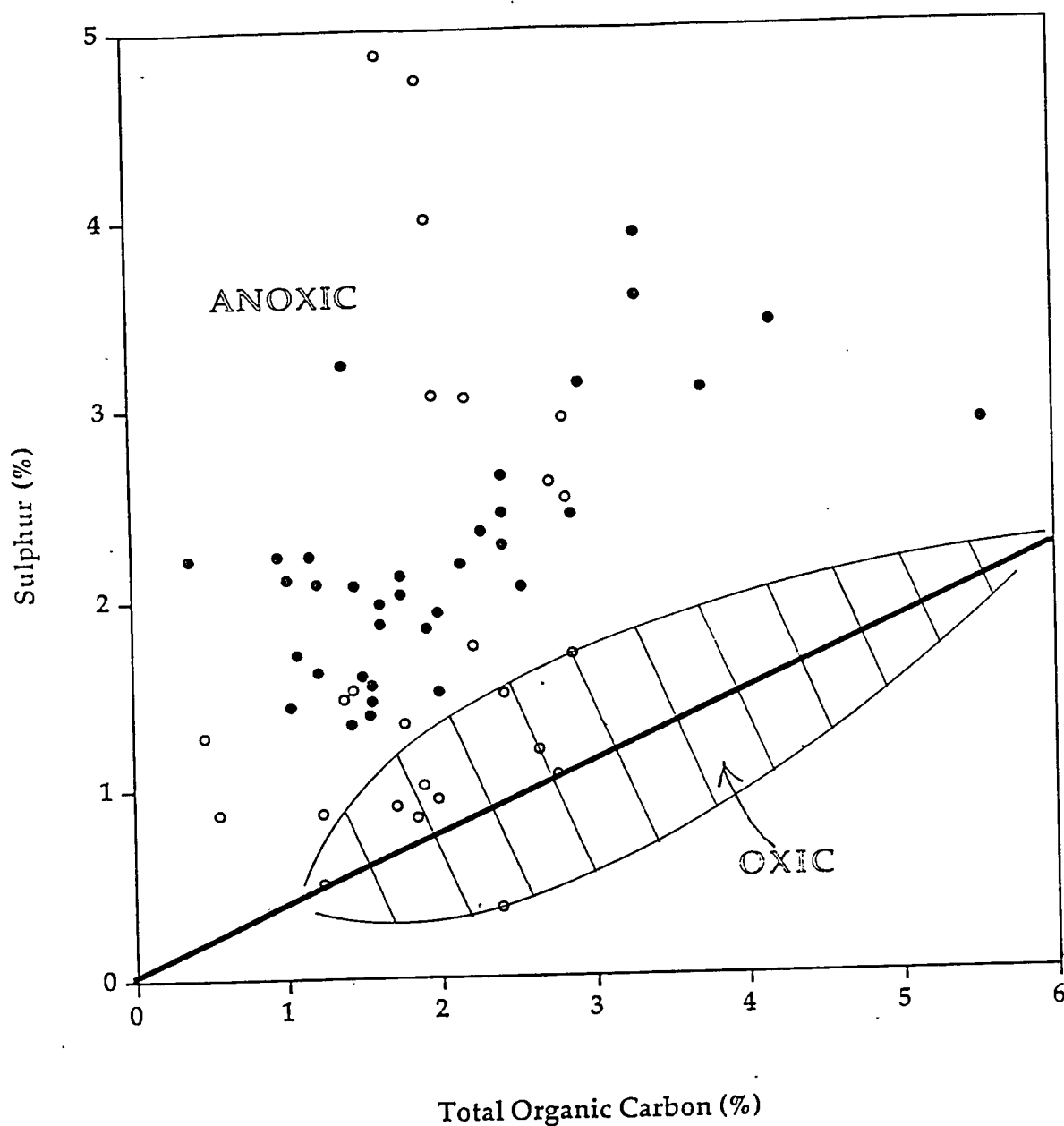


Figure 4.10 - Plot of present day total S<sub>pyrite</sub> (%) = Total sulfur (%) versus present day Total Organic Carbon (%) for samples of the Taconic Foreland Basin. Also plotted is the relationship between organic carbon content and (pyritic) sulfur in marine environments. Distinction between oxic and anoxic environments according to Leventhal (1983) and Berner (1984). For Quaternary normal marine, fine-grained detrital sediment, mean C/S ratio = 2.8 (Berner, 1984; Goldhaber and Kaplan, 1974); envelope of regression line encloses several hundred data points (Berner, 1989). Solid filled dots = from Black Sea sediments (Taken from Stein, 1991); Open circles = Utica Formation samples. Utica Formation data plotted are present day TOC values because possible changes in Total S<sub>pyrite</sub> (%) during maturation are not established.

In addition, if  $S_{\text{pyrite}}$  was forming under true anoxic conditions during the deposition of the Utica Formation,  $C_{\text{org}}/S_{\text{pyrite}}$  ratios would also be lower than those observed in Figure 4.10, since less  $C_{\text{org}}$  would be needed for the production of  $S_{\text{pyrite}}$  within the sediment column. Under anoxic conditions, where sedimentation rates and  $C_{\text{org}}$  flux rates can be low, maximization of  $S_{\text{pyrite}}$  production would have occurred since the residence time of reactive detrital iron-minerals for reaction with free  $\text{H}_2\text{S}$  would have been longer (Berner, 1983).

The presence of elevated concentrations of uranium within samples from the Taconic Foreland Basin are also indicative of the establishment of anoxic conditions on the outer slope of the foreland basin during deposition of the Utica Formation (Demailson and Moore, 1980) (Fig. 4.11), with the likely source of the additional uranium coming from seawater (Hein et al., 1987). The preferential extraction of uranium from seawater occurs, under anaerobic conditions, by the reduction of dissolved  $\text{U}^{6+}$  ions to less soluble  $\text{U}^{4+}$  in the presence of decaying organic matter. The presence of  $\text{H}_2\text{S}$  above the sediment-water interface, a consequence of bacterial sulfate reduction, also helps to increase the rate of  $\text{U}^{6+}$  reduction and its incorporation into previously-deposited organic matter (Hein et al., 1987). The inferred subsequent remobilization of  $\text{U}^{4+}$  probably occurred when thermal maturation and diagenesis of the MPSR unit developed, causing degradation of the organic-rich Utica Formation. The appearance of a correlation between  $\text{P}_2\text{O}_5$  and U concentrations (Fig. 4.12) also points towards the notion that phosphatic material (i.e degraded organic matter), which normally contains abundant uranium, served as the primary source for the bulk of the uranium present (Hein et al., 1987).

A general trend of enrichment of Co, Cu, and Ni concentrations is also seen within the lower 40 meters of the Taconic Foreland Basin samples, relative to PAAS (Post-Archean Average Shale). It is interpreted, within the context of this thesis, that implies infers the existence of long term anoxic conditions during their deposition (Demailson and Moore, 1980). Also, based upon major and trace element analyses from McGill University, oxic bottom water conditions are interpreted to have been re-established within the Taconic Foreland Basin during deposition of the upper 100

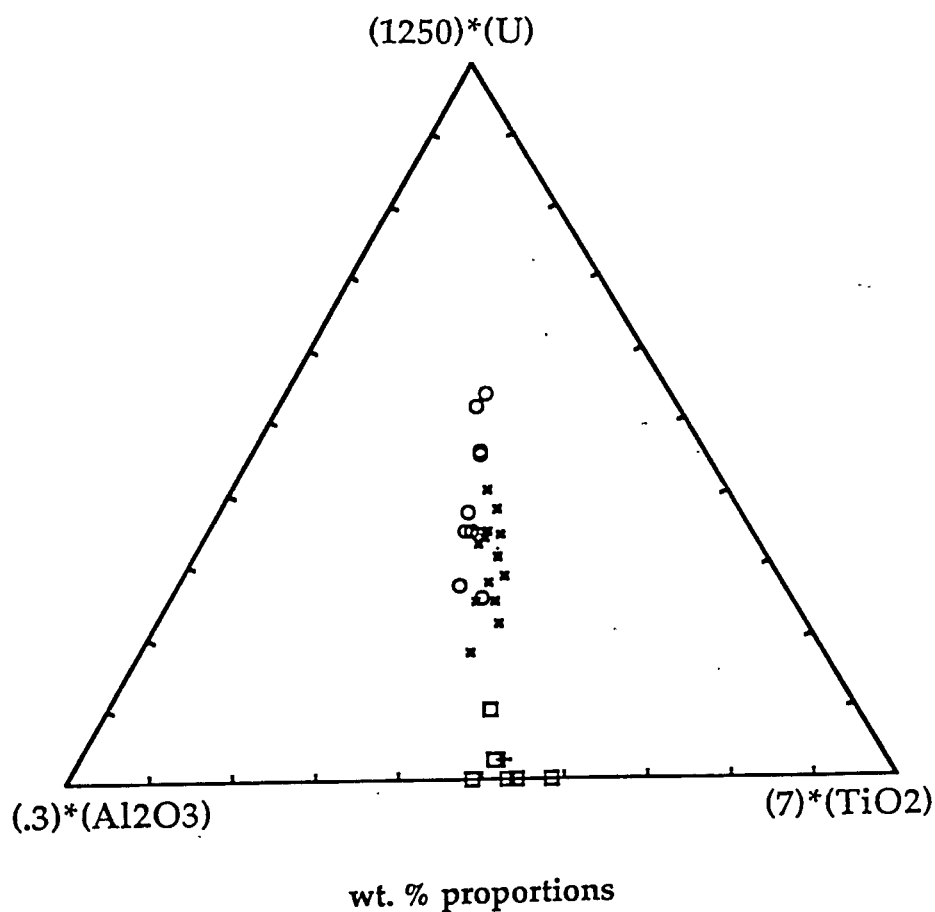


Figure 4.11 - Ternary plot of Al<sub>2</sub>O<sub>3</sub>-U-TiO<sub>2</sub> concentrations of Taconic Foreland Basin samples. Open circles = samples within first 25 meters of stratigraphic section; X-marks = samples within lower 25 to approximately 150 meters of stratigraphic section; Squares = samples approximately 150 meters and higher in stratigraphic section; Cross = Post Archean Average Shale. Note that samples above 150 meters of section (Nowadaga Creek, Yatesville Creek, Otsquago Creek, Route 171 samples) plot within the area that PAAS occupies within Al<sub>2</sub>O<sub>3</sub>-U-TiO<sub>2</sub> space.

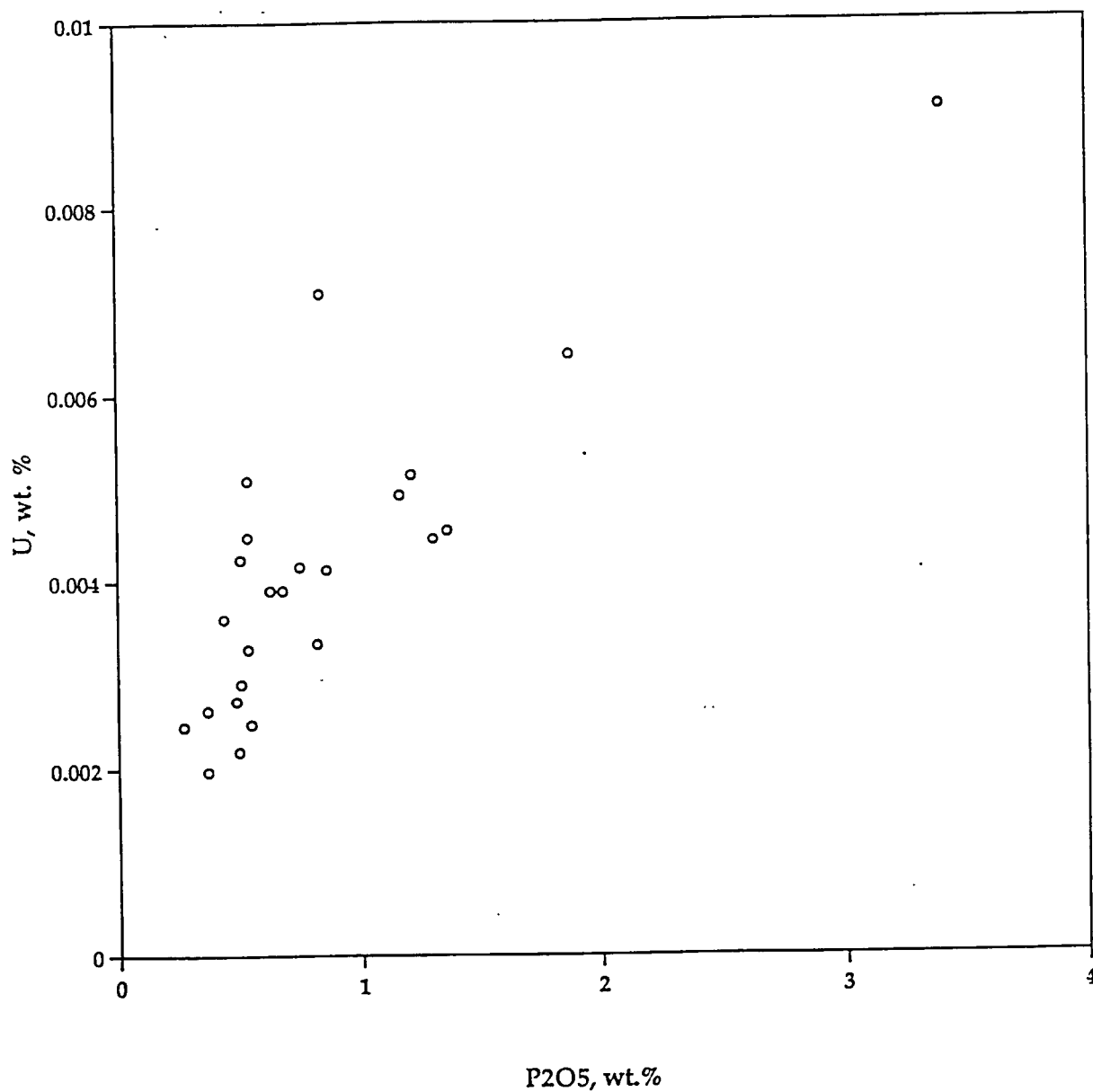


Figure 4.12 - Plot of U versus P<sub>2</sub>O<sub>5</sub> (LOI - CaO free weight basis) concentrations of Taconic Foreland Basin samples. Open circles = samples done for XRF analysis at University of Mass. and McGill University.

meters of the Utica Formation. This is inferred from U concentrations of the Nowadaga Creek, Yatesville Creek, and overlying samples plotting close to PAAS observed concentrations within  $\text{Al}_2\text{O}_3$ -U-TiO<sub>2</sub> space (Fig. 4.12).

#### 4.3.3 Establishment of Primary Productivity Conditions within the Taconic Foreland Basin

From major element oxide analyses, performed at the University of Massachusetts at Amherst and at McGill University on a suite of samples from the Taconic Foreland Basin (Table XIII), an assessment of the possible existence of high primary organic productivity conditions, relative to detrital sedimentation rate, was made. The effects of diagenesis and thermal maturation however, allows only for a qualitative estimate of the existence of high primary productivity conditions during deposition of the Utica Formation. Determination of the potential quantity of marine organic matter produced within the basin is unattainable; consequently, elements chosen as representative indicators of high primary productivity (such as P and Ba concentrations on a CaO-LOI free weight basis) can only be considered as proxies for the establishment of the spatial and temporal existence of high primary productivity on the outer slope of the collisional foreland basin.

Phosphates are consumed by planktonic organisms in surficial waters; on dying, these fall through the water column as 'organic rain'. Through the oxidation of decaying organic matter, a phosphate 'sink' exists in the deep ocean, 500-1000 meters below the surface. Due to the mechanics of upwelling currents however, surface waters depleted in phosphates can be continually replenished with nutrient-rich (phosphate-enriched), deeper, oceanic water (Hein et al., 1987; Parrish, 1982). Following planktonic consumption, decaying organic matter deposited on sea bottoms may experience the effects of long-term anoxic conditions. If the conditions are anoxic this would result in the concentration of phosphate in the deposited bottom sediments, due to the inability of the deposited organic matter to be microbially degraded (Hein et al., 1987). Therefore high  $P_2O_5$  concentrations within a deposited sediment should be indicative of high primary productivity during the time of its deposition. A plot of  $TiO_2$ - $Al_2O_3$ - $P_2O_5$  concentrations of samples from the Taconic Foreland Basin points to the possibility of enhanced primary

Table XIII: Major Element Analyses, Taconic Foreland Basin

Sample	Strat Height (m)	SiO <sub>2</sub>	TiO <sub>2</sub>	Al <sub>2</sub> O <sub>3</sub>	ΣFe	MnO	MgO	CaO	Na <sub>2</sub> O	K <sub>2</sub> O	P <sub>2</sub> O <sub>5</sub>	MC LOI	SUNYA LOI	Total
NASC1		64.8	0.78	16.9	5.7	0.06	2.85	3.56	1.15	3.99	0.11			99.9
NASC2		64.82	0.79	16.88	5.59	0.07	2.86	3.68	1.12	3.87	0.17			99.85
PAAS		62.8	1	18.9	6.5	0.11	2.2	1.3	1.2	3.7	0.16			97.87
MC CCUS 02	0.88	13.28	0.16	3.69	1.96	0.04	1.36	41.83	0.26	0.65	0.30	35.22	34.70	98.80
MC CCUS 03	2.20	7.68	0.10	2.07	0.89	0.05	1.43	47.23	0.22	0.33	0.45	39.41	39.38	99.89
MC CCUS 04	3.23	15.79	0.20	4.79	2.65	0.04	1.84	38.97	0.30	0.89	0.22	33.38	32.21	99.10
MC CCUS 06	5.24	13.40	0.16	3.62	1.19	0.04	1.79	42.79	0.30	0.57	0.26	35.77	35.78	99.95
MC CCUS 08	7.50	13.50	0.18	3.98	1.40	0.04	1.87	41.85	0.29	0.71	0.26	35.47	35.31	99.60
MC CCUS 09	8.51	15.79	0.19	3.99	1.20	0.04	1.78	39.53	0.39	0.79	0.32	35.18	34.99	99.22
MC CCUS 10	9.60	11.98	0.13	2.64	1.14	0.04	1.51	44.03	0.35	0.48	0.35	37.19	37.08	99.87
MC ASUS 03	14.12	24.29	0.24	4.98	2.24	0.04	3.07	32.71	0.27	0.99	0.20	30.98	29.77	100.10
MC ASUS 04	16.68	17.44	0.13	2.47	0.79	0.02	0.98	41.96	0.21	0.38	0.19	35.59	35.36	100.20
MC CCUS 13	24.97	18.20	0.11	2.23	0.94	0.02	1.43	41.86	0.27	0.39	0.12	34.77	34.64	100.38
MC ASUS 08	27.56	25.84	0.32	7.12	2.44	0.03	2.82	30.03	0.28	1.34	0.15	29.15	28.31	99.58
MC ASUS 10	38.31	22.99	0.24	5.01	1.79	0.02	1.73	35.33	0.37	0.93	0.21	31.42	30.50	100.09
MC ASUS 11	40.98	17.92	0.20	4.18	1.74	0.03	1.59	39.85	0.22	0.63	0.23	33.56	32.71	100.19
MC CCUS 16	43.38	15.88	0.18	3.65	1.18	0.02	2.03	40.72	0.37	0.64	0.18	35.38	34.14	100.27
MC ASUS 12	52.56	32.98	0.21	3.89	1.05	0.02	1.35	31.86	0.48	0.76	0.11	27.54	26.96	100.28
MC CCUS 19	70.09	21.98	0.24	4.49	1.78	0.03	2.05	35.56	0.40	0.88	0.16	32.03	31.41	99.64
MC ASUS 14	72.26	22.51	0.21	4.12	1.36	0.02	1.30	37.30	0.35	0.75	0.21	32.13	32.25	100.31
MC NCUS 04	100.61	22.07	0.27	5.30	2.42	0.04	1.96	35.43	0.46	0.96	0.18	31.20	28.66	100.35
MC NCUS 05	118.90	28.37	0.31	5.86	2.33	0.03	1.63	31.58	0.59	1.16	0.20	28.17	27.43	100.30
MC TC US 01	122.44	28.02	0.24	4.25	1.22	0.03	0.86	34.41	0.54	0.82	0.16	29.66	27.12	100.25
MC TCUS 02	136.95	26.02	0.27	5.75	2.09	0.04	2.28	32.01	0.39	1.08	0.14	29.78	26.74	99.89
MC SCUS 01	148.35	22.95	0.22	3.97	1.37	0.03	1.45	37.07	0.45	0.76	0.17	31.87	31.52	100.36
MC SCUS 02	178.84	32.30	0.32	5.64	2.65	0.04	1.94	28.38	0.59	1.13	0.23	26.97	26.03	100.25
MC YKSUS 01	192.07	19.15	0.19	3.69	1.66	0.04	1.77	39.27	0.35	0.62	0.15	33.36	33.25	100.29
MC JWD STD		50.25	0.95	20.86	7.99	0.05	2.76	4.52	0.86	4.65	0.16	8.27	7.65	101.47
UM 171 FF 02	255.78	61.94	0.99	18.43	7.50	0.09	3.19	0.99	0.83	4.62	0.16		5.13	98.74
UM YC FF 02	326.13	61.21	1.10	16.46	6.49	0.07	2.20	1.06	1.15	4.25	0.16		3.12	94.13
UM YC FF 01	318.30	63.81	0.99	17.49	6.52	0.09	2.83	2.39	1.19	4.17	0.15		5.69	99.61
UM NCUS 08	170.73	51.49	0.52	10.37	5.93	0.07	2.41	21.17	0.95	0.29	0.29		16.94	93.47
UM NCUS 06	143.29	53.95	0.66	13.09	4.81	0.07	2.44	18.35	0.90	3.00	0.34		16.63	97.62
UM OTC FF 01	347.44												5.26	

MC: McGill University analyses

UM: University of Mass. samples



productivity conditions, relative to detrital sedimentation rate, during deposition of the organic-rich Utica Formation (Figure 4.13). The standard chosen for this study, Post-Archean Average Shale (PAAS), is thought to be representative of shales deposited under normal oxic conditions and indicative of average primary biological productivity conditions.  $\text{TiO}_2$  and  $\text{Al}_2\text{O}_3$  were used as coplotted elements in ternary diagrams, used in this study, because they are thought to represent the detrital component of the organic-rich shales of the Utica Formation and are resistant to diagenetic mobilization following deposition. Because the  $\text{TiO}_2/\text{Al}_2\text{O}_3$  ratio of samples chosen for analysis remain relatively constant throughout the entire stratigraphic thickness of the Utica Formation, plotting elements that are thought to be proxies of specific conditions existing during deposition of the Utica Formation (e.g.,  $\text{P}_2\text{O}_5$  for the proxy of enhanced biological productivity) against their relatively constant  $\text{TiO}_2/\text{Al}_2\text{O}_3$  ratios should identify specific conditions, (e.g., enhanced primary productivity), on the outer slope of the foreland basin. Using the same methodology, a plot of  $\text{P}_2\text{O}_5/\text{Al}_2\text{O}_3$  and/or  $\text{P}_2\text{O}_5/\text{TiO}_2$  versus stratigraphic height of samples from the Taconic Foreland Basin shows that the highest degree of biological enrichment is within the first 25 meters of the Utica Formation (Fig 4.14; Fig 4.15). This enrichment is considered the result of very low detrital sedimentation rates existing during contemporaneous organic deposition of biogenic debris within the first 25 meters of the Utica Formation.

Barium has also been determined to be a proxy of the nutrient content of the ocean, with barium enrichments in sediments being interpreted as indicating the deposition of those sediments under a high productivity paleo-upwelling site (Stein, 1991). Barium has been previously recognized as a biologic productivity indicator by Goldberg (1958). This is a consequence of the inorganic precipitation of barite in the presence of decaying organic matter. As with Figure 4.14, a plot of  $\text{TiO}_2$ - $\text{Al}_2\text{O}_3$ - $\text{BaO}$  concentrations of samples from the Taconic Foreland Basin could also point to the possibility of high primary productivity conditions, relative to detrital sedimentation rate, existing on the outer slope of the Taconic Foreland Basin during deposition of the Utica Formation. However, this is not observed to be the case (Fig. 4.16), with all samples of the Taconic

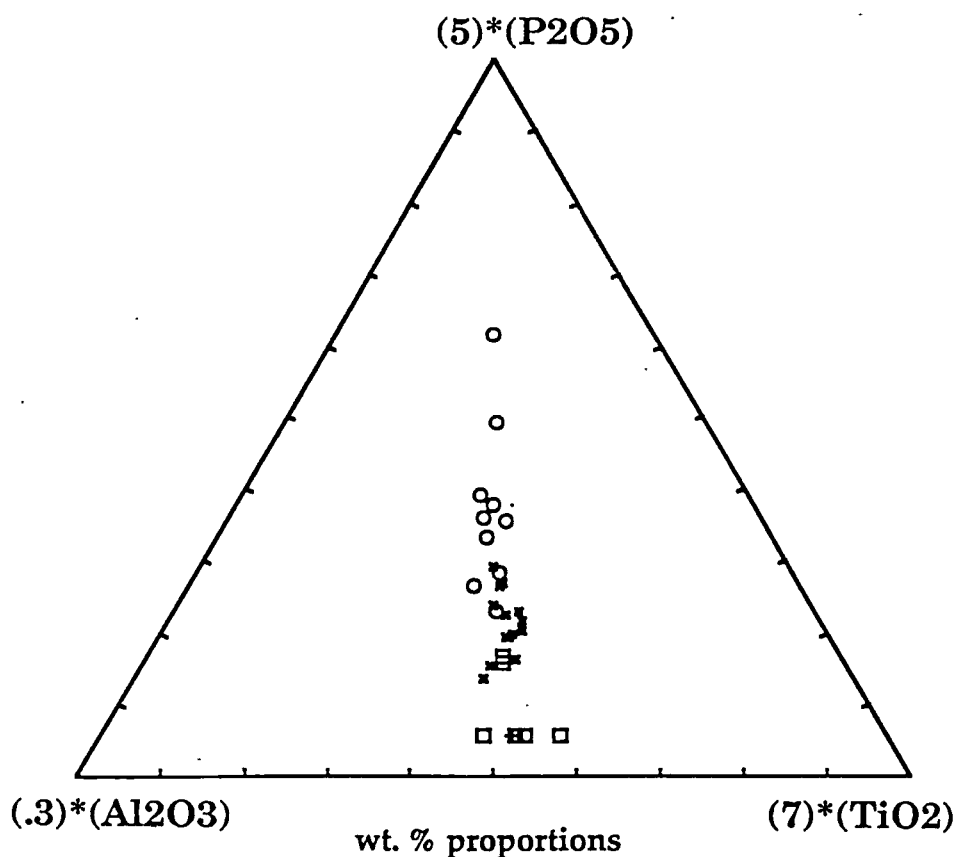


Figure 4.13 - Ternary plot of  $\text{Al}_2\text{O}_3$ - $\text{P}_2\text{O}_5$ - $\text{TiO}_2$  concentrations of Taconic Foreland Basin samples. Open circles = samples within first 25 meters of stratigraphic section; X-marks = samples approximately between 25 meters and 150 meters of stratigraphic section; Squares = samples approximately 150 meters and higher; Cross = Post Archean Average Shale. Note that samples above 150 meters of section (Nowadaga Creek, Yatesville Creek, Otsquago Creek, Route 171 samples) plot within the area PAAS occupies within  $\text{Al}_2\text{O}_3$ - $\text{P}_2\text{O}_5$ - $\text{TiO}_2$  space.

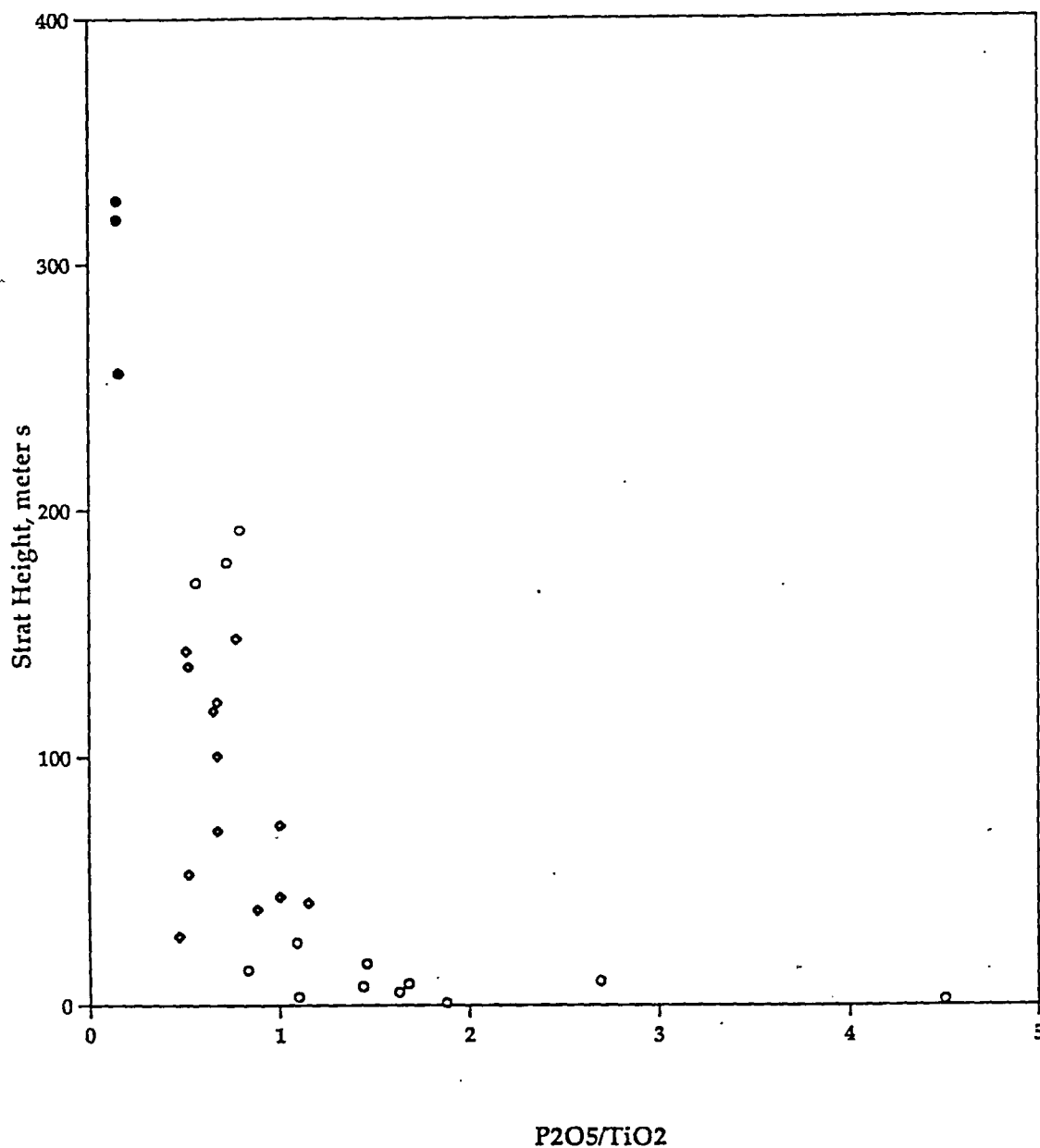


Figure 4.14 - Plot of  $P_2O_5/TiO_2$  (LOI - CaO free weight concentrations) versus stratigraphic height of Taconic Foreland Basin samples. Open circles = samples within first 25 meters of stratigraphic section; Diamonds = samples approximately between 25 meters and 150 meters of stratigraphic section; Closed circles = samples approximately 150 meters and higher (Nowadaga Creek, Yatesville Creek, Otsquago Creek, Route 171 samples).

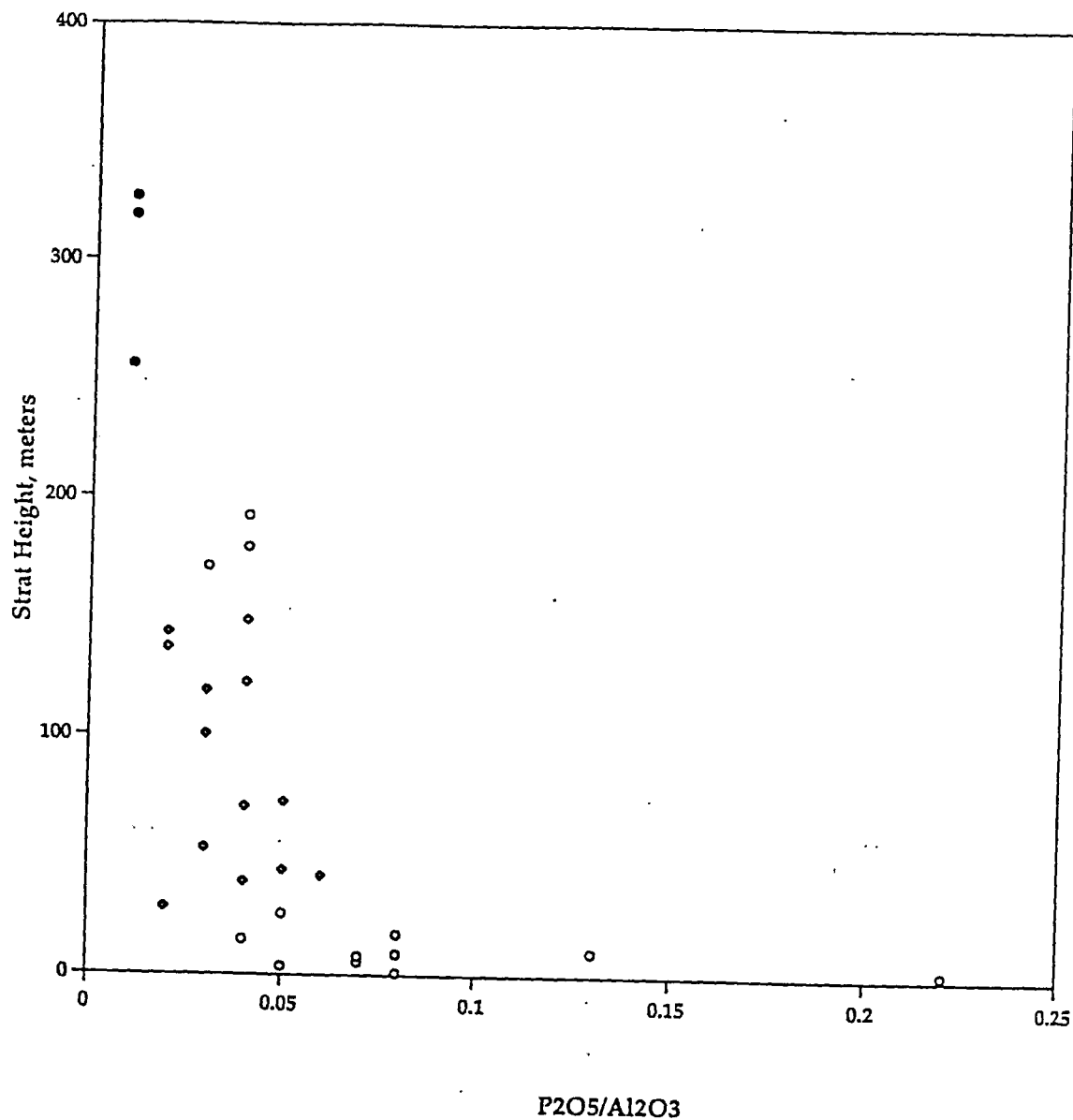


Figure 4.15 - Plot of  $P_2O_5/Al_2O_3$  (LOI - CaO free weight concentrations) versus stratigraphic height of Taconic Foreland Basin samples. Open circles = samples within first 25 meters of stratigraphic section; Diamonds = samples approximately between 25 meters and 150 meters of stratigraphic section; Closed circles = samples approximately 150 meters and higher (Nowadaga Creek, Yatesville Creek, Otsquago Creek, Route 171 samples).

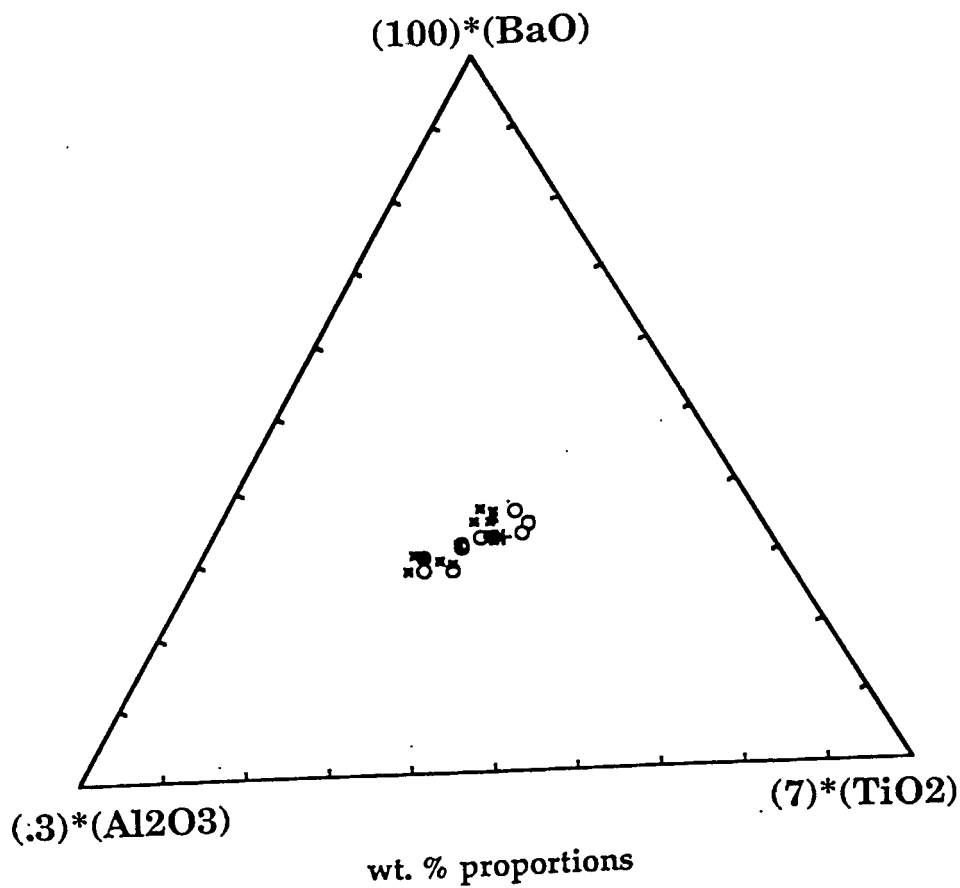


Figure 4.16 - Ternary plot of Al<sub>2</sub>O<sub>3</sub>-BaO-TiO<sub>2</sub> concentrations of Taconic Foreland Basin samples. Open circles = samples within first 25 meters of stratigraphic section; X-marks = samples approximately between 25 meters and 150 meters meters of stratigraphic section; Cross = Post Archean Average Shale.

Foreland Basin chosen for analysis plotting within the same field. Plots of  $\text{BaO}/\text{TiO}_2$  versus stratigraphic height (Fig 4.17), as well as  $\text{BaO}/\text{Al}_2\text{O}_3$  versus stratigraphic height (Fig 4.18), are also inconclusive regarding the interpretation that the first 25 meters within the Utica Formation is the most biologically enriched within the unit. The observation that all samples possess the same relative Ba concentrations may be the result of several processes occurring. First, as mentioned earlier, thermal maturation of the MPSR unit has probably resulted in diagenetic remobilization of original Ba concentrations within the Taconic Foreland Basin. Another possibility is that feldspars, derived from the volcanic arc complex colliding with the eastern Laurentian passive margin, may have had Ba incorporated into the mineral lattice structure. This would have enabled an additional potential source of Ba to have existed during the phase of high clastic, and low biologic, input at the late stages of the foreland basin sedimentation. This could have resulted in relative Ba concentrations remaining similar to the earlier phase of low clastic input and high biologic productivity in the overlying water column. Ultimately, additional biological proxies, more resistant to the effects of diagenetic remobilization, such as Cd, will have to be analyzed in order to help determine the degree to which biologic productivity played in producing a prolific MPSR unit within the Taconic Foreland Basin during late medial Ordovician times.

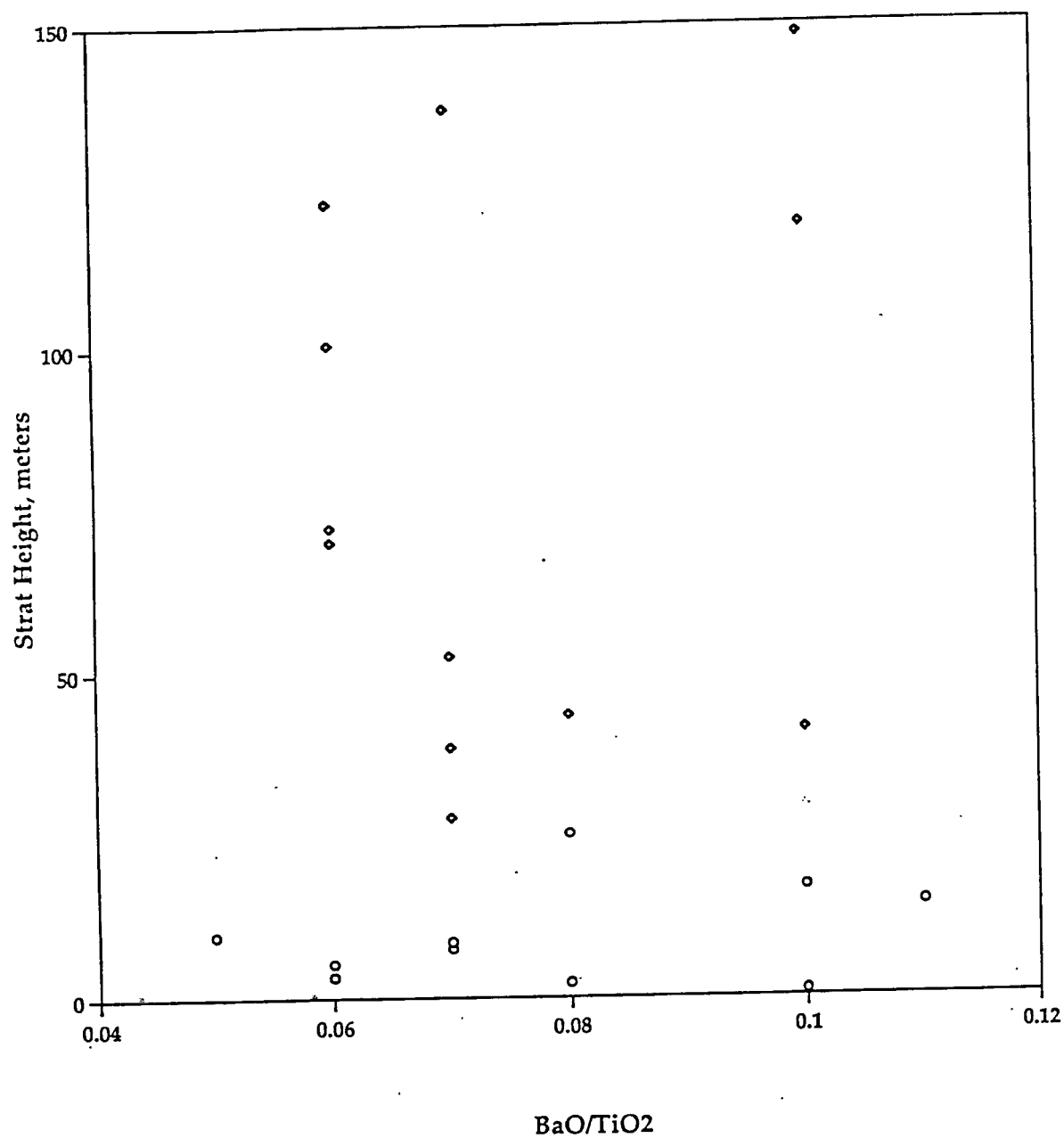


Figure 4.17 - Plot of BaO/TiO<sub>2</sub> (LOI - CaO free weight concentrations) versus stratigraphic height of Taconic Foreland Basin samples. Open circles = samples between first 25 meters of stratigraphic section; Diamonds = samples approximately within 25 meters and 150 meters of stratigraphic section.

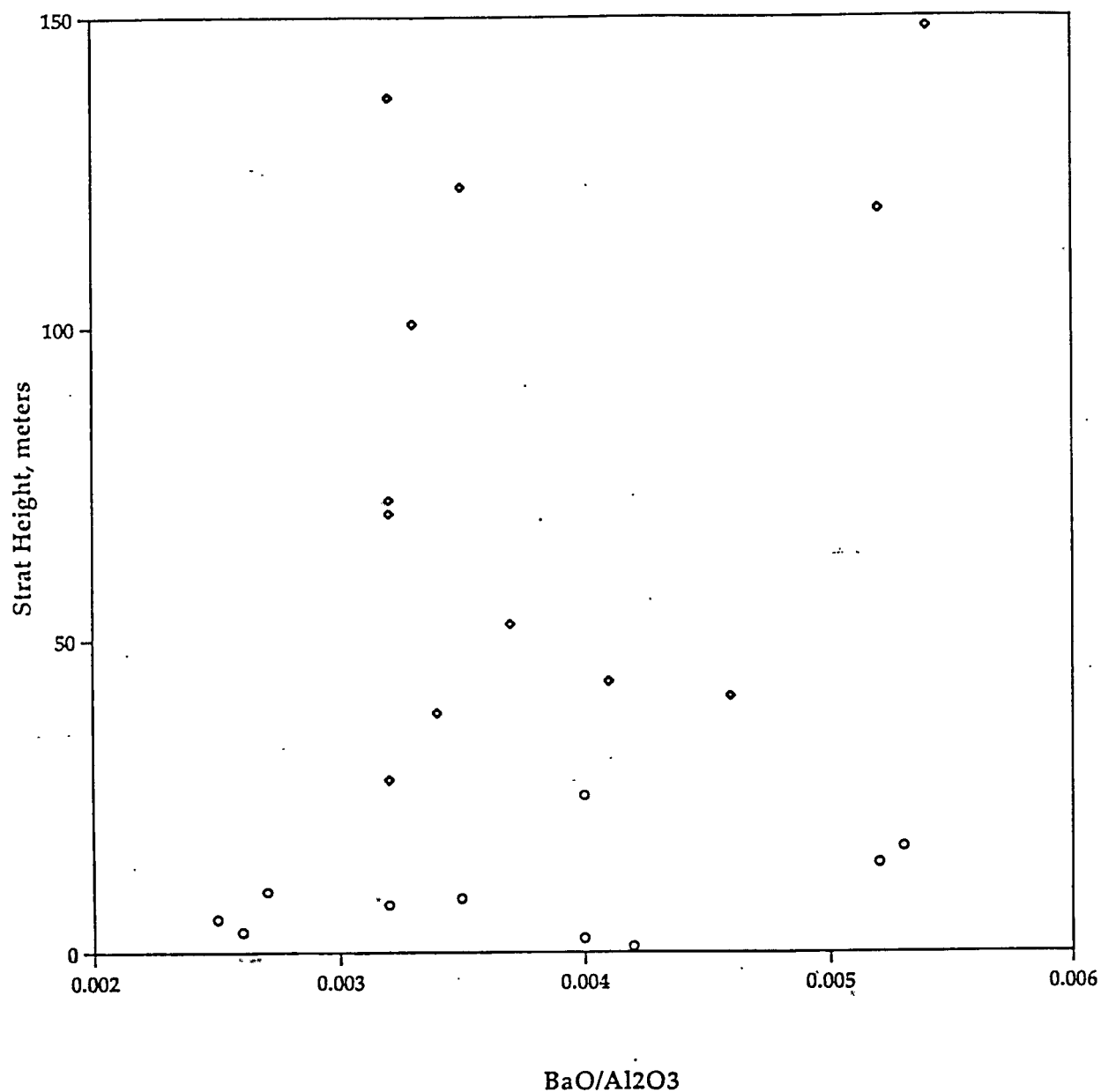


Figure 4.18 - Plot of BaO/Al<sub>2</sub>O<sub>3</sub> (LOI - CaO free weight concentrations) versus stratigraphic height of Taconic Foreland Basin samples. Open circles = samples between first 25 meters of stratigraphic section; Diamonds = samples approximately between 25 meters and 150 meters of stratigraphic section.



#### 4.3.4 Provenance Determination of Deposited Sediments within the Taconic Foreland Basin

Based upon major and trace element analyses, an assessment of potential sources of sediment eventually deposited with the Taconic Foreland Basin was made (Table XIII; Table XIV). Using plots of  $\text{Al}_2\text{O}_3\text{-Nb-TiO}_2$  (Fig. 4.19), and  $\text{Al}_2\text{O}_3\text{-Zr-TiO}_2$  (Fig. 4.20), it can be shown when the approaching volcanic arc began to influence and dominate the depositional patterns with the foreland basin. Two distinct fields are observed, with PAAS values separating the two. It is believed that clastic sediment derived from the volcanic arc/accretionary complex was not an important factor within the first 150 meters of sediment deposited within the Taconic Foreland Basin, with all samples exhibiting a higher  $\text{Zr/TiO}_2$  ratio than PAAS (Fig. 4.20). This is consistent with the theory that a substantial portion of the volcanic arc complex was submerged due to the highest sea-level stands occurring during deposition of the Utica Formation and that the lower 150 meters of the Utica Formation are biologically enriched passive margin deposits. However, samples approximately 150 meters and above in stratigraphic position (Nowadaga Creek, Yatesville Creek, Otsquagó Creek and Route 171 samples) possess lower  $\text{Zr/TiO}_2$  ratios than PAAS. This is felt to be the result of the volcanic arc/accretionary complex being spatially close enough, to the then eastern Laurentian margin, so that clastic sediment derived from the arc was able to be deposited onto the lower part of the outer slope of the foreland basin. This caused higher sedimentation rates and associated long-term oxic bottom water conditions within this part the basin. This is consistent with the progressive decrease of TOC content of samples above 150 meters in section observed within the Taconic Foreland Basin. Similar arguments can be made from a plot of  $\text{Al}_2\text{O}_3\text{-Nb-TiO}_2$  with all proposed biologically-enriched passive margin deposits plotting on the  $\text{Al}_2\text{O}_3\text{-TiO}_2$  join of the ternary plot, while volcanic arc/accretionary complex derived sediments plot closer to PAAS determined values (Fig. 4.19).

Table XIV : Trace Element Analyses, Taconic Foreland Basin

Sample	Strat Height (m)	BaO	Ce	Co	Cr2O3	Cu	Ni	Sc	V	Zn	Nb	Zr	Y	Sr	U	Rb	Th	Pb	Ga
NASC1		636	66.7	25.7	124.5		58	14.9				200		142	2.66	125	12.3		
NASC2		650	80		110		55	16	150		19	210	27	200	3.1	160	14.6	20	
PAAS																			
MC CCUS 02	0.88	156	24	15	47	34	58	30	30	16	0	44	13	1629	10	37	0	8	3
MC CCUS 03	2.20	82	47	0	11	83	37	31	14	19	0	31	17	1879	12	20	0	5	2
MC CCUS 04	3.23	123	36	19	16	52	37	24	31	17	0	51	12	1522	9	51	0	9	5
MC CCUS 06	5.24	89	38	6	107	55	122	27	28	15	0	42	12	1722	11	36	0	5	4
MC CCUS 08	7.50	126	35	6	21	63	33	24	23	20	0	43	13	1735	11	40	0	6	4
MC CCUS 09	8.51	139	43	2	27	37	32	30	28	28	0	52	18	1685	11	37	0	5	4
MC CCUS 10	9.60	70	40	10	7	93	27	27	22	17	0	43	16	1774	12	23	0	6	3
MC ASUS 03	14.12	257	75	17	201	47	225	24	61	27	0	64	15	1505	9	47	0	6	5
MC ASUS 04	16.68	130	74	0	28	51	30	26	36	16	0	38	13	2333	16	23	0	4	2
MC CCUS 13	24.97	89	51	0	3	56	18	28	17	13	0	40	10	1775	10	19	0	4	2
MC ASUS 08	27.56	229	66	21	57	40	46	22	53	40	0	80	14	1377	8	68	0	7	8
MC ASUS 10	38.31	168	66	9	41	100	39	22	40	38	0	71	15	1939	13	46	0	7	5
MC ASUS 11	40.98	194	81	12	29	42	26	24	33	20	0	58	13	1710	11	39	0	7	4
MC CCUS 16	43.38	149	47	4	22	54	30	27	30	21	0	62	13	1544	10	33	0	4	4
MC ASUS 12	52.56	142	49	0	26	63	29	24	37	23	0	83	11	1662	10	33	0	5	4
MC CCUS 19	70.09	144	55	13	36	59	55	23	30	30	0	75	15	1280	7	41	0	4	4
MC ASUS 14	72.26	130	54	8	15	8	29	25	41	25	0	62	15	1684	12	38	0	5	4
MC NCUS 04	100.61	173	53	17	30	43	45	26	57	30	0	65	18	1583	11	46	0	6	6
MC NCUS 05	118.90	306	43	20	41	57	38	21	62	52	0	74	19	1676	11	49	0	7	7
MC TCUS 01	122.44	147	67	4	38	60	31	24	35	22	0	60	16	1729	13	36	0	4	4
MC TCUS 02	136.95	184	64	18	44	42	24	23	60	30	0	65	13	1593	10	51	0	7	7
MC SCUS 01	148.35	215	68	5	33	76	34	22	53	34	0	60	17	1881	14	33	0	5	4
MC SCUS 02	178.84	316	56	18	40	51	44	26	78	36	0	86	20	1573	13	48	0	6	6
MC YKSUS 01	192.07	212	63	7	34	45	31	25	40	28	0	56	13	1971	14	33	0	7	4
MC JWD STD		892	153	87	136	91	62	15	137	101	14	152	38	127	0	171	9	16	27
UM 171 FF 02	255.78											12	149	32	94	0	158	3	7
UM YC FF 02	326.13											15	185	31	75	0	150	6	14
UM YCFF 01	318.30											12	155	30	93	0	148	0	9
UM NCUS 08	170.73											2	96	28	706	6	74	0	11
UM NCUS 06	143.29											5	114	29	594	2	94	0	8
UM OTC FF 01	347.44											13	150	31	88	0	167	3	5

MC : McGill University analyses; UM : University of Mass. analyses

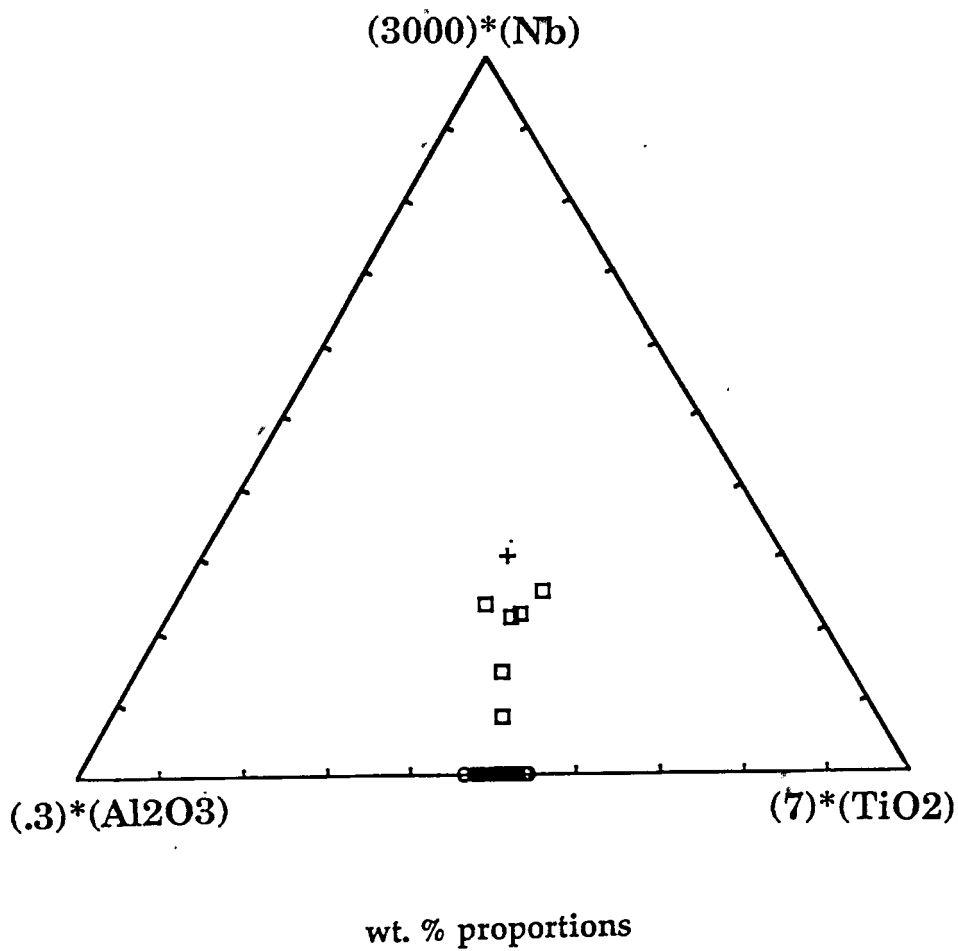


Figure 4.19 - Ternary plot of  $\text{Al}_2\text{O}_3$ -Nb- $\text{TiO}_2$  concentrations of Taconic Foreland Basin samples. Open circles = samples of passive margin origin; Squares = samples derived from the volcanic arc complex (Nowadaga Creek, Yatesville Creek, Otsuago Creek, Route 171 samples); Cross = Post Archean Average Shale.

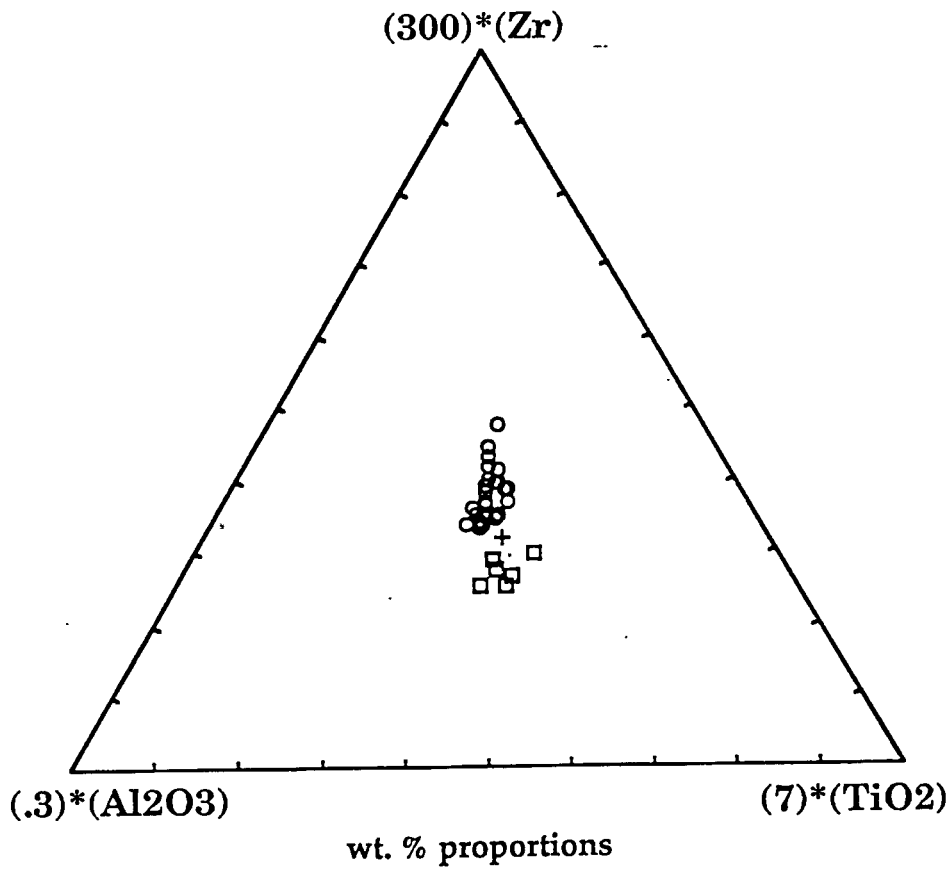
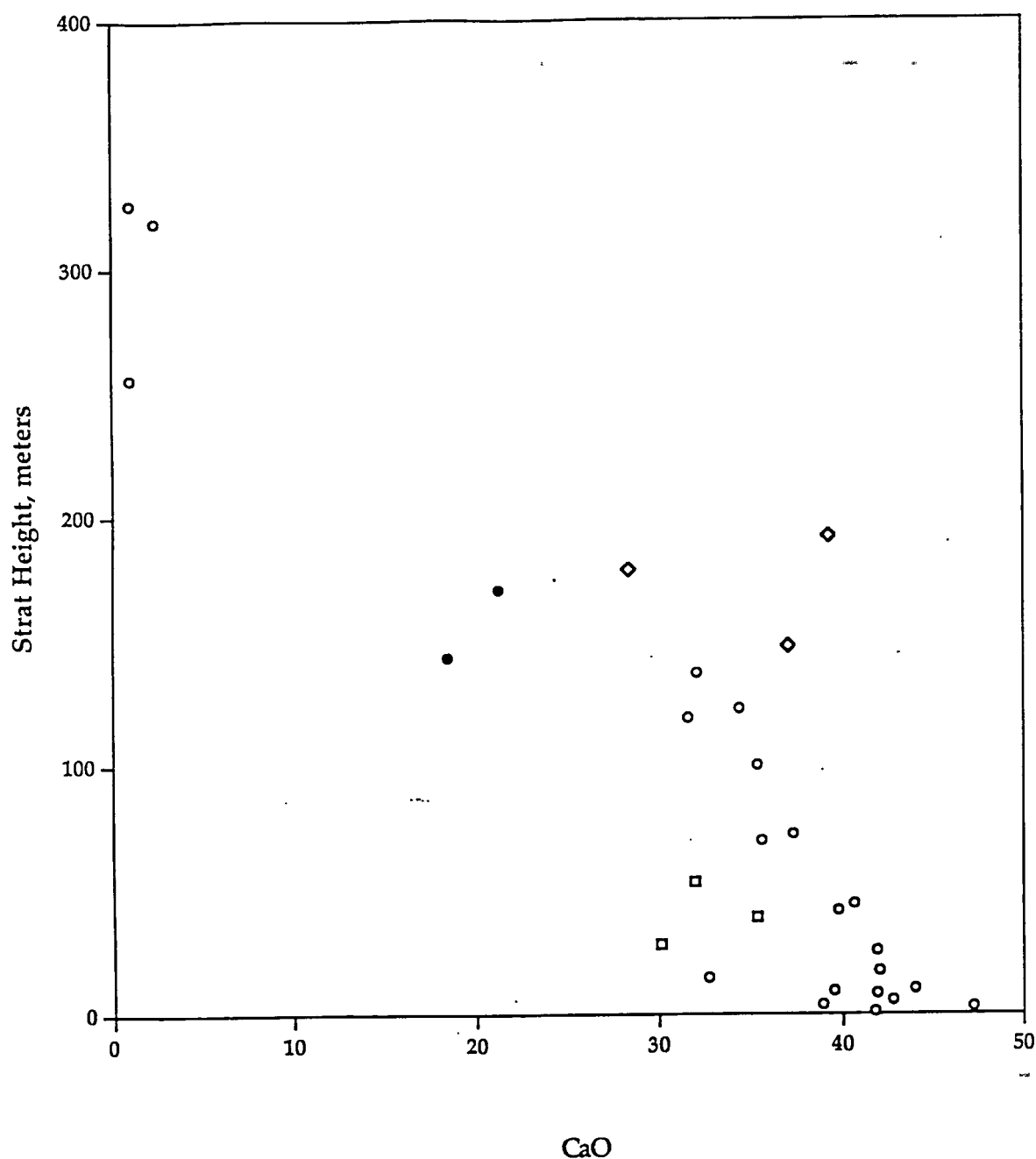


Figure 4.20 - Ternary plot of Al<sub>2</sub>O<sub>3</sub>-Zr-TiO<sub>2</sub> concentrations of Taconic Foreland Basin samples. Open circles = samples of passive margin origin; Squares = samples derived from the volcanic arc complex (Nowadaga Creek, Yatesville Creek, Otsquago Creek, Route 171 samples); Cross = Post Archean Average Shale.

#### 4.3.5 Preliminary Geochemical Analyses and Implications for Previously Unmapped Faults within the Taconic Foreland Basin

Previous analyses, and interpretation of data, of samples of the Utica Formation from the Taconic Foreland Basin determined a potentially effective way for quickly determining a sample's approximate stratigraphic position within the foreland basin (Delano, personal communication, 1992). A simple linear trend of several major and trace elements versus stratigraphic height was observed to hold throughout the entire thickness of the Utica Formation. From this, it was proposed that the use of such plots could quickly ascertain a sample's position. A plot of CaO concentrations versus stratigraphic height of samples from this study shows that this holds to a first approximation, with concentrations of CaO decreasing as one progresses upsection (Fig. 4.21). A similar type of chronostratigraphic tool can be developed with  $\text{Al}_2\text{O}_3$  concentrations; plotted against stratigraphic height,  $\text{Al}_2\text{O}_3$  concentrations are observed to generally show a trend of enrichment (Fig. 4.22). Minor trace elements, such as Co and Sc, show similar linear trends of enrichment or depletion when plotted against stratigraphic height. If this linear trend is assumed to hold true for the entire thickness of the Utica Formation, samples that then fall either above or below the linear trend could be result of faulting, not previously mapped, producing the observed discrepancies. Based upon Figure 4.21 and 4.22, three fields of samples deviating from the general linear trend have been observed; three samples from Chuctanunda Creek (ASUS08, ASUS10, ASUS12), both samples from Nowadaga Creek (NCUS06, NCUS08) and both samples from Schoharie Creek, and the samples from Youngs Lake (SCUS01, SCUS02, YKSUS01). (see Fig 4.21 and Fig. 4.22 for explanation of symbols used for highlighting proposed deviations). Based upon these preliminary geochemical conclusions, it is proposed that previously unmapped faults exist near each of these sample localities. The existence of pronounced westward tilting at the Nowadaga Creek section near Newville strengthens the possibility of unmapped faulting existing at that location, while for the Schoharie Creek and Youngs Lake samples, the continuation of the normal faults bounding the eastern side of the Sacanadaga Reservoir, from Fisher's (1970) geologic



**Figure 4.21** - Plot of CaO versus stratigraphic height of Taconic Foreland Basin samples. Squares = samples ASUS08, ASUS10, ASUS12 that show deviation of general trend between CaO concentrations and stratigraphic height. Diamonds = samples SCUS01, SCUS02, YKSUS01 that show deviation of general trend between CaO concentrations and stratigraphic height. Closed circles = samples NCUS06 and NCUS08 that show deviation of general trend between CaO concentrations and stratigraphic height.

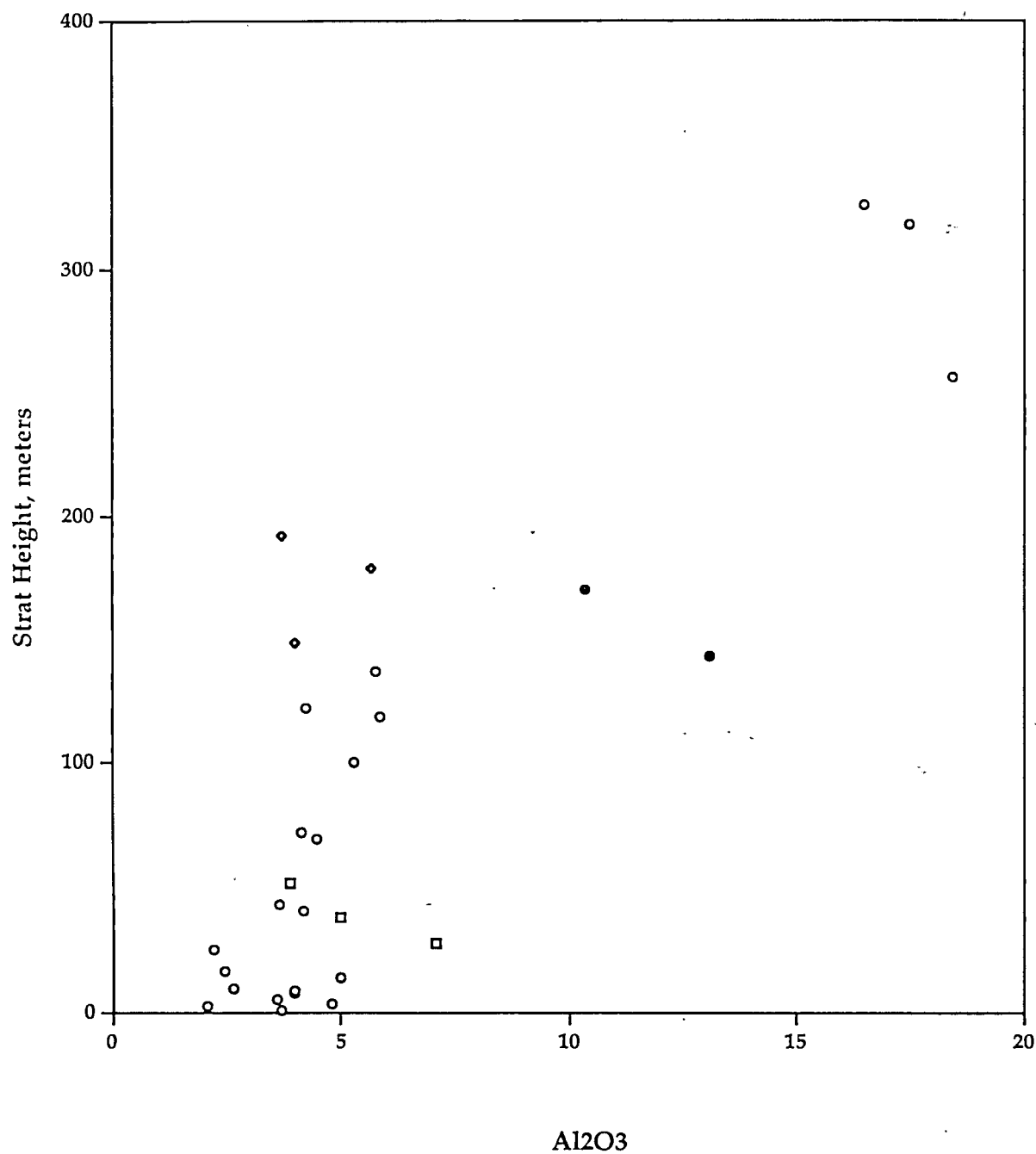


Figure 4.22 - Plot of  $\text{Al}_2\text{O}_3$  concentrations versus stratigraphic height of Taconic Foreland Basin samples. Squares = samples ASUS08, ASUS10, ASUS12 that show deviation of general trend between  $\text{CaO}$  concentrations and stratigraphic height. Diamonds = samples SCUS01, SCUS02, YKSUS01 that show deviation of general trend between  $\text{CaO}$  concentrations and stratigraphic height. Closed circles = samples NCUS06 and NCUS08 that show deviation of general trend between  $\text{CaO}$  concentrations and stratigraphic height.

map, down to these localities could explain these anomalies. The anomalous samples from Chuctanunda Creek near Amsterdam may also be explained by the continuation of normal faults from the eastern side of Sacanadaga Reservoir. However, pronounced weathering observed in the field from these particular samples may also be a valid explanation for their anomalous composition against stratigraphic height. With recent advances, and successes, of using Ordovician bentonites as a more precise chronostratigraphic tool (Delano et al., in press), the possibility may soon arise for a more definitive explanation of the observed discrepancies. Reconstruction of the entire thickness of the normal-faulted Utica Formation, based upon chemically 'fingerprinting' and correlating individual Ordovician ash beds, will enable geologists to establish a precise stratigraphic framework for these selected samples.



#### 4.4 Conclusions

##### 4.4.1 Re-Evaluation of the Utica Formation as an Extensive Spent Marine Petroleum Source Rock (MPSR) Unit

In a comprehensive assessment of the depositional environment of the Taconic Foreland Basin during late medial Ordovician times, Hay (1982) concluded that there was sufficient organic carbon within the Utica Formation during its deposition for its qualification as a good source rock. This was based upon the observation that present-day TOC contents of the Utica Formation average 1.75 wt. % (1.5-3.5 wt. %), and that during thermal diagenesis, increasing maturation of a source rock can lower its total organic carbon content by a minimum of 18 percent (Hay, 1982). It was also concluded that the thermal diagenesis of the calcareous shales of the Utica Formation was presently into the catagenic stage of hydrocarbon generation, presently making the late medial Ordovician Utica Formation a spent source rock unit (Hay, 1982).

Hay (1982) ascribed the deposition of this MPSR unit only to paleoclimatic conditions existing during medial Ordovician times. A paleoclimatically-controlled density stratification, caused by a local thermocline (and halocline ?), which was augmented by the occurrence of a worldwide 'Oceanic Anoxic Event', was proposed as the mechanism for the deposition of the organic-rich Utica Formation. Hay (1982), without presenting any direct evidence, determined that the potential role of high primary productivity, relative to detrital sedimentation rate, in surficial waters was not an important factor in controlling  $C_{org}$  values on the outer slope of the Taconic Foreland Basin (Hay, 1982). Recently, Jenden et al. (1993), in a study of potential sources of thermogenic natural gases in the Northern Appalachian Basin, eastern United States, also concluded that oil-prone black shales, correlative with the late medial Ordovician Utica Formation, were at one time extensive MPSR units (Jenden et al., 1993). It was reported that presently the Utica Formation averages 1.3 wt.% TOC and yields  $4\text{kg(ton)}^{-1}$  of pyrolytic hydrocarbon products upon programmed pyrolysis (Jenden et al., 1993).

From this study, it is believed that qualitative paleoclimatic modeling techniques developed by Parrish (1982) also predicts extensive MPSR deposition off the (present eastern) coast of proto-North America during late medial Ordovician times. Based upon the integrated use of programmed pyrolysis and geochemical analyses of the Taconic Foreland Basin, a re-assessment of the previous mechanism(s) thought responsible for the deposition of the Utica Formation has been undertaken. Consequently, it is proposed that the existence of the Utica Formation is the result of 'channeled flow upwelling' occurring in a bathymetrically-constricted basin during late medial Ordovician times. A west-vergent volcanic arc, progressively colliding with proto-North America and closing the Iapetus Ocean, created a seaway for northeasterly trade winds that promoted the establishment of high primary productivity conditions near this margin of proto-North America. Occurring simultaneously, the impingement of the oxygen-minimum zone of the water column on the outer slope of the Taconic Foreland Basin established long-term anoxic conditions, promoting the preservation of deposited organic matter (Fig. 4.23). Also crucial to the formation of a prolific MPSR unit within the Taconic Foreland Basin was the drowning of the outer slope, and the probable submergence of the developing flexural bulge and partial submergence of the colliding volcanic arc. These developments were due, respectively, to the mechanical flexure and consumption of the Laurentian continental margin within the subduction zone, and the occurrence of the highest inferred sea-level stand in the Paleozoic. The occurrence of these five factors, which are considered to be crucial for the development of prolific MPSR unit production, (i.e. surficial depression of the Laurentian passive margin, high sea-level stand, long term anoxic conditions being established with the basin, optimum paleogeographic configuration and beneficial paleoclimatic conditions), combined to produce an extensive MPSR unit during late medial Ordovician times. MPSR unit accumulation within the basin ceased when the primary source of sediment deposition within the Taconic Foreland Basin changed from passive margin sediments to clastic sediments derived from the colliding volcanic arc/accretionary complex during the later

# late medial Ordovician Taconic Foreland Basin

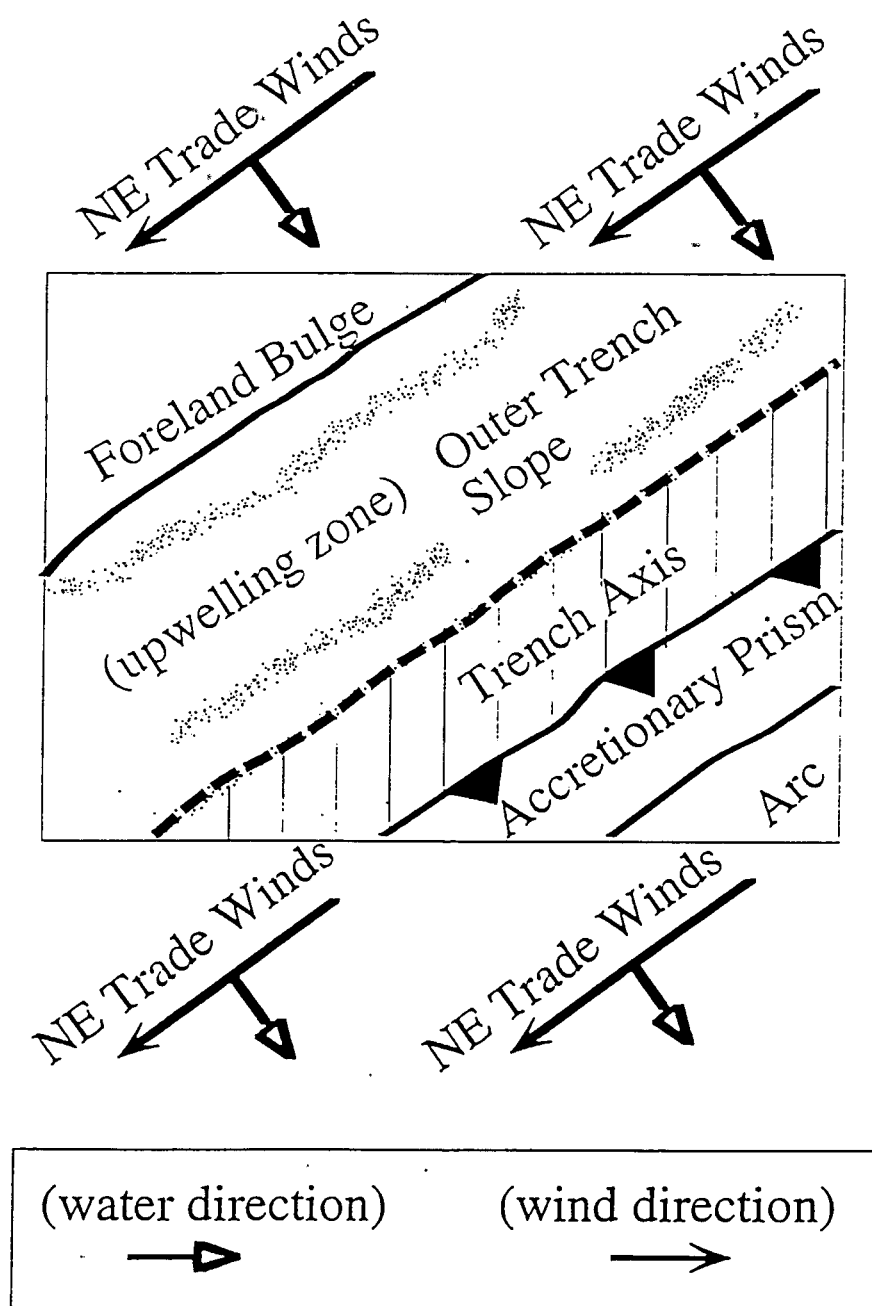


Figure 4.23 - Diagrammatic representation of how channeled flow upwelling within the Taconic Foreland Basin allowed for the deposition of the MPSR Utica Formation unit.

stages of the Taconic Orogeny. The increased flux of clastic sediment into the foreland basin quickly filled the basin and enabled oxic conditions to be re-established within the basin.

The presence of an extensive, spent, MPSR unit within the Taconic Collisional Foreland Basin, as with the La Luna Formation of the Maracaibo Basin of northwestern Venezuela, highlights the potential utility of paleogeography and paleoclimatology towards locating yet-to-be discovered MPSR sites. It also shows that the quantity of marine organic matter preserved in paleo-upwelling sites by wind-driven upwelling, when optimum conditions for its preservation prevail, is sufficient for the production of large commercial quantities of hydrocarbons.

## CHAPTER 5: CONCLUSIONS

### 5.1 Conclusions

#### 5.1.1 Overall Conclusions

This study has considered the potential utility of identifying specific variables associated with MPSR accumulation, and preservation, towards predicting their spatial and temporal distribution. New analyses by programmed pyrolysis, and XRF-techniques, for the organic, and inorganic geochemical composition of samples from the Taconic Foreland Basin of eastern New York, and the synthesis of data from previously published authors regarding the Maracaibo Basin of northwestern Venezuela and the Taconic Foreland Basin, has been undertaken within the context of this thesis. From the integration of these analyses, and interpretations derived from them, it has been established that for both active foreland basin outer slopes, and for passive continental margins and shelves, when positioned and correctly oriented in low paleolatitudes, the formation of prolific, commercial-size, MPSR units may be enhanced in these situation during high sea level intervals.

Geochemical analyses of samples from the Utica Formation of the Taconic Foreland Basin performed in this study have allowed the re-assessment of conditions responsible for the deposition of the prolific MPSR unit of the area, the Utica Formation. The organic-rich Utica Formation is suggested here to have been the result of 'channeled flow upwelling', within a bathymetrically-constricted foreland basin, establishing high primary biological conditions within the western part of the basin. Based upon inorganic geochemical analyses, it has been determined that: 1) the highest degree of biological enrichment is within the first 25 meters of the Utica Formation, 2) the lower 150 meters of the Utica Formation, interpreted as biologically enriched passive margin deposits, was not influenced by the approaching volcanic arc/accretionary complex, 3) the upper 150 meters of the Utica Formation was influenced by clastic sediment derived from the volcanic

arc/accretionary complex, because the arc/accretionary complex was close enough to the eastern Laurentian margin during that time of deposition of the Utica Formation and its overlying units, 4) previously unmapped faulting exists within the Schoharie Creek, Youngs Lake, Nowadaga Creek, and possibly Chuctanunda Creek, localities within the Taconic Foreland Basin, and 5) the variation of organic carbon values, documented within this study, throughout the entire thickness of the Utica Formation is as large as are the variations seen within the basal 20 meters of this unit, consequently casting doubt on the original first-order increases of organic carbon both through time and downslope within the Taconic Foreland Basin, as postulated by Hay and Cisne (1988).

During optimum times of hydrocarbon generation, it is calculated that the Utica Formation was capable of generation at least  $175 \times 10^6$  BOE (barrels of oil equivalent) per  $1\text{km}^3$  of source rock undergoing petroleum conversion. This was a result of the diachronous collision of a volcanic arc with the then eastern passive margin of Laurentia (proto-North America), and its subsequent drowning, when ideally oriented in a low paleolatitude during late medial Ordovician times. This contrasts with Hay's (1982) original conclusion that a paleoclimatically-controlled density stratification, augmented by the occurrence of a late Paleozoic 'Oceanic Anoxic Event', was the primary mechanism responsible for the deposition of the key MPSR unit within the Taconic Foreland Basin.

Geochemical analyses of whole rock extracts and derived petroleum oils within the Maracaibo Basin have identified the La Luna Formation as the primary MPSR unit of the region. The formation of hydrocarbon reserves within the area is due to a marine, anoxic, environment, with high primary biological productivity conditions being established off the northern coast of South America during medial Cretaceous times. Calculations show that the La Luna Formation is capable of generating  $290 \times 10^6$  BOE for every  $1\text{km}^3$  of source rock undergoing hydrocarbon conversion. This was a result of the drowning of the northern passive margin of South America during the highest sea level interval in late medial Cretaceous times. Additional research is still needed however concerning how much of the deposition of the La Luna Formation is the result of

passive margin as opposed to collisional foreland basin outer slope deposition. Newly published data points to most, if not all, of the La Luna Formation being a passive margin-deposited sediment. The maturation and migration of hydrocarbons however, is directly linked to Eocene-age collisional foreland basin development off the northwestern coast of South America.

The quantity of hydrocarbon reserves being produced within the passive margin-deposited MPSR unit of the Maracaibo Basin is greater than the calculated quantity that could have been derived from the active continental margin-deposited MPSR unit within the Taconic Foreland Basin. This is a consequence of active continental margin-deposited MPSR units having a smaller temporal window for significant MPSR production and accumulation than passive margin-deposited MPSR units. Effective MPSR accumulation within active continental margin-produced foreland basins begins only when the area passes the foreland bulge, is quickly subsided, and sea-level stand is sufficiently high enough to cover substantial portions of the flexural bulge and the volcanic arc/accretionary complex. This enables organic carbon flux rates to be higher than detrital sedimentation rates within the basin, which is key towards producing significant MPSR accumulations. The temporal window for active continental margin-deposited MPSR production is closed when the proximity of the volcanic arc/accretionary complex floods the basin with clastic sediments, making clastic sedimentation rates higher than organic carbon flux rates. In contrast, continental passive margin-deposited MPSR units may have a longer time for the accumulation of organic matter into a significant MPSR unit, since there is not necessarily any major clastic source to potentially flood the depositional site with clastic sediment; the controlling factors in this case are sea level and the position/orientation of the continental margin relative to prevailing winds that control wind-driven upwelling mechanisms.

The 'basin-specific' model developed, within this thesis, for the occurrence of prolific, commercial-size MPSR units, is also capable of explaining why the Utica Formation of the Taconic Foreland Basin and the Colon Formation of the Maracaibo Basin, both being units deposited on the outer trench slope of a collisional foreland basin, possess dramatically different TOC values. The

effect of lower sea level stand (less than 200 meters above present conditions) during the deposition of the Colon Formation, and its lateral equivalents, enabled for the clastic dilution of this unit, because organic carbon flux rates were significantly lower than detrital sedimentation rates. This resulted in the formation of a non-MPSR unit during this time of deposition within the Maracaibo Basin of northwestern Venezuela. The occurrence of high sea level stand (higher than 250 meters above present conditions) during deposition of the Utica Formation however, allowed for organic carbon fluxes to be greater than detrital sedimentation rates on the outer slope of the collisional foreland basin during its deposition. This consequently resulted in the production of a prolific, although spent, MPSR unit.



### 5.1.2 Future Work and Study

Much work remains to be undertaken towards gaining a better understanding the accumulation and preservation of hydrocarbon reserves within foreland basins in general. It is believed that the potential utility of using key variables identified towards locating extensive MPSR paleo-depositional sites should be extended towards identifying the temporal and spatial distribution of ideal paleo-depositional sites (such as the ideal locations of the impingement of O<sub>2</sub>-minimum zones on the outer slopes of foreland basins formed at active plate margins). This is based on Demaison and Moore's (1982) conclusion that O<sub>2</sub>-minimum zone development is dependent upon paleogeographic and paleoclimatic effects, and not directly linked only to high primary biological productivity conditions (Demaison and Moore, 1980). Using the same techniques developed by Parrish (1982) and Barron (1985), for identifying potential paleo-upwelling sites, identification of potential paleo-anoxic preservation sites will help towards the future exploration and exploitation of yet-to-be discovered petroleum reserves. One could test the predicted sites of these paleo-anoxic sites by the use of strontium isotope stratigraphy, and their comparison to contemporaneous global values. Significant deviations between the two values is believed to be indicative of long-term anoxic conditions being established within areas restricted from global oceanic circulation patterns (Derry, personal communication, 1993).

A more accurate assessment of surficial water productivity could be attained through a detailed study of the variation of carbon isotope concentrations within the Utica Formation of the Taconic Foreland Basin. Surficial waters experiencing high biologic activity are expected to be enriched in <sup>13</sup>C because of the preferential uptake of <sup>12</sup>C by marine organisms during photosynthesis (White, personal communication, 1993). The degree of enrichment would depend primarily on the biologic activity existing within the water column, with high productive areas showing the highest <sup>13</sup>C enrichment values. Subsequent decay, and deposition, of marine organisms on the ocean floor would produce organic-rich sediments enriched with <sup>12</sup>C, if detrital sedimentation rates were low enough. Therefore, elevated <sup>12</sup>C values in shales would be a

qualitative measurement of biologic activity when compared to marine oxic shale values. Both of the proposed projects however will require the accurate restoration of normal faulted sections of the Utica Formation back to their original stratigraphic positions. Through the use of bentonite chronostratigraphy to reconstruct the original relative stratigraphy of the Utica Formation, these problems can be undertaken in earnest within the near future (Delano, personal communication, 1993).

Finally, another problem that needs addressing is the information obtainable from the fact that the foreland basin was produced as a consequence of the diachronous collision of the Taconic Orogeny. If the overall Taconic basins had similar TOC concentrations and theoretical hydrocarbon generative potential as the Taconic Foreland Basin, the summation of hydrocarbons produced from it could have been significantly greater than the production of hydrocarbons from the continental passive margin-produced Maracaibo Basin MPSR unit. A study, similar in scope to the one undertaken within the context of this thesis of the Taconic Foreland Basin, should be undertaken along the strike of the whole length of the Appalachian Taconic Foreland Basin, for an assessment of the present and original TOC concentrations. The diachronous development of the Taconic Foreland Basin might allow better discrimination, and testing, of the 'global ocean anoxic event' explanation from the 'basin-specific' explanation of the existence of the Utica Formation MPSR unit favored within this thesis.

## APPENDIX I

### DETERMINATION OF STRATIGRAPHIC POSITION OF SAMPLES

The determinations of the stratigraphic positions of samples from the Trenton Limestone, Utica Formation and the Frankfort/Schenectady Formations were accomplished by the use of structural contouring principles. Using geological maps compiled by Fisher (1979), and topographic maps published by the New York State Department of Transportation (1978), and by using an average south-southwestward dip of  $1^{\circ}$  (100ft/mile), a series of parallel structure contours for the base of the Utica Formation, and the base of the Frankfort Formation, were constructed. The structure contours were keyed upon mapped contacts between the Utica Formation/Trenton Limestone and Utica Formation/Frankfort Formations. This resulted in the construction of a series of parallel structure contours that are of non-uniform strike. The construction presumes that the thickness of the Utica Formation throughout most of the study area remains essentially constant (300 meters); no data have been encountered that flatly contradict this assumption. Every point where a structure contour crosses a topographic contour of equal elevation would constitute a potential surface outcrop for that level. Consequently, the difference between identified topographic elevation of an outcrop and the intersecting structural contour line would represent the approximate stratigraphic height of the outcrop within the Utica Formation.

Possible errors associated with stratigraphic height determinations include:

- normal faults which occur throughout the Taconic Foreland Basin (Bradley and Kidd, 1991) could generate the duplication or removal (depending on the location of particular sample localities) of portions of the various sections within the Utica Formation. Outcrops for sampling were chosen as far as possible to be away from identified normal fault traces within the Utica Formation to minimize this possible problem. However, it has to be admitted that the mapping of such faults within the Utica Formation is problematical; samples SCUS01,

SCUS02, YKSUS01, NCUS06, and NCUS08 are most likely to be mislocated stratigraphically for this reason.

- the absence of many observable contacts between the Utica Formation and Trenton Limestone could contribute to the inaccurate positioning of structure contours on geologic maps compiled by Fisher (1979) and consequently produce inaccurate stratigraphic height determinations. Therefore, the probable error on the stratigraphic position of samples will range between 5-20 meters and will approach zero where samples were taken from locations that possess an identifiable stratigraphic contact for data to be keyed upon (i.e. Canajoharie Creek samples in particular). Errors are probably largest within the middle 100 meters of the Utica Formation. If particular outcrops are located near (undetected) normal faults, large errors of stratigraphic position are possible, perhaps as much as 100 meters if the fault has displacement of this amount or more, such as with samples around Nowadaga Creek, Youngs Lake, and Schoharie Creek.

## APPENDIX II

### PROGRAMMED PYROLYSIS OF SAMPLES

Representative samples were collected from shale outcrops spanning the whole stratigraphic thickness of the Utica Formation, while from the Frankfort Formation they were taken from the shaliest beds within the first 1000 meters of stratigraphic section. Up to 10lbs. (4.5kg) of sample was taken from each location and were stored in plastic air-tight bags until preparation. After removal of weathered surfaces, each sample was washed with tap water and then air dried. Subsequently, 2.2lbs. (1 kg) of each sample was pulverized to a 200 mesh size and was subsequently prepared for delivery to Texaco Inc. for determination of the quantity, type, and thermal maturity of organic matter, and total sulfur, present in each sample, by programmed pyrolysis. The experimental procedures documented below are from A. Bissada (personal communication, 1993).

For the determination of the total organic carbon (TOC) of the samples, approximately 200mg of each sample was weighed into a ceramic filtering crucible and acidized with 6N HCl solution for the removal of carbonate carbon. TOC measurements were made from these carbonate-free samples using an automatic Leco CS-12 carbon-sulfur analyzer equipped with an induction furnace to combust the organic carbon to CO<sub>2</sub>, and an infra-red detector to measure the generated CO<sub>2</sub>. The standard error was less than 0.16% for all of the samples analyzed (Bissada, personal communication, 1993).

In order to determine the free hydrocarbon content (S1) and the residual hydrocarbon generation potential (S2) of the samples, approximately 100mg of each sample was weighed into a stainless steel crucible equipped with a fritted-disk base and introduced into a Delsi RockEval instrument for programmed pyrolysis analysis. The instrument was set to heat each of the samples isothermally at 300°C for three minutes, then incrementally heated from 300°C to 550°C at a

programmed rate of 25°C/minute, and finally heated isothermally at 550°C for one additional minute. By doing so, all free hydrocarbons (S<sub>1</sub>) within the pores of the pulverized rock samples would have been volatilized within the first three minutes of heating, with the residual kerogen thermally degrading to hydrocarbons (S<sub>2</sub>) within the next eleven minutes of heating. The standard error for the S<sub>1</sub> analyses of all the samples was 0.03mg/gm, while the standard error for all of the S<sub>2</sub> analyses was 0.35mg/gm (Bissada, personal communication, 1993).

The existence of vitrinite-like organic matter within six of the samples sent to Texaco Inc. enabled a rough measurement of the thermal maturity of the samples. The use of the changes in color of organic particles as viewed under transmitted light microscopy (Thermal Alteration Index - TAI) was used as a second indicator of the thermal maturity of the samples. Recovery of the kerogen particles used for these analyses consisted of the dissolution of the mineral matrix by a series of acid digestion steps of concentrated HCl and HF acids for the removal of the carbonates and silicates respectively. The recovered kerogen particles were split into two fractions, one for slide-mount preparation for TAI determinations and one for polished-plug preparation for reflectance microscopy measurements. TAI determination was carried out using a Zeiss Universal transmitted-light microscope using a 12 watt xenon source, and reflectance measurements were carried out using a Zeiss Universal reflectance microscope using a 100 watt halogen bulb (546nm incident light) and a model M-003 digital recording photometer (Bissada, personal communication, 1993).

The majority of samples sent for programmed pyrolysis analysis were chosen from the middle transect of the foredeep basin (Canajoharie Creek and other associated locations, see Table IV). The primary reason for this choice included the fact that the middle transect was the only location where there was an observable contact between the Trenton and Utica Formations, and where the underlying Trenton Limestone sample was of relatively good quality. In addition, the middle transect possesses the most continuously exposed section of the lower 80 meters of the Utica Formation. Several problems regarding the nature of samples from the eastern transect limits its

usefulness for detailed geochemical analysis and its incorporation into a comprehensive assessment of the evolution of petroleum deposits within the Taconic Foreland Basin. These include: 1) that it is probably missing exposure of the basal 10 meters, or so, of the Utica Formation, 2) that it is composed of several localities, which could have introduced larger errors in stratigraphic position, and 3) that it has no Trenton sample for geochemical analysis. Similar problems existed within the western transect of the field area, namely that the Trenton Limestone sample of the area is of relatively poor quality, the basal (lower 50 meters or so) part Dolgeville Formation/Utica Formation is not fully exposed. This made the precise determination of the location of the basal contact of the Utica Formation not possible. For the same reasoning behind using the best exposed and continuous stratigraphic sections for detailed geochemical analysis, the samples chosen for the top 100 meters of the Utica Formation were selected from the eastern transect (Bean Hill Creek). This allowed a relatively even (?) spaced sampling coverage of the Utica Formation above the 30 meter level. There is a persistent outcrop gap in the 192-220 meter (650-720ft) stratigraphic interval throughout the eastern and central transect areas of the Utica Formation; from this investigation there was no explanation for this observation.

### APPENDIX III

#### X-RAY FLUORESCENCE OF SAMPLES

Thirty samples of the Taconic Foreland Basin were chosen for analysis by either the Ronald B. Gilmore X-Ray Analytical Facility at the University of Massachusetts at Amherst or at the Geochemical Laboratories Facility at McGill University, Montreal, Canada. Samples with less than twenty weight percent CaO were analyzed for major element oxide concentrations the at University of Massachusetts, while the remaining samples were sent to McGill University for major element analysis. All samples for trace element geochemical analysis were sent to McGill University.

Both sets of samples, after removal of weathered surfaces, were washed with tap water and air-dried. 2-3kg of each sample was then crushed to less than 200 mesh by use of a tungsten carbide shatterbox. All samples until further preparation and analysis were stored in plastic air-tight bags.

For samples analyzed at the University of Massachusetts for major element oxide concentrations, 30-40 g of each sample was previously ignited for a minimum of 24 hours at approximately 800°C to drive off all volatiles present and after cooling stored in 8 dram glass vials at the State University of New York at Albany (see Appendix IV see detailed explanation). From this, 1 g of each sample was placed into a quartz crucible and subsequently ignited for additional LOI drive-off at 1000°C for a minimum of 4 hours and then placed into an aluminum desiccator until cooled off to room temperature. The samples were then ground back into a powder with a quartz mortar and pestle and immediately placed into labeled plastic vials for storage in an aluminum desiccator, arresting H<sub>2</sub>O and CO<sub>2</sub> adsorption.

Using a lithium-borate flux dried for a minimum of 8 hours before its use,  $1.6070 \pm .0010$  g of this flux was thoroughly mixed with  $.3000 \pm .0003$  g of the oven-dried samples in glass vials. This



powder was then fused into a glass disk by pouring the sample from the glass vial into a dry Pt-Au crucible and then heating to 1200°C, being periodically stirred over about 6 minutes until a homogeneous glass bead formed. This was subsequently poured onto a graphite disk and pressed into a glass disk by an aluminum plunger. Each disk was then transferred to an annealing plate and allowed to cool to room temperature. Before the disks were analyzed on a Siemens MRS at the X-Ray Analytical Facility, all samples were wiped with acetone and handled with plastic gloves to minimize possible Na contamination.

Originally all samples were taken to the University of Massachusetts for major element oxide concentration determination. However several of the disks possessed unusual total yields. Further 'quality-control' inspection of the glass disks showed the effects of incipient crystallization and bubble formation during the molten bead pressing process. In addition, the facility at the University of Massachusetts was not calibrated for the high calcium samples. It is interpreted that the high calcium concentrations present in several samples promoted immediate crystallization which is responsible for the observed unusual total yields. Consequently, all samples that possessed high calcium concentrations ( $\geq 20$  wt. %) were sent to McGill University for re-analysis. The samples that were sent to McGill University consisted of 25g of each of the samples. An Austin Glen Shale from Ravena, New York, supplied by Dr. J.W. Delano of the State University of New York at Albany was used as an internal standard at both the Univ. of Massachusetts at Amherst and at McGill University to check the accuracy of the reported analyses. Trace element analyses at McGill University were performed on pressed pellets of the shale powders.

#### APPENDIX IV

##### LOI DETERMINATION OF SAMPLES

All samples analyzed at the University of Massachusetts and McGill University were independently measured for volatile content at the State University of New York at Albany. After removal of weathered surfaces and crushing to less than 200 mesh, between 30-40g of each sample was weighed and placed into a pre-weighed porcelain crucible. Each crucible was then placed into a furnace preset at 650°C and left for 4 hours; the temperature was then raised to 800°C and the sample heated for a minimum of 24 hours to drive off any volatiles present. Originally, both VYCOR and quartz crucibles were used; however, after ignition some high-CaO samples that were in the VYCOR crucibles showed unusual color pigmentation. In addition, these VYCOR crucibles upon cooling began to crack. It is interpreted that calcium from the high-CaO samples reacted with the VYCOR crucibles, causing the subsequent cracking. As a result, all samples were re-done in porcelain crucibles, with this discoloration and cracking not occurring with these crucibles.

After ignition, all samples were taken out and allowed to cool on asbestos mats for a maximum of 15 minutes. The crucibles were then re-measured with the oven-dried powder for determination of the samples' weight loss, and hence its volatile content (see Table IX). These LOI-absent samples were then used at the University of Mass. at Amherst for major element oxide concentration determinations.

Table IX: LOI Weight Loss Calculations, Taconic Foreland Basin

Sample Code	Crucible, g	Combined Weight, g	Sample Weight, g	Post Weight, g	Weight Loss, g	LOI Fraction	LOI Percentage
OTC FF 01	17.1666	40.189	23.0224	38.9775	1.2115	0.052622663	5.26
171 FF 02	17.5729	39.4237	21.8508	38.3036	1.1201	0.051261281	5.13
YC FF 02	6.6214	37.624	31.0026	36.6581	0.9659	0.031155451	3.12
YC FF 01	17.0961	38.5628	21.4667	37.3412	1.2216	0.056906744	5.69
YKS US 01	17.6929	47.058	29.3651	37.2931	9.7649	0.332534199	33.25
SC US 02	17.5974	43.0257	25.4283	36.4074	6.6183	0.260273003	26.03
NC US 08	15.8671	38.7652	22.8981	34.8865	3.8787	0.1693896	16.94
SC US 01	16.321	40.3992	24.0782	32.8095	7.5897	0.315210439	31.52
NC US 06	16.9753	38.1007	21.1254	34.5878	3.5129	0.166287976	16.63
TC US 02	17.3114	40.747	23.4356	34.4801	6.2669	0.267409411	26.74
TC US 01	15.867	34.4196	18.5526	29.3875	5.0321	0.271234221	27.12
NC US 05	17.3317	42.9424	25.6107	35.9178	7.0246	0.274283795	27.43
NC US 04	17.5986	45.8967	28.2981	37.786	8.1107	0.286616416	28.66
AS US 14	18.1926	39.1774	20.9848	32.4092	6.7682	0.322528687	32.25
CC US 19	18.2629	40.3024	22.0395	33.3801	6.9223	0.314086073	31.41
AS US 12	17.024	38.9974	21.9734	33.0736	5.9238	0.269589595	26.96
CC US 16	17.9735	42.1879	24.2144	33.9201	8.2678	0.341441456	34.14
AS US 11	17.7067	41.2437	23.537	33.5441	7.6996	0.327127501	32.71
AS US 10	18.2624	41.9241	23.6617	34.7084	7.2157	0.30495273	30.50
AS US 08	16.9698	40.2015	23.2317	33.625	6.5765	0.283083029	28.31
CC US 13	16.6639	39.161	22.4971	31.3674	7.7936	0.346426873	34.64
AS US 04	16.6327	37.9971	21.3644	30.4416	7.5555	0.353649061	35.36
AS US 03	17.9688	43.7097	25.7409	36.0469	7.6628	0.297689669	29.77
CC US 10	17.0726	39.151	22.0784	30.964	8.187	0.370814914	37.08
CC US 09	16.9888	38.878	21.8892	31.218	7.66	0.349944265	34.99
CC US 08	17.5886	38.6008	21.0122	31.1804	7.4204	0.353147219	35.31
CC US 06	16.5828	38.304	21.7212	30.5325	7.7715	0.3577841	35.78
CC US 04	18.2336	38.8462	20.6126	32.2078	6.6384	0.322055442	32.21
CC US 03	16.6037	39.832	23.2283	30.6841	9.1479	0.393825635	39.38
CC US 02	18.1664	39.2042	21.0378	31.9045	7.2997	0.346980198	34.70
JWDSID	21.1243	43.6427	22.5184	41.9195	1.7232	0.076524087	7.65

# APPENDIX V

## ORIGINAL STRATIGRAPHIC FIELD NOTES OF SELECTED SAMPLE LOCALITIES

Chuctanunda Creek, Amsterdam, New York  
23 June 1992 pm with C. M. Achong and W.S.F. Kidd

Large gap with intermittent till exposures to N of Utica shale outcrop. Significant part of outcrop shown on Fisher's map is till, and therefore there is no close approach to Trenton-Utica contact. Furthermore, the dip is significantly more than usual; at N end outcrop, 4-9, average 7°S dip (to 205°). Whole section exposed in stream is cut by substantial calcite-filled veins, most trending 255-265, range 250-270, vertical, with horizontal slickensides, and clear examples of left-lateral offset from filled pull-aparts. Displacements shown by these pull-aparts are up to 60cm on a 2cm wide vein, maximum seen ~1m. One example seen with some dip-slip component, shown by offset calciturbidite layer at falls, with ~25cm down to S displacement.

Samples acquired by C.M. Achong are labeled as AS US in bold lettering. Samples were acquired with Dr. W.S.F. Kidd. Original column developed by W.S.F. Kidd

Measured section starting from N end outcrop on W bank; thicknesses in meters

1.90	1.90	black shale (AS US 01 : 01.4m)
1.95	0.05	calciturbidite (?), or more calcareous shale
3.05	1.10	black shale (AS US 02 : 2.3m)
3.17	0.12	moderate reentrant in black shale; fully exposed, perhaps with an intermittent 1mm pale seam in center (at 3.13) (AS US 03 : 3.45m)
5.55	2.38	black shale; sample at 3.45m; top 0.15 is prominent weathering reentrant, without any separate bentonite (?mixed in)
5.90	0.35	black shale
6.00	0.10	weathering reentrant in black shale (no separate bentonite); two reentrants separated by ~2cm (AS US 04 : 6.0m)
7.20	1.20	black shale; sample just above base of interval (6.0m+)
7.34	0.14	calciturbidites; 4cm below parting, then 10cm top layer; layers are also somewhat vaguely defined, particularly where the outcrop is more weathered
8.44	1.10	black shale
8.48	0.04	calciturbidite
8.49	0.01	shale parting
8.57	0.08	calciturbidite
8.70	0.13	shale
8.74	0.04	calciturbidite
10.54	1.80	black shale; sample at ~9.30m from face of lower part of falls on E side (AS US 05 : 9.3m)
10.66	0.12	calciturbidite, prominent and clearly defined; can be traced all across the first shelf on the falls. This is the one offset by one of the calcite vein faultlets, 260-265,

with down to S displacement component, which forms the base of the falls on the W side of the stream.

- 13.66 3.00 black shale to base of bridge abutment on W side of creek bed. First 0.75-1.0 of this interval is probably more calcareous than above since it forms the second part of the falls. Sample at ~11.70m. About 9m up to level of roadbed at west side of bridge; this interval can be sampled in the creek bed to south of bridge. Dip at and to S of bridge is  $\sim 4^{\circ}$ S. (AS US 06 : 11.70m)

3/7/92 - Chuctanunda Creek, continued

Upstream from bridge west abutment NW end; measured by compass on unipod allowing for dip  
 sample at 14.00m (AS US 07 : 14.0m); ~1cm or less thick calciturbidite just above sampled  
 layer  
 sample at ~16.85m (AS US 08 : 16.85m)  
 ~17.15m v. narrow weathering reentrant at base of west bank (~15 paces from S end  
 abutment)  
 ~19.05m and 19.15m two thin reentrants with rusty weathering, no bentonitic clay  
 sample at 19.90m (AS US 09 : 19.9m)  
 ~23.20m weathering reentrant, no bentonite  
 up to 25.70m no other prominent reentrants or calciturbidites or ledges from harder  
 shale

-----  
 measured with 1.5m wooden stick from 13.66m at base of NW bridge abutment up the exposure next  
 to NW side of the bridge.

- ~+9.0m (total 22.66m) to base of ditch at break in slope; +10.5m to mark on side outcrop  
 above;
- outcrop adequate to ~+15m, mostly rubble to +18m (31.66m)
- sample at 25.16m (AS US 10 : 25.16m) (+11.5)
- sample at 30.30m (AS US 11 : 30.30m)
- 31.66 good outcrop face on N side. From paint mark at 31.66m +1.34 (33.00m) up to 33.00  
 prominent weathering reentrant, which has small pyritiferous very rusty weathering  
 nodules scattered along it. No bentonite.
- 36.00 +3.0m to prominent weathering reentrant, no bentonite
- 36.40 +0.40m to another prominent weathering reentrant, no bentonite; this one is slightly more  
 prominent; measured to the top of this and previous one
- 36.75 +0.35m to another very prominent weathering reentrant, no bentonite; This and the next one  
 can be correlated across to S side outcrop
- 36.90 +0.15m thickness of reentrant starting at 36.75m
- 38.90 +2.00m next prominent reentrant up on exposed cliff face on N side road
- 41.75 +2.85m to base of first bentonite (labeled 36 in red paint)
- 41.77 +0.02m bentonite A
- 43.05 +1.28m to base of 2nd bentonite (labeled 37 in red paint); sample of shale at 41.90m (AS US  
 12 : 41.90m)
- 43.07 +0.02m bentonite B1
- 43.12 +0.05m shale/hard band
- 43.14 +0.02m bentonite B2; this layer is persistent across the exposure, but the B1 lower layer is  
 not, disappearing in about 2m from E to W, and then reappearing again about 4m to W  
 before going below ground; both layers vary up to perhaps 3cm thick locally; the separating  
 hard ?shale layer also is thinner to E (~2cm).
- 44.24 +1.10 shale up to thin rusty layer with reentrant, probably no discrete bentonite
- 45.74 +1.50m shale [interval previously 1.0m - error]
- 45.75 <0.01 bentonite C; prominent reentrant
- 46.97 +1.22 shale to reentrant with rusty weathering lensing lamination, no bentonite
- 47.72 +0.75m shale
- 47.73 +0.01m bentonite D; prominent reentrant, rusty weathering
- 51.12 +3.39m shale; small reentrant at +2.45, no bentonite
- 51.13 +0.01m bentonite E
- 52.43 +1.30m shale (AS US 13 : 51.70m)
- 52.46 +0.03m bentonite F

- 55.01 +2.55m shale with several partings, ?pyritiferous  
 55.03 +0.02m Bentonite G; grey colour, locally 3cm thick; labeled 48.8m in red paint; last bentonite exposed; can be correlated across to N side road, to avoid poison ivy on S side.  
 56.08 +1.05m to pyritiferous layer (with reentrant)  
 57.25 +1.17m to next hard layer (~1cm thick) in reentrant, ?pyritiferous  
 58.73 +1.48m to next reentrant, no bentonite; measured to base of 2cm hard layer  
 58.75 +0.02m calciturbidite?, or cementation related to reentrant?  
 61.40 +2.65m to reentrant about 2/3 the way up the cliff on N side road, to W of tree  
 64.70 +3.30m shale to top of cliff, top of exposed section. Bedding has flattened out just before this part of exposure (AS US 14 : 61.7m)

#### SUMMARY OF SAMPLES OF SHALE FROM CHUCTANUNDA CREEK

ASUS 01	1.4m	-	v. shaly; close to edge of outcrop and till; fair-poor
ASUS 02	2.3m	0.90	fair sample
AS US 03	3.45	2.05	full of ?calcite blebs; fairly good
ASUS 04	6.00	2.55	first sample; good
ASUS 05	9.30	3.30	base of falls; v. good
ASUS 06	11.70	2.40	top of falls; v. good
ASUS 07	14.00	2.30	next to bridge abutment; v. good
ASUS 08 <sup>1</sup>	16.85	2.85	good
ASUS 09	19.90	3.05	(v.) good
ASUS 10	25.16	2.16	fair-good; small sample; N side road
ASUS 11	30.30	5.14	good; N side road
ASUS 12	41.90	11.60	fair; S side road
ASUS 13	51.70	9.80	
ASUS 14	61.7	10.0	

Bean Hill Creek Utica Shale section

Samples taken by C.M. Achong labeled as **BHC US** in bold lettering

Samples taken by J.W. Delano labeled as **JWD BHC** in bold lettering

Original stratigraphic column developed by W.S.F. Kidd

Thicknesses in meters.

Cumulative thickness; Interval thickness;		Description
0	0	-
1.23	1.23	First exposures in creek bed; flat-lying black shale, just outside (~10m) the edge of the trees lining the creek above.
1.97	0.74	Bend in stream bed to N; shale; at 1.48 a 3 cm calciturbidite with central 1cm having pyrite laminations.
2.87	0.90	Gap in outcrop.
3.47	0.60	Shale; bend in stream to south.
4.74	1.27	patchy outcrop, only in bank.
6.14	1.40	shale; exposure in south bank and onto base of falls.
6.19	0.05	strong reentrant - ? bentonite.
7.69	1.50	Black shale in step below main falls; top of interval is at base of falls.
11.64	3.95	Black shale; top of interval is lip of steep part of falls. At 10.34, base of a calciturbidite 6cm thick occurs. ( <b>BHC US 01 : 8.34m</b> )
14.29	2.65	Black shale; Lowest Sample of previous visit at 12.24 ( <b>JWD BHC 88, 063 : 12.24m</b> )
15.79	1.50	Black shale; small steep falls in this interval; beginning of small bend to N.
17.29	1.50	Black shale; center of bend to S.
18.34	1.05	black shale.
18.47	0.13	Calciturbidite sample ( <b>JWD BHC 88, 062 : 18.35m</b> ).
19.42	0.95	Black shale; bend to N.
19.97	0.55	Black shale.
20.09	0.12	Calciturbidites; two beds 6-7cm each; ? bentonite at base.; small step in outcrop. Bend in stream to SW.
28.00	7.91	Black shale: ( <b>BHC US 02 : 20.60m</b> ); ( <b>JWD BHC 88, 060 : 26.5m</b> )
29.85	1.85	black shale; outcrop in bank only, until upper 30cm. ( <b>BHC US 03 : 28.60m</b> )
31.15	1.30	black shale. Fence crosses brook near base of this interval.
32.05	0.90	black shale; small dry stream enters from S near base of interval.
32.06	0.01	calciturbidite (micrite).
32.41	0.35	black shale.
32.43	0.02	calciturbidite (micrite).
32.68	0.25	Harder black pyritic mudstone; forms a ledge.
33.82	1.14	black shale.
33.83	0.01	calciturbidite (micrite).
34.26	0.43	black shale; thin bentonite at top.
34.28	0.02	calciturbidite (micrite); pyritic layer in center; rippled top, crests trend 250, steep faces to N.
35.52	1.24	black shale.
35.58	0.06	bentonite, with a hard layer in it; exposed in S bank. Sampled ( <b>JWD BHC 88, 065 and 88, 066 : 35.55m</b> ) previously.
38.28	2.70	black shale; sample ( <b>JWD BHC 88, 059 : 36.5m</b> ) ; thin calciturbidite in interval 36.4-37.1.
38.30	0.02	calciturbidite (micrite).
43.61	5.31	black shale; fence crosses in interval 39.61- 40.46 ( <b>BHC US 04 : 38.94m</b> )
43.62	0.01	calciturbidite (micrite).
45.07	1.45	black shale.



47.52	2.45	black shale - outcrop in bank only.
49.67	2.15	black shale (JWD BHC 88, 058, 49.25m)
50.42	0.75	black shale; bend to N; small dry stream enters on S side. (BHC US 05 : 50.40m)
51.62	1.20	black shale; bend to W.
59.74	8.12	black shale; at ~58.8 graptolites [Climacograptus sp.]; shale very calcareous (fizzes with HCl) (JWD BHC 88, 057 : 55.25m).
60.71	0.97	black shale
61.86	1.15	black shale - outcrop in banks only. (BHC US 06 : 61.73m)
65.53	3.67	black shale; ? thin bentonite at 65.23.
65.61	0.08	calciturbidite.
66.46	0.85	black shale; stream (chute) enters from N side.
67.96	1.50	black shale.
69.01	1.05	black shale; outcrop poor, only in S bank.
70.96	1.95	black shale; some is argillite/mudstone. Not much reaction with HCl. Top of interval is at intersection of larger side stream from SW. (BHC US 07 : 70.73m)
75.52	4.56	black shale.
75.77	0.25	black shale; previous sample taken here.
76.08	0.31	black mudstone; top 8cm sampled previously (JWD BHC 88, 054 and 88, 055).
76.98	0.90	shale; outcrop in bank only.
79.16	2.18	shale.
79.29	0.13	pair of calciturbidites; 5, and 7cm thick separated by 1cm of shale. Sampled previously (JWD BHC 88, 052 and 88, 053).
80.49	1.20	shale; top is just below junction of two streams; section measured up SW branch.
83.47	2.98	shale; bend to S begins at top of interval.
86.82	3.35	shale; at top, junction of steep stream from N.
88.54	1.72	shale, just below waterfall.
88.72	0.18	thin calciturbidite at base of interval; otherwise shale.
88.82	0.10	thin sandstone (flysch) at base, then shale.
-	-	base of first thick turbidite sandstone. Section continues, but not measured.

Joint sets in much of section 056 and 330, vertical.

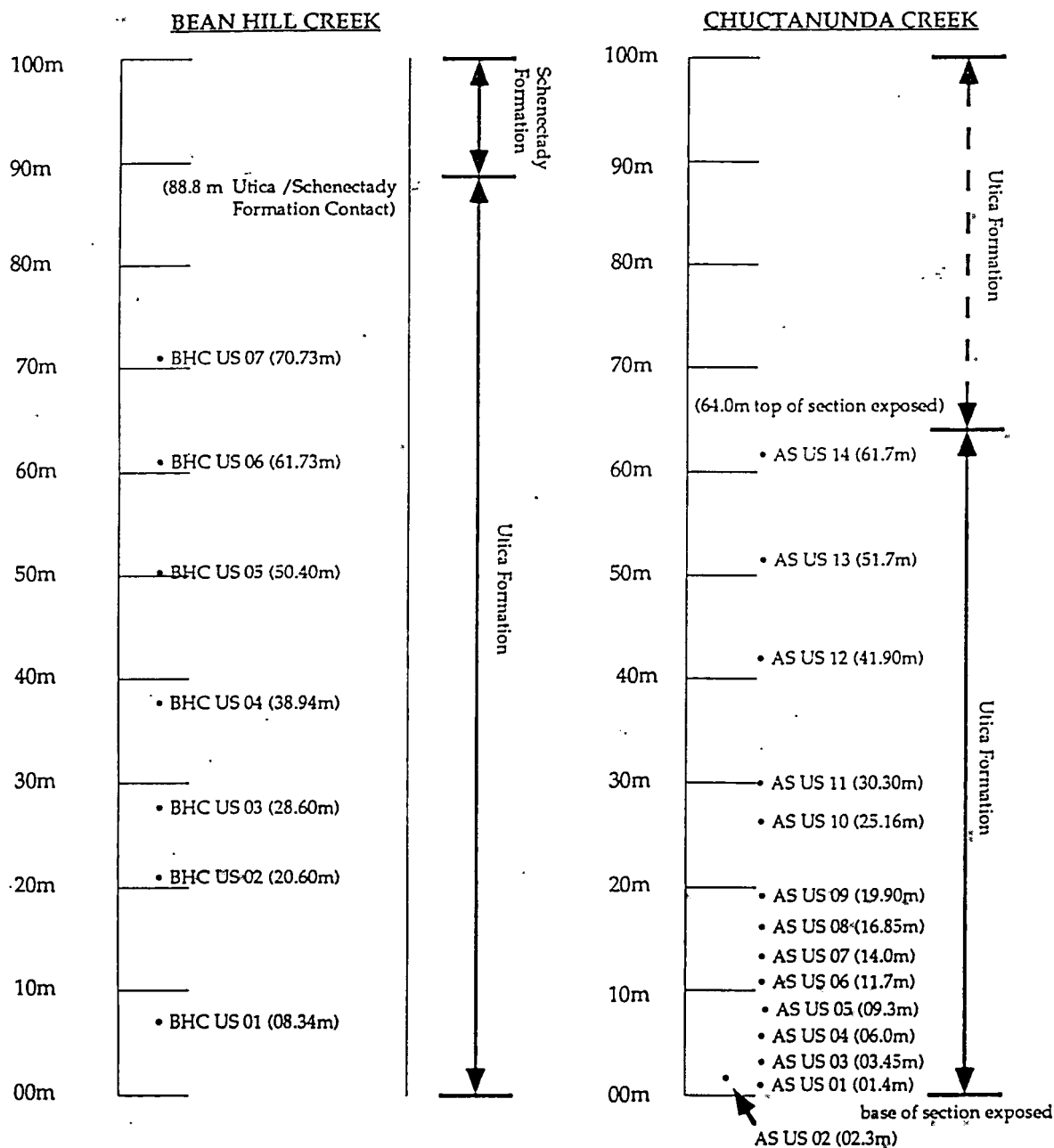
Section summary: Top 88.7m of Utica shale exposed here (about 30% of the full thickness of the unit).

Geochemical transition according to Dr. J.W. Delano is in interval 25-35m

SUMMARY OF SHALE SAMPLES FROM BEAN HILL CREEK  
BY C.M. ACHONG

BHC US 01	8.34m	shale
BHC US 02	20.60m	shale
BHC US 03	28.60m	shale
BHC US 04	38.94m	shale
BHC US 05	50.40m	shale
BHC US 06	61.73m	shale
BHC US 07	70.73m	shale

# UNMODIFIED STRATIGRAPHIC POSITIONS OF SELECTED SAMPLES



Harter Hill Creek samples - Utica Formation base placed at 45m for sample strat.  
Samples acquired by C.M. Achong are labeled as HHC US, TL, or DF in bold lettering  
Samples acquired by J.W. Delano are labeled as JWD HHC in bold lettering  
Original stratigraphic column was developed by W.S.F. Kidd

Harter Hill Creek measured section. Thicknesses in meters. Section is essentially flat-lying.

Cumulative thickness	Interval thickness	Description
0	0	-
4.5	4.5	Good outcrop of medium-thin bedded Trenton limestone, with shell fragments and calcite spar cement. Sample (JWD HHC 88, 105 : 0m) of thin shale layer from this interval. Sample (JWD HHC 88, 106 : 0.25m) of limestone bed just below shale sample. (HHC TL 01 : 3.0m)
7.5	3.0	Not so good outcrop of same limestone; Sample (JWD HHC 88, 107 : 7.375m) of micrite; uppermost layer exposed.
12.5	5.0	Unexposed. Fence crosses in this interval.
15.4	2.90	Limestone and shale; some shell fragments at bed bases. Tops and bases of beds are wavy, not planar, in some cases, but this interval has dominantly lime mudstone with flat tops and bases, and shales of significant thicknesses. Transitional to Dolgeville type; closer to Dolgeville than Trenton.
22.7	7.3	No exposure
23.7	1.0	Closely bedded Dolgeville limestone; beds up to 15cm, and thin shales. At 23m, Sample (JWD HHC 88, 108 : 23.25m) of calciturbidite bed.
27.0	3.3	No exposure
29.0	2.00	Thin limestone (10cm calciturbidite micrites) and shales; limestone-rich; poorly exposed, especially at top.
33.0	4.00	No exposure.
36.3	3.30	Shale at base, 20cm thick, Sample (JWD HHC 88, 109 : 33.06m). Then ~12-15cm calciturbidite, Sample (JWD HHC 88, 110 : 33.5m). Dominantly micrites, some shale, poorly exposed, and only in bank, after first 50cm.
37.0	0.70	No exposure.
41.5	4.50	Micrite limestone ~60-70%, shale ~30-40%. Calciturbidites ~5-10cm, shales ~1-5cm typically; Limestone-rich Dolgeville. At ~39.0m, 20+cm calciturbidite. small stream from N at ~40m. (HHC DF 02 : 38.7m)
48.8	7.30	Unexposed. dry streamlet from S at ~43+
73.0	24.20	Shale and much less abundant calciturbidites. Sample (JWD HHC 88, 111 : 53.125m) of shale; At 55.8m - fence crosses stream; ~60.0m - 5cm calciturbidite; Sample (JWD HHC 88, 112 : 65.25m) of shale; Sample (JWD HHC 88, 113 : 65.63m) of calciturbidite; 67.0-71.5m - steeper chute and good outcrop; several ~5cm calciturbidites scattered in this interval; outcrop stops in stream bed at 73.0m, very poor continuation in S bank for ~5m. New(?) power line crosses creek at ~60-61m; small stream from N at ~63m; larger stream from N at ~64m (HHC US 03 : 51.0m) ; (HHC US 04 : 61.0m) ; (HHC US 05 : 71.0m)
75.3	2.30	No exposure.
96.3	21.0	Shale. A few thin (<5cm) calciturbidites in this section. Sample (JWD HHC 88, 114 : 82.75m) at ~82.50m; Sample (JWD HHC 88, 115 : 89.0m) at approx. 88.80m. Stream from S at 85.5m, and at 86.5m (HHC US 06 : 80.0m) ; (HHC US 07 : 91.0m)
98.3	2.00	No exposure; dam of stones below track crossing creek.
100.8	2.50	Shale continues. (HHC US 08 : 100.5m)
104.3	3.50	No exposure.
108.5	4.20	Shale; Sample (JWD HHC 88, 116 : 107.0m) at 107.0.
111.0	2.50	No exposure.

112.0	1.00	Shale. (HHC US 09 ; 111.3m)
117.0	5.00	No exposure.
119.2	2.20	Shale.
122.2	3.00	No exposure.
137.2	15.00	Shale. At 127.2m, stream comes in from S side; Stream is of significant size; comes from below Davis farm. Shale sample at (JWD HHC 88, 117 : 131.875). Sample (JWD HHC 89, 002 : 137m) of shale taken. Additional shale samples (HHC US 10 : 124.2m); (HHC US 11 : 131.5m) taken
140.2	3.00	No exposure; shale poorly exposed in N bank for ~2m above the base of this interval.
141.00	0.80	Shale. Sample (JWD HHC 89, 003 : 140.75) of shale taken.
141.35	0.35	35cm calciturbidite base at 141.0m, sample (JWD HHC 89, 004 : 141.63m) taken. Also sample of shale (HHC US 12 : 141.6m) taken.
141.7	0.35	Shale sample (JWD HHC 89, 005 : 141.65) taken.
144.8	3.10	unexposed to fence line. fence [border of Crosset Farm to Davis farm] crosses at 145m and small stream enters from S here
144.9	0.1	unexposed
145.5	0.6	Sample of shale (HHC JWD 89, 006 : 144.0m) at around 144.9m
148.5	3.0	unexposed
150.0	1.5	shale sample (HHC US 13 : 149m) at 149.0m Sample (JWD HHC 13F) at 149.0m (poor exposure in N bank for ~2m above this) also taken.
154.0	4.0	little or no exposure; shale in S bank ~3.0-3.3; Sample (JWD HHC 13G) at 152 m 1.5 to base of large erratic of anorthosite in stream; 2.0-3.0 track from S crosses (new), also gully from N
155.3	1.3	shale top and base of this interval [patchy outcrop]; 1.5 to base of large erratic of gneiss on N bank, 2.5 to top [156.5m]
156.6	1.3	no outcrop in stream; poor shale outcrop in S bank along this and previous intervals
157.4	0.8	shale; sample (HHC US 14 : 157.0m) at 157.0m Sample (JWD HHC 88, 118 : 156.9m) at 156.9m
159.5	2.1	tree in creek; probably no outcrop
160.6	1.1	shale; outcrop in creek and N bank
171.2	10.6	no outcrop; 0.4 [161m] stream from S and gully; 3.9-4.9 [164.5-165.5m] poor shale outcrop in N bank; 6.0 [166.6m] significant stream from S enters with outcrop in this from about 2m up from junction; 10.0 [170.6m] base of largest erratic on N bank and poor outcrop starts up in S bank
171.6	0.4	shale outcrop in N bank
175.9	4.3	shale in stream bed; top is at sharp meander bend to S going upstream
176.6	0.7	no outcrop
179.4	2.8	shale; sample (HHC US 15 : 179.0m) at 179.0 m. Sample taken at (JWD HHC 88, 119 : 179.2m) 179.4 m.
180.4	1.0	poor exposure of shale [under logs in bend to N going upstream]. Base of interval is at fence crossing stream [upstream border of Davis property]. Top is where significant stream [main branch] enters from S; main stream bends sharply back to N here.
180.9	0.5	shale in S bank
181.9	1.0	no outcrop; stream bends sharply back to W
183.2	1.3	shale
185.4	2.2	no outcrop
187.4	2.0	shale; old interval measurements from this one up to 240.5m; small stream from N at 1.2
192.4	5.0	boulders; no outcrop - error in old printed version
196.4	4.0	shale; basal 2.0 is good outcrop, top patchy; sample (HHC US 16 : 195.0m) 195.0m

212.7	16.3	no outcrop - boulders
213.7	1.0	shale; junction of two streams; main turns to S
218.7	5.0	no outcrop - boulders
223.2	4.5	shale; good outcrop in stream bed; sample (HHC US 17 : 219.0m) at 219.0m Sample (JWD HHC 88, 120 : 220.7m) at 220.7m
225.7	2.5	no outcrop
227.0	1.3	black shale; sample (HHC US 18 : 226m) at 226.0m
232.5	5.5	grey shale; sample at 229.0; first 0.4 is outcrop, then gap to ~1.2, then good outcrop Sample (JWD HHC 88, 121 : 229.7m) taken at 229.7 m
237.7	5.2	no outcrop; 2.7-3.7m in this interval and track and fence on upstream side cross stream; elevation from topographic map approximately 1100 feet
239.5	1.8	grey shale; one ~1cm rusty weathering ?silty/sandy layer
240.5	1.0	gap - no outcrop
241.8	1.3	grey shale in stream; sample at 241.5m; very thin silts to 1cm, mostly 1mm present, sampled; (HHC US 20.241.5m)
246.0	4.2	no outcrop; poor outcrop above in S bank in this interval Sample (JWD HHC 88, 122 : 243.6m) at ?243.6 m
246.3	0.3	grey shale.
249.8	3.5	no outcrop; tiny shale outcrop in S bank at 3.0-3.2 ; major stream junction at top of this interval
251.8	2.0	no outcrop
254.3	2.5	grey shale with siltstone layers, patchy outcrop Shale sample (JWD HHC 88, 123 : 253.1m) at ~253.1m
260.8	6.5	grey shale up side stream to N; Sample (HHC US 21 : 258.0m) at 258.0m
260.8	6.50	No outcrop on main stream; side stream enters from N at base of interval, and outcrop occurs for several meters thickness upstream from the mouth; section also measured up this - see below.
269.8	9.0	No outcrop. Junction with smaller stream from N at base of interval; section also measured up this - see below.
272.8	3.0	Grey shale below sandstone bed ~10cm thick at ~270.3; Sample (JWD HHC 88, 125 : 275.25m) taken of this bed. Altimeter elevation 1230 feet. Stream bed flattens out; no outcrop past this point.

Side stream section beginning at 260.8m.

265.3	4.50	No outcrop.
266.3	1.00	Shale; 1cm fine-grained sandstone at 265.8m; 2cm similar sandstone at 266.3m; Sample (JWD HHC 88, 124 : 270.63m) of shale No outcrop beyond this.

Side stream section beginning at 254.3m.

260.8	6.50	Shale.
264.8	4.00	Gap in outcrop.
264.9	0.10	Very small outcrop of shale.
		No outcrop beyond this to overgrown road on the south flank of Harter Hill peak.

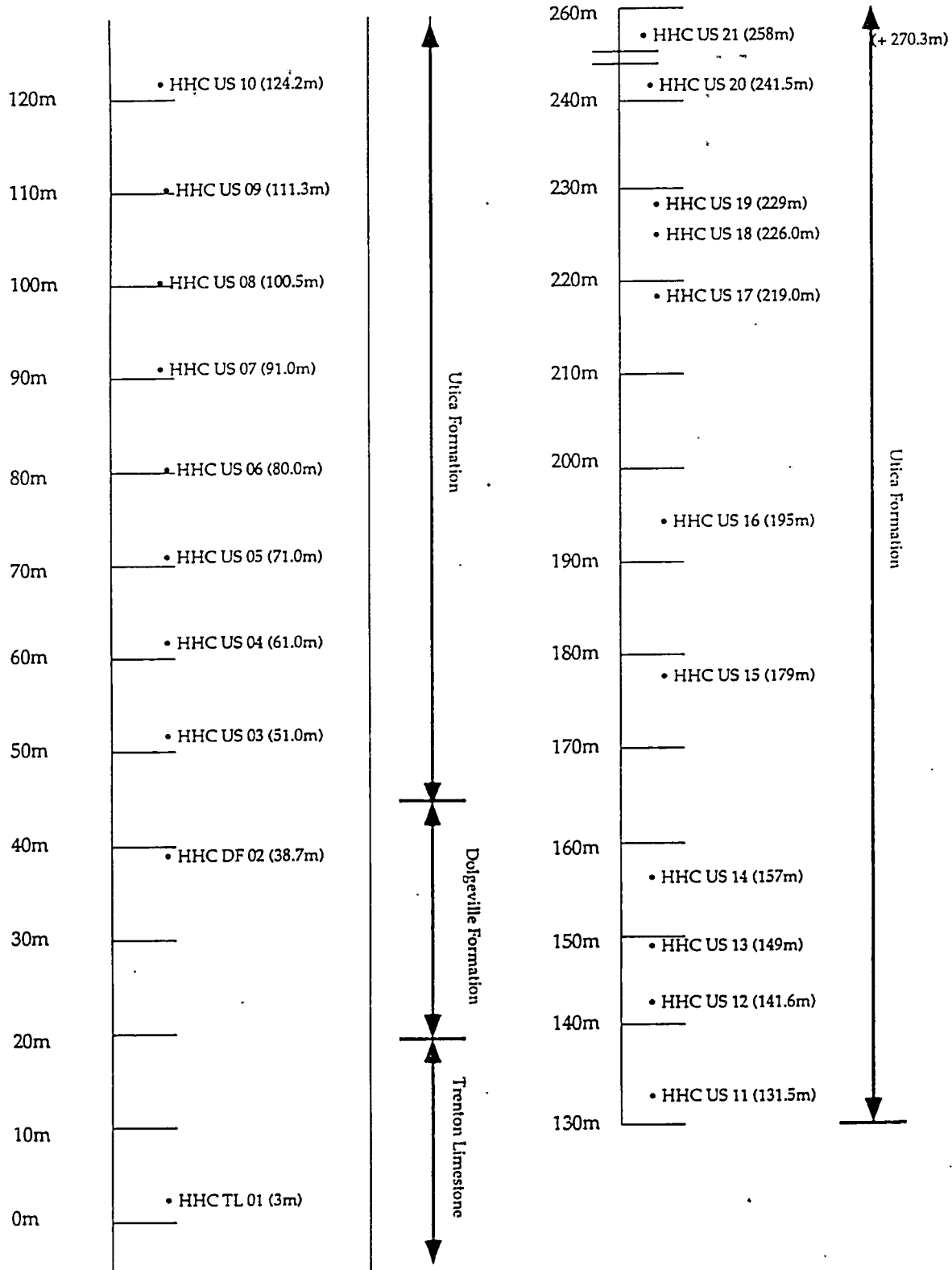
SUMMARY OF SAMPLES FROM HARTER HILL CREEK

HHC US 01	~3m	Trenton limestone shaly sample
HHC US 02	38.7m	shale from micritic limestone [Dolgeville]
HHC US 03	51.0m	shale - near base of exposed Utica [anywhere from 2.2 to 9.5m above base]
HHC US 04	60-61.0 m	shale
HHC US 05	71.0m	shale
HHC US 06	80.0m	shale
HHC US 07	91.0m	shale
HHC US 08	100.5m	shale
HHC US 09	111.3m	shale
HHC US 10	124.2m	shale
HHCUS 11	131.5m	shale
HHC US 12	141.6m	shale - section ok up to this point
HHC US 13	149.0	shale - new measurements for position of this and higher samples
HHC US 14	157.0m	shale
HHC US 15	179.0m	shale
HHC US 16	195.0m	shale
HHC US 17	219.0m	shale
HHC US 18	226.0m	shale, black
HHC US 19	229.0m	shale, grey
HHC US 20	241.5m	shale, grey
HHC US 21	258.0m	shale, grey

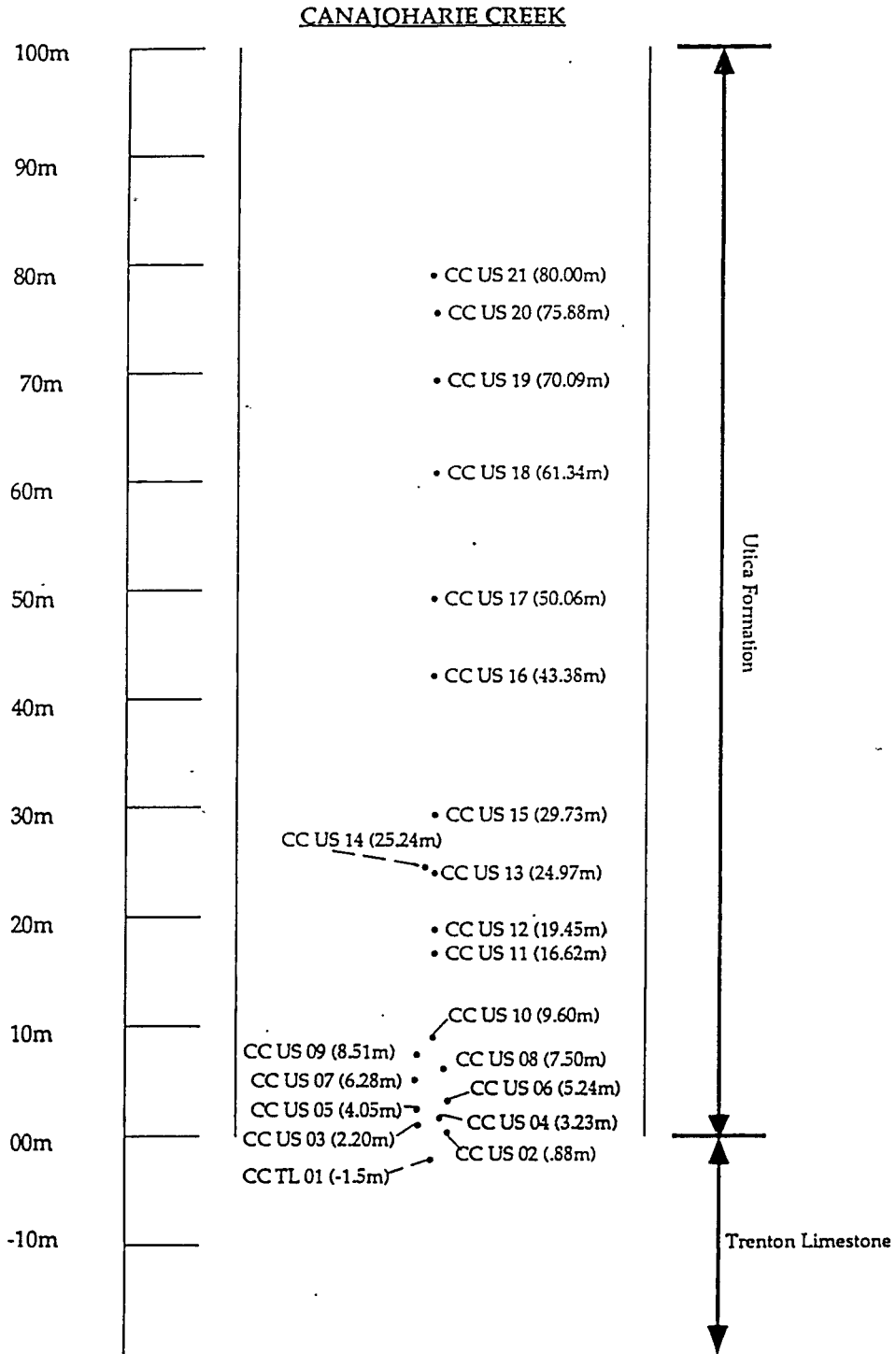
Harter Hill section unit summary: Utica Shale overall (including Dolgeville) 253.3-258.3m. Base 7.5 to 12.5m in section measured; top at 265.8m. Top Dolgeville between 41.5 and 48.8m; thickness 29.0-41.3m. Total Utica without Dolgeville 217.0-224.3m. Grey shale laminae start at 227.0m; thickness to first sandstone above at 265.8 is 38.8m; first thin sandstone/siltstone at ~239.0 - minimum of 12.0m grey shale.

# UNMODIFIED STRATIGRAPHIC POSITIONS OF SELECTED SAMPLES

## HARTER HILL CREEK



UNMODIFIED STRATIGRAPHIC POSITIONS OF SELECTED SAMPLES





Nowadaga Creek 24/11/92 with C.M. Achong and W.S.F. Kidd  
creek high

Samples acquired by C.M. Achong and W.S.F. Kidd are labeled as NC DF, US in bold lettering.  
Stratigraphic position of samples were determining through structure contouring on  
geologic maps by Fisher (1979)

- A] Outcrop to north of old railroad bridge, north of Thruway. Dip  $\sim 4^{\circ}\text{S}$ , strike  $\sim 320-325$ . 80-90% shale - i.e. rather sparse Dolgeville; calciturbidites to 30cm thick. About 5m exposed. **Sample 1 [NC DF-01]** near top. Calcite veins 287 88N, left-lateral rhombic openings. Another vein/fracture set 248 vertical [no shear sense seen]
- B] Just above Thruway bridge. About 2m exposed,  $\sim 80\%$  shale with calciturbidites to 40cm. Strike  $\sim 330-335$ , dip  $\sim 4^{\circ}\text{S}$ .
- C] Black shale with minor thin [1-2cm] calciturbidites. Strike  $\sim 335$ , dip  $4^{\circ}\text{S}$ . **Sample 2 [NC US-02]** from N-facing low E-W ledge 10 paces south of cedar tree in west bank. Prominent fracture set 243 vertical. Elevation from topo map at downstream end of outcrop estimated at 370ft.
- C<sub>2</sub>] All underwater; flexure in 30-40 cm calciturbidite near south end outcrop is down to east, with strike of hinge of 210 and parallel fractures.
- D] Black shale with prominent calciturbidites [locally 25% of section] at sample site at east end of outcrop near bridge. **Sample 3 [NC US-03]** from just below 25cm thick calciturbidite bed [about 50m plus elevation change up from sample 1]. Strike not easily definable from outcrop observed; dip  $\sim 2^{\circ}\text{S}$ .
- E] Next bridge upstream; shale, dip  $\sim 1^{\circ}\text{S}$ ; about 12m plus elevation change up from sample 3.
- F] Shale, no large calciturbidites. **Sample 4 [NC US-04]** by foot of north bridge abutment. Difficult to measure dip, but not greater than  $1.5^{\circ}\text{S}$ , and probably near  $1^{\circ}$ . About 17m plus elevation change up from outcrop E.
- G] Well-exposed shale, with dip  $1.2^{\circ}\text{S}$  [i.e. 100 ft/mile!]. Picnic site visited with Delano previously. Three thin bentonite reentrants seen in cliff across river.
- H] Just north of Bladec's garage, and just south of house immediately north of this. Shale, dip  $\sim 3^{\circ}\text{S}$ , strike  $\sim 110$ . **Sample 5 [NC US-05]**; about 20m up from sample 4 plus elevation change - assuming dip of outcrop G.
- I] Shales, dip  $\sim 1.5^{\circ}\text{S}$ , strike  $\sim 110$ .
- J] Tibbits Road bridge, Newville. Shales, dip  $\sim 4-5^{\circ}\text{W}$ , strike  $\sim 150$ . **Sample 6 [NC US-06]** from south bank, at second ledge upstream from corner of bridge abutment, about 20 paces from it. At upstream end of outcrop, elevation from topo map is 520ft, about 150ft above bottom of outcrop C.

- K] Bridge at intersection in west end of Newville. To east, downstream, outcrop is flat-lying to begin with, but into cliff on SE bank it dips prominently west, then may flatten again to north. Outcrop to west of bridge looks flattish, dip probably less than 20. Sample 7 [NC US-07] from base of southwest bridge abutment. Elevation from topo map ~550ft.
- L] Shale, dip ~3-40E, strike ~275. Sample 8 [NC US-08] from north bank about 40 feet west of bridge. Calcite vein 243 vertical.
- M] Roadcut with grey shale and thin silty greywackes, Sample 9 [OTC FF-01]; also a few sandy greywackes to ~30 cm, prominently cross-laminated with N-flowing currents. Otsquago Creek, south-west of Starkville.

9/12/92 with C.M. Achong and Dr. W.S.F. Kidd.

all stratigraphic positions of the following samples were determined by use of structure contours on geologic maps published by Fisher (1979)

- 1/ Ohisa Creek. Junction with small creek from Maby Road to SW. About 50% thin sandstone and siltstone typically 1-3cm thick, a few up to 10cm thick. Flat [max  $<1^{\circ}$  S-W dip]. Much ice and snow. No outcrop seen, allowing for ice, down to this stream junction. Ohisa creek has flat bottom; outcrop likely to be intermittent [OC FF-01].
- 2/ Rte 171 SW of Frankfort. Large outcrop on N side road near base of gorge, sampled at base [171 FF-01], where about 5m of thin sandstone/siltstone and shale, with typically 1-5cm thick sandstones, some to 10cm or so, make up about 40-50% of the interval. Next part of outcrop above is 4m+/- of shale, then about 7+m above is similar to bottom interval, with perhaps a thicker sandstone at top.
- 3/ Just south of bridge by fault offset sandstone and parking area by creek. New roadcut with fresh shale and thin sandstone/siltstone. Light grey-dark grey shale transition seen and sampled [171 FF-02; 2 bits]. Thick sandstone at top of roadcut ~70cm+.
- 4/ Route 30A about 3 miles north of Central Bridge, on west side of road, opposite junction with side road that crosses creek on old girder bridge. Schenectady Fm nominally. About 40-50% sandstone, most 10cm or less thick, a couple to ~30cm. Sample of shale ~2m up from base of cut [30A FF-01]. Gentle SW dip  $\sim 1.5^{\circ}$ . Very thick [1.5m+] sandstone exposed to south round corner. Two perpendicular directions of tool/groove marks seen on loose slab and on underside of prominent 30cm sandstone in face of cut. This bed has parallel lamination for bottom 5cm or so, then convoluted lamination, overturned south, then ?climbing cross-laminated top 20cm, climbing to south. Is this within wave base? Many of tool marks on sandstone base are large and look like shell margin marks; but no shells visible in sandstone! Top of this bed is not planar, also suggesting reworking of original turbidite; shale and next thin sandstone above thicken over depressions in top of this bed.
- 5/ Wolf Hollow, east of Amsterdam. Schenectady Fm. near Hoffmans Fault. About 60-70 % coarse thick sandstones [turbidites] with shales; one shale sampled [WH FF-01]. Dip about  $20^{\circ}$  E, because of bending near the Hoffmans Fault. Fisher's map implies that these beds are not far above the contact with the Utica [assuming that there are not any splays to the main fault].

Yatesville Creek below Buttermilk Falls. 29.95m is base of "Frankfort" or "Schenectady"  
C.M. Achong samples YC US-01 at 11.60m; YC US-02 at 27.77m; YC FF-01 at 44.4m; YC FF-  
02 at 51.3m

## APPENDIX VI

### PALEOGEOGRAPHIC AND PALEOCLIMATIC RECONSTRUCTION TECHNIQUES

#### VI.i Introduction

The distribution of organic-rich sediments is partially controlled by oceanographic processes which affect the distribution of phytoplankton (Parrish and Curtis, 1982), constituting ninety-five percent of all primary organic producers in the ocean (Krujic and Barron, 1990). Because organic productivity, and preservation of the matter produced, are the main forces controlling the distribution of marine petroleum source rock (MPSR) beds, oceanographic processes affect the spatial and temporal distribution of MPSR beds (Barron, 1985). Oceanographic processes are driven by continental geographic setting and climate; therefore, organic productivity and preservation of organic matter can be described essentially as a function of continental geography and climatic conditions (Barron, 1985). The successful prediction of past times and locations of MPSR occurrences could be enhanced if past paleogeographic positions and motions, and paleoclimatic conditions, can be accurately known.

Paleo-locations of persistent, wind-driven, upwelling zones are one of the most important results that are derived from paleogeographic and paleoclimatic modeling. The enhanced production of marine organic matter observed at these sites presently is a consequence of upwelling currents continually replenishing the photic zone of the water column with nutrients, in particular phosphates and nitrates, for planktonic consumption (Barron, 1985). These currents are driven by surface winds that are associated with the largest-scale features of atmospheric circulation (Parrish, 1982). Therefore, accurate modeling of atmospheric circulation on paleogeographic reconstructions should enable more accurate and precise predictions of MPSR beds, if it is correct that they are dominantly a consequence of wind-driven upwelling.

While accurate paleogeographic reconstructions have become attainable with the combined use of paleomagnetic, biogeographic, tectonic and climatic methods (Ziegler et al., 1987), accurate paleoclimatic prediction is still in its developmental stages. Two different approaches towards the development of better paleoclimatic/paleoproductivity predictive techniques have progressed in the past two decades. Parrish (1982) has pioneered the use of a 'qualitative' paleoclimatic model, using analogies with the present-day climatic conditions and the effects of continental positioning in the modification of global atmospheric circulation patterns, to isolate probable paleo-upwelling sites (Parrish, 1982). More recently, Barron (1985) has used numerical modeling based on the 'presumed', more fundamental, physical laws controlling global atmospheric circulation to predict the time and locations of paleo-upwelling sites.

A review of previously published material (Parrish, 1982, 1982a; Barron, 1985) discusses further whether these qualitative and numerical models can predict the former existence of wind-driven upwelling zones. These sites have been observed to have extensive organic-rich sediments. The paleoclimatic predictive capabilities of both models can be tested by assessing:

- Is there an actual connection between present-day upwelling and the observation of high primary productivity?
- Can current climatic modeling attempts accurately and precisely simulate present-day observations of upwelling?
- Are these climatic models capable of predicting sites of paleo-upwelling and paleoproductivity using specific, field-observed, paleoclimatically-sensitive sediments to test the potential usefulness of climatic modeling towards identifying prolific MPSR deposits?

## VI.ii Atmospheric Circulation

### VI.ii.i Review of the Derivation of ideal, present-day, zonal circulation patterns

The development of accurate global atmospheric models for the Cretaceous and the Ordovician is predicated on the ability to ascertain the necessary parameters for the correct explanation of present-day atmospheric circulation and extrapolation to the past. Present-day atmospheric and oceanic circulation patterns are controlled by the distribution of heat over the Earth and the effect of planetary motion (Parrish, 1982). The construction of present-day atmospheric circulation patterns begins first with an ideal situation, a water-only planet, and its subsequent modification into present-day climatic observations.

On an ideal, globally uniform, water-planet, present-day circulation would be a function of heating differences between the equator and the pole and the rotation of the planet. A temperature gradient is continually generated as a consequence of the surface of the planet receiving more sunlight at the equator than at the poles (Parrish, 1982). In the absence of planetary rotation, air heated at the equator would rise and flow directly poleward, while air cooled at the poles would sink and flow equatorward. The Coriolis Effect, a consequence of planetary rotation, causes the deflection of the developing air masses; equatorward moving air is shunted to the west, while poleward moving air is moved to the east (Parrish, 1982). Additional heat and mass balance constraints cause the development of a global wind system on this ideal water-only planetary system, consisting of six general wind belts. Each of these belts are parallel to latitude, three in each hemisphere. They are:

- the equatorial easterlies, lying between the equator and 20°N and 20°S
- the westerlies, occupying the areas between 40°N-55°N and 40°S-55°S
- the polar easterlies lying between the poles and 65°S and 65°N respectively (Fig. VI.i)

The imposition of additional heat and mass balance constraints causes the development of present-day zonal pressure regimes. Equatorial-derived air flowing to the poles will sink at about

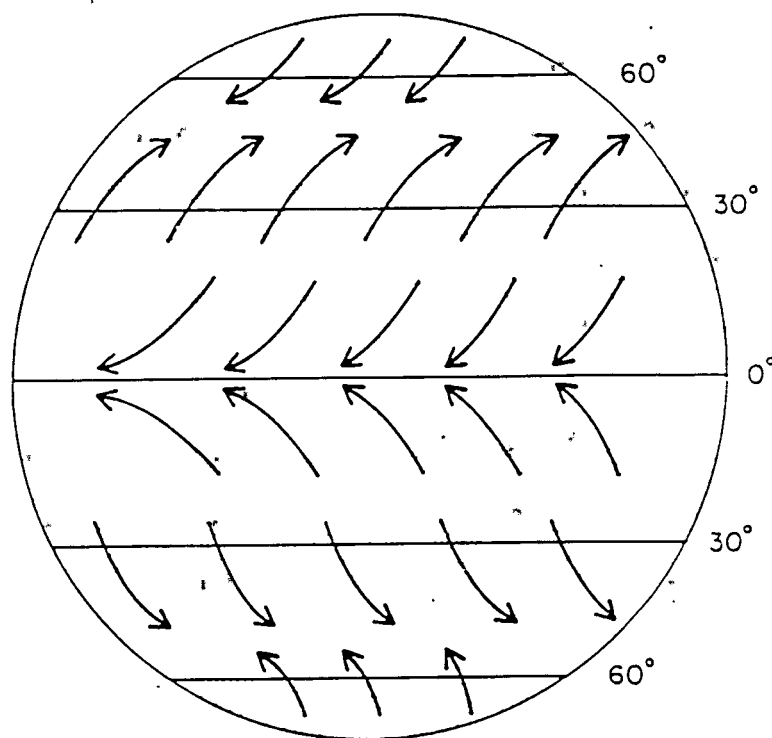


Figure VI.i - Idealized surface atmospheric circulation, showing easterly and westerly wind belt systems. Arrows show wind direction (After Barron, 1985).



30° in each hemisphere, causing barometric high development at these locations. Poleward-derived air flowing to the equator rises at 60° in both hemispheres, consequently forming barometric lows in these regions. Therefore, the ideal zonal pressure regimes are also parallel to latitude; high pressure zones are located at the poles and parallel to 30°N and 30°S, while low pressure zones form at the equator and parallel to 60° in both hemispheres (Fig. VI.ii) (Parrish, 1982).

The first barrier confronting the development of accurate paleoclimatic predictive techniques is whether or not this 'idealized' zonal construction of present-day atmospheric circulation was valid for the past. The rotation of the Earth has slowed down since Paleozoic times; the modeling of tidal friction forces that would have slowed down the Earth's rotation is thought by some to require that planetary rotation was then fifteen to twenty percent faster than the present (Parrish, 1982). A faster-rotating planet would cause the compression of the ideal zonal wind and pressure regime construction towards the equator. If a faster critical rotational speed was reached earlier in Earth's history, the creation of additional wind and pressure regimes still would have occurred parallel with latitude (Parrish, 1982). Modeling predicts that a fifteen to twenty percent increase in planetary rotation speed would have caused a 4°-6° compression of zonal wind and pressure belts in each hemisphere. However, because of a minimum 5°-10° error on the positioning of paleocontinents, the possible error associated with the compression of zonal wind and pressure belts enables this potential factor to be discarded as significant (Parrish, 1982).

The obliquity of the planet also has the potential to seriously affect the past overall global atmospheric patterns on this ideal 'water-only' planet (Parrish, 1982). However there is no supporting evidence for assertions that the tilt of the Earth's rotational axis relative to the plane of the orbit of the Earth around the Sun has changed since Paleozoic times. Consequently, obliquity can also be discarded as a potential threat to extrapolating this present-day zonal atmospheric construction to the past. These two factors, obliquity and faster planetary rotation, are the only primary 'challenges' that could pose problems for the ability of modeling an ideal 'water-only' planetary atmospheric system in the past by using present-day considerations.

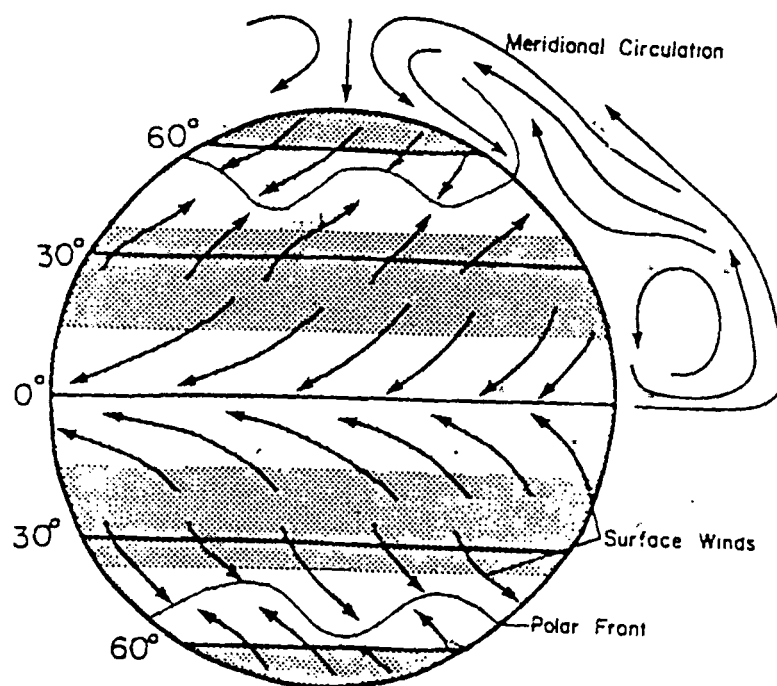


Figure VI. ii - Idealized surface atmospheric circulation, showing pressure belt systems and associated wind belt system development. Isobars are parallel to latitude.  
 dark shading = relative high pressure belt; light shading = relative low pressure belt  
 (After Parrish, 1982).

VI.ii.ii      Modification of ideal present-day zonal circulation into present-day cellular circulation patterns

The introduction of continental landforms on this idealized 'water-only' planetary construction causes the modification of ideal zonal atmospheric circulation into our present-day cellular atmospheric circulation patterns. This is a direct consequence of the differing thermal properties between land and water (Parrish, 1982).

A continual temperature contrast exists between the continents and the adjacent oceans because land is able to thermally equilibrate faster than the ocean. The greater the contrast between an area and the idealized 'water-only' situation, (i.e. more continental mass in a given area), the greater the disruption of the idealized zonal atmospheric model into present-day observed cellular circulation patterns. The effect of the latitudinal position of a continent can also contribute to the degree of zonal modification. At mid-latitudes, the magnitude of difference between land and oceanic temperatures are greater which can contribute to even more severe modification of the 'ideal' zonal atmospheric patterns (Parrish, 1982). Seasonality can also play a role in the modification of atmospheric circulation; some aspects of present-day circulation patterns are created and destroyed on a seasonal basis. Zonal pressure belts can shift as much as  $10^{\circ}$  between summer and winter seasons due to seasonality alone (Parrish, 1982).

The combined effects of the aforementioned processes is the intensification of the oceanic pressure belts and the creation of contrasting pressure regimes on the adjacent landform, all relative to the ideal zonal atmospheric model construction (Fig. VI.iii) (Barron, 1985). For example, even though permanent high-pressure cells are located at the poles presently, during the winter the southern pole high-pressure cell is more intense than its northern counterpart. This is because the presence of the Antarctic continent ideally situated around the South Pole.

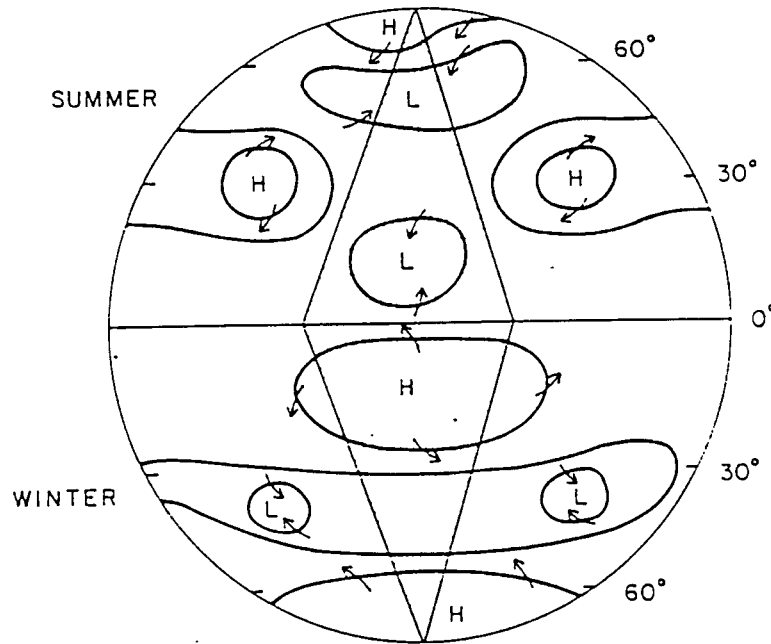


Figure VI. iii - An idealized surface atmospheric circulation for summer and winter hemispheres on a hypothetical continental landform.  
 L = relative low pressure cell development  
 H = relative high pressure cell development  
 (After Barron, 1985).

With these fundamental principles, coupled with the assumptions of atmospheric circulation, paleoclimatic circulation maps can be constructed in the following manner:

- superimposing the reconstructed paleogeography for the time desired on the ideal zonal atmospheric model
- modification of high and low-pressure belts and cells on these maps as a consequence of paleocontinental mass, positioning, and seasonality (Parrish, 1982).

### VI.iii Wind-Driven Upwelling

#### VI.iii.i Conditions for wind-driven upwelling

It is currently observed that the areas of highest primary marine productivity occur in upwelling regions located in coastal waters (Fig. VI.iv) (Barron, 1985). These regions occupy only one-tenth of one percent of the world's surface area. However, they are presently observed to be six to fourteen times as biologically productive as the least productive area of the world's oceans and more than three times more productive than normal shelf waters (Parrish, 1982a). Average productivity in these regions is observed to be  $250 \text{ gC}_{\text{Org}}\text{m}^{-2}\text{yr}^{-1}$ , compared to  $50 \text{ gC}_{\text{Org}}\text{m}^{-2}\text{yr}^{-1}$  in open-oceanic environments.

While there are several types of processes which can produce upwelling currents, the most important ones are those that are large-scale, persistent, and wind driven (Parrish, 1982). Wind-driven upwelling occurs whenever surface wind currents create a surface divergence in the water column (Barron, 1985). This enables surface water depleted in nutrients, due to its consumption by organisms in the photic zone, to be replaced by nutrient-rich water from below the photic zone. The mechanics of how these divergences occur is important to modeling attempts for the prediction of marine petroleum source rock (MPSR) occurrences.

In the absence of planetary rotation, a particle on the surface of a water column, composed of several hypothetical layers, would move in the same direction of the wind. The Coriolis Effect, due to planetary rotation, however causes the particle not to travel in the same direction of the wind. Instead it is deflected at an angle to the right of the wind in the Northern Hemisphere. Because the water layer immediately beneath the surface layer is in frictional contact with it, movement of this layer also occurs. However, the Coriolis Effect also affects this layer so that a particle in this layer would be deflected at an angle to the right greater than the first layer (Parrish, 1982). Energy loss, caused by frictional contact with the above layer, causes this layer to move slower than the first layer. This process continues until at some depth, no further motion occurs. The summation of the magnitudes and directions of these frictionally coupled layers is

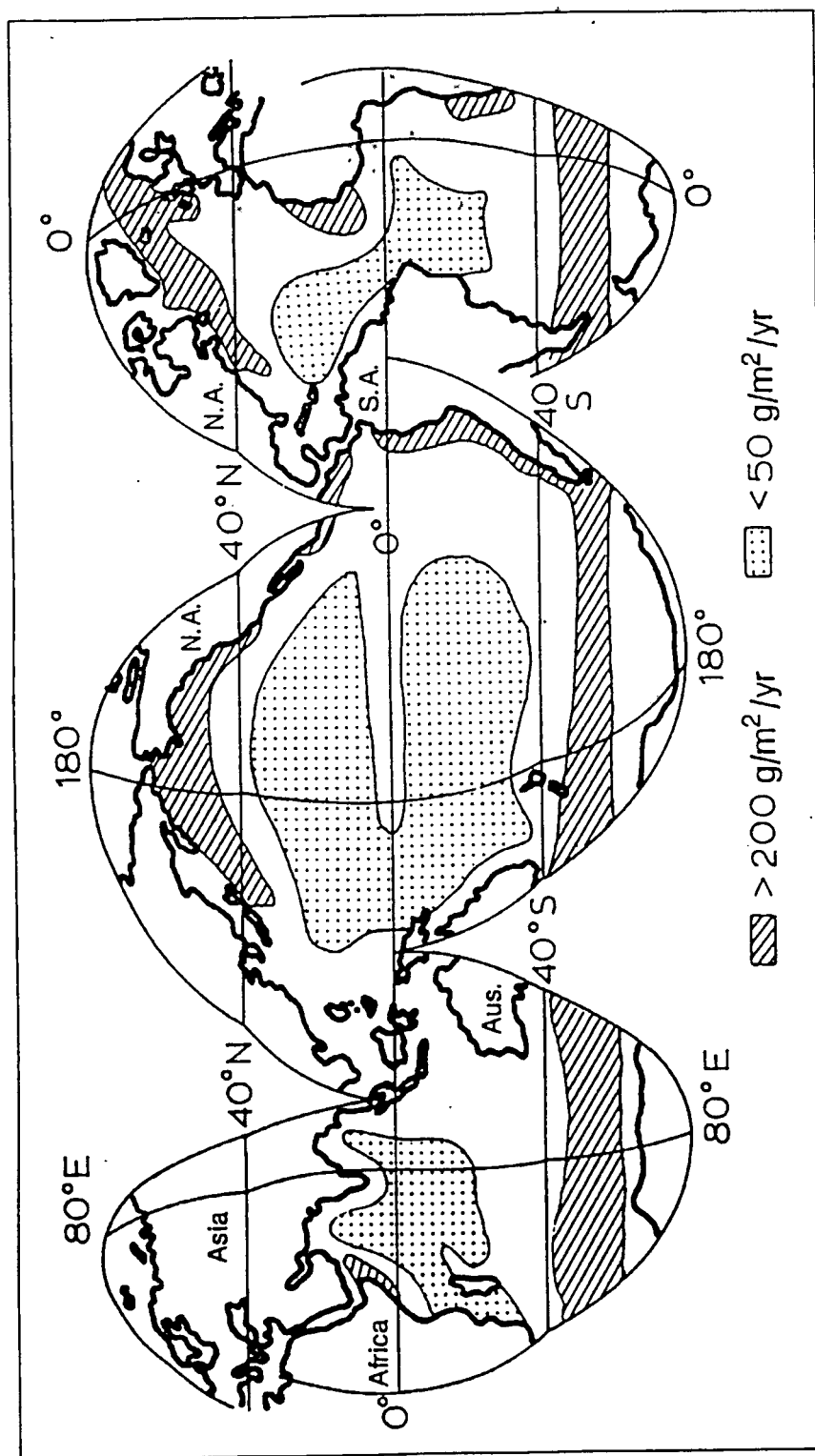


Figure VI. iv - Primary organic production in the present-day ocean in  $\text{g/m}^2/\text{yr}$ .  
 Reproduced by permission of the Geological Society from Calvert (1987). Aus = Australia;  
 N.A. = North America; S.A. = South America (After Pedersen and Calvert, 1990).

called an Ekman spiral (Barron, 1985). The net transport of the water column beneath the open atmosphere, called the Ekman transport, is perpendicular to the wind direction (Fig. VI.v). In the Northern hemisphere water deflection is observed to be to the right of the wind; in the Southern hemisphere it is to the left (Barron, 1985). Using this observation, two situations have been determined to be favorable for the long term existence of wind-driven upwelling: open-oceanic divergences and coastal upwelling (Parrish, 1982).



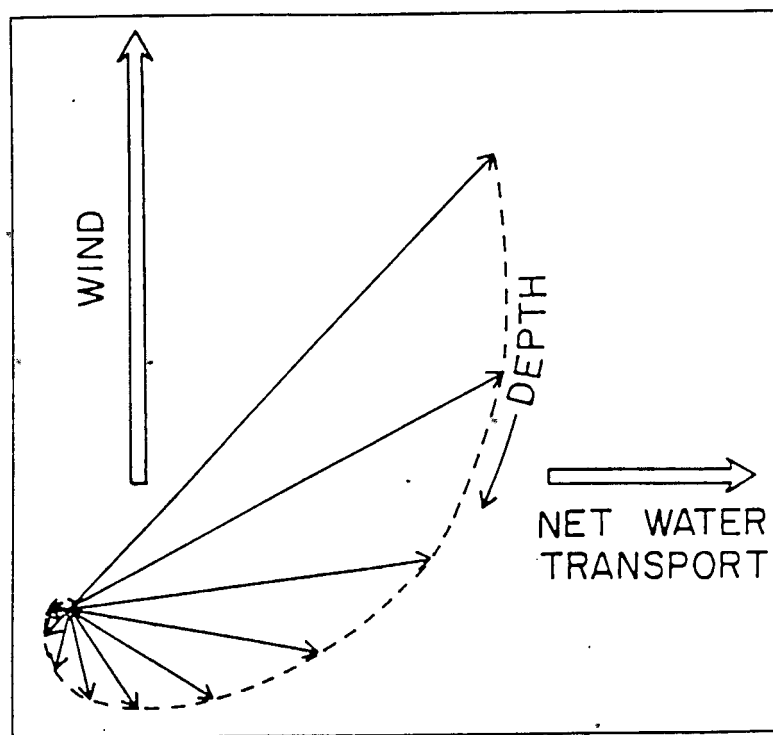


Figure VI. v - Ekman spiral, highlighting the gradual change in current direction and strength with increasing depth, and the 90° relationship of net water transport with wind direction (After Barron, 1985).

VI.iii.iiCoastal wind-driven upwelling

Coastal surface wind-driven upwelling occurs whenever the wind direction is parallel to the coastline of a continent. The coastline must be on the right side (looking downward) of the wind direction in the Northern hemisphere, while the coastline must be on the left side in the Southern hemisphere, if the net transport of water is to be in an offshore direction. This causes surface water to be transported out to the open sea and nutrient-rich water to take its place. Presently, coastal wind-driven upwelling is observed off western South and North America, and off the coast of northwestern and southwestern Africa (Fig. VI.iv). Presently, and probably in the past, coastal wind-driven upwelling occurs on west-facing coasts within sub-tropical high-pressure belts, or on east facing coasts within the middle latitude low-pressure belts known as meridional coastal upwelling zones (Parrish, 1982). Present-day meridional coastal upwelling zones, such as the one off the Peruvian coast, can generate productivity values as high as  $600 \text{ gC}_{\text{Org}}\text{m}^{-2}\text{yr}^{-1}$ , and up to 20 wt. % carbon in underlying sediments. Coastal upwelling can also develop on north or south facing coasts that coincide with zonal wind and pressure belts such that enable surface water divergences occur. Presently this situation occurs off the coast of northern Venezuela (Fig. VI.iv), with productivity averaging  $100 \text{ gC}_{\text{Org}}\text{m}^{-2}\text{yr}^{-1}$  in these areas. Monsoonal upwelling combines the effects of large-scale continental positioning and seasonality to produce extensive productivity, which is presently observed adjacent to northeastern Africa (Parrish, 1982) (Fig. VI.iv).

### VI.iii.iii Open-oceanic divergences and upwelling

Open-oceanic divergences form whenever low-pressure cells form over the ocean. In this situation, air flows counterclockwise into the low-pressure system from adjacent high-pressure systems in the Northern hemisphere, while in the Southern hemisphere air flows clockwise into the cell. The air flows in a circular path into the low-pressure cell because of the Coriolis Effect (Parrish, 1982). The wind convergence into the low-pressure cell causes a water divergence within the water column; water is transported perpendicularly away from the low-pressure system. This type of open-oceanic divergence is called radial in nature (Fig. VI.vi) (Parrish, 1982). A symmetric version of open-ocean divergences occurs at the equator when the equatorial easterlies converge at the equator. Perpendicular transport of the water relative to the direction of the wind direction causes divergence to occur (Fig. VI.vi) (Parrish, 1982). Both versions of open-oceanic divergence mechanisms presently are not seriously considered as optimum sites for marine petroleum source rock deposition, because presently both types of open-oceanic divergences occur mostly over abyssal depths of the oceans. In addition, presently observed productivity values are only as high as  $50\text{gC}_{\text{org}}\text{m}^{-2}\text{yr}^{-1}$ . All organic productivity that could be produced as a product of upwelling would be biodegraded, since the vertical distance traveled by the organic matter is large enough for complete oxidation of the matter before it reaches the sea floor (Demaison and Moore, 1980). However, this type of divergence could have been of importance during past times when sea-level stands were considerably higher. The formation of relatively shallow, intercontinental seas could have enabled the production and significant preservation of organic matter if the continents were in the correct latitudinal position. If the production rate was high enough, and the epeiric seas not too deep, organic matter could have exhausted the oxygen content of the waters, allowing for its deposition and possible preservation. This is presently occurring in the Black Sea, where in the middle of this basin productivity is only between  $50\text{--}90\text{ gC}_{\text{org}}\text{m}^{-2}\text{yr}^{-1}$ . However, average total organic carbon (TOC) values are at least 4 wt. % and higher. This contrasts the observation that

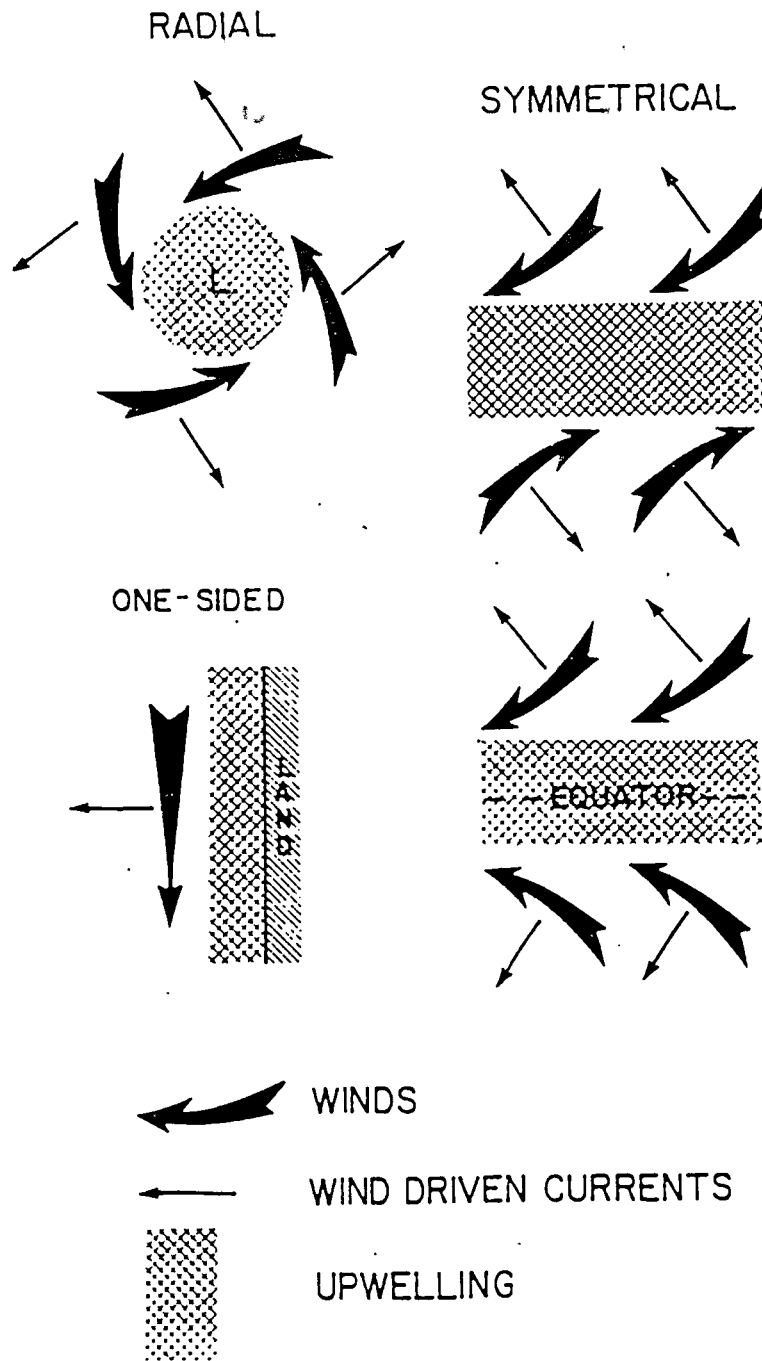


Figure VI. vi - Schematic diagram highlighting upwelling types. Radial and symmetrical wind-driven upwelling occurs under stable, low atmospheric pressure systems. Except for the equatorial area, diagram illustrating wind and water currents are for northern atmospheric orientation. Southern hemisphere wind patterns would be mirror images of the ones pictured above, with water transported to the left of wind direction (facing downwind) (After Parrish, 1982).

productivity values are as high as  $500 \text{ gC}_{\text{org}}\text{m}^{-2}\text{yr}^{-1}$  on the coastal edges of the Black Sea, yet TOC values there are observed to be less than 1 wt. % (Stein, 1991).

VI.iii.iv      The connection between primary productivity and wind-driven upwelling: Is there actually one ?

One of the most critical assumptions used to justify the use of paleogeography and paleoclimatology towards predicting marine petroleum source rock (MPSR) occurrences is that wind-driven upwelling indicates productivity (Moore et al, 1993). The actual connection between wind-driven upwelling and marine productivity is that the transport of surface water depleted in nutrients by winds is replaced by nutrient-rich water from underneath. But is this actually the case? Does wind-driven upwelling actually indicate high primary productivity? And is the converse - that high primary productivity indicates wind-driven upwelling - a valid assumption?

The most direct means towards resolving this issue would be determining upwelling rates for various areas for comparison. However, because upwelling rates are relatively small in the world ocean ( $\approx 10^{-2} \text{ cm}^1 \text{ sec}^{-1}$ ), the determination of surface wind conditions is used as a proxy for wind-driven upwelling in a specific area. A divergent wind condition would indicate the existence of wind-driven upwelling. The measurement of surface wind conditions indicative for wind-driven upwelling consists of a two-stage process:

- computation of surface wind stress from observed wind velocities
- determination of divergent wind conditions possibly existing from the surface wind stress

A global wind velocity data base spanning 106 years with a  $2^\circ$  by  $2^\circ$  resolution was constructed by Hellerman and Rosenstein (1983). From this a global wind stress diagram, a map was created showing  $2^\circ$  by  $2^\circ$  areas of predicted wind-driven upwelling (Fig. 1, of Krujic and Barron, 1990). In an ideal situation, a global map with  $2^\circ$  by  $2^\circ$  resolution showing high primary productivity would be used to directly compare the locations observed for wind-driven upwelling and high primary productivity. However, the data set for primary production is far from ideal. The spatial and temporal distribution of sampling was biased, multiple techniques were used for determining the primary productivity ( $\text{mg C}_{\text{org}} \text{ m}^{-2} / \text{day}$ ) of specific areas, and the original data is unavailable for

its possible manipulation into a workable format (Krujis and Barron, 1990). Therefore, is it the best available map showing global productivity.

For comparison, both maps were re-digitized over an evenly spaced grid 5° by 5° in resolution. Both were then superimposed for direct comparison (Fig. 3, of Krujis and Barron, 1990). At first glance, it appears that the assumption that wind-driven upwelling is indicative of high primary productivity is not promising. Only 18 percent of annual wind-driven upwelling regions are associated with high primary productivity areas, with many of the wind-driven upwelling regions occurring in the open ocean and permanent ice cover areas. However, while present-day open oceanic divergences are potential sites for extensive wind-driven upwelling, they are observed to be poor sites for marine petroleum source rock deposition. Therefore, all areas that are at least one grid-point away from a land source can be discarded. Doing this causes the association between wind-driven upwelling and high primary productivity to rise to 63 percent (Krujis and Barron, 1990). An interesting note is that there are very few sites of high primary productivity not associated with wind-driven upwelling (Diagram 3c, of Krujis and Barron, 1990), suggesting that high primary productivity is an indication of wind-driven upwelling. However, the assertion that the converse is true, that wind-driven upwelling requires high primary productivity, is not confirmed and must be determined for each individual case presented (Krujis and Barron, 1990).

The assertion that wind-driven upwelling is an indicator of high primary productivity must be used conditionally. Wind-driven upwelling can be used only as an indicator of productivity if all other factors associated with marine petroleum source rock deposition are favorable. These include the rate at which organic debris sinks through the water column, the burial rate of the deposited organic matter and the oxygen concentration in the water column (Moore et al, 1993). This represents the next major predictive step; the temporal and spatial prediction of organic matter preservation through paleogeography and paleoclimatology (Barron, 1985). However, a sixty-three percent occurrence of primary productivity and wind-driven upwelling provides strong

support for the use of paleoclimatology and paleogeography for the prediction of paleoproductivity.



#### VI.iv Paleoclimatic Reconstruction Modeling

##### VI.iv.i Paleogeographic Reconstructions

A critical parameter that directly affects the accuracy of global paleoclimatic patterns is the accuracy of the paleogeographic maps on which they are based. The proportion of paleocontinental landforms, and their latitudinal and longitudinal positioning, will have important effects on the distribution of world temperature, precipitation, climate (Ziegler et al, 1979). The importance of this can be seen when comparing the paleogeography and its associated general climatic features of various time intervals. The distribution of paleocontinental landforms in the high latitudes in the Permo-Carboniferous and late Precambrian allowed world climate to be relatively cool, with evidence of substantial glaciation during these times. During the early Paleozoic however, the proposed low latitude configurations of the various paleocontinents would have caused world climate to be relatively hot (Ziegler et al, 1979). Therefore, the temporal and spatial distribution of marine petroleum source rock (MPSR) occurrences is highly dependent on paleogeography as well as paleoclimatology.

Paleogeographic reconstructions are still active areas of research. The unavailability of quantitative data to help constrain paleogeographic motions and locations has required subjective interpretations. For paleogeography, paleomagnetic evidence is scarce and often inconsistent, due to secondary magnetizations of rocks through metamorphism and weathering. Coupled with the inability to measure the longitudinal separation of continental pairs, the inaccuracies of paleogeographic reconstructions based solely on paleomagnetic data are high (Ziegler et al., 1979). As a consequence, more qualitative techniques, such as biogeographic and paleoclimatic evidence, have been combined with paleomagnetic data to develop more accurate paleogeographic reconstructions. However, each of these qualitative techniques have limitations too.

The biogeographic distribution of faunal provinces allows for independent checks on paleomagnetically determined latitudes, in addition to inferring the longitudinal separation of paleocontinents. An effect of biogeographic barriers being a function of climate and geographic

distance, this has enabled better determination of general east-to-west paleogeographic configurations during the lower Paleozoic (Ziegler et al., 1979). However, the robust nature of some faunal provinces, such as the present-day Indo-Pacific Province which spans 180° of longitude, places limitations on biogeography alone for constraining paleogeographic motions and locations.

The use of geochronology and sedimentology have also allowed better control on the timing of continental disruptions and collisions, while tectonic patterns presently existing can be used in producing more accurate paleogeographic reconstructions. Present-day subduction zones, such as the 'Ring of Fire' surrounding the Pacific Ocean, possess a degree of continuity from continent to continent. Because all the major Paleozoic paleocontinents show evidence of active continental margins along at least one of their margins, the assumption that paleo-subduction zones were also continuous belts has been incorporated into paleogeographic reconstructions (Ziegler et al., 1979).

The occurrence of climatically sensitive sediments, such as evaporites, coal beds and tillites, also helps constrain paleogeographic modeling. The observation of relatively wet conditions, indicated by coal swamps and thick clastic sequences on eastern coasts in low latitudes and on western coasts in mid latitudes, has also enabled better construction of paleogeographic maps (Fig. 1, of Ziegler et al., 1979).

With the combined use of these fields, paleogeographic maps have undergone major revisions. Paleogeographic maps of Ziegler et al. (1979) originally placed Baltica in higher latitudes of the Southern Hemisphere (Fig. 3, of Ziegler et al., 1979). The errors of paleomagnetic poles in the Cambrian and Ordovician caused its inaccurate positioning. However, evidence from planktonic graptolites and pelagic trilobites have repositioned Baltica in more intermediate latitudes in the medial Ordovician (Fig. 8, of Scotese and McKerrow, 1990). The difficulty of reconstructing previous paleogeographies is not limited to the Paleozoic. Mesozoic-Cenozoic paleogeographic reconstructions have also been difficult to constrain. The Cretaceous Quiet Zone hampers the use of paleomagnetism for quickly and accurately determining the paleo-positions and motions of the continents in the Caribbean Inter-Realm (Pindell et al., 1988). Therefore the

necessity of producing highly accurate paleogeographic reconstructions, used for deducing paleoclimatic patterns and paleoproductivity sites, forces the use of more qualitative techniques for outlining continental motions (Ziegler et al., 1979). Care must be taken when using these paleogeographic reconstructions; research must be undertaken on an individual basis for determining what, paleobiological, paleoclimatic, sedimentological and tectonic evidence was used for the interpretation of a particular paleogeographic reconstruction.

VI.iv.ii      Bathymetric considerations of wind-driven upwelling

An additional factor that can influence the location of paleo-upwelling sites is bathymetry. Wind-driven upwelling draws oceanic water not from abyssal depths but from water ranging tens of meters to at most a few hundreds meters deep (Demaision and Moore, 1980). The minimum water thickness that is needed for Ekman, wind-driven, water transport to develop has been estimated between fifty to one hundred fifty meters. Water depths less than this allow for turbulence between the surface and bottom layers to effectively smother Ekman water transport effects (Parrish, 1982). Therefore, the point where wind-driven upwelling ceases is not the actual position of the shoreline, but the depth where turbulence dominates over Ekman transport in the water column. Currently, it is a plausible assumption that the wind-driven upwelling shoreline and the geographic shoreline are essentially the same; this may not have been valid in the past. Until recently, paleoclimatic models have not attempted to superimpose geographic contouring onto their paleogeographic reconstructions. If they were made, they were highly subjective at best, having the world being divided only into mountains, lowlands, shelves and oceans (Ziegler et al., 1979). As a consequence, many predicted paleo-upwelling sites have been placed at the location for preserving(?) paleocontinental shelf breaks. There is no quantitative way to determine the optimum water depth for organic-rich sediments in an existing paleo wind-driven upwelling system; the necessary resolution does not exist. This allows for substantial error to be introduced in the spatial prediction of paleo-upwelling sites on continental shelves.

#### VI.iv.iii      Non-numerical, qualitative, paleoclimatic modeling

Parrish (1982) pioneered the use of non-numerical modeling of paleoclimate and its effectiveness in localizing paleo-upwelling sites. The paleo-circulation maps were constructed on the following assumptions:

- previous atmospheric patterns were analogous to the present day
- paleocontinental configurations were the key factors controlling the severity of the disruption of idealized zonal atmospheric patterns and the location of paleo-upwelling sites (Parrish, 1982a, Parrish, 1982, Parrish and Curtis, 1982)

The spatial and temporal distribution of paleoclimatically-sensitive sediments and organisms were then predicted from the paleoclimatic constructions. Field observations of paleoclimatic indicators, such as glauconite, phosphate, coal beds and evaporites, were then used to test the predictions (Parrish, 1982). Because paleoclimatically-sensitive sediments have been used to constrain the paleogeographic positions, however, the validity of using these reconstructions towards identifying prolific MPSR occurrences has been questioned. However, in addition to evaporites, coals and tillites, non-paleoclimatic rock types were used for the reconstruction of past paleogeographies (Ziegler et al., 1987). Also, because Parrish (1982) attempted the prediction of locations of a paleoclimatically-controlled sediment that was not used to constrain paleogeographic positioning, specifically MPSR units, the potential conflict of using the same variables for localizing paleogeographies and petroleum occurrences was avoided.

Her modeling attempts were able to correctly predict 55% of all presently observed organic-rich deposits as being a consequence of wind-driven upwelling alone (Table 2, of Parrish 1982a). However, non-numerical modeling attempts of MPSR distributions worked better during certain time intervals. A better association was observed for the late Devonian, most of the Cretaceous and the later Tertiary, while a poorer association was seen for the Jurassic and early Paleozoic. (Parrish, 1982a). Several explanations for why qualitative paleoclimatic modeling could only identify 55% of all organic-rich rocks included:

- that not all upwelling sites are underlain by organic-rich sediments. If bottom waters are accessible to, and replenished by, highly oxygenated waters, efficient degradation of deposited organic matter will continue. This is observed presently in Antarctica, where very low water temperatures enables the polar waters to be highly oxygenated. Consequently,  $C_{org}$  values in the bottom sediments are only .52 wt. %. Similar situations exist offshore of southeastern Brazil (Demaïson and Moore, 1980).
- that not all petroleum source rock beds are a consequence of wind divergences (Parrish, 1982). Upwelling zones are not the only optimum location for the deposition of marine petroleum source rocks (Demaïson and Moore, 1980). In addition to upwelling sites, large anoxic lakes, anoxic silled basins and open ocean anoxic layers can also be sites conducive for the production and preservation of organic-rich sediments.

However, with as many as half of all organic-rich sediments being correctly predicted as a consequence of wind-driven upwelling Parrish (1982a) inferred that non-numerical paleoclimatic modeling holds promise for predicting the time and location of MPSR occurrences.

VI.iv.ivNumerical paleoclimatic modeling

The observation that some periods of the Phanerozoic in the non-numerical paleoclimatic modeling gave better predictions for the occurrences of MPSR units than others caused some to question the validity of assuming that present-day atmospheric circulation was the same in the past. It was argued that some paleocontinental configurations would not allow for accurate prediction of paleoclimatic conditions and paleoproductivity if one assumed that atmospheric conditions have remained constant throughout time. This would be due to the qualities of atmospheric circulation constantly changing in response to a changing paleogeography. Changing paleogeographic configurations would also force angular and energy momentum balances of the earth-atmosphere system, which ultimately control climate, to change. The validity of non-numerical paleoclimatic modeling was challenged on the assertion that it was incapable of accounting for a changing paleogeography which affects the overall energy, momentum and climatic balances of the earth-atmosphere system (Barron, 1985). By relying on analogies of present-day continental configurations and atmospheric circulation, non-numerical paleoclimatic models would be inherently biased, perhaps predicting paleoclimates and paleo-upwelling sites incorrectly. Only when paleocontinental configurations were similar to present-day conditions would the probability that the predictions were right increase. The more grossly dissimilar the paleogeography, such as during the Jurassic, the more likely that non-numerical predictions would be incorrect.

Barron (1985) attempted to solve this potential problem of non-numerical paleoclimatic modeling by developing numerical climatic models that were based only upon the 'presumed', fundamental, physical laws that govern atmospheric and oceanic circulation. These models have the capability of determining whether or not the general features of atmospheric and oceanic circulation remain stable in a constantly evolving paleogeography (Barron, 1985; Krujis and Barron, 1990).

In order to test the potential usefulness of this version of paleoclimatic modeling, a series of sensitivity experiments were developed that ascertained the ability of the model to accurately predict present day climatic patterns (Barron, 1985). It was shown capable of correctly predicting sites of present-day wind-driven upwelling and their associated high productivity sites (Diagrams 7-9, Barron, 1985). The model was then used on a medial Cretaceous paleogeography under high and low sea level stands to address whether or not atmospheric circulation was stable under a changing paleogeography. Numerical modeling showed that present-day atmospheric conditions are valid for this past paleogeography only in low latitude locations. Inaccurate predictions were made for higher-latitudinal positions. Therefore, paleo-upwelling predictions in high latitude locations must be treated with caution since numerical modeling was able to show that paleoclimatic modeling is highly sensitive to geography (Barron, 1985).



VI.iv.vComparison between both paleoclimatic models

The comparison between similar paleogeographic reconstructions for both models during the Cenomanian (Figure 4, of Parrish and Curtis, 1982 and Figure 13C, of Barron, 1985) shows that in a general sense both produce similar predictions. Both models show wind-driven upwelling existing off western South America and northwestern Africa. However, numerical modeling shows wind-driven upwelling off the northern coast of South America during the Cenomanian while it is not on the qualitative maps. Comparison of paleoclimatic maps of the late Silurian (Diagram 8, of Parrish and Curtis, 1982 and Diagram 3, of Moore et al., 1993) reinforces the assertion that both models can predict paleo-upwelling sites relatively well. This and other comparisons highlight the effectiveness of qualitative models in low latitude areas. Numerical models have the potential to be more accurate in higher-latitudinal positions. However, they have been developed only for the medial Cretaceous (Barron, 1985; Kruijs and Barron, 1990) and recently for the late Silurian (Moore et al., 1993).

Additionally, paleoclimatic reconstructions are only as good as the paleogeographic maps on which they are constructed. Because the minimum error on the latitudinal positioning of paleocontinents is 5°-10°, and even perhaps greater for longitudinal positioning, even if numerical modeling is more accurate, its effectiveness is reduced by the large errors associated with paleo-positioning. Therefore non-numerical paleoclimatic models should be considered as potential, first-order, predictive tools for marine petroleum source rock occurrences. However, the unreliability of the prediction will be greater in high latitudinal positions and on paleocontinental configurations that are grossly dissimilar to present-day situations. Both numerical modeling and qualitative modeling should be used to predict MPSR occurrences, with field observations used to either strengthen or reject a proposed paleo-upwelling occurrence. The predictions should be used only as a starting point from which further investigation will yield a more comprehensive explanation concerning the existence of prolific MPSR deposits.

## REFERENCE LIST

- Barron, E.J., 1985, Numerical Climate Modeling, A Frontier in Petroleum Source Rock Prediction: Results Based on Cretaceous Simulations: American Association of Petroleum Geologists Bulletin, v. 69, p. 448-459.
- Berner, R.A., 1983, Sedimentary pyrite formation: An update: *Geochimica et Cosmochimica Acta*, v. 48, p. 605-615.
- Bockmeulen, H., Barker, C. and Dickey, P.A., 1983, Geology and Geochemistry of Crude Oils, Bolivar Coastal Fields: American Association of Petroleum Geologists Bulletin, v. 67, p. 242-270.
- Bosworth, W., and Vollmer, F.W., 1981, Structures of the medial Ordovician flysch of eastern New York: Deformation of Synorogenic Deposition in an Overthrust Environment: *Journal of Geology*, v. 48, p. 551-568.
- Bradley, D.C., and Kusky, T.M., 1986, Geologic Evidence for Rate of Plate Convergence During the Taconic Arc-Continent Collision: *Journal of Geology*, v. 94, p. 667-681.
- Bradley, D.C., 1989, Taconic Plate Kinematics as Revealed by Foredeep Stratigraphy, Appalachian Orogen: *Tectonics*, v. 8, p. 1037-1049.
- Bradley, D.C., and Kidd, W.S.F., 1991, Flexural Extension of the Upper Continental Crust in Collisional Foredeeps: *Geological Society of America Bulletin*, v. 103, p. 1416-1438.
- Brooks, J., Conford, C., and Archer, R., 1987, The role of hydrocarbon source rocks in petroleum exploration. From Brooks, J. and Fleet, A.J., (eds), 1987, *Marine Petroleum Source Rocks*, Geological Society Special Publication No. 26, p. 17-46.
- Burke, K., 1988, Tectonic Evolution of the Caribbean. From, *Annual Review Earth and Planetary Science*, v. 16, p. 201-230.
- Cisne, J.L., et al., 1982, Topography and tectonics of the Taconic outer trench slope as revealed through gradient analysis of fossil assemblages: *Lethaia*, v. 15, no. 3, p. 229-246.
- Delano, J.W., et al., 1990, Petrology and geochemistry of Ordovician K-bentonites in New York State; constraints on the nature of a volcanic arc: *Journal of Geology*, v. 98, p. 157-170.
- Delano, J.W., Tice, S.J., Mitchell, C.E., and Goldman, D., 1993, Rhyolitic glass in Ordovician K-bentonites: A new stratigraphic tool: *Geology*, (in press).
- Demaison, G.J. and Moore, G.T., 1980, Anoxic Environments and Oil Source Bed Genesis: American Association of Petroleum Geologists Bulletin, v. 64, p. 1179-1209.
- Emerson, S., and Hedges, J.I., 1988, Processes Controlling the Organic Carbon Content of Open Ocean Sediments: *Paleoceanography*, v. 3, p. 621-634.
- Erikson, J.P., and Pindell, J.L., 1993, Analysis of subsidence in northeastern Venezuela as a discriminator of tectonic models for northern South America: *Geology*, v. 21, p. 945-948.

- Goldberg, E.D., 1958, Determination of opal in marine sediments: *Journal of Marine Research*, v. 17, p. 178-182.
- Hallam, A., 1984, Pre-Quaternary Sea-Level Changes. From Wetherill, G.W., Albee, A.L., and Stehli, F.G., (eds), 1984, *Annual Review of Earth and Planetary Science* v. 12, p. 205-244.
- Hallam, A., 1987, Mesozoic marine organic-rich shales. From Brooks, J. and Fleet, A.J., (eds), 1987, *Marine Petroleum Source Rocks*, Geological Society Special Publication No. 26, p. 251-261.
- Haq, B.U., Hardenbol, J., Vail, P.R., 1987, Chronology of Fluctuating Sea Levels Since the Triassic: *Nature*, v. 235, p. 1156-1166.
- Hay, B.J., 1982, Depositional Environment in the late middle Ordovician Taconic Foreland Basin (New York State): Evidence from Geochemical, Sedimentological and Stratigraphic Studies: M.S. Thesis, Cornell University, Ithaca, New York, 191 p.
- Hay, B.J., and Cisne, J.L., 1988, Deposition in the Oxygen Deficient Taconic Foreland Basin, late Ordovician. From Keith, D.B., (ed), 1988, *The Trenton Group (upper Ordovician Series) of Eastern North America. Deposition, Diagenesis and Petroleum*, American Association of Petroleum Geologists Studies in Geology, 29, American Association of Petroleum Geologists, Tulsa, Oklahoma, p. 113-134.
- Hein, J.R., Morgenson, L.A., and Sliney, R.E, 1987, Concentration of Uranium in Marine Siliceous Rocks. From Hein, J.R., (ed), 1987, *Siliceous Sedimentary Rock-Hosted Ores and Petroleum*, Van Nostrand Reinhold Company, 304 p.
- James, K.H., 1990, The Venezuelan Hydrocarbon Habitat. From Brooks, J., (ed), 1990, *Classic Petroleum Provinces*, Geological Society Special Publication No. 50, p. 9-35.
- Jenden, P.D., Drazan, D.J., and Kaplan, I.R., Mixing of Thermogenic Natural Gases in Northern Appalachian Basin: American Association of Petroleum Geologists Bulletin, vol. 77, p. 980-988.
- Jenkyns, H.C., 1980, Cretaceous anoxic events: from continents to oceans: *J. Geol. Soc. London*, v. 137, p. 171-188.
- Krujic, E., and E. Barron, 1990, Climate Model Prediction of Paleoproductivity and Potential Source Rock Distribution. From Huc, A.Y., (ed), 1990, *Deposition of Organic Facies*, American Association of Petroleum Geologists Studies in Geology No. 30, p. 195-211.
- Leggett, J.K., McKerrow, W.S., Cocks, L.R.M., and Rickards, R.B., 1981, Periodicity in the early Palaeozoic marine realm: *J. Geol. Soc. London*, v. 138, p. 167-176.
- Longman, M.W., and Palmer, S.E., 1987, Organic Geochemistry of Mid-Continent Middle and Late Ordovician Oils: American Association of Petroleum Geologists Bulletin, v. 71, p. 938-950.
- McDonald, W., 1990, Survey of Caribbean Paleomagnetism. From Dengo, G., and Case, J.E., (eds), 1990, *The Caribbean region*: Boulder, Colorado, Geological Society of America, The Geology of North America, v. H.

- Moore, G.T., D.N. Hayashida and C.A. Ross, 1993, Late Early Silurian (Wenlockian) general circulation model-generated upwelling, graptolitic black shales, and organic-rich rocks-An accident of plate tectonics?: *Geology*, v. 21, p. 17-20.
- Parrish, J.T., 1982, Upwelling and Petroleum Source Beds, With Reference to Paleozoic: *American Association of Petroleum Geologists Bulletin*, v. 66, p. 750-774.
- Parrish, J.T. and Curtis, R. L., 1982, Atmospheric Circulation, Upwelling, and Organic-Rich Rocks in the Mesozoic and Cenozoic Eras: *Palaeogeography, Paleoclimatology, Paleoecology*, v. 40, p. 31-66.
- Parrish, J.T., 1987, Paleo-Upwelling and the distribution of organic-rich rocks. From Brooks, J. and Fleet, A.J., (eds), 1987, *Marine Petroleum Source Rocks*, Geological Society Special Publications No. 26, p. 199-205.
- Pedersen, T.E., and Calvert, S.E., 1990, Anoxia vs. Productivity: What Controls the Formation of Organic-Carbon-Rich Sediments and Sedimentary Rocks?: *American Association of Petroleum Geologists Bulletin*, v. 74, p. 454-466.
- Peters, K.E., 1986, Guidelines for Evaluating Petroleum Source Rock Using Programmed Pyrolysis: *American Association of Petroleum Geologists Bulletin*, v. 70, p. 318-329.
- Pindell, J.L. and Dewey, J.F., 1982, Permo-Triassic Reconstruction of Western Pangea and the Evolution of the Gulf of Mexico/Caribbean Region: *Tectonics*, v. 1, p. 179-211.
- Pindell, J.L., Cande, S.C., Pitman, W.C., Rowley, D.B., Dewey, J.F., Labrecque, J., Haxby, W., 1988, A Plate-Kinematic Framework for Models of Caribbean Evolution: *Tectonophysics*, v. 155, p. 121-138.
- Pindell, J.L., and Barrett, S.F., 1990, Geological evolution of the Caribbean region: A plate-tectonic perspective. From Dengo, G., and Case, J.E., (eds), 1990, *The Caribbean region*: Boulder, Colorado, Geological Society of America, *The Geology of North America*, v. H.
- Pindell, J.L., 1991, Geologic Rationale For Hydrocarbon Exploration in the Caribbean and Adjacent Regions: *Journal of Petroleum Geology*, v. 14, p. 237-257.
- Pindell, J.L., and Erikson, J.P., (in press), The Mesozoic Passive Margin of Northern South America. From Salfity, J.A. (ed), *Cretaceous Tectonics of the Andes* : Weisbaden, Vieweg, p. 1-60.
- Press, F., and Siever, R., *Earth*, (Fourth Edition), 1986.W.H. Freeman and Company: New York, 656 p.
- Rowley, D.B., and Kidd, W.S.F., 1980, Stratigraphic Relationships and Detrital Composition of the medial Ordovician Flysch of western New England: Implications for the Tectonic Evolution of the Taconic Orogeny: *Journal of Geology*, v. 89, p. 199-218.
- Scotese, C.R., Snelson, S., Ross, W.C., and Dodge, L.P., 1980, A Computer Animation of Continental Drift. From McElhinny, M.W., Khramov, A.N., Ozima, M., and Valencio, D.A., (Eds), 1980, *Global Reconstruction and the Geomagnetic Field during the Paleozoic*, *Advances in Earth and Planetary Sciences* 10, Center for Academic Publications, 142 p.

- Scotese, C.R. and McKerrow, W.S., 1990, Revised World maps and introduction. From McKerrow, W.S. and Scotese, C.R., (eds), 1990, *Paleozoic Paleogeography and Biogeography*, Geological Society Memoir No. 12, p. 1-21.
- Sheldon, R.P., 1987, Association of Phosphatic and Siliceous Marine Sedimentary Deposits. From Hein, J.R., (ed), 1987, *Siliceous Sedimentary Rock-Hosted Ores and Petroleum*, Van Nostrand Reinhold Company, 304 p.
- Spicer, R.A., 1989, Physiological characteristics of land plants in relation to environment through time: Royal Society of Edinburgh Transactions, Earth Sciences, v. 80, p. 321-329.
- Stein, R., 1991, Accumulation of Organic Carbon in Marine Sediments. From Bhattacharji, S., Freidman, G.M., Neugebauer, H.J., and Seilacher, A., (eds), *Lecture Notes in Earth Sciences*, vol. 34, Springer-Verlag, 217 p.
- Sweeney, J., Talukdar, S., Burnham, A., Vallejos, C., 1990, Pyrolysis kinetics applied to prediction of oil generation in the Maracaibo Basin, Venezuela: *Organic Geochemistry*, v. 16, p. 189-196.
- Tyson, R.V., 1987, The genesis and palynofacies characteristics of marine petroleum source rocks. From Brooks, J. and Fleet, A.J., (eds), 1987, *Marine Petroleum Source Rocks*, Geological Society Special Publications No. 26, p. 74-67.
- Talukdar, S., Gallango, O., and Chin-A-Lien, M., 1986, Generation and migration of hydrocarbons in the Maracaibo Basin, Venezuela: An integrated basin study: *Organic Geochemistry*, v. 10, p. 261-279.
- Talukdar, S., Gallango, O., Vallejos, C., Ruggiero, A., 1987, Observations on the Primary Migration of Oil in the La Luna Source Rocks of the Maracaibo Basin, Venezuela. From Doligez, B., (ed), 1987, *Migration of Hydrocarbons in Sedimentary Basins*, p. 59-78, Technip Paris.
- Titus, R., 1988, Facies of the Trenton Group. From Keith, D.B., (ed), 1988, *The Trenton Group (upper Ordovician Series) of Eastern North America. Deposition, Diagenesis and Petroleum*, American Association of Petroleum Geologists Studies in Geology, 29, American Association of Petroleum Geologists, Tulsa, Oklahoma, p. 77-86.
- Ulmishek, G.F., and Klemme, H.D., 1990, Depositional controls, distribution, and effectiveness of world's petroleum source rocks: U.S. Geological Survey Bulletin 1931, 59 p.
- Van Der Voo, R., 1988, Paleozoic paleogeography of North America, Gondwana and intervening displaced terranes: Comparisons of paleomagnetism with paleoclimatology and biogeographical patterns: *Geological Society of America Bulletin*, v. 100, p. 311-324.
- Waples, D., 1980, *Organic Geochemistry for Exploration Geologists*:: Minneapolis, Burgess Publishing Company. 151p.
- Wilson, J.T., 1966, Are the Structures of the Caribbean and Scotia Arc Regions Analogous to Ice Rafting?: *Earth and Planetary Science Letters*, v. 1, p. 335-338.
- Witzke, Brian J., 1990: Palaeoclimatic constraints for Palaeozoic Paleolatitudes of Laurentia and Euramerica. From McKerrow, W.S. and Scotese, C.R., (eds), 1990, *Palaeozoic Palaeogeography and Biogeography*, Geological Society Memoir No. 12, pp. 57-73.

- Ziegler, A.M., C.R. Scotese, W.S. McKerrow, M.E. Johnson and R.K. Bambach, 1979: Paleozoic Paleogeography. From Donath, F.A., Stehli, F.G., and Wetherill, G.W., (eds), 1979, *Annual Review of Earth and Planetary Sciences*, v. 7, p. 473-502.
- Zerrahn, G.J., 1978, Ordovician (Trenton to Richmond) depositional patterns of New York State, and their relation to the Taconic Orogeny: *Geological Society of America Bulletin*, v. 89, p. 1751-1760.